UNIVERSITY OF CALIFORNIA
IRVINE

The Chemistry of the Lanthanides Using Nontraditional Ligand Sets

DISSERTATION

Submitted in partial satisfaction of the requirements
for the degree of

DOCTOR OF PHILOSOPHY

in

CHEMISTRY

By

KITO GILBERT-BASS

Dissertation Committee:
Professor Dr. William J. Evans, Chair
Professor Dr. Jenny Yang
Professor Dr. Alan Heyduk
May 14th, 2025

–Table of Contents–

–List of Figures–

–List of Schemes–

–List of Tables–

–Acknowledgements–

An appreciation of those who helped me along my journey

The past five years have been the most challenging, frustrating, confusing, and arduous of my life thus far. They have been hallmarked by late nights at the laboratory, threats to give up, and a plethora of experiments that did not go the way I had hoped. However, the ease at which I am able to make these acknowledgements should be a testament how much these people have helped me through the hardest parts of this journey, have celebrated the breakthroughs, and offered me guidance when I felt lost. This thesis is dedicated to them.

First and foremost, I would like to thank my Primary Investigator, Dr. William J. Evans. Throughout my five years in his lab, he has been generous with his funding for my research, kind and willing to talk me through any difficult times I was having, and supportive in my education and job search. Dr. Evans is a true inspiration in his enthusiasm for chemistry and his excitement for education. I know for a fact that without his guidance, speedy return of drafts and persistence, I would not have been able to accomplish what I have during this year.

I would also like show my appreciation to the current and past members of the Evans lab. Domonic Caruth, the undergraduate student that I plucked straight out of the inorganic chemistry laboratory class, CHEM 107L, and brought into the lab to work with me is an incredible chemist with an envious curiosity for chemical synthesis. Thank you for your assistance and consistent positive attitude and for convincing me to get a climbing gym class membership (although it is probably time to cancel it); I only wish that we could have met sooner. It has been an absolute pleasure to watch as you develop your synthetic technique, from the happy accidents that landed you a new Ce(IV) complex and an impressive way to purify products, to the wonderful intentional results you have been getting lately, and I wish you only the best at UC Riverside.

Makayla Luevano, you are the first undergraduate that I worked with and you not only have incredible and award-winning chemistry prowess, but also impeccable taste in music and you make a fantastic Learning Assistant. Thank you for sharing your love for Saya Gray with me, working with Cary and me on our terphenylthiolate project, and for assisting me when I was Instructor of Record. You deserve all of the accolades you have earned, and I cannot wait to see what you do next with Dr. La Pierre.

To Dr. Cary Stennett, I cannot say that I have directly learned more from anyone in this lab than him. Whether it was with "Argument Fridays" or late nights working up laborious ligand syntheses, the conversations I have had with you have opened my mind in ways that I would otherwise have never considered. Thank you for challenging me be better, like doing "just one more thing" before I leave for the day, or taking much needed beach breaks even if they were too early in the morning. I will Cary your wisdom along to my future endeavors.

Jonah Stiel, you have been an incredible help, especially in the final stages of writing this dissertation. I admire your passion for home chemistry and the profound curiosity you bring to the laboratory, despite the challenges you face daily. Good luck with the next few years, I am confident you will do excellently.

I will never not be jealous of the ability for Dr. Joshua Queen to discover groundbreaking organometallic complexes on a whim. Thanks for coming over to my corner of the lab and inspiring me not to give up on projects when they don't work out right away. You have helped me think more intuitively about the chemistry I am conducting to produce better results.

To the previous Evans lab members Dr. Sierra Ciccone, Dr. Lauren Anderson-Sanchez, Dr. Joseph Nguyen, Dr. William Moore, Dr. Justin Wedal, Gabriella Godinho, Brynn Turpin and honorary member Safa Yosafi, I want to express my utmost gratitude for welcoming me so

warmly into the lab and showing me the ropes of lanthanide synthesis. Time spent with you all has been precious to me, and your mentorship has been invaluable.

Drs. Jenny Yang, Alan Heyduk, Andy Borovik, Sarah Finkeldei, and Suzanne Blum, your guidance with my orals presentations and your overall kindness and graciousness, even if it is just saying hello or simply asking “how is your chemistry going” when passing me in the hallway, has meant a tremendous amount to me and has kept my spirits high throughout this process.

Jasmine Peña, your entry into my life has been so much more than impactful; you feel like family. You are always a pleasure to spend time with and the little tunes that you sing get stuck in my head like nothing ever has. Your encouragement, compassion and excitement to celebrate accomplishments is second to none, and I am not afraid to admit that I admire your ability to give and receive love so freely.

Genesis Escobar, I am routinely impressed with your drive to learn about science and the brightness of your future is blinding at times. I don’t know how you light up every room you enter the way you do with your wit, charisma, and style, but I love that about you and I consider myself lucky to even be able to witness it.

To the close friends that I have made throughout my schooling: Matthew Nguyen, Enrique Valerdi, Dr. Rain Talosig. You have shaped my personality, supported me at my worst, and partied with me at my best.

Matt, thank you for teaching me to work smarter, not harder, to appreciate the music in my life, and to effectively treat myself when I’ve earned it. Your attention to detail is immaculate and your steadfastness when it comes to perfection is without question. You are hilarious, generous and thoughtful, and being friends with you has been one of the most rewarding parts of

my life. You have introduced me so much about the world, including the pleasures of actual ramen, Elden Ring, and so much that if I put it all here, this thesis would be at least twice as large.

Enrique, thank you for allowing me to share an apartment with you and to grow with you as I have. I am blessed to have a friend that laughs at my throwaway jokes, feels comfortable coming to me for relationship advice, and acts as a shoulder to lean on when I need it. Your support, encouragement, and overall fraternity has been tantamount to my success, and so I thank you for that. I look forward to the billions of laughs we will share over the coming decades.

Rain, you have always been there for me, from Ithaca to now, encouraging me to leave the house, riding on weekend Brews Cruises with me, and letting me crash at your place on numerous occasions for various reasons. I am beyond delighted that we have become such close friends. Thank you for letting me follow you to UCI, and I hope you don't mind if I follow you again to the bay area.

To my partner, my love, Jessamyn Gilbert, my gratitude toward you is Boundless. I am infinitely indebted to you for all of the laughs, the silly cat pictures, the love and commitment you have given to me over these past five years. You have been the reason that I am excited to come home, my confidant and my most loyal ally throughout all of this. You are smart as a tack, as sharp as a whip, and so, so incredibly fast. Needless to say, none of this would have been possible without you by my side, and I am so excited to start this next chapter of our lives together and to see how we grow from here. You are the best thing that has ever happened to me. Thank you for being my person.

To my mother, Stacey Gilbert, my father Eric Bass, and my brother Gyasi Gilbert-Bass, I love you all like family. You have nourished me, advocated for me, invested in me, and educated

me since day one (and in some cases, before that). There is not a thing that I have ever done of which the credit is not owed to you. From the bottom of my heart, thank you.

I absolutely would not have gotten to this point without the help of all of those mentioned above, but I would also like to thank the following people who have made my life that much more improved (in no particular order):

Olive and Opal, my cats

My close friends:

Adrian Soria, Maria Soria, Kendra Johnson, Gregory Rowley, Anya Atkins, Rockee Adams, Kokie Adams, Karen Vogel (thanks for letting me use your car to come here in the first place), Claire Levitt, Dr. Darnell Harris, Adam Rabayda, Otto Euler, Megan Holman, Rochelle Radzyminski

My previous and current mentors and people who have helped me along the way:

Anja Rosengarth, Dr. Tyler Kerr, Dr. Janet Hunting, Dr. Mike Haaf, Dr. Scott Ulrich, Dr. Dewey Moody, Dr. Suvrajit Sengupta, Dr. Sarah Finkeldei, Britney Pham, Dr. Joseph Ziller.

All other people significant to me not mentioned here, know that I am immensely grateful.

The text of portions of Chapter 2 of this dissertation is an adaptation of the material as it appears in Gilbert-Bass, K., Stennett, C. Grotjahn, R. Ziller J., Furche F., Evans, W. J. Exploring sulfur donor atom coordination chemistry with La(II), Nd(II), and Tm(II) using a terphenylthiolate ligand. *Chem. Commun., 2024,* ***60****, 4601*. Used with permission form RSC publishing. The coauthors listed in this publication are Kito Gilbert-Bass, Cary Stennett, Robin Grotjahn, Filipp

Furche, and William J. Evans. Oski T. Bear directed and supervised research which forms the basis for the dissertation.

Financial support was provided by the University of California, Irvine, NSF Grant CHE- 2154255 and an NSF Grant GRS-AGEP-2302297

–VITA–

KITO GILBERT-BASS

Department of Chemistry
University of California, Irvine

U.S. Citizen

EDUCATION

PhD University of California Irvine, *Irvine, CA* — Sept 2020 - Present
Overall GPA: 3.9

BS Ithaca College, *Ithaca, NY* — Aug 2015 – May 2019
Cum Laude
Minor: Sociology
Overall GPA: 3.6

HONORS AND AWARDS

NSF AGEP-GRS Award — January 2023 - Present
Dean's List — Fall 2015 and 2017, Spring 2019
Goldwater Scholarship Nominee — 2017
ALANA Outstanding Academic Achievement Award — Fall 2016 and 2017
ALANA Excellent Academic Performance Award — Fall 2018
Russel Drago Chemistry Award — Fall 2018
ACS Undergraduate Award in Inorganic Chemistry — 2018
Sigma XI Member — Spring 2018

CHEMISTRY WORK EXPERIENCE

UC Irvine Chemistry Department
Irvine, CA

Instructor of Record — Jan 2024 – Mar 2024
Acted as instructor for a class of over 360 students teaching General Chemistry (Chem 1A) for one quarter

Chemistry Teaching Assistant — Sept 2020 – Present
Taught weekly four-hour lab classes in-person and online. Offered guidance for 12-50 students at a time in General Chemistry Laboratory (Chem 1A, 1LC and 1LD), Nuclear and Radiochemistry (Chem 133/233), and Inorganic Chemistry Laboratory (Chem 107L)

Freelance tutoring
Seattle, WA
Irvine, CA

Chemistry Tutor — Jan 2020 – Present
Created a small for-hire business within the greater Seattle area for chemistry tutoring for up to 4 students at a time

DeepCell Industries
Seattle, WA

Operations Staff at CBD Product Startup — Jul 2019 – Aug 2020
Assisted with research and development of CBD products. Improved operations methods. Managed inventory.

Ithaca College Tutoring Services
Ithaca, NY

Head tutor — Aug 2016 – May 2019
Showed exemplary peer tutoring skills and shared knowledge in previously mastered classes. Provided advice from experience to other peer tutors seeking guidance in tutoring sessions. Led peer tutor workshops to help other tutors develop their tutoring abilities

Ithaca College Chemistry Department *Ithaca, NY*	**Chemistry Teaching Assistant** Was a student resource and sat in on various chemistry classes including Principles of Chemistry, Organic Chemistry I and II, and Quantitative Chemistry. Helped in paper grading and experiment set-up.	Aug 2016 – May 2019

RESEARCH EXPERIENCE

Graduate Student Research University of California, Irvine *Irvine, CA*	**Graduate Student Researcher** Studying the expansion of the chemistry of the rare-earth elements by finding ligand systems that stabilize the 2+ oxidation state in the lab of Dr. William Evans.	May 2020 – Present
	Laboratory Safety Representative Managed lab inventory, was liaison with the safety department, and developed strategies for improved safety practices in the lab	Aug 2023 – Jan 2025
Clean Energy Institute REU University of Washington *Seattle, WA*	**Visiting Student Researcher** Explored quantum dot catalysis for the degradation of a lignin substrate in the lab of Dr. Brandi Cossairt. Participated in a poster exposé for undergraduate summer research.	May 2018 – Aug 2018
Honors Student Research Ithaca College *Ithaca, NY*	**Student Researcher** Conducted synthesis and analysis of new quaternary lithium calcium transition metal nitrides in Dr. Janet L. Hunting's solid state chemistry lab. Explored new perovskite compositions and techniques for increased solar fuel cell efficiency. Became proficient in utilizing SC-XRD and powder diffraction methods for chemical examination	Jan 2016 – May 2019
Dana Summer Scholar Research *Ithaca, NY*	**Student Researcher** Constructed a detailed poster explaining research for presentation at Ithaca college's 125th anniversary	May 2017 – Jul 2017

JOURNAL PUBLICATIONS

Exploring the Stabilization of Ln(IV) Coordination Complexes with the Di(mesityl)boroxide ligand
Kito Gilbert-Bass, Domonic Caruth, Joseph W. Ziller, and William J. Evans* *Manuscript in Progress, Expected* **2025**

The Variable Di(mesityl)boroxide Coordination Chemistry of the Lanthanide Metals
Kito Gilbert-Bass, Domonic Caruth, Joseph W. Ziller, and William J. Evans* *Submitted to Inorganic Chemistry, Publication Expected* **2025**

Exploring sulfur donor atom coordination chemistry with La(ii), Nd(ii), and Tm(ii) using a terphenylthiolate ligand
Kito Gilbert-Bass, Cary R. Stennett, Robin Grotjahn, Joseph W. Ziller, Filipp Furche , and William J. Evans* *Chemical Communications,* **2024**, *60,* 4601-4604.

Photolytic C–O Bond Cleavage with Quantum Dots

Michael J. Enright, Kito Gilbert-Bass, Harrison Sarsito, and Brandi M. Cossairt* *Chemistry of Materials* **2019** *31* (7), 2677-2682.

CONFERENCE PRESENTATIONS

Poster: *Synthesis and characterization of new lithium calcium transition metal quaternary nitrides*
Kito Gilbert-Bass *Abstracts of Papers, ACS National Meeting & Exposition* March 18-20, **2017**, p.CHED-1165

Oral Presentation: *The Variable Di(mesityl)boroxide Coordination Chemistry of the Lanthanide Metals*
Kito Gilbert-Bass: *Abstracts of Papers, ACS National Meeting & Exposition* March 23-27, **2025**, p.INOR- 4192978

ANALYTICAL PROFICIENCIES

Instrumentation Capabilities	X-Ray Diffractometry: Single-crystal and Powder, NMR and EPR Spectroscopy, HPLC, Mass Spectrometry, Fluorimetry, UV-Visible Spectroscopy, Infra-Red Spectroscopy, X-Ray Fluorimetry
Software Capabilities	Mestre Nova, TopSpin, ChemDraw Prime, Olex, Spectragryph, Easyspin, SpinCount, Apex 2-5, Microsoft Office

ADDITIONAL EXPERIENCE

Big Brothers Big Sisters of America *Irvine, CA*	**Big Brother** Met weekly with and mentored a sophomore high school student with my own life experiences and in some laboratory science	Apr 2023 - Present
ChemUNITY University of California, Irvine *Irvine, CA*	**Chemistry Grad Student First Year Mentor** Guided three incoming chemistry graduate students through their first year with quarterly meetings and advice when requested.	May 2021 - May 2022
Poster Presentation 255th American Chemical Society National Meeting *New Orleans, LA*	**Poster Presenter** Presented nitride synthesis research to a symposium of chemists and undergrad researchers.	May 2017
Faculty Search Committee Ithaca college *Ithaca, NY*	**Committee Member** Participated in the hiring of three new biochemistry and physical chemistry professors. Learned to discern useful qualities in viable and respectable professorial position candidates. Gained fundamental teamwork skills to reach desired and productive outcomes.	Sept 2016 - Mar 2017

–Abstract of the Dissertation–

The Chemistry of the Lanthanides Using Nontraditional Ligand Sets
By
Kito Gilbert-Bass
Doctor of Philosophy in Chemistry
University of California, Irvine, 2025
Professor Dr. William J. Evans, Chair

This dissertation focuses on the utilization of uncommon ligands for the stabilization of rare-earth metal complexes in unusual oxidation states (rare-earth metal = Y, Sc, and the lanthanides). Discussed here are the syntheses and spectroscopic and crystallographic characterization of complexes of these ligands and an evaluation of their value in stabilizing unusual oxidation states. An introduction to the nuances of rare-earth metal coordination chemistry, details of the redox chemistry of these metals and the definitions of "traditional" $4f^{n+1}$ and "nontraditional" $4f^n5d^1$ rare-earth metal ions in the +2 oxidation state can be found in Chapter 1.

Chapter 2 discusses the coordination chemistry of the hexa-iso-propyl-terphenylthiolate ligand with various lanthanide metals. In this Chapter, the synthesis of new La(II), Nd(II) and Tm(II) complexes this thiolate ligand are described as well as their characterization by analytical techniques including EPR spectroscopy and density functional theory. Use of this ligand with lanthanum led to the formation of a long-lasting $4f^05d^1$ Ln(II) species with a very small eight-line hyperfine coupling constant of 67.3 MHz.

Chapters 3 and 4 are concerned with the electron-deficient alkoxide analog, di(mesityl)boroxide, $(OBMes_2)^-$ (Mes = C_6H_2-2,4,6-Me_3), and the various lanthanide oxidation states that it can support. In Chapter 3, the $(OBMes_2)^-$ ligand was explored as a possible less-electron-rich ligand that may better coordinate the less-electropositive +2 oxidation state

lanthanides. This ligand was shown to coordinate to +3 lanthanide ions in a plethora of modalities. Structural and spectroscopic information is described for many complexes including dimeric compounds like $[(Mes_2BO)_2Ln(\mu\text{-}OBMes_2)]_2$ (Ln = La, Ce, Nd, Gd) and monomers like $Ln(OBMes_2)_3(THF)_3$ (Ln = La, Nd), as well as mixed ligand complexes like $Nd(OBMes_2)(NR_2)_2(THF)$. Although reduction of these di(mesityl)boroxide complexes did not result in identifiable Ln(II) complexes, crystallographic analysis of the complexes such as $K(\mu\text{-}Mes_2BO)_3Sm(OBMes_2)(THF)$ led to the discovery that many of the complexes are able to form "ate-salts" in which four $(OBMes_2)^-$ ligands bind to a single Ln(III) ion in a compound that is charge-balanced by a potassium countercation that is encapsulated by ligands. However, a complex of a +2 lanthanide ion was isolated for samarium from reactions with SmI_2: the tetrameric Sm(II) oxo cluster, $Sm_4(OBMes_2)_6(\mu_4\text{-}O)$. This complex reacts with the xylyl isocyanide CNXyl (Xyl = C_6H_3-2,6-Me_2) to form an unusual pair of closely related cocrystallized Sm(III) complexes, $Sm(OBMes_2)_3(CNXyl)(Et_2O)$ and $Sm(OBMes_2)_3(CNXyl)_3$.

This potassium-encapsulation theme is the basis of Chapter 4 which explores the di(mesityl)boroxide ligand in heteroleptic $K(\mu\text{-}Mes_2BO)_2Ln(NR)_2)_2$ (Ln = Ce, Pr, Nd, Sm, Tb; R = $SiMe_3$) complexes as starting materials to form Ln(IV) complexes. For $K(\mu\text{-}Mes_2BO)_2Ce(NR)_2)_2$, treatment with AgI led to the elimination of KI and Ag metal, along with the formation of a new tetravalent cerium complex, $Ce^{IV}(OBMes_2)_2(NR_2)_2$. Treatment of these heteroleptic complexes with the strong oxidizing agent, "magic blue," $[N(C_6H_4\text{-}4\text{-}Br)_3][SbCl_6]$, led to characterization of the unexpected complex $Sb(OBMes_2)_3$. Additionally, another Ce(IV) complex could be formed from the treatment of $Ce^{IV}(OTf)_4$ with four equivalents of $KOBMes_2$.

Chapter 5 of this dissertation describes the use of the di-tert-butylmethylsilanide ligand, [$(SiMe^tBu_2)^-$, to make the "ate-salt" $(Na(THF)_3Cl\text{-}\mu)Y(SiMe^tBu_2)_3(THF)$. This is the first example of a rare-earth metal complex containing three Y-Si bonds.

Chapter 6 describes the use of a ligand isoelectronic to the widely used cyclopentadienide and its derivatives, the tripodal oxygen donor ligand, tris(2-oxo-1-tert-butylimidazolyl)hydroborato (TpO^{tBu}). The formation of $Yb^{II}(TpO^{tBu})_2$ shows that the ligand can coordinate to a traditional Ln(II) ion. In Appendix A, the synthesis and spectroscopic information on the complex $Bi(OBMes_2)_3$ are described in detail. Finally, in Appendix B, the synthesis and characterization of heteroleptic terphenyl complexes $Y(SAr^{iPr6})I_2(THF)_3$ and $Sm(SAr^{iPr6})(NPh_2)I(THF)$, as well as the samarium bisamide iodide, $Sm(NPh_2)_2I(THF)_2$) are described.

–Chapter 1–

Introduction

The Rare Earth Metals. Making up nearly 10% of the members of the periodic table of the elements, the rare-earth metals, also called rare-earth elements or just rare-earths, are 17 metals that possess similar qualities and include yttrium, scandium and lanthanum, which reside in the first group of the d-block, and cerium through lutetium which make up the occupants of the 4f period, all of which are colloquially abbreviated Ln. Contrary to what the name suggests, these elements are not rare at all, and in fact, most are more abundant in the earth's crust than commonly used metals such as gold, silver, mercury and tungsten.[1] The element cerium is the 25th most abundant element, which is higher than that of copper.[2–4] After the discovery of the first rare earth compounds in Ytterby, Sweden in 1787[5] and the development of separation and purification processes in the 1940s,[5] more about the chemistry of these elements was uncovered, including the development of rare-earth coordination complexes[6–18] even with radioactive promethium. It was found that not only is the dominant oxidation state of all 17 of these elements +3, but their chemistry is also similar in that oxidation state and they were thus seen as interchangeable.[1–5,19]

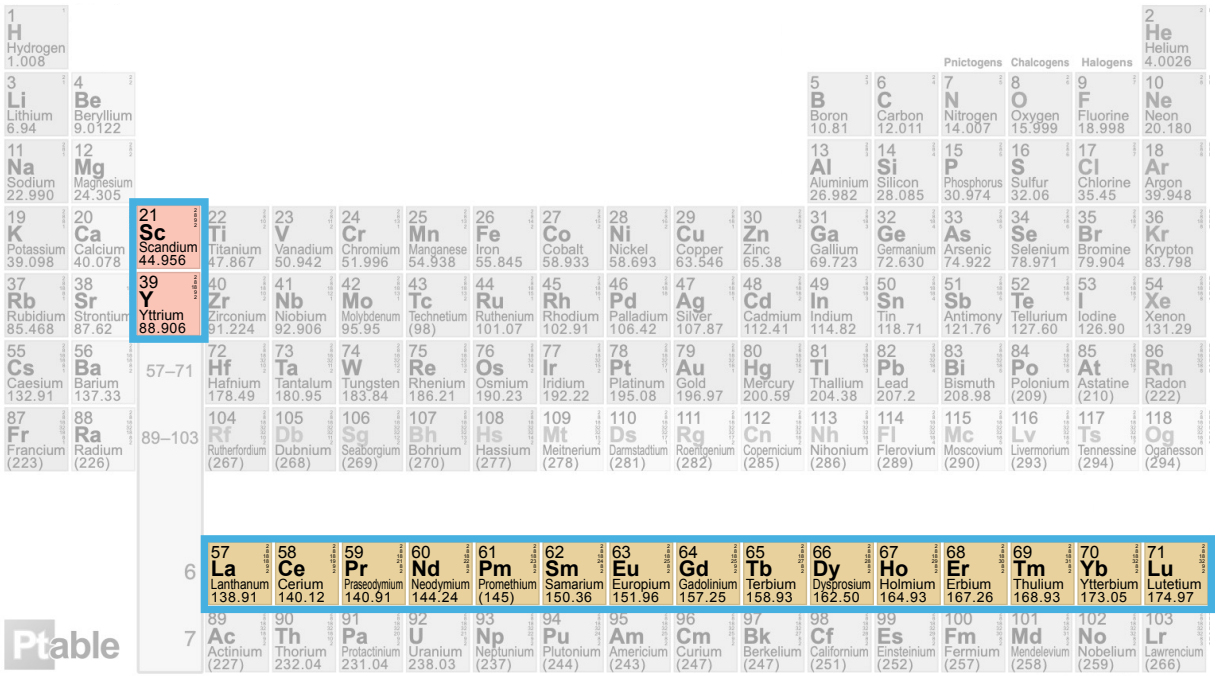

Figure 1.1. The Periodic Table of the Elements with the rare earth metals highlighted.[20]

The +3 Oxidation State of the Rare Earth Metals. The commonness of the +3 ionization state of these ions comes from the stability of triply charged ions gained from environmental interactions being larger than the energy loss from removing these electrons. As long as the hydration energy of these ions is higher than that of the energy to remove a fourth electron, these ions will default to the Ln(III) state, and thus are found in the 3+ oxidation state in the natural world. [2,21] The similarity of these ions to one another in the +3 oxidation state is due to the phenomenon called the lanthanide contraction[22] in which the 4f valence orbitals of these metals do not extend past the 54-electron xenon gas core, resulting in an unexpectedly rapid decrease in size across the 4f period, and the inability to participate in covalent bonds that are common in complexes of the d-block elements.[3,19]

The +2 Oxidation State of the Rare Earth Metals. However, although the +3 ions are the most stable, other oxidation states are accessible for the select lanthanide elements. Specifically, Ln(II) complexes can be isolated for Ln = Nd, Sm, Eu, Dy, Tm, Yb. This is possible

for Eu and Yb because their Ln(II) valence electron configurations of $4f^7$ and $4f^{14}$ offer the added stability of a half-filled and fully-filled 4f orbital, respectively.[2,3] Likewise, the $4f^6$ and $4f^{13}$ valence electron configurations of Sm and Tm are approaching half- and fully- filled 4f orbitals give some stability to +2 ions of those metals although not as much as to Eu and Yb. It should be noted here that in this dissertation, complexes of Sm, Eu, Tm and Yb in the Ln(II) oxidation state are referred to as "traditional divalent lanthanides" due to the fact that reduction of their $4f^n$ Ln(III) ions generates Ln(II) ions with $4f^{n+1}$ electron configurations.

Interestingly, the Nd(II) and Dy(II) valence electron configurations of $4f^4$ and $4f^{10}$ do not claim the status of approaching or achieving half- or fully-filled 4f orbitals upon the addition of an electron. These ions have the ability, depending on their coordination environment, to form tradition $4f^{n+1}$ electron configurations or to place the electron in a 5d orbital to adopt a $4f^n5d^1$ electron configuration, which is called "nontraditional." Nd(II) and Dy(II) are accordingly called "configurational crossover ions".[23–26]

Although Nd(II) and Dy(II) were known to exist in the solid state, it was generally considered that the only rare-earth metals that could form soluble molecular complexes of Ln(II) ions were the traditional divalents, Eu, Yb, Sm, and Tm. However, a divalent form of lanthanum was crystallographically characterized in a 2008 publication by Lappert[27] specifically the complexes $[K(chelate)][La^{II}(Cp'')_2]$ (chelate = 2.2.2-cryptand, 18-crown-6; Cp'' = C_6H_3-1,3-$(SiMe_3)_2$), figure 1.2.[27]

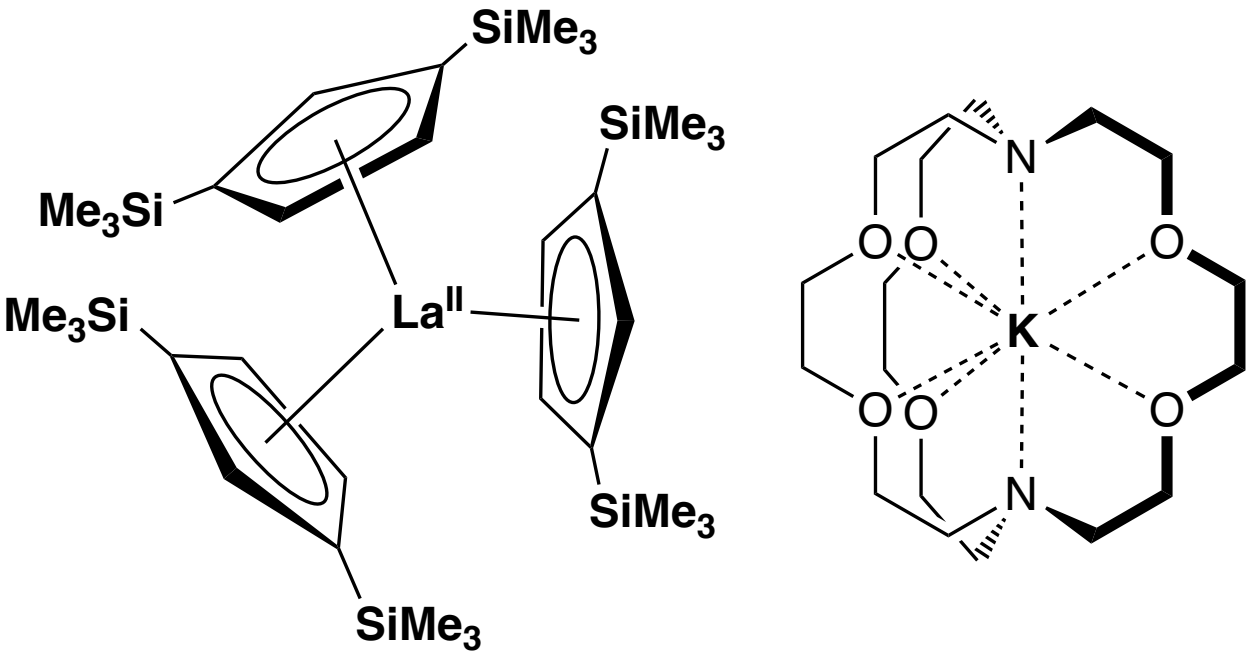

Figure 1.2. One of the first two crystallographically characterizable La^{II} complexes, [K(2.2.2-cryptand)][$La^{II}Cp''_3$]; the other being [K(18-crown-6)][$La^{II}Cp''_3$].[27]

This led to the discovery that all of the non-radioactive lanthanides that were not traditional or configurational crossover divalents (Ln = La, Ce, Pr, Gd, Tb, Ho, Er, Lu) adopted the nontraditional $4f^n5d^1$ coordination.[15,28] Similarly, it was found that yttrium and scandium could also make divalent compounds, however without having f orbitals, these metals adopt the $3d^1$ and $4d^1$ electron configurations[29–31]

Oxidation States Beyond Ln(II) and Ln(III). Although the most common oxidation states of the rare earths are +3, complexes of rare earths in the Ln(0),[13,32–34] Ln(IV)[7,35–42] and even Ln(V)[43] oxidation states have been isolated and characterized. Through metal vapor deposition, complexes of $Ln^0(C_6H_3\text{-}1,3,5\text{-}^t\text{Bu})$ (Ln = Sc,[13] Y,[33] La,[34] Pr,[34] Nd,[34] Sm,[34] Gd,[33] Tb,[34] Dy,[34] Ho,[34] Er,[34] Lu,[34])[32] were formed. And, while Ce(IV) is a rather attainable oxidation state for that metal due to its [Xe] noble gas electron configuration, with powerful oxidizing agents, high valent species such as Tb(IV),[37,39,42] Pr(IV)[40] and Pr(V)[43] could also be formed. Needless to say, the rare earth metals are not limited to one oxidation state.

Expanding the Range of Traditional Ligands for the Rare-Earth Metals. In a broader sense, this thesis aims to challenge the notions that the coordination chemistry of the lanthanides is limited to ligands in the known literature through the exploration of the coordination of non-standard ligands that have not previously shown to coordinate to the rare earth metals. Of the complexes discussed so far, the vast majority consist of only a few negatively charged donor atoms: carbon, nitrogen, oxygen and the halogens. This is because the small, highly positively-charged rare earth metals are considered "hard" Lewis acids and thus are quite compatible with these "hard" Lewis bases.[2,19,44] However, ignoring the "softer" electron donor atoms excludes the possibility for significant discoveries to be made. For example, in Chapter 2 of this dissertation, the chemistry of a divalent lanthanide complex that employs a "softer" thiolate ligand is described that has a decomposition rate of 5% over 36 h at room temperature and an uncharacteristically small La(II) hyperfine coupling constant of 67.3 MHz. [45,46] In Chapter 3, the chemistry of the di(mesityl)boroxide $(OBMes_2)^-$ ligand, a less-electron-rich analog of an alkoxide ligand,[47–50] is presented and includes the synthesis of to a Sm(II) oxo cluster.. In Chapter 4, that same ligand is shown to support a tetravalent cerium ion in the complex $Ce^{IV}(OBMes_2)_2(N(SiMe_3)_2)_2$. In Chapter 5, the first yttrium complex with three Y—Si bonds is described using the $(SiMe^tBu_2)^-$ ligand, which had previously been used to form Ln(II) complexes.[51] Finally, in Chapter 6, the use of a ligand isoelectronic to the cyclopentadienide ligand to form a coordination complex of Yb(II) is described.

REFERENCES

(1) Muecke, G. K.; Möller, P. The Not-So-Rare Earths. **1988**, *258* (1), 72–77.

(2) Liddle, S. T.; Mills, D. P.; Natrajan, L. P. *The Lanthanides and Actinides Synthesis, Reactivity, Properties and Applications*; World Scientific Publishing Europe Ltd., 2022.

(3) Atwood, D. A. *The Rare Earth Elements: Fundamentals and Applications*; John Wiley & Sons, Ltd., 2012.

(4) Haskin, L. A.; Frey, F. A. Dispersed and Not-So-Rare Earths. *Science* **1966**, *152* (3720), 299–314.

(5) Mingos, D. M. P.; Macgregor, S. A.; Neese, U. F.; An Der Ruhr, M.; Pariente, G. J. P.; Schneider, S. S. *The Periodic I Development and Essential*; Mingos, D. M. P., Ed.; Springer Nature Switzerland AG, 2019; Vol. 1.

(6) Morss, L. R. Thermochemical Properties of Yttrium, Lanthanum, and the Lanthanide Elements and Ions. *Chemical Reviews* **1976**, *76* (6), 827–841.

(7) Evans, W. J.; Deming, T. J.; Ziller, J. W. The Utility of Ceric Ammonium Nitrate Derived Alkoxide Complexes in the Synthesis of Organometallic Cerium(IV) Complexes: Synthesis and First X-Ray Crystallographic Determination of a Tetravalent Cerium Cyclopentadienide Complex, $(C_5H_5)_3Ce(OCMe_3)$. *Organometallics* **1989**, *8* (6), 1581–1584.

(8) Bradley, D. C.; Chudzynska, H.; Hursthouse, M. B.; Motevalli, M.; Wu, R. *VOLATILE FLUORINATED TERTIARY ALKOXIDES OF SOME LANTHANIDES, TRIS-HEXAFLUORO-TERTIARY BUTOXIDES OF LANTHANUM, PRASEODYMIUM AND EUROPIUM*; 1994; Vol. 13.

(9) Evans, W. J.; Nyce, G. W.; Clark, R. D.; Doedens, R. J.; Ziller, J. W.; Evans, W. J.; Nyce, G. W.; Clark, R. D.; Doedens, R. J.; Ziller, J. W. The Trivalent Neodymium Complex [(C 5 Me 5) 3 Nd] Is a One-Electron Reductant! *Angewandte Chemie International Edition* **1999**, *38* (12).

(10) Evans, W. J.; Gummersheimer, T. S.; Ziller, J. W. Coordination Chemistry of Samarium Diiodide with Ethers Including the Crystal Structure of Tetrahydrofuran-Solvated. *Journal of the American Chemical Society* **1995**, *117*, 8999–9002.

(11) Evans, J. W.; Drummond, D. K. Samarium-Mediated Functionalization of N=N Bonds: Double Insertion of Carbon Monoxide into the N=N of Azobenzene1. *Journal of the American Chemical Society* **1986**, *108* (1), 7440–7441.

(12) Brennan, J. G.; Cloke, F. G. N.; Sameh, A. A.; Zalkin Allan. Synthesis of Bis(η-1,3,5-Tri-t-Butylbenzene) Sandwich Complexes of Yttrium(0) and Gadolinium(0); the X-Ray Crystal Structure of the First Authentic Lanthanide(0) Complex, [Gd(η-But3C6H3)2]. *Journal of the Chemical Society, Chemical Communications* **1987**, No. 21, 1668–1669.

(13) Cloke, F. G. N.; Khan, K.; Perutzb, R. N. η-Arene Complexes of Scandium(0) and Scandium(II). *Journal of the Chemical Society, Chemical Communications* **1991**, No. 19, 1372–1373.

(14) Evans, W. J.; Allen, N. T.; Ziller, J. W. The Availability of Dysprosium Diiodide as a Powerful Reducing Agent in Organic Synthesis: Reactivity Studies and Structural Analysis of DyI2((DME)3 and Its Naphthalene Reduction Product [13]. *Journal of the American Chemical Society*. November 29, 2000, pp 11749–11750.

(15) MacDonald, M. R.; Bates, J. E.; Fieser, M. E.; Ziller, J. W.; Furche, F.; Evans, W. J. Expanding Rare-Earth Oxidation State Chemistry to Molecular Complexes of Holmium(II) and Erbium(II). *Journal of the American Chemical Society* **2012**, *134* (20), 8420–8423.

(16) Pfeiffer, D.; Ximba, B. J.; Liable-Sands, L. M.; Rheingold, A. L.; Heeg, M. J.; Coleman, D. M.; Bernhard Schlegel, H.; Kuech, T. F.; Winter, C. H. Synthesis, Structure, and Molecular Orbital Studies of Yttrium, Erbium, and Lutetium Complexes Bearing H2-Pyrazolato Ligands:

Development of a New Class of Precursors for Doping Semiconductors. *Inorganic Chemistry* **1999**, *38* (20), 4539–4548.

(17) Bochkarev, M. N.; Fedushkin, I. L.; Fagin, A. A.; Petrovskaya, T. V.; Ziller, J. W.; Broomhall-Dillard, R. N. R.; Evans, W. J. Synthesis and Structure of the First Molecular Thulium(II) Complex: [TmI2(MeOCH2CH2OMe)2]. *Angewandte Chemie (International Edition in English)* **1997**, *36* (1–2), 133–135.

(18) Bochkarev, L. N.; Makarov, V. M.; Hrzhanovskaya, Y. N.; Zakharov, L. N.; Fukin, G. K.; Yanovsky, A. I.; Struchkov, Y. T. Synthesis and Structure of Organosilicon and Organogermanium Complexes of Ytterbium (Ph3E)2Yb(THF)4 with YbSi and YbGe Bonds. *Journal of Organometallic Chemistry* **1994**, *467* (2).

(19) Wedal, J. C.; Evans, W. J. A Rare-Earth Metal Retrospective to Stimulate All Fields. *Journal of the American Chemical Society* **2021**, *143* (44), 18354–18367.

(20) Dayah, M. *Ptable*. ptable.com (accessed 2025-05-03).

(21) Robert Connick, B. E. Oxidation States of the Rare-Earth and Actinide Elements. **1949**.

(22) Pyykko, P. Relativistic Effects in Structural Chemistry. *Chemical Reviews* **1988**, *88* (3), 563–594.

(23) Fieser, M. E.; Palumbo, C. T.; La Pierre, H. S.; Halter, D. P.; Voora, V. K.; Ziller, J. W.; Furche, F.; Meyer, K.; Evans, W. J. Comparisons of Lanthanide/Actinide +2 Ions in a Tris(Aryloxide)Arene Coordination Environment. *Chemical Science* **2017**, *8* (11), 7424–7433.

(24) Evans, W. J.; Allen, N. T.; Workman, P. S.; Meyer, J. C. Large Scale Synthesis of Dysprosium and Neodymium Diiodides. *Inorganic Chemistry* **2003**, *42* (9), 3097–3099.

(25) Trinh, M. T.; Wedal, J. C.; Evans, W. J. Evaluating Electrochemical Accessibility of $4f^n5d^1$and $4f^{n+1}$Ln(II) Ions in $(C_5H_4SiMe_3)_3Ln$ and $(C_5Me_4H)_3Ln$ Complexes. *Dalton Transactions* **2021**, *50* (40), 14384–14389.

(26) Meyer, G. Small Cause – Great Effect: What the $4f^{n+1}5d^0 \rightarrow 4f^n5d^1$ Configuration Crossover Does to the Chemistry of Divalent Rare-Earth Halides and Coordination Compounds. *Journal of Solid State Chemistry* **2019**, *270*, 324–334.

(27) Hitchcock, P. B.; Lappert, M. F.; Maron, L.; Protchenko, A. V. Lanthanum Does Form Stable Molecular Compounds in the +2 Oxidation State. *Angewandte Chemie International Edition* **2008**, *47* (8), 1488–1491.

(28) Macdonald, M. R.; Bates, J. E.; Ziller, J. W.; Furche, F.; Evans, W. J. Completing the Series of +2 Ions for the Lanthanide Elements: Synthesis of Molecular Complexes of Pr^{2+}, Gd^{2+}, Tb^{2+}, and Lu^{2+}. *Journal of the American Chemical Society* **2013**, *135* (26), 9857–9868.

(29) MacDonald, M. R.; Ziller, J. W.; Evans, W. J. Synthesis of a Crystalline Molecular Complex of Y2+, [(18-Crown-6)K][(C5H4SiMe3)3Y]. *Journal of the American Chemical Society* **2011**, *133* (40), 15914–15917.

(30) Queen, J. D.; Rajabi, A.; Ziller, J. W.; Furche, F.; Evans, W. J. Redox Studies of the Scandium Metallocene (C5H2tBu3)2ScII Lead to a Terminal Side-On (N═N)2- Complex: [(C5H2tBu3)2ScIII(H2-N2)]−. *Journal of the American Chemical Society* **2025**.

(31) Queen, J. D.; Anderson-Sanchez, L. M.; Stennett, C. R.; Rajabi, A.; Ziller, J. W.; Furche, F.; Evans, W. J. Synthesis of Crystallographically Characterizable Bis(Cyclopentadienyl) Sc(II) Complexes: (C5H2tBu3)2Sc and {[C5H3(SiMe3)2]2ScI}1-. *Journal of the American Chemical Society* **2024**, *146* (5), 3279–3292.

(32) Cloke, F. G. N. Zero Oxidation State Compounds of Scandium, Yttrium, and the Lanthanides. *Chemical Society Reviews* **1993**, *22* (1), 17–24.

(33) Brennan John G.; Cloke Geoffrey N.; Sameh, A. A.; Zalkin, A. Synthesis of Bis(n-1,3,5-Tri-t-Butylbenzene) Sandwich Complexes of Yttrium(0) and Gadolinium(0); the X-Ray Crystal

Structure of the First Authentic Lanthanide(0) Complex, [Gd(η-Bu$^t_3$C$_6$H$_3$)$_2$]. *Journal of the Chemical Society, Chemistry Communications* **1987**.

(34) Anderson, D. M.; Geoffrey, F.; Cloke, N.; Cox, P. A.; Edelstein, N.; Green, J. C.; Pang, T.; Sameh, A. A.; Shalimoffb, G. On the Stability and Bonding in Bis(n-Arene)Lanthanide Complexes. *Journal of the Chemical Society, Chemistry Communications* **1989**, *3*.

(35) Willauer, A. R.; Douair, I.; Chauvin, A. S.; Fadaei-Tirani, F.; Bünzli, J. C. G.; Maron, L.; Mazzanti, M. Structure, Reactivity and Luminescence Studies of Triphenylsiloxide Complexes of Tetravalent Lanthanides. *Chemical Science* **2022**, *13* (3), 681–691.

(36) Gompa, T. P.; Ramanathan, A.; Rice, N. T.; La Pierre, H. S. The Chemical and Physical Properties of Tetravalent Lanthanides: Pr, Nd, Tb, and Dy. *Dalton Transactions* **2020**, *49* (45), 15945–15987.

(37) Rice, N. T.; Popov, I. A.; Russo, D. R.; Gompa, T. P.; Ramanathan, A.; Bacsa, J.; Batista, E. R.; Yang, P.; La Pierre, H. S. Comparison of Tetravalent Cerium and Terbium Ions in a Conserved, Homoleptic Imidophosphorane Ligand Field. *Chemical Science* **2020**, *11* (24), 6149–6159.

(38) Ma, C. G.; Brik, M. G.; Liu, D. X.; Feng, B.; Tian, Y.; Suchocki, A. Energy Level Schemes of FN Electronic Configurations for the Di-, Tri-, and Tetravalent Lanthanides and Actinides in a Free State. *Journal of Luminescence* **2016**, *170*, 369–374.

(39) Willauer, A. R.; Palumbo, C. T.; Scopelliti, R.; Zivkovic, I.; Douair, I.; Maron, L.; Mazzanti, M. Stabilization of the Oxidation State +IV in Siloxide-Supported Terbium Compounds. *Angewandte Chemie - International Edition* **2020**, *59* (9), 3549–3553.

(40) Willauer, A. R.; Palumbo, C. T.; Fadaei-Tirani, F.; Zivkovic, I.; Douair, I.; Maron, L.; Mazzanti, M. Accessing the +IV Oxidation State in Molecular Complexes of Praseodymium. *Journal of the American Chemical Society* **2020**, *142* (12), 5538–5542.

(41) Tricoire, M.; Hsueh, F. C.; Keener, M.; Rajeshkumar, T.; Scopelliti, R.; Zivkovic, I.; Maron, L.; Mazzanti, M. Siloxide Tripodal Ligands as a Scaffold for Stabilizing Lanthanides in the +4 Oxidation State. *Chemical Science* **2024**, *15* (18), 6874–6883.

(42) Palumbo, C. T.; Zivkovic, I.; Scopelliti, R.; Mazzanti, M. Molecular Complex of Tb in the +4 Oxidation State. *Journal of the American Chemical Society* **2019**, *141* (25), 9827–9831.

(43) Boggiano, A. C.; Studvick, C. M.; Roy Chowdhury, S.; Niklas, J. E.; Tateyama, H.; Wu, H.; Leisen, J. E.; Kleemiss, F.; Vlaisavljevich, B.; Popov, I. A.; La Pierre, H. S. Praseodymium in the Formal +5 Oxidation State. *Nature Chemistry* **2025**.

(44) Pearson, R. G. Hard and Soft Acids and Bases. *Journal of the American Chemical Society* **1963**, *85* (22), 3533–3539.

(45) Gilbert-Bass, K.; Stennett, C. R.; Grotjahn, R.; Ziller, J. W.; Furche, F.; Evans, W. J. Exploring Sulfur Donor Atom Coordination Chemistry with La(II), Nd(II), and Tm(II) Using a Terphenylthiolate Ligand. *Chemical Communications* **2024**, *60* (34), 4601–4604.

(46) Moehring, S. A.; Evans, W. J. Evaluating Electron Transfer Reactivity of Rare-Earth Metal(II) Complexes Using EPR Spectroscopy. *Organometallics* **2020**, *39* (8), 1187–1194.

(47) Le Coz, E.; Hammoud, J.; Roisnel, T.; Cordier, M.; Dorcet, V.; Kahlal, S.; Carpentier, J. F.; Saillard, J. Y.; Sarazin, Y. Bonding in Barium Boryloxides, Siloxides, Phenoxides and Silazides: A Comparison with the Lighter Alkaline Earths. *Chemistry - A European Journal* **2021**, *27* (46), 11966–11982.

(48) Yan, H.; Wu, B.; Zhao, X. K.; Yu, C.; Wei, J.; Hu, H. S.; Zhang, W. X.; Xi, Z. Rare-Earth Metal Boroxide with Formal Triple Metal–Oxygen Orbital Interaction: Synthesis from B(C6F5)3·H2O and Radical-Anion Ligated Rare-Earth Metal Amides. *CCS Chemistry* **2021**, *3* (11), 2772–2781.

(49) Arnold, P. L.; Puig-Urrea, L.; Wells, J. A. L.; Yuan, D.; Cruickshank, F. L.; Young, R. D. Applications of Boroxide Ligands in Supporting Small Molecule Activation by U(III) and U(IV) Complexes. *Dalton Transactions* **2019**, *48* (15), 4894–4905.

(50) Cole, S. C.; Coles, M. P.; Hitchcock, P. B. Boroxide Complexes of the Group 4 Metals: A "Noninnocent" Ligand in Olefin Polymerization †. *Ogranometallics* **2005**, *24* (13), 3279–3289.

(51) Réant, B. L. L.; Berryman, V. E. J.; Basford, A. R.; Nodaraki, L. E.; Wooles, A. J.; Tuna, F.; Kaltsoyannis, N.; Mills, D. P.; Liddle, S. T. ^{29}Si NMR Spectroscopy as a Probe of S- And f-Block Metal(II)-Silanide Bond Covalency. *Journal of the American Chemical Society* **2021**, *143* (26), 9813–9824.

–Chapter 2–

Exploring Sulfur Donor Atom Coordination Chemistry with La(II), Nd(II), and Tm(II) using the Hexa-iso-propyl-terphenylthiolate Ligand

INTRODUCTION†

Investigations of the redox chemistry of the rare-earth metals have shown that molecular complexes of the $4f^n$ Ln(III) ions can be reduced not only to $4f^{n+1}$ Ln(II) complexes for Eu, Yb, Sm, Tm, Dy, and Nd, but also to $4f^n5d^1$ Ln(II) ions of all the other lanthanides (except radioactive Pm).[1–3] Complexes of $4d^1$ Y(II) can also be obtained.[4] Many variations in ligands have been found to stabilize the new $4f^n5d^1$ Ln(II) complexes since Lappert, et al. reported the first examples with La and Ce in 2008[1] and examples for the rest of the lanthanides were described in 2013,[2] eq 2.1. Nd(II) and Dy(II) are configurational crossover ions which can display $4f^{n+1}$ or $4f^n5d^1$ electron configurations depending on the specific ligand.[5]

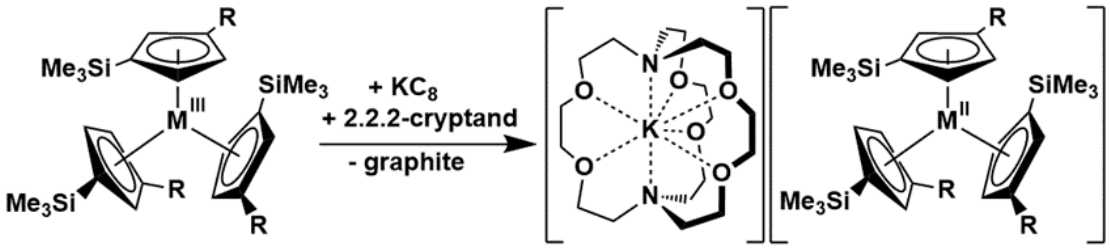

(2.1)

R = H, $SiMe_3$
M = Y, La, Ce, Pr, Nd, Sm, Gd, Tb, Dy, Ho, Er, Tm, Lu, Th, U, Pu

Although this new Ln(II) chemistry has been extended to a variety of other ligands,[6–12] they all involve C, N and O donor atoms from the first row of the main group. It was of interest to determine if the new Ln(II) ions could be stabilized with second row donor atoms.[13]

† Portions of this Chapter have been published: Gilbert-Bass, K., Stennett, c., Grotjahn, R., Ziller J., Furche F., Evans, W. J. Exploring sulfur donor atom coordination chemistry with La(II), Nd(II), and Tm(II) using a terphenylthiolate ligand *Chem. Commun., 2024,**60**, 4601*. DOI: 10.1039/d4cc01037j

Since the aryloxide ligand, $(OAr^*)^{1-}$ [Ar* = C_6H_2-2,6-(1-adamantyl)$_2$-4-^{t}Bu] provided some of the most thermally stable complexes of the $4f^n5d^1$ Ln(II) ions,[10] it was of interest to look at a sterically bulky congeneric thiolate.

The hexa-iso-propyl terphenylthiolate ligand, SAr^{iPr6} [Ar^{iPr6} = C_6H_3-2,6-(C_6H_2-2,4,6-^{i}Pr$_3$)$_2$], was attractive because Power, et al. had previously shown the efficacy of this ligand framework to stabilize two-coordinate M(II) thiolate complexes of Si, Ge, Sn, and Pb,[14] as well as Cr, Mn, Fe, Co, Ni, and Zn[15] and Mg.[16] Furthermore, with the $NHAr^{iPr6}$ analog, formally two-coordinate M(II) complexes were isolated for V,[17] Cr,[18] Mn,[19] Fe,[20] Co,[21] and Ni.[21]

The hexa-iso-propyl terphenylthiolate ligand also had been used in the rare-earth area. Niemeyer, et al. isolated Ln(SAr^{iPr6})$_2$ complexes for the traditional $4f^{n+1}$ Ln(II) ions, namely, Sm,[22] Eu,[23] and Yb,[24] as well as the THF and DME solvates, ($Ar^{iPr6}S$)$_2$Yb(THF)$_4$[25] and ($Ar^{iPr6}S$)$_2$Yb(DME)$_2$.[24] The OAr^{iPr6} analog was used to synthesize Sm(OAr^{iPr6})$_2$,[26] while the $NHAr^{iPr6}$ was used to generate U($NHAr^{iPr6}$)$_2$[27] and Y($NHAr^{iPr6}$)$_2$.[8] Described here is the expansion of the initially reported Ln(SAr^{iPr6})$_2$ series to La, Nd, and Tm. These metals were examined since La(II) has a distinctive EPR spectrum, Nd(II) is a configurational crossover ion,[5] and Tm was an unreported example of the $4f^{n+1}$ series.

RESULTS AND DISCUSSION

The Ln(SAr^{iPr6})$_2$I complexes of Ln = La and Nd were prepared by reaction of $KSAr^{iPr6}$ [28,29] with LnI_3, eq 2.2.

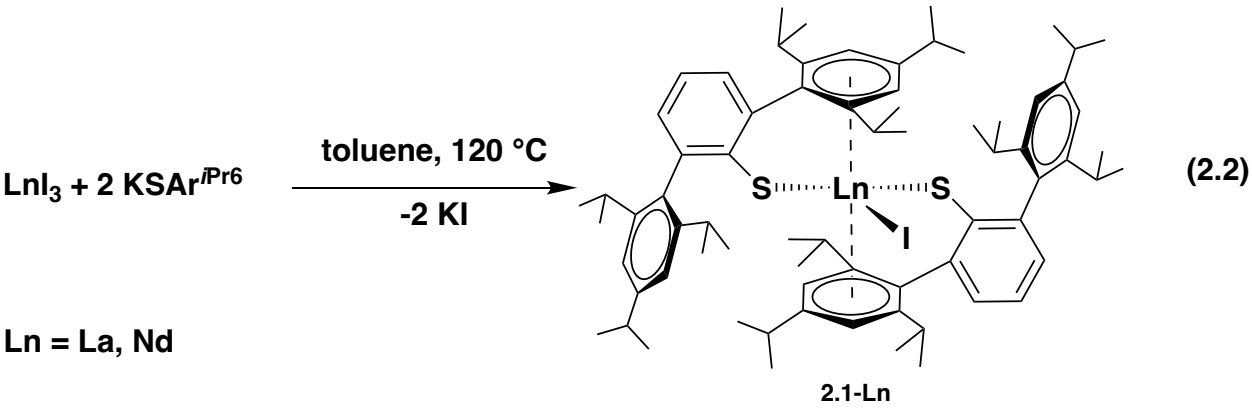

(2.2)

The **2.1-Ln** complexes (Figures 2.1 and 2.2) are structurally similar to and crystallize in the same space group as the previously reported $Eu(SAr^{iPr6})_2Cl$[30] complex, the $Ln(SAr^{iPr6})_2$ complexes of Ln = Sm,[22] and Eu,[30] and the $Ln(SeAr^{iPr6})_2Cl$ complexes of Ln = Nd[30] and Pr[30] with nearly identical unit cell constants. Evidently, the steric bulk of two SAr^{iPr6} ligands is sufficient to generate the overall molecular structure independent of the rare-earth metal and the presence or absence of a halide ligand.

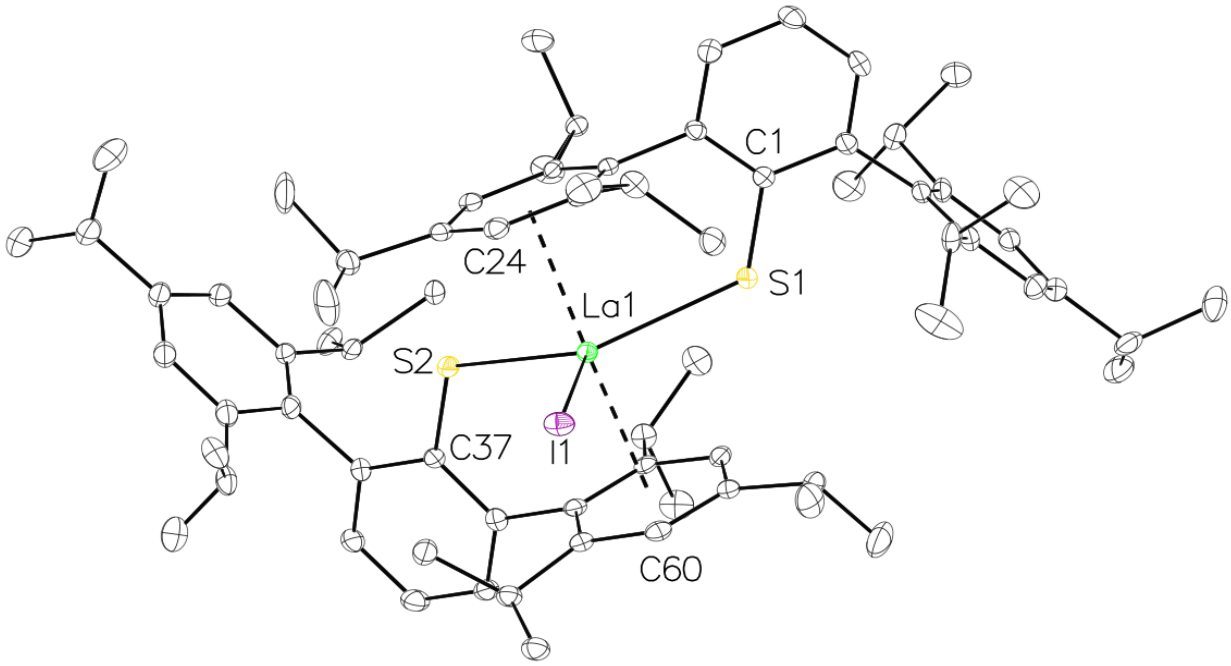

Figure 2.1. The molecular structure of La(SAr^{iPr6})$_2$I, **2.1-La**, with thermal ellipsoids drawn at 30% probability. For clarity, hydrogen atoms and disorder in the isopropyl groups are not shown.

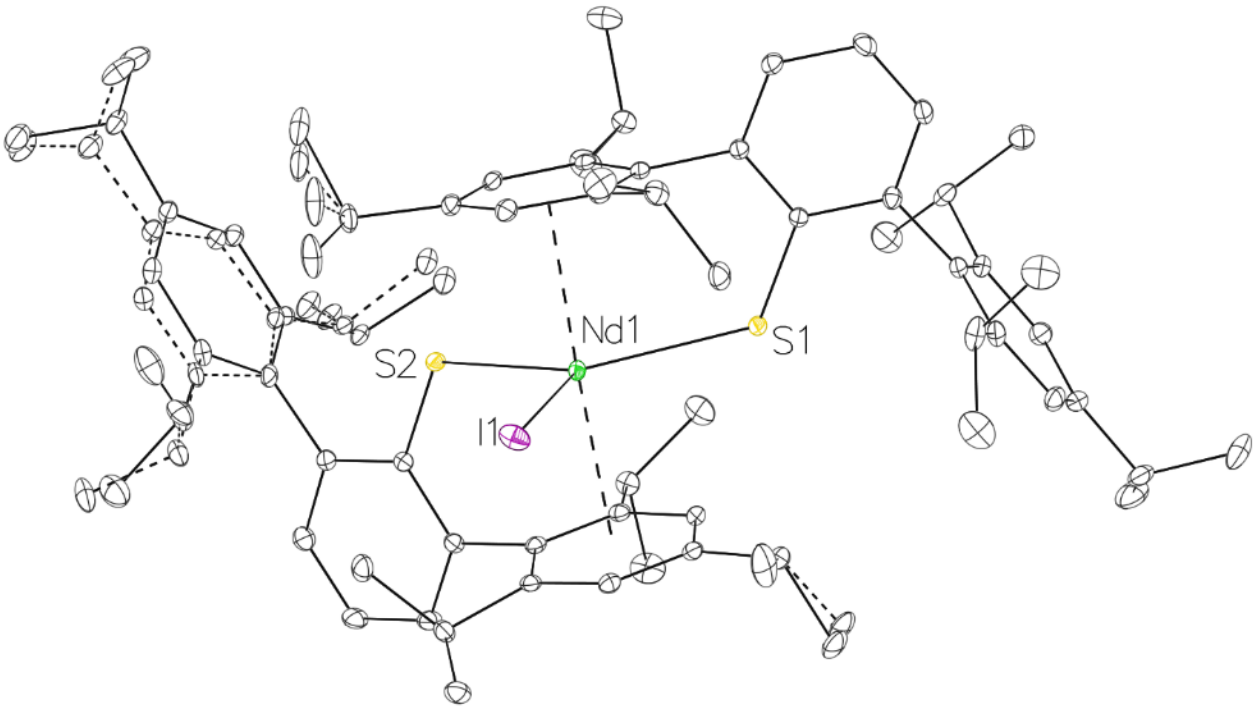

Figure 2.2. The molecular structure of Nd(SAr^{iPr6})$_2$I, **2.1-Nd**, showing modeled disorder. Thermal ellipsoids have been drawn at 30% probability. For clarity, hydrogen atoms are not shown.

In **2.1-La**, the two sulfur donor atoms and the iodide ligand have a trigonal geometry around La with a 125.32(3)° S-La-S angle and 116.42(3)° and 118.26(2)° I-La-S angles that sum to 360°. In **2.1-Nd**, the 127.389(3)° S-Nd-S angle is similar to that in **2.1-La**, but the I-Nd-S angles differ substantially at 111.914(2)° and 120.696(3)°. The Ln-I and Ln-S distances of **2.1-Nd** are 0.04-0.07 Å shorter than those of **2.1-La** which is consistent with the 0.053 Å[31] smaller Shannon radius of 9-coordinate Nd(III) versus La(III) (Table 2.1).

Table 2.1. Selected interatomic distances and angles in Ln(SAr^{iPr6})$_2$I complexes (2.1-Ln)		
	2.1-La	**2.1-Nd**

Ln-I	3.1213(4)	3.0542(6)
Ln-S	2.8235(12), 2.8173(10)	2.7490(5), 2.7734(4)
Ln-C_{arene}	3.096 – 3.187(5); avg: 3.142(1)	3.0619(5) – 3.1876(5); avg: 3.1293(2)
Ln-Cnt	2.8090(16), 2.8165(15)	2.7972(4), 2.7980(4)
S-Ln-S	125.32(3)	127.334(10)
S-Ln-I	116.42(2), 118.26(2)	120.689(11), 111.977(7)
Cnt-Ln-Cnt	173.22(5)	175.2358(9)
Cnt-Ln-I	93.52(4), 93.25(4)	92.741(12), 92.013(13)
Cnt-Ln-S	88.75(4), 87.71(4), 87.87(4), 89.45(4)	88.849(15), 88.957(14), 88.450(15), 89.561(14)

The flanking arene rings of each SAr^{iPr6} ligand in the **2.1-Ln** compounds are oriented toward the metal to form a sandwich-like structure for the **2.1-Ln** compounds. The La-Cnt distances of 2.809(2) and 2.817(2) Å and the Nd-Cnt distances of 2.799(1) and 2.793(1) Å (Cnt = flanking arene ring centroid) are more similar than the difference between their radii.

The corresponding Nd-Cnt distances in the similar selenolate complex $Nd(SeAr^{iPr6})_2Cl$ are 2.816 and 2.822 Å.[30] The Cnt1-Ln-Cnt2 angles are 173.22(5)° for **2.1-La** and 175.38(1)° for **2.1-Nd.**

Treatment of Et_2O solutions of **2.1-Ln** chilled to −35 °C with slurries of KC_8 in Et_2O at −35 °C generated intensely dark brown solutions for both La and Nd. Recrystallization of the products from hexane at −35 °C produced brown blocks of $Ln(SAr^{iPr6})_2$, **2.2-Ln**, in 80% (La) and 70% (Nd) yield, eq 2.3, which were identified by X-ray crystallography. The stability of the **2.2-Ln** complexes in hexane solution was monitored by UV-vis spectroscopy. The absorption of **2.2-La** at 409 nm decreases by only 25% over 24 h, Figure 2.3. For **2.2-Nd** at 274 nm, the decrease was 5% in 36 h, Figure 2.4.

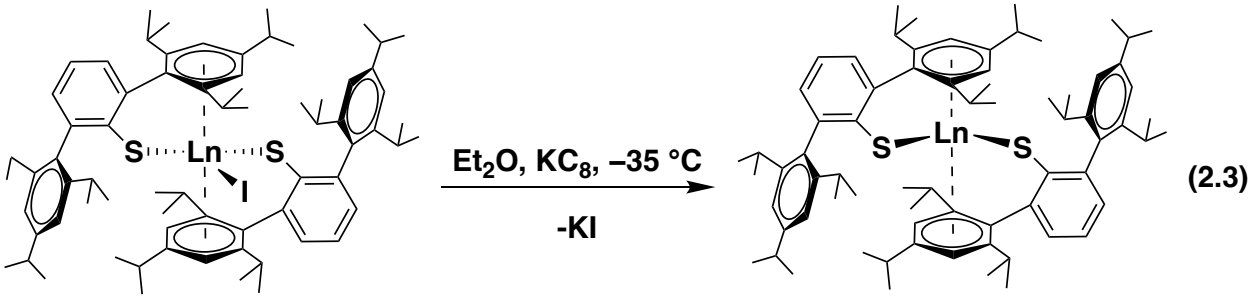

2.1-Ln

Ln = La, Nd

2.2-Ln

(2.3)

Figure 2.3. UV-vis spectrum of $La(SAr^{iPr6})_2$, **2.2-La**, (1.2 mM in hexane, 0.1 cm path length, ambient temperature). Spectra were recorded every 30 minutes for 24 h. The absorbance at 409 nm at t = 0 h is 0.49 and the absorbance at the same wavelength at t = 24 h is 0.36, which indicates that **2.2-La** has decomposed by ca. 26% during the period of this study.

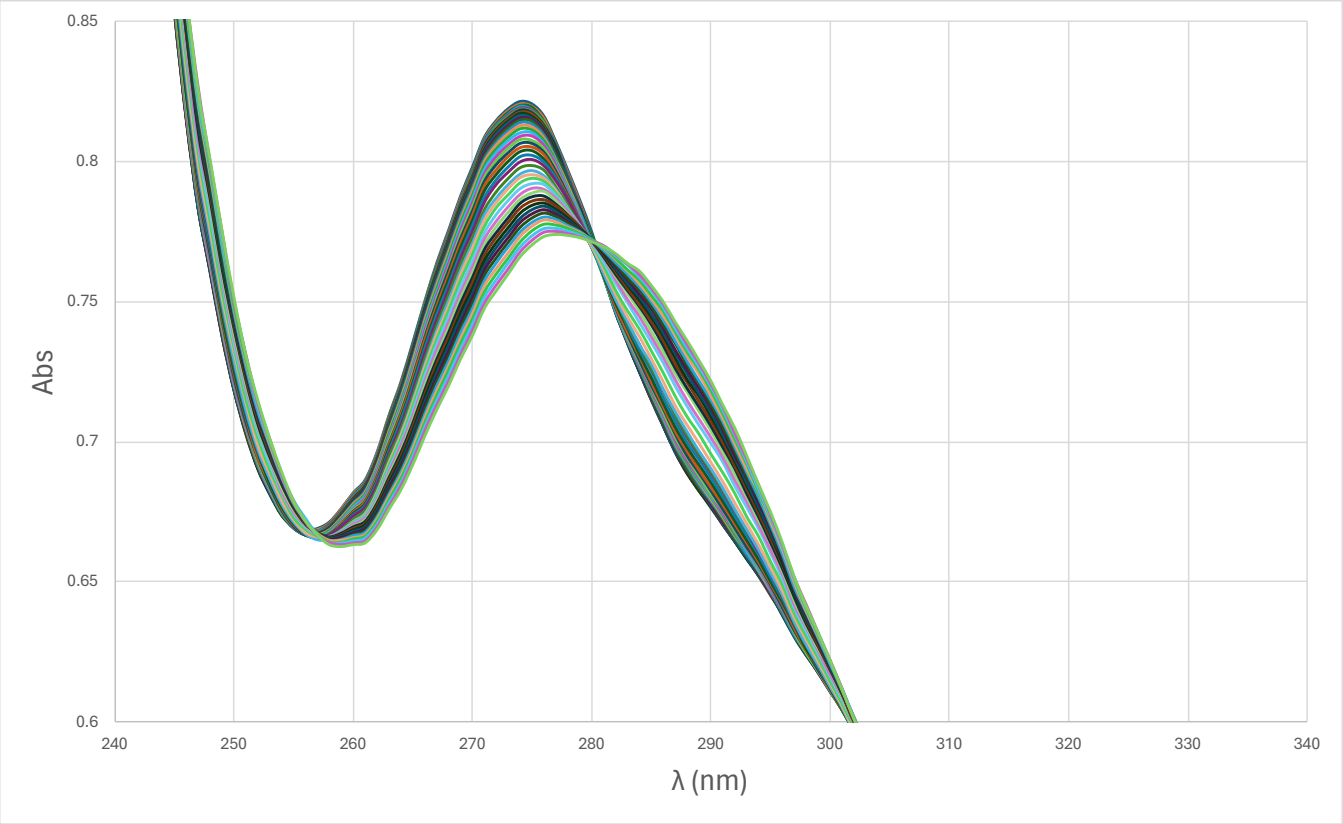

Figure 2.4. UV-vis spectrum of $Nd(SAr^{iPr6})_2$, **2.2-Nd**, (0.9 mM in hexane, 0.1 cm path length, ambient temperature). Spectra were recorded every h for 36 h. The absorbance at 274 nm at t = 0 h is 0.82 and the absorbance at the same wavelength at t = 36 h is 0.78, which indicates that **2.2-Nd** has decomposed by ca. 5% during the period of this study.

The **2.2-Ln** complexes crystallize in the same space group as the **2.1-Ln** complexes and for both La and Nd, there is residual unreacted **2.1-Ln** co-crystallized with **2.2-Ln**. The amount of **2.1-Ln** contained in the samples of **2.2-Ln** varied from 13% to 84%. Longer reaction times, using THF as an alternative solvent, and performing reactions in the presence of 2.2.2-cryptrand (crypt) and 18-crown-6 (18-c-6) did not solve the iodide contamination problem.

However, iodide-free **2.2-Nd** could be prepared in 70% yield through an alternate route by the reaction of NdI_2[32,33] with $KSAr^{iPr6}$ in Et_2O over two days at room temperature.

This synthesis was modeled on a reaction of $TmI_2(DME)_3$ and of $KSAr^{iPr6}$ in Et_2O which provided the previously unreported **2.2-Tm**, eq 2.4, Figure 2.5. The structure of **2.2-Tm** is similar to the previously reported **2.2-Sm**, **2.2-Eu**, and **2.2-Yb** and the Ln-S bond distances scale like the ionic radii (Table 2.2). In all of these complexes, both flanking rings of the SAr^{iPr6} ligand sandwich the metal. In **2.2-Tm**, the Ln-Cnt distances are 2.642(1) and 2.663(1) Å and the Cnt-Ln-Cnt angle is 164.09(3) °.

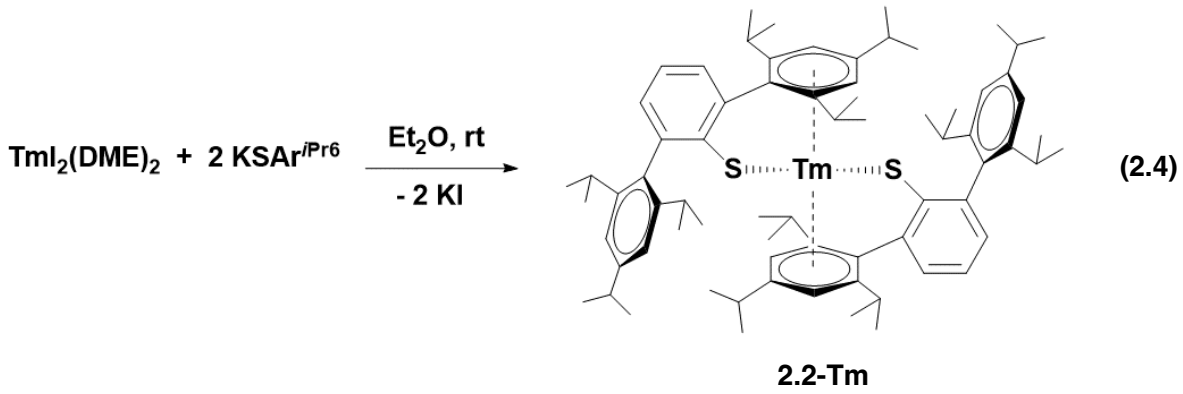

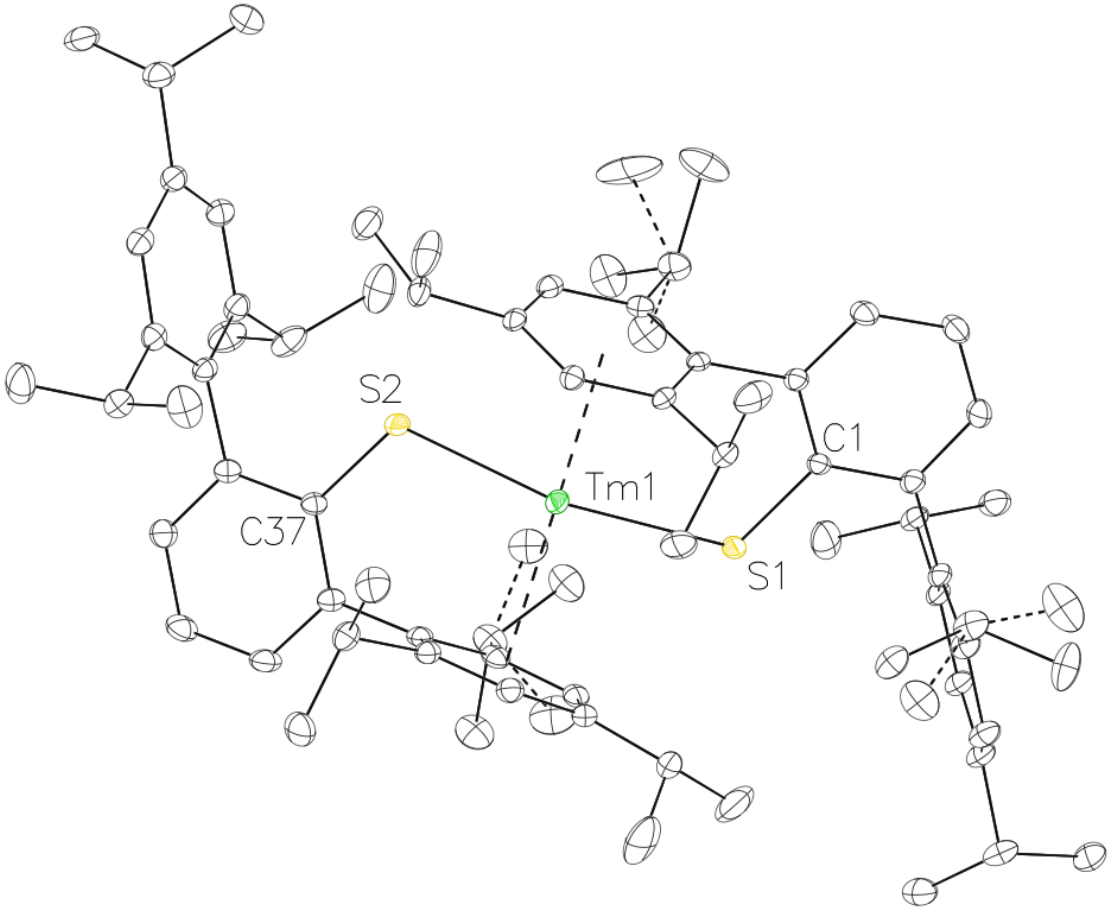

Figure 2.5. The molecular structure of $Tm(SAr^{iPr6})_2$, **2.2-Tm**, showing modelled disorder. Thermal ellipsoids have been drawn at 30% probability. For clarity, hydrogen atoms are not shown.

Table 2.2. Selected interatomic distances of $Ln(SAr^{iPr6})_2$ complexes (2.2-Ln)							
	2.2-La	**2.2-Nd**	**2.2-Sm**[7]	**2.2-Eu (173 K)**[23]	**2.2-Eu (100 K)**[23]	**2.2-Tm**	**2.2-Yb**[24]
Ln-S	2.805(3), 2.810(3)	2.7763(11), 2.741(1)	2.8187(16), 2.8141(13)	2.8164(10), 2.8177(12)	2.8104(9), 2.8031(11), 2.8303(9), 2.8174(10)	2.7182(6), 2.7203(5)	2.696(3), 2.685(2)
$Ln\text{-}C_{arene}$	Ring1: 2.819(12) – 2.957(10) avg: 2.892(4) Ring 2: 3.073(13) – 3.201(11) avg: 3.137(4)	Ring 1: 2.697(3) – 2.858(3) avg: 2.779(1) Ring 2: 3.048(3) – 3.201(3) avg: 3.135(1)	2.993(6) – 3.149(5); avg: 3.071(2)	2.968(3) – 3.161(3); avg: 3.065(1)	2.973(4) – 3.240(4); avg: 3.095(2)	2.884(2) – 3.117(2); avg: 2.999(1)	2.823(9) – 3.139(8); avg: 2.974(3)

Ln-Cnt	2.524(4) 2.808(5)	2.3950(13), 2.8044(13)	2.726(2), 2.741(2)	2.7344(14), 2.7218(15)	2.7834(15), 2.7394(16), 2.7583(15), 2.7616(15)	2.6631(9), 2.6423(9)	2.624(4), 2.650(4)
S-Ln-S	135.97(10)	140.36(3)	139.76(4)	141.89(3)	139.04(3), 143.84(3)	143.31(2)	142.73(4)
Ln-S-C_{aryl}	118.8(4) 113.4(3)	118.71(11), 112.22(10)	116.11(18), 116.20(15)	115.43(10), 115.85(9)	115.50(12), 115.51(12), 115.69(11), 115.32(12)	115.76(7), 115.33(7)	115.0(3), 115.7(3)
Cnt-Ln-Cnt	170.92(17)	164.68(5)	168.88(7)	166.92(4)	172.61(4), 170.55(4)	164.09(3)	164.50(12)
Cnt-Ln-S	89.33(9) 87.71(8) 95.37(9) 94.23(9)	97.27(4), 96.77(4), 90.18(4), 85.74(4)	91.60(6), 91.93(6), 91.26(5), 92.84(6)	91.52(4), 94.08(4), 92.12(4), 90.68(4)	92.01(4), 90.51(4), 91.04(4), 91.59(4),	93.90(2), 91.03(2), 90.68(2), 94.38(2)	93.63(10), 93.80(9), 94.71(10), 87.43(9)

					91.16(4), 95.81(9), 92.03(3), 91.67(4)		

The molecular structure of **2.2-Nd** is shown in Figure 2.7 and the structurally similar **2.2-La** (including the ca. 14% iodide impurity) is shown Figure 2.6. **2.2-La** and **2.2-Nd** differ from **2.1-Ln** and the other **2.2-Ln** structures (Ln = Sm, Eu, Tm, and Yb) in that one flanking ring of a terphenyl ligand is substantially closer to the Ln ion than the other. **2.2-La** has La-Cnt distances of 2.524(4) and 2.808(5) Å; for **2.2-Nd**, they are 2.395(1) and 2.804(1) Å.

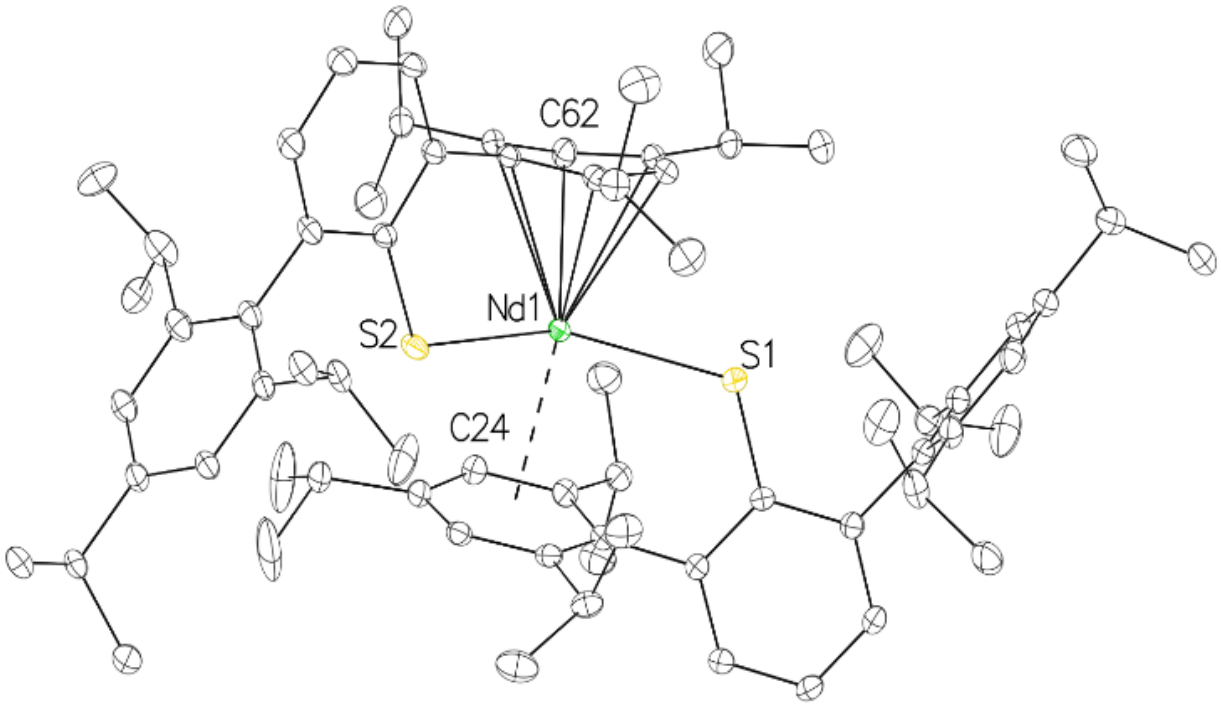

Figure 2.6. Top: The molecular structure of Nd(SAr^{iPr6})$_2$, **2.2-Nd**, with thermal ellipsoids drawn at 30% probability. For clarity, hydrogen atoms and the minor components of modelled disorder (isopropyl substituents, 20% site disorder of Nd atom) are not shown.

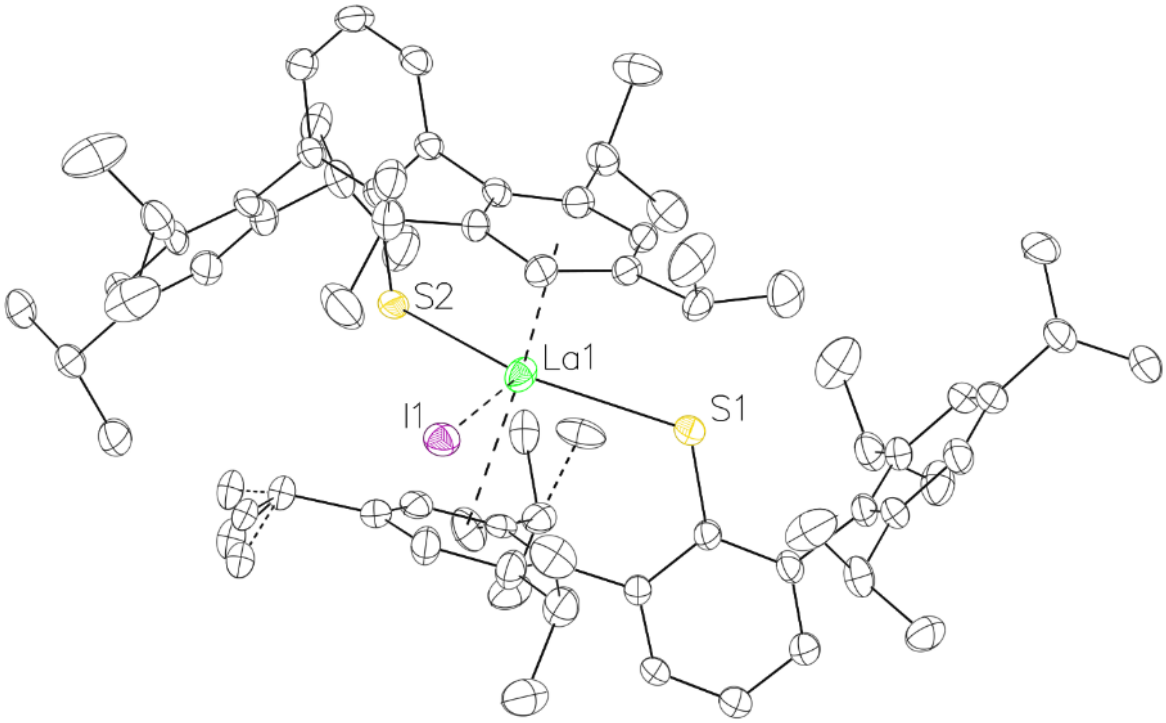

Figure 2.7. The molecular structure of La(SAr^{iPr6})$_2$, **2.2-La**, showing modelled disorder. Thermal ellipsoids have been drawn at 30% probability. For clarity, hydrogen atoms are not shown. The occupancy of the iodine atom in the crystal structure is 13%.

In both **2.2-La** and **2.2-Nd**, the ring that is closer to the Ln ion has a boat-like distortion from planarity. The C-C distances in the proximal ring of **2.2-Ln** do not differ as widely as those of fully reduced arene rings as detailed in Figure 2.8, although a range of distances has been observed in reduced arene complexes.[34–39]

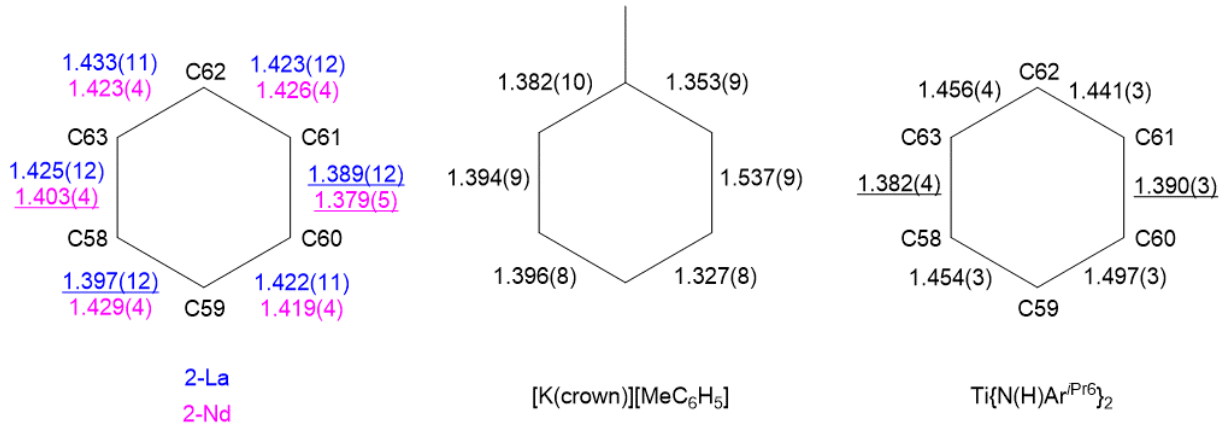

Figure 2.8. A comparison of interatomic C–C distances in the proximal flanking ring of **2.2-La** and **2.2-Nd** (left), the anion of [K(crown)][MeC_6H_5][34] (center), and the doubly reduced flanking ring of Ti[N(H)Ar^{iPr6}]$_2$.[35] The carbon atoms in the right diagram have been numbered to reflect their identical substitution to those of **2.2-Ln**. The two shortest C–C distances have been underlined in the left and right diagrams.

The dihedral angle between the C(59)C(60)C(61)C62) and C(59)C(58)C(63)C(62) planes of **2.2-Nd** is 10.9(3)° and the corresponding angle for **2.2-La** is 9.0(7)°. In Figure 2.8, the C-C distances in these rings are compared to those in [K(crown)][C_6H_5Me][34] which is viewed as a $(C_6H_5Me)^{1-}$ complex and the titanium terphenyl amide complex Ti[N(H)Ar^{iPr6}]$_2$,[35] which is considered a Ti(IV) complex wherein a flanking ring of one ligand is reduced by two electrons.[40] The C-C distances in the proximal ring of **2.2-Ln** do not differ as widely as those of the fully reduced arene rings although a range of distances has been observed in reduced arene complexes.[41–44]

The EPR spectra of THF solutions of **2.2-La** (Figure 2.9) and [La(SAr^{iPr6})$_2$I/KC$_8$/chelate reaction products (Table 2.3) at room temperature have eight-line patterns characteristic of La(II). The spectrum of **2.2-La** was fitted using EasySpin[45] which indicated g = 1.99 and A = 67.3 MHz (22.9 G).

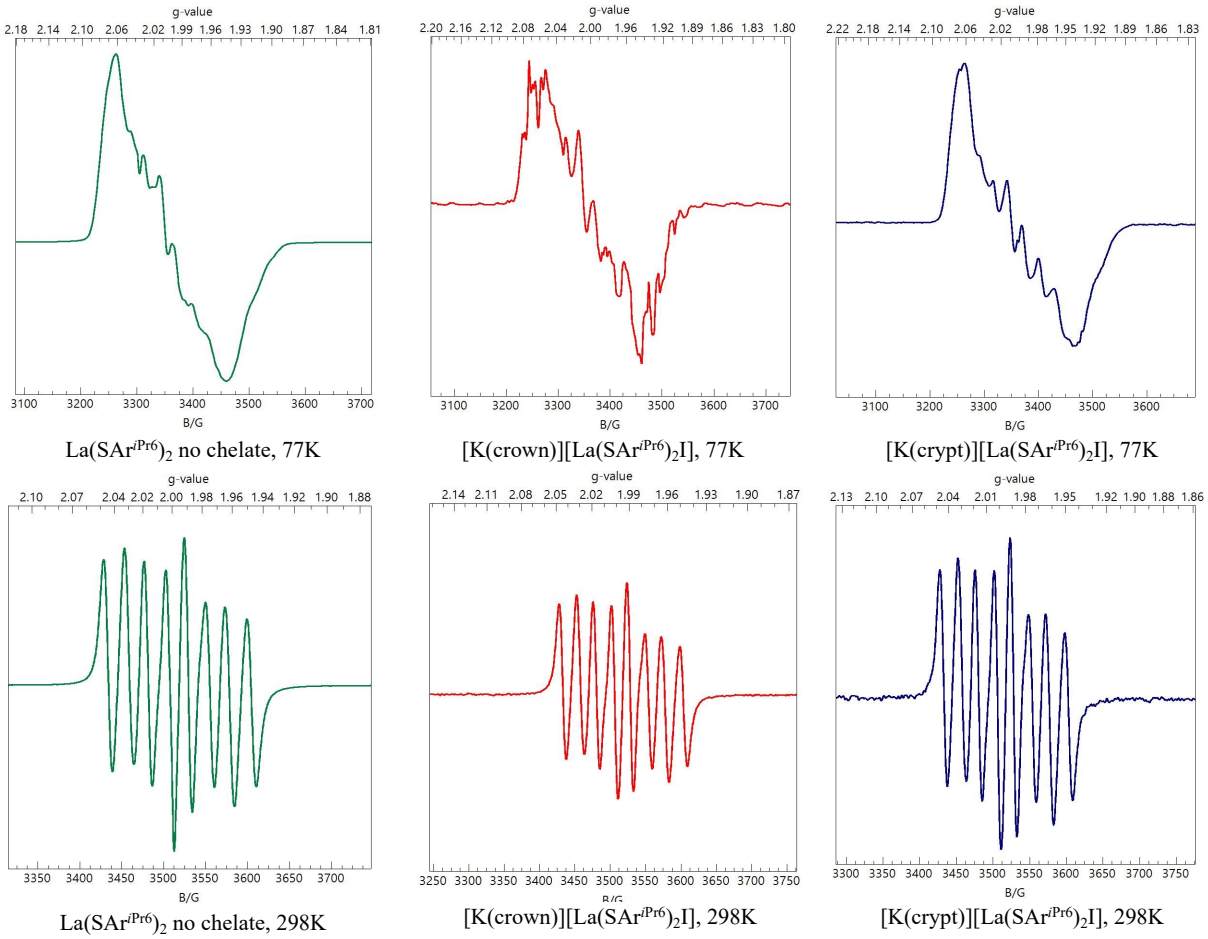

Figure 2.9. EPR spectra at 77K (top row) and 298 K (bottom row) of the products formed by reduction of **2.1-La** at −35 °C in THF with 1.1 equiv KC$_8$ with and without (**2.2-La**) chelates.

Table 2.3. EPR Spectral Data of 2.2-La and selected La(II) complexes.			
Complex			**g**

	Hyperfine Coupling (MHz)	**Hyperfine Coupling (Gauss)**	
$La(SAr^{iPr6})_2$, **2.2-La**	67.3	24.2	1.99
"[K(crypt)][$La(SAr^{iPr6})_2I$]"	67.3	24.2	1.99
"[K(18-c-6)][$La(S\ Ar^{iPr6})_2I$]"	66.9	24.0	1.99
$[La\{OC_6H_2\text{-}2,6\text{-}(1\text{-}Ad)_2\text{-}4\text{-}tBu\}_3]^{1-}$ [8]	1840.0	657.3	2.00
$[La\{C_5H_4(SiMe_3)\}_3]^{1-}$ [9]	430.4	154	1.994
$[La\{C_5H_3\text{-}1,3\text{-}(SiMe_3)_2\}_3]^{1-}$ [10]	371.8	133.5	1.99
$[La(C_5H\text{-}1,2,3,4\text{-}Me_4)_3]^{1-}$ [11]	802.4	291	1.97
$[La\{C_5H_4(tBu)\}_3]^{1-}$ [12]	550.1 565.1	$A_{\|\|}$ = 197 $A_\perp$ = 208	$g_{\|\|}$ 1.995 $g_\perp$ = 1.941
$[La\{C_5H_4(Me)\}_3]^{1-}$ [13]	537.9	195	1.971
$[La\{C_5H_4{}^tBu_2\}_3]^{1-}$ [14]	A_z = 630.7 A_{xy} = 648.8	A_z = 233 A_{xy} = 232	g_z = 1.934 g_{xy} = 1.998

The g value is similar to all previously reported La(II) complexes, but the A value is smaller: (g, A MHz) $\{La[C_5H_3(SiMe_3)_2]_3\}^{1-}$ (1.99, 372);[1] $[La(C_5H_4SiMe_3)_3]^{1-}$ (1.994, 430.4);[46] $[La(C_5H_4Me)_3]^{1-}$ (1.971, 537.9);[47] $[La(C_5H_4{}^tBu)_3]^{1-}$ (1.959, 559 MHz);[48] $\{La[C_5H_4(^tBu)_2]_3\}^{1-}$ (1.977, 642.8); $[La(C_5HMe_4)_3]^{1-}$ (1.97, 802);[49] $\{La[OC_6H_2\text{-}2,6\text{-}(1\text{-}Ad)_2\text{-}4\text{-}tBu]_3\}^{1-}$(2.00, 1840).[50] It should be noted that in [K(crypt)][$U(TDA)_2$] (TDA = N-

(2,6-di-isopropylphenyl)pivalamido), which contains a monoreduced arene in one of the TDA ligands, a nearly axial single-line EPR signal is observed with g = [2.042, 2.021, 2.013] which is assigned to the arene radical anion.[39] The EPR spectrum of a solid sample of **2.2-La** (Figure 2.10) displayed a single broad signal with g = 1.98 and no resolved hyperfine coupling similar to that of the La(II) complex [K(crown)][LaCp″$_3$] (Cp″ = η^5-1,3-(SiMe$_3$)$_2$-C$_5$H$_3$).[1]

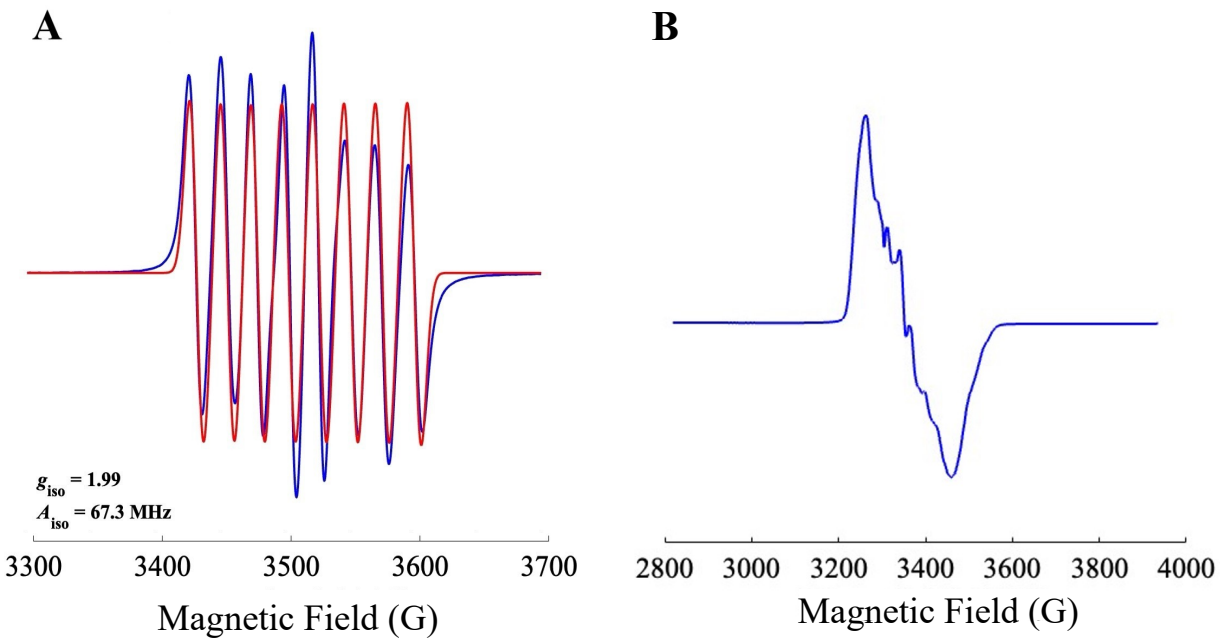

Figure 2.10. EPR spectra at 298 K (A) and 77 K (B) of **2.2-La** in blue with a simulated spectrum superimposed in red. The g and hyperfine coupling constants determined at 298 K are g_{iso} = 1.99 and A_{iso} =67.3 MHz (21.2 Gauss).

Density functional theory calculations were carried out by Dr. Robin Grotjahn in the group of Professor Filipp Furche to evaluate the electronic structure of the **2.2-Ln** complexes at the TPSSh-D3(BJ)/def2-TZVP level of theory. The calculations of simulated EPR data and Mulliken analysis led to the conclusion that for **2.2-La**, the electron in the highest occupied spin orbital (HOSO) consists of 34.4% 5*d*, 36.0% arene *p* orbitals, and

only 4.3% *s* character. For **2.2-Nd**, Mulliken population analysis shows distinct *f* character (90%+) for α HOSO-3, α HOSO-2, and α HOSO-1, but it is only 61.5% for α HOSO with most of the remaining character (23.3%) being described by the six carbon p-orbitals involved in the d-type interaction. Hence, this is not a $4f^3 5d^1$ Nd(II) ion and a $4f^4$ designation with significant electron transfer to the ring is a more appropriate description. More details can be found in the publication.†

The reductive chemistry of **2.2-Nd** was examined by treating it with azobenzene. The reaction forms $Nd^{III}(SAr^{iPr6})_2(PhNNPh)$, **2.3-Nd**, eq 2.5, Figure 2.11, which has structural and spectroscopic features characteristic of Ln(III) complexes containing $(PhNNPh)^{1-}$ anions (see publication† for ^1H NMR, IR, UV Vis, EPR and crystallographic data).[51–53] The reaction of **2.2-Sm** with azobenzene gives the analogous compound, **2.3-Sm** eq 2.5, Figure 2.12. The structure of **2.3-Nd** demonstrates the steric flexibility of the SAr^{iPr6} ligand which can obviously change the orientation of the flanking arene rings to accommodate a ligand as large as $(PhNNPh)^{1-}$.

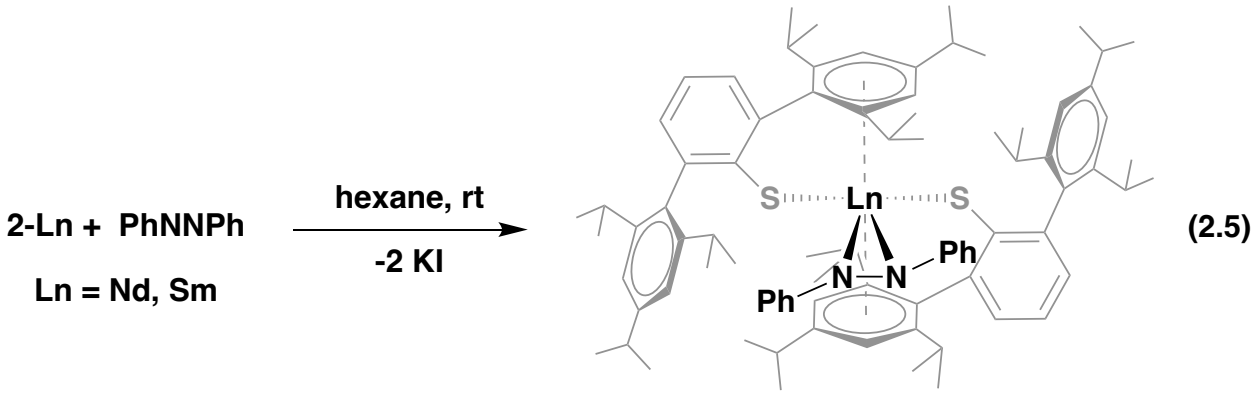

2.3-Ln

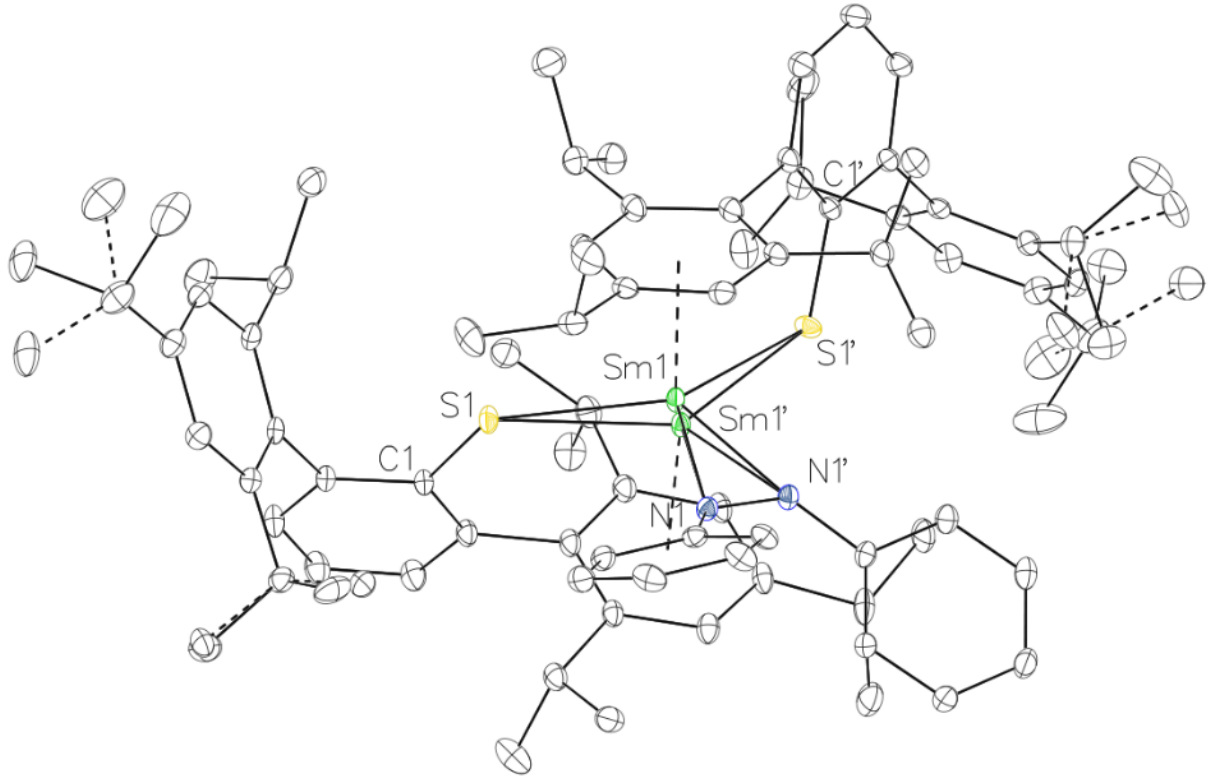

Figure 2.11. The molecular structure of $Nd(SAr^{iPr6})_2(N_2Ph_2)$, **2.3-Nd**, showing modelled disorder. Thermal ellipsoids have been drawn at 30% probability. For clarity, hydrogen atoms are not shown.

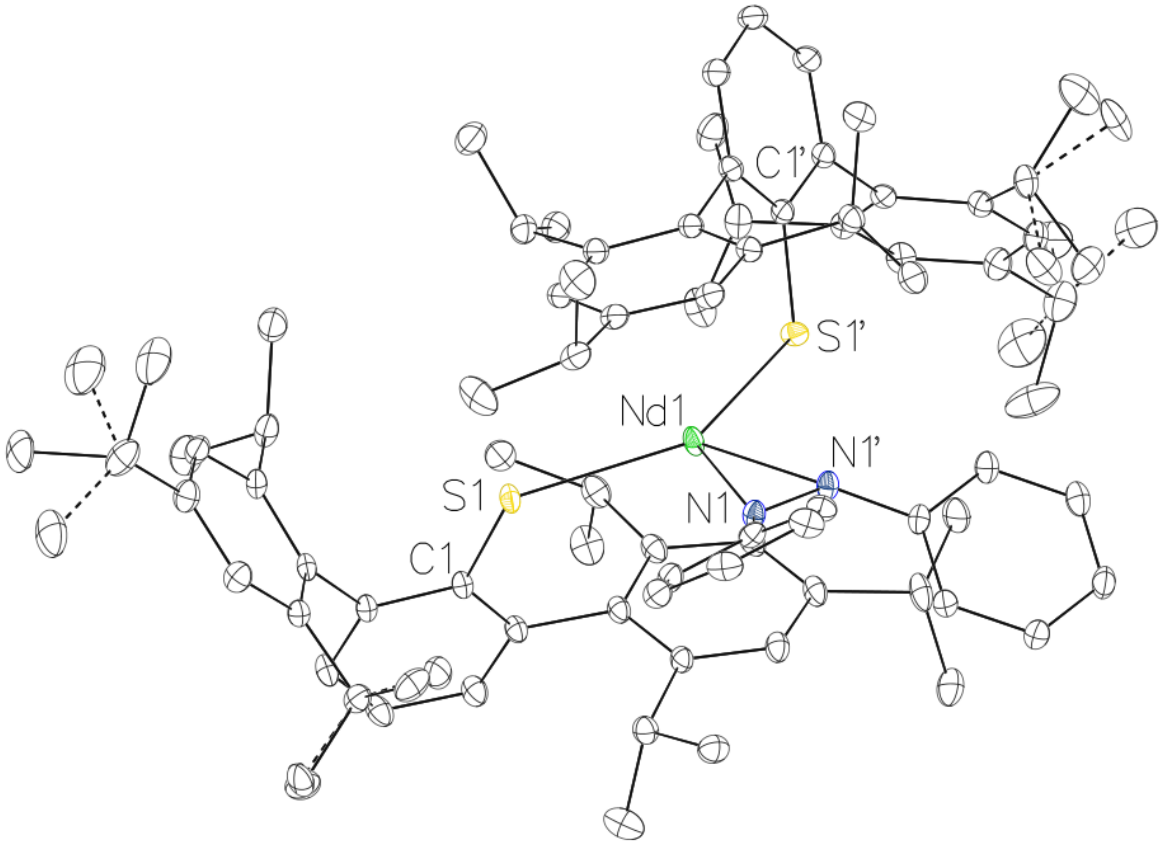

Figure 2.12. The molecular structure of $Sm(SAr^{iPr6})_2(N_2Ph_2)$, **2.3-Sm**, showing modelled disorder. Thermal ellipsoids have been drawn at 30% probability. For clarity, hydrogen atoms are not shown. Unlike the analogous complex **2.3-Nd**, the metal atom in **2.3-Sm** does not lie on the 2-fold crystallographic axis. Thus, the Sm atom resides on two sites of equal occupancy, with the Sm atom interacting with only one flanking ring of the ligand.

CONCLUSION

In summary, sulfur donor atom ligands can be used to isolate La(II) and Nd(II) ions, but with the SAr^{iPr6} ligand this involves partial reduction of a flanking arene ring. This apparently stabilizes the complexes compared to other La(II) and Nd(II) complexes and may make them better reagents for Ln(II) reductive chemistry. The reaction of **2.2-Nd** with azobenzene shows that it is a competent one electron reductant equivalent to the traditional

rare-earth reductant Sm(II).[54] In the case of **2.2-Nd**, the DFT analysis suggests a $4f^4$ electron configuration rather than $4f^35d^1$. This is consistent with complexes such as $[K(crypt)]_2\{[(KX_3Ce)(C_6H_5Me)]_2Ce\}$ [X =$OSi(O^tBu)_3$],[6] $[K(crypt)][(^{Ad,Me}ArO)_3U]$,[55] $(NHAr^{iPr6})_2U$,[27] and $[K(crypt)][U(TDA)_2]$[39] which contain arene rings near a metal ion in the +2 oxidation state and are assigned f^{n+1} electron configurations instead of f^nd^1 configurations.

EXPERIMENTAL DETAILS

General Considerations. All manipulations were performed by using modified Schlenk techniques or in a Vacuum/Atmospheres glovebox under argon. Solvents were degassed by sparging with dry argon before drying and collection using an S2 Grubbs-type[56] solvent purification system (JC Meyer). All physical measurements were recorded under strictly anaerobic and anhydrous conditions. Infrared spectra were recorded on compressed solid samples using an Agilent Cary 630 ATR/FTIR instrument. Electronic spectra were recorded as dilute solutions in the indicated solvent in quartz cuvettes (1 cm or 1 mm path length) using an Agilent Cary 60 UV/vis spectrophotometer. NMR spectra were recorded using a Bruker AVANCE 600 MHz spectrometer or a Bruker AVANCE 500 MHz spectrometer at 298 K unless otherwise stated and referenced to residual solvent signals. Assignment of the signals of NMR spectra have been provided where possible; but for the paramagnetic complexes, assignments were not possible due to broadening of the signals by the paramagnetism. Elemental analyses were conducted on a Thermo Scientific FlashSmart CHNS/O Elemental Analyzer at UC Irvine Materials Research Institute's TEMPR facility in Irvine, California. LaI_3 and NdI_3 were prepared using a modification of Meyer's procedure for the preparation of $LnCl_3$.[57] NdI_2 was prepared from neodymium metal and iodine as previously described.[32,33] $TmI_2(DME)_3$ was prepared from thulium metal and iodine

in dimethoxyethane as previously described[58] and the final content of DME in the bulk material was determined by combustion analysis. KSAr$^{i\text{Pr6}}$ was prepared by the reaction of HSAr$^{i\text{Pr6}}$ with potassium metal in toluene as previously described.[59]

Synthesis of La(SAr$^{i\text{Pr6}}$)$_2$I, 2.1-La. A suspension of LaI_3 (0.12 g, 0.23 mmol) in toluene (20 mL) was added to a Teflon-tapped, heavy-walled flask. To this, a clear, colorless solution of KSAr$^{i\text{Pr6}}$ (0.25 g, 0.452 mmol) in toluene (30 mL) was added. This was heated in an oil bath at 120-130 °C overnight, forming a white slurry. Solvent was removed under reduced pressure, and the white residue was extracted in ca. 20 mL of hexane. The mixture was centrifuged and the supernatant was filtered to give a clear, colorless solution. Hexane was removed from the filtrate under reduced pressure. The product was recrystallized by heating to near-boiling in ca. 2 mL hexane until dissolution and allowing the solution to return to room temperature before placing in a freezer at −35 °C. Colorless, X-ray quality crystalline blocks were collected after overnight storage of this solution (0.044 g, 15%). Anal. Calcd for $LaIS_2C_{72}H_{98}$: C, 66.86; H, 7.64. Found: C, 68.36; H, 8.00. ^{1}H NMR (600 MHz, C_6D_6): δ = 8.21 (s, 2H, aryl H)), 7.45 (s, 2H, aryl H)), 7.27 (d, 4H, aryl H), 7.14 (d, 2H, aryl H), 6.89 (t, 2H, aryl H), 6.79 (d, 2H, aryl H), 3.43 (m, 4H, *p*-C*H*(CH)$_3$), 2.98 (m, 4H, *o*-C*H*(CH)$_3$), 2.84 (m, 4H, *o*-C*H*(CH)$_3$), 1.48-0.85 (m, 72H, *o*,*p*-CH(C*H*$_3$)$_3$).

Synthesis of Nd(Ar$^{i\text{Pr6}}$S)$_2$I, 2.1-Nd. In a 100 mL Teflon-tapped, heavy-walled flask, NdI_3 (0.047 g, 0.090 mmol) and solid KSAr (0.10 g, 0.18 mmol) were combined in ca. 10 mL of toluene. The flask was sealed, and mixture was heated in an oil bath warmed to 120 °C and stirred for 18 h, after which the solution became pale green with concomitant formation of a colorless precipitate. The solvent was then removed under reduced pressure and the pale green residue was extracted in ca. 10 mL of hexane. The mixture was centrifuged, and the pale green supernatant was filtered.

The solvent was then removed from the filtrate under reduced pressure to afford **2.1-Nd** as a pale green solid (0.084 g, 0.065 mmol, 72%). Crystals suitable for study by X-ray diffractometry were grown by overnight storage of a concentrated solution of **2.1-Nd** in hexane at -35 °C. Anal. Calcd for $NdIS_2C_{72}H_{98}$: C, 66.58; H, 7.61. Found: C, 65.93; H, 7.44. ^{1}H NMR (600 MHz, benzene-D_6): broad signals characteristic of **2.1-Nd** were found at δ = 8.49 ($\Delta\nu_{1/2}$ = 14 Hz) and 1.95 ($\Delta\nu_{1/2}$ > 620 Hz) No additional signals were observed in the region between -150 and 150 ppm. UV-vis: λ_{max}/nm (ε/$M^{-1}cm^{-1}$): 290 (shoulder, 18000), 325 (shoulder, 11000).

Synthesis of La(SAr^{iPr6})$_2$, 2.2-La. A clear, colorless solution of freshly prepared **2.1-La** (0.039 g, 0.030 mmol) in ca. 2 mL Et_2O was chilled to −35 °C for 30 minutes in a 20 mL scintillation vial. Similarly, a slurry of freshly made KC_8 (0.0082 g, 0.061 mmol) in ca. 2 mL Et_2O was chilled to −35 °C for 30 minutes in a separate scintillation vial. The solution of **2.1-La** was then added quickly by pipette into the vial containing KC_8. This was stirred for 2 minutes at room temperature and then placed back in the freezer overnight. The intense dark brown solution was then filtered through a pipette packed with ca. 1 cm of filter paper and the solvent was removed from the filtrate under reduced pressure. The intensely dark brown solid was extracted in ca. 2 mL hexanes and filtered through a pipette packed with ca. 1 cm of filter paper once more and stored for 18 h at -35 °C to afford intensely colored dark brown crystal blocks suitable for X-ray diffraction (0.028 g, 80% yield). Anal. Calcd for $LaS_2C_{72}H_{98}$: C, 74.13; H, 8.47. Found: C, 75.16; H, 8.62. ^{1}H NMR (600 MHz, C_6D_6): The 1H NMR spectrum of **2.2-La** is essentially silent save for a broad signal of low intensity at δ = 8.47 which was apparent across several experiments along with resonances of diamagnetic KSAr^{iPr6} which may be formed in small amounts during the reduction of **2.1-La** with KC_8.

Reduction of 2.1-La in the presence of [2.2.2]cryptand. A clear, colorless solution of freshly prepared **2.1-La** (0.052 g, 0.03 mmol) in ca. 2 mL THF was chilled to −35 °C for 30 minutes in a 20 mL scintillation vial. Similarly, a slurry of freshly prepared KC_8 (0.006 g, 0.06 mmol) in ca. 2 mL solution of 2.2.2-cryptand (0.016 g, 0.04 mmol) in THF was chilled to −35 °C for 30 minutes in a separate scintillation vial. The colorless solution of **2.1-La** was then quickly transferred by pipette into the vial containing KC_8. This was stirred for 5 minutes at room temperature and filtered immediately. The resulting yellow/green solution was then filtered using a pipette filter and the solvent was removed under reduced pressure. The yellow/green solids were extracted with ca. 2 mL toluene and the extract was filtered through a glass pipette packed with ca. 1 cm of filter paper. The solvent was then removed under reduced pressure to afford 0.028 g of yellow/green powder. The EPR spectrum of a solution of this material dissolved in THF showed a characteristic 8-line pattern with g = 2.00 (A = 67.7 MHz) at 298 K. ^{1}H NMR (600 MHz, benzene-D_6, 298K): no resonances indicative of a new paramagnetic complex were observed in the ^{1}H NMR spectrum (Figure 2.13).

Reduction of 2.1-La in the presence of 18-crown-6. A clear, colorless solution of freshly prepared **2.1-La** (52 mg, 0.030 mmol) in ca. 2 mL of THF was chilled to −35 °C for 30 minutes in a 20 mL scintillation vial. Similarly, a slurry of freshly made KC_8 (0.006 g, 0.06 mmol) in ca. 2 mL solution of 18-crown-6 (0.013 g, 0.05 mmol) in THF was chilled to −35 °C for 30 minutes in a separate scintillation vial. The black solution of **2.1-La** was then quickly transferred by pipette into the vial containing KC_8. This was stirred for 5 minutes at room temperature and then the mixture was filtered twice through a pipette packed with ca. 1 cm of filter paper to afford a dark brown/red solution. The solvent was then removed from the filtrate under reduced pressure. The dark brown solids were extracted with ca. 2mL of toluene and the extract was filtered through a

glass pipette packed with ca. 1 cm of filter paper. The solvent was then removed from the filtrate under reduced pressure to afford 0.028 g of yellow/green powder. The EPR spectrum of a solution of this material dissolved in THF showed a characteristic 8-line pattern with g = 1.99 (A = 67.6 MHz) at 298 K. ^{1}H NMR (600 MHz, benzene-D_6, 298K): no resonances indicative of a new paramagnetic complex were observed in the ^{1}H NMR spectrum (Figure 2.14).

Synthesis of Nd(SAr^{iPr6})$_2$, 2.2-Nd, by reduction of 2.1-Nd. Dark brown **2.1-Nd** (0.050 g, 0.043 mmol) was dissolved in ca. 5 mL of diethyl ether in a 20 mL vial. KC_8 (0.077 g, 0.090 mmol) was then added in one portion and the mixture was stirred for 4 h. The solvent was then removed under reduced pressure and the residue was extracted in ca. 4 mL of hexane. The mixture was then centrifuged and the supernatant was filtered. The solvent was then removed from the filtrate under reduced pressure until small, dark brown crystals began to form on the wall of the vial. The vial was then sealed and gently warmed by hand until the crystalline material had dissolved and the vial was allowed to stand at ambient temperature. After ca. 18 h., a small amount of dark brown/orange crystals had grown from this solution which were suitable for study by X-ray diffraction experiments. The structural data showed a significant impurity of **2.1-Nd**, which has the same unit cell as **2.2-Nd**. Thus, a route to **2.2-Nd** through NdI_2 was pursued (vide infra). The formation of **2.2-Nd** was confirmed by ^{1}H NMR and IR spectroscopy (Figures 2.15 and 2.16 respectively). No signals for **2.1-Nd** were apparent in the NMR spectrum, although several additional paramagnetically shifted and broadened signals were present which has not been identified.

Synthesis of Nd(SAr^{iPr6})$_2$, 2.2-Nd, from NdI$_2$. NdI_2 (0.36 g, 0.90 mmol) and KSAr^{iPr6} (0.50 g, 0.90 mmol) were combined in a 20 mL vial. Diethyl ether (15 mL) was then added. The vial was canted by ca. 15 degrees to assure effective stirring of the insoluble NdI_2 and the mixture

was stirred at room temperature. After stirring for 18 h, the mixture had become dark brown in color. The diethyl ether was removed from the mixture under reduced pressure and the residue was then extracted with ca. 5 mL of hexane. The mixture was then centrifuged and the supernatant was filtered through a pipette packed with ca. 1 cm of filter paper. The solvent was then completely removed from the filtrate under reduced pressure to afford 0.40 g (0.34 mmol, 76%) of **2.2-Nd** as dark brown, nearly black powder. Dark red/orange crystals which were suitable for study by X-ray diffraction experiments were grown from a concentrated hexane solution of **2.2-Nd** stored at ambient temperature for 24 h. Anal. Calcd. for $NdS_2C_{72}H_{98}$: C, 73.79; H, 8.43. Found: C, 73.39; H, 7.33. ^{1}H NMR (600 MHz, C_6D_6): δ = 8.28 (d, br), 7.63 (d, br), 7.56 (t, br), 7.37 (s, $\Delta\nu_{1/2}$ = 14 Hz), 3.35 (s, $\Delta\nu_{1/2}$ = 99 Hz), 2.98 (mult.), 2.89 (mult.), 1.33-1.19 (mult.), 0.63 (s, $\Delta\nu_{1/2}$ = 36 Hz), -3.80 ($\Delta\nu_{1/2}$ = 112 Hz), -5.12 (s, $\Delta\nu_{1/2}$ = 45 Hz). UV-vis: λ_{max}/nm (ε/$M^{-1}cm^{-1}$): 272 (25000), 300 (shoulder, 15000).

Synthesis of Sm(SAr$^{i\text{Pr6}}$)$_2$, 2.2-Sm. The preparation of **2.2-Sm** by the reaction between KSAr$^{i\text{Pr6}}$ and excess SmI_2 has been previously described by Cofone and Niemeyer.[22] However, it has been have found that **2.2-Sm** may also be reliably obtained through the following route: $SmI_2(THF)_2$ (0.25 g, 0.45 mmol) and ca. 15 mL of diethyl ether were combined in a 20 mL vial. KSAr$^{i\text{Pr6}}$ (0.25 g, 0.45 mmol) was added to this mixture while stirring. The mixture was then stirred for 18 h. The solvent was removed under reduced pressure to afford a violet solid. The residue was extracted in ca. 10 mL of hexane and the mixture was centrifuged. The supernatant was then filtered through a pipette packed with ca. 1 cm of filter paper. The solvent was then removed from the filtrate under reduced pressure to afford 0.18 g (0.15 mmol, 68%) of **2.2-Sm** as a dark violet, microcrystalline solid. ^{1}H NMR (600 MHz, C_6D_6): δ = 29.54 ($\Delta\nu_{1/2}$ = 442 Hz), 25.42 ($\Delta\nu_{1/2}$ = 299 Hz), 7.25 ($\Delta\nu_{1/2}$ = 7 Hz), 7.21 ($\Delta\nu_{1/2}$ = 8 Hz), 4.92 ($\Delta\nu_{1/2}$ = 22 Hz), 3.76 ($\Delta\nu_{1/2}$ = 23

Hz), 3.61 ($\Delta\nu_{1/2}$ = 29 Hz), 0.12 ($\Delta\nu_{1/2}$ = 19 Hz), -0.20 ($\Delta\nu_{1/2}$ = 159 Hz), -0.67 ($\Delta\nu_{1/2}$ = 49 Hz), -0.76 ($\Delta\nu_{1/2}$ = 31 Hz), -1.19 ($\Delta\nu_{1/2}$ = 38 Hz), -3.43 ($\Delta\nu_{1/2}$ = 102 Hz), -7.31 ($\Delta\nu_{1/2}$ = 107 Hz). UV-vis: λ_{max}/nm (ε/$M^{-1}cm^{-1}$): 274 (25000), 300 (shoulder, 15000) 350 (shoulder, 6000).

Synthesis of Tm(SAr^{iPr6})$_2$, 2.2-Tm. In a 20 mL vial, solid KSAr^{iPr6} (0.15 g, 0.27 mmol) was added in one portion to a stirred mixture of $TmI_2(DME)_2$ (0.082 g, 0.14 mmol) in ca. 4 mL of diethyl ether. The mixture was stirred for 18 h, after which a colorless precipitate had formed and the dark green $TmI_2(DME)_2$ had been consumed. The solvent was then removed under reduced pressure to afford a dark green, solid residue. The residue was extracted in ca. 4 mL of hexane. The mixture was centrifuged, and the dark green supernatant was filtered. The solvent was then removed from the filtrate under reduced pressure to afford a dark green oil. The oil was dissolved in ca. 1 mL hexane and the solvent was again removed under reduced pressure. Another ca. 1 mL portion of hexane was added and the above process was repeated three times to afford 0.13 g (0.0.11 mmol, 78%) of **2.2-Tm** as a dark green, microcrystalline solid. Crystals suitable for study by X-ray diffractometry were grown by overnight storage at ambient temperature of a concentrated solution of **2.2-Tm** in hexane. Anal. Calcd. for $TmS_2C_{72}H_{98}$: C, 72.27; H, 8.26. Found: C, 72.29; H, 8.51. ^{1}H NMR (600 MHz, C_6D_6): δ = 12.99 ($\Delta\nu_{1/2}$ = 673 Hz), -2.24 ($\Delta\nu_{1/2}$ = 176 Hz), -2.74 ($\Delta\nu_{1/2}$ = 133 Hz), -3.73 ($\Delta\nu_{1/2}$ = 27 Hz), -6.80 ($\Delta\nu_{1/2}$ = 407 Hz), -8.14 ($\Delta\nu_{1/2}$ = 434 Hz), -10.80 ($\Delta\nu_{1/2}$ = 133 Hz), -53.56 ($\Delta\nu_{1/2}$ = 230 Hz). UV-vis: λ_{max}/nm (ε/$M^{-1}cm^{-1}$): 274 (24000), 300 (shoulder, 14000), 345 (5600).

Synthesis of Nd(SAr^{iPr6})$_2$(N_2Ph_2), 2.3-Nd. In a 20 mL vial, azobenzene (0.006 g, 0.034 mmol) was added in one portion to a stirred, dark brown solution of Nd(SAr^{iPr6})$_2$ (**2.2-Nd**, 0.040 g, 0.034 mmol) in ca. 2 mL of hexane at room temperature. The solution immediately became dark green and was stirred for 20 min. The solvent was then removed under reduced pressure to

afford a dark green solid. A minimal amount of hexane (ca. 0.5 mL) was added dropwise to the dark green residue until it was dissolved, and the vial was then sealed and laid on its side. Dark red, almost black crystals of $Nd(SAr^{iPr6})_2(N_2Ph_2)$, **2.3-Nd**, which were suitable for study by X-ray diffraction had grown on the walls of the vial after ca. 1 h (0.010 g, 0.0074 mmol, 34%). Anal. Calcd for $NdS_2C_{84}H_{108}N_2$: C, 74.51; H, 8.04; N, 2.07. Found: C, 75.03; H, 8.34; N, 2.48. ^{1}H NMR (500 MHz, C_6D_6): δ = 13.25 ($\Delta\nu_{1/2}$ = 153 Hz), 8.55 ($\Delta\nu_{1/2}$ = 12 Hz), 8.48 ($\Delta\nu_{1/2}$ = 18 Hz), 8.02 (d, br), 5.71 ($\Delta\nu_{1/2}$ = 51 Hz), 5.45 ($\Delta\nu_{1/2}$ = 30 Hz), 4.96 ($\Delta\nu_{1/2}$ = 85 Hz), 3.93 ($\Delta\nu_{1/2}$ = 21 Hz), 2.55 ($\Delta\nu_{1/2}$ = 61 Hz), 2.30 ($\Delta\nu_{1/2}$ = 21 Hz), 2.21 (d, br), 1.86 ($\Delta\nu_{1/2}$ = 30 Hz), 1.77 ($\Delta\nu_{1/2}$ = 53 Hz), 1.65 ($\Delta\nu_{1/2}$ = 34 Hz), 0.40 ($\Delta\nu_{1/2}$ = 114 Hz), -2.56 ($\Delta\nu_{1/2}$ = 24 Hz), -3.29 ($\Delta\nu_{1/2}$ = 27.2 Hz).

Synthesis of $Sm(SAr^{iPr6})_2(N_2Ph_2)$, 2.3-Sm. In a 20 mL vial, azobenzene (0.008 g, 0.034 mmol) was added in one portion to a stirred, violet solution of $Sm(SAr^{iPr6})_2$ (**2.2-Sm**, 0.025 g, 0.021 mmol) in ca. 2 mL of hexane at room temperature. The solution immediately became dark green and was stirred for 20 min. The solvent was then removed under reduced pressure. A minimal amount of hexane (ca. 0.5 mL) was added dropwise to the dark green residue until it was dissolved, and the vial was then sealed and laid on its side. Dark red, almost black crystals of $Sm(SAr^{iPr6})_2(N_2Ph_2)$, **2.3-Sm**, which were suitable for study by X-ray diffraction had grown on the walls of the vial after ca. 1 h (0.011 g, 0.008 mmol, 37 %). Anal. Calcd for $SmS_2C_{84}H_{108}N_2$: C, 74.17; H, 8.00; N, 2.06. Found: C, 74.40; H, 8.23; N, 2.35. ^{1}H NMR (600 MHz, C_6D_6): δ = 70.40 ($\Delta\nu_{1/2}$ = 412 Hz), 25.30 ($\Delta\nu_{1/2}$ = 347 Hz), 8.02 ($\Delta\nu_{1/2}$ = 89 Hz), 5.90 ($\Delta\nu_{1/2}$ = 172 Hz), 4.52 ($\Delta\nu_{1/2}$ = 175 Hz), 4.15 ($\Delta\nu_{1/2}$ = 128 Hz), 3.81 ($\Delta\nu_{1/2}$ = 155 Hz), 3.23 ($\Delta\nu_{1/2}$ = 133 Hz), 2.89 ($\Delta\nu_{1/2}$ = 142 Hz), 1.83 ($\Delta\nu_{1/2}$ = 128 Hz), 1.39-0.93 (mult.), 0.11 ($\Delta\nu_{1/2}$ = 170 Hz), -0.77 ($\Delta\nu_{1/2}$ = 202 Hz), -1.77 ($\Delta\nu_{1/2}$ = 200 Hz), -148.17 ($\Delta\nu_{1/2}$ = 573 Hz), -159.83 ($\Delta\nu_{1/2}$ =

344.2 Hz). UV-vis: λ_{max}/nm (ε/$M^{-1}cm^{-1}$): 277 (17000), 293 (shoulder, 15000), 315 (shoulder, 13000), 329 (shoulder, 10000), 345 (shoulder, 6000).

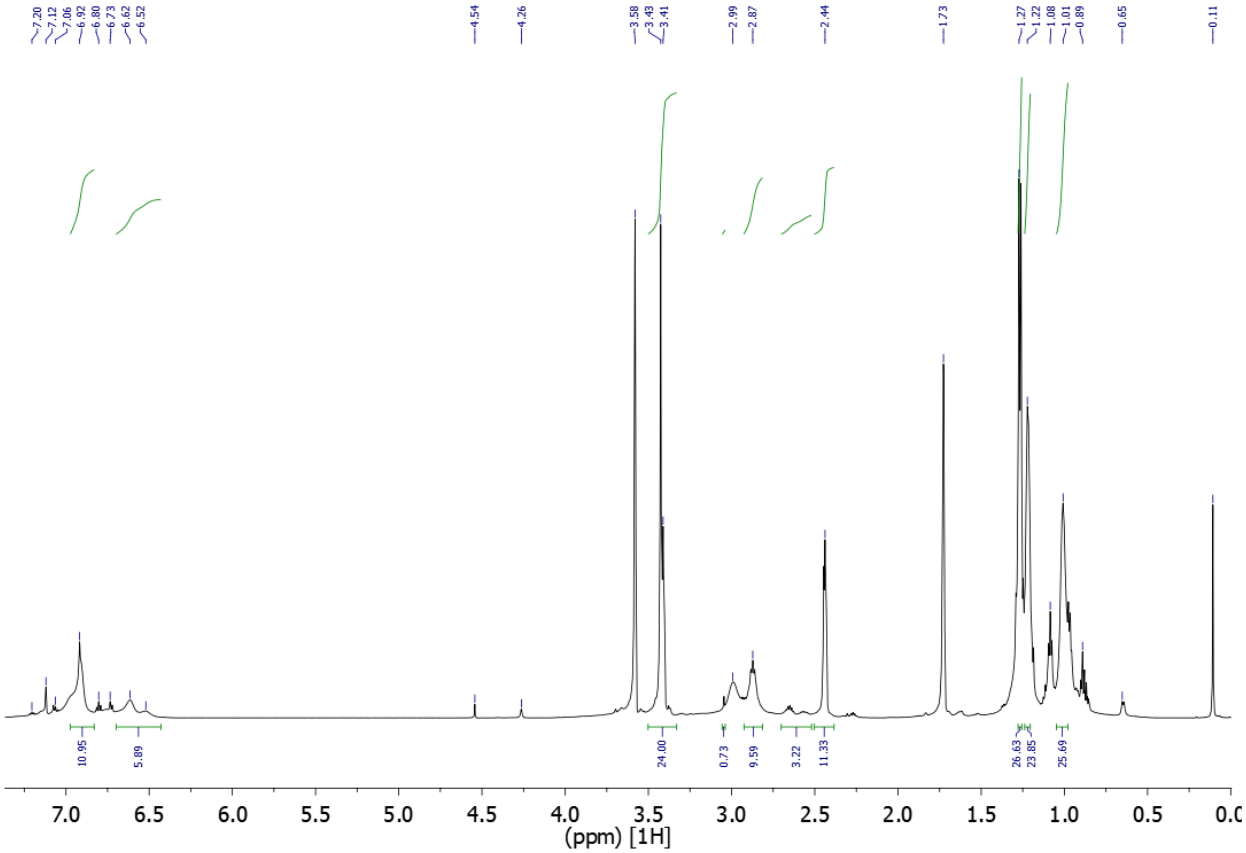

Figure 2.13. ^{1}H NMR (600 MHz, 298K) of **2.1-La** treated with 2.2.2-cryptand and KC_8. Note: resonance of of $HSAr^{ipr6}$ impurity, hexane impurity at 0.89, unknown impurities at 4.54, 4.26 and 0.65, silicon grease at 0.11, and residual THF-D_8 solvent at 3.58 and 1.73 ppm.

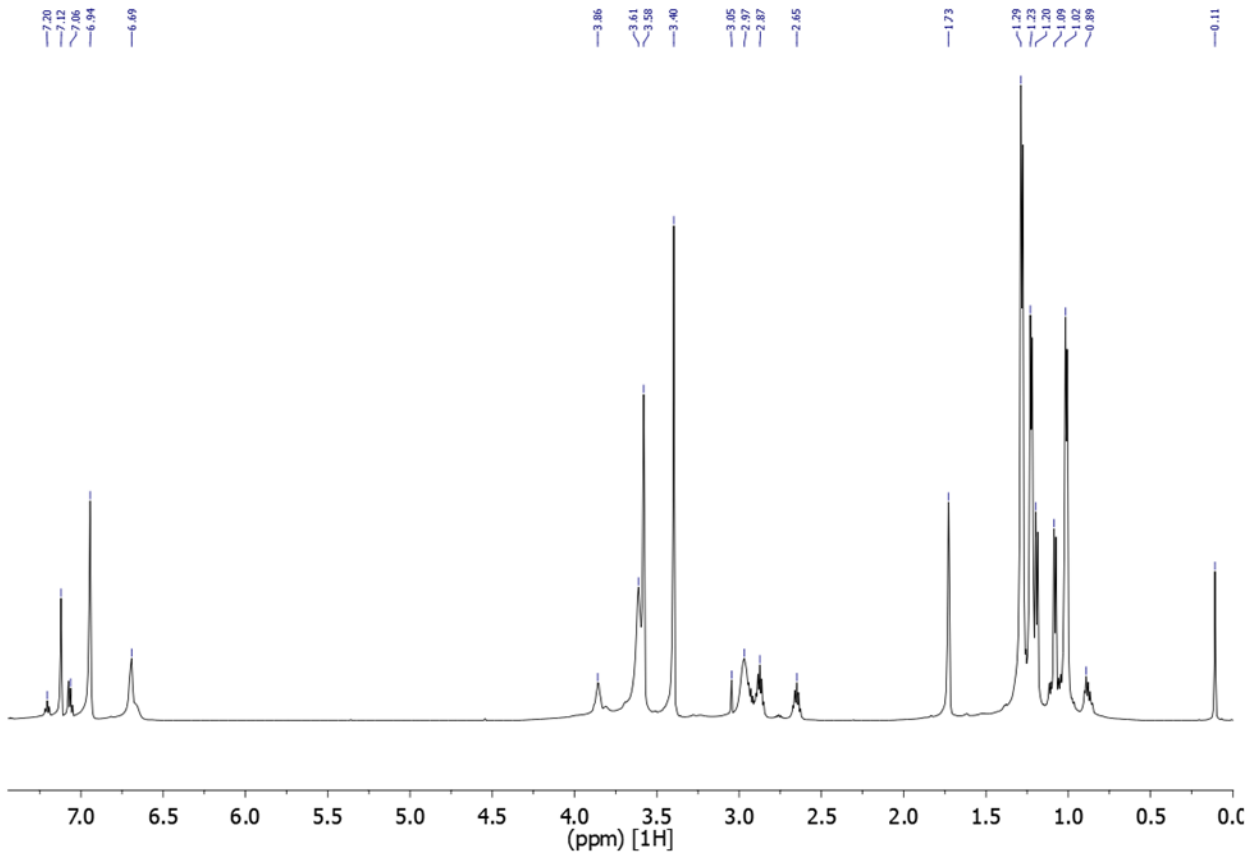

Figure 2.14. ^{1}H NMR (500 MHz, 298K) of **2.1-La** treated with 18-crown-6 and KC_8. Note: sample contains resonances of $HSAr^{iPr6}$ impurity, hexane at 0.89, silicon grease at 0.11, and residual THF-D_8 solvent at 3.58 and 1.73 ppm.

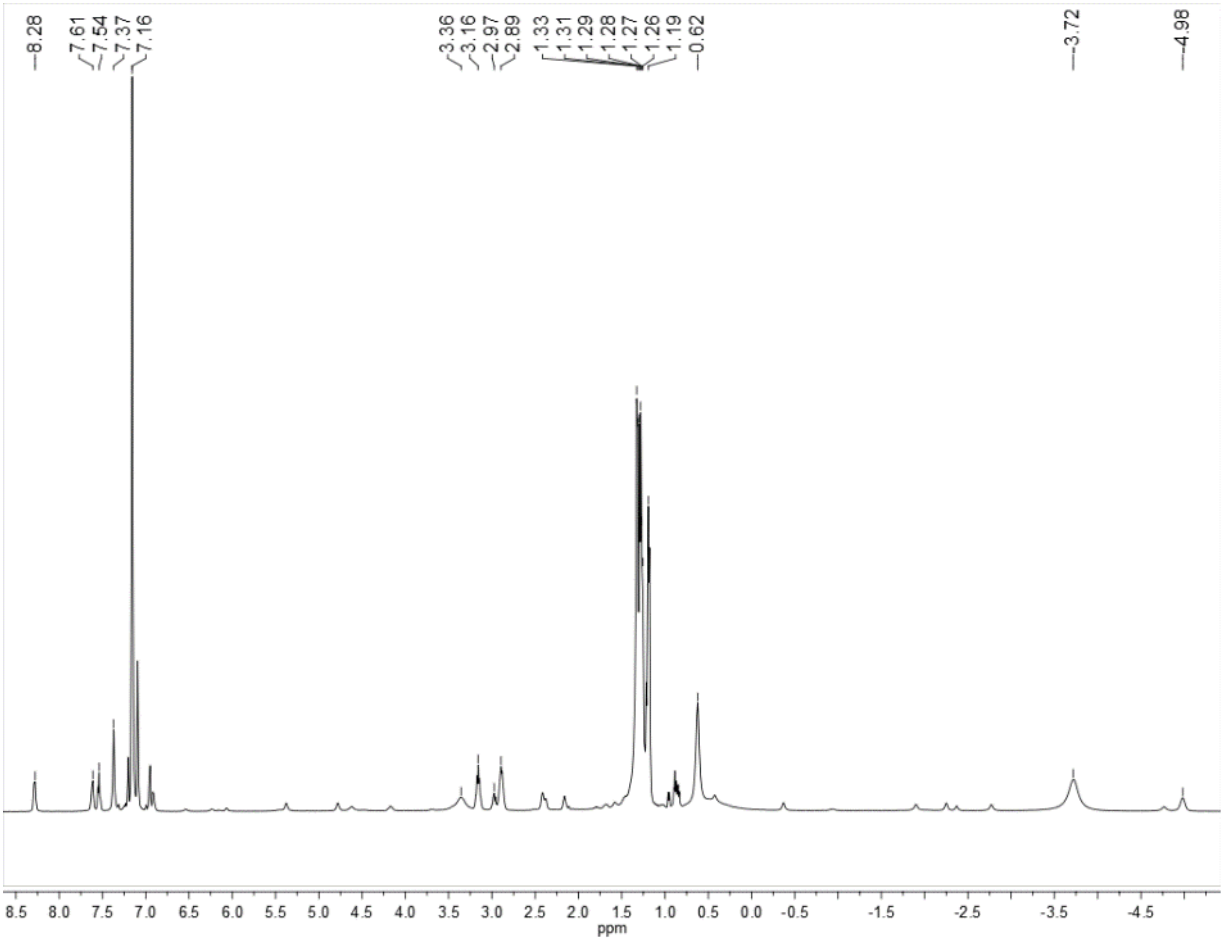

Figure 2.15. ^{1}H NMR spectrum (500 MHz, 298K, benzene-D_6) of the crude residue of the reaction between **2.1-Nd** and KC_8. Signals at 8.28, 7.61, 7.54, 7.37, 3.36, 2.97, 2.89, 1.30-1.20, 0.63, -3.72, and -4.98 are indicative of the formation of **2.2-Nd**. The signal at 7.16 ppm is due to residual benzene in the deuterated solvent.

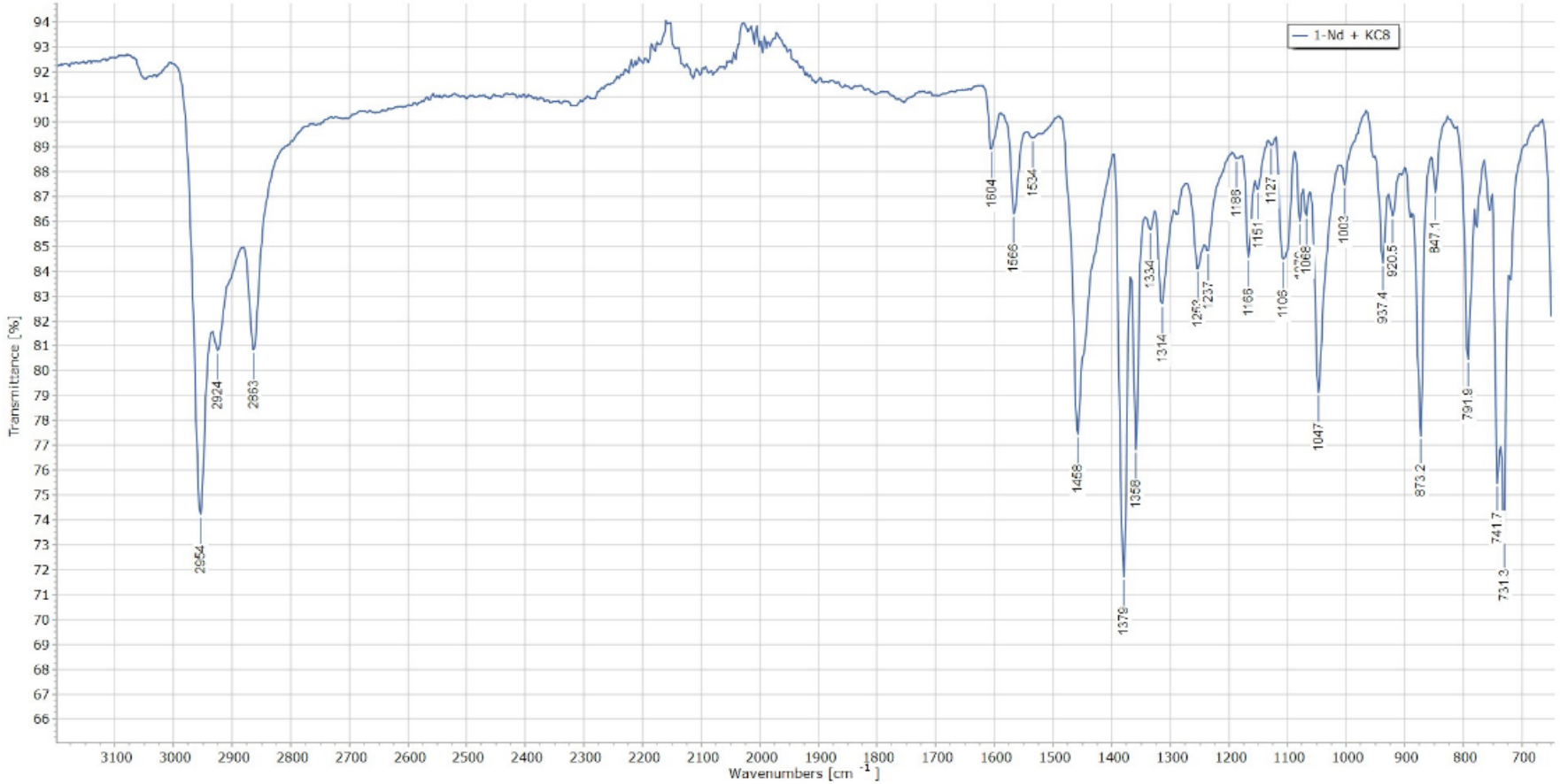

Figure 2.16. Infrared spectrum of $Nd(SAr^{iPr6})_2$, **2.2-Nd**, prepared by the reaction between **2.1-Nd** and KC_8

Crystallographic information can be found in the publication[†].

REFERENCES

(1) Hitchcock, P. B.; Lappert, M. F.; Maron, L.; Protchenko, A. V. Lanthanum Does Form Stable Molecular Compounds in the +2 Oxidation State. *Angewandte Chemie International Edition* **2008**, *47* (8), 1488–1491.

(2) Macdonald, M. R.; Bates, J. E.; Ziller, J. W.; Furche, F.; Evans, W. J. Completing the Series of +2 Ions for the Lanthanide Elements: Synthesis of Molecular Complexes of Pr^{2+}, Gd^{2+}, Tb^{2+}, and Lu^{2+}. *Journal of the American Chemical Society* **2013**, *135* (26), 9857–9868.

(3) Evans, W. J. Tutorial on the Role of Cyclopentadienyl Ligands in the Discovery of Molecular Complexes of the Rare-Earth and Actinide Metals in New Oxidation States. *Organometallics* **2016**, *35* (18), 3088–3100.

(4) MacDonald, M. R.; Ziller, J. W.; Evans, W. J. Synthesis of a Crystalline Molecular Complex of Y^{2+}, [(18-Crown-6)K][$(C_5H_4SiMe_3)_3Y$]. *Journal of the American Chemical Society* **2011**, *133* (40), 15914–15917.

(5) Fieser, M. E.; Palumbo, C. T.; La Pierre, H. S.; Halter, D. P.; Voora, V. K.; Ziller, J. W.; Furche, F.; Meyer, K.; Evans, W. J. Comparisons of Lanthanide/Actinide +2 Ions in a Tris(Aryloxide)Arene Coordination Environment. *Chemical Science* **2017**, *8* (11), 7424–7433.

(6) Kelly, R. P.; Maron, L.; Scopelliti, R.; Mazzanti, M. Reduction of a Cerium(III) Siloxide Complex To Afford a Quadruple-Decker Arene-Bridged Cerium(II) Sandwich. *Angewandte Chemie International Edition* **2017**, *56* (49), 15663–15666.

(7) McClain, K. R.; Gould, C. A.; Marchiori, D. A.; Kwon, H.; Nguyen, T. T.; Rosenkoetter, K. E.; Kuzmina, D.; Tuna, F.; Britt, R. D.; Long, J. R.; Harvey, B. G. Divalent Lanthanide Metallocene

Complexes with a Linear Coordination Geometry and Pronounced 6s-5d Orbital Mixing. *Journal of the American Chemical Society* **2022**, *144* (48), 22193–22201.

(8) Jena, R.; Benner, F.; Delano, F.; Holmes, D.; Mccracken, J.; Demir, S.; Odom, A. L. A Rare Isocyanide Derived from an Unprecedented Neutral Yttrium(II) Bis(Amide) Complex. *Chemical Science* **2023**, *14*, 4257–4264.

(9) Wang, Y.; Liang, J.; Deng, C.; Sun, R.; Fu, P. X.; Wang, B. W.; Gao, S.; Huang, W. Two-Electron Oxidations at a Single Cerium Center. *Journal of the American Chemical Society* **2023**, *145* (41), 22466–22474.

(10) Anderson-Sanchez, L. M.; Yu, J. M.; Ziller, J. W.; Furche, F.; Evans, W. J. Room-Temperature Stable Ln(II) Complexes Supported by 2,6-Diadamantyl Aryloxide Ligands. *Inorganic Chemistry* **2023**, *62* (2), 706–714.

(11) Ryan, A. J.; Ziller, J. W.; Evans, W. J. The Importance of the Counter-Cation in Reductive Rare-Earth Metal Chemistry: 18-Crown-6 Instead of 2,2,2-Cryptand Allows Isolation of $[Y^{(II)}(NR_2)_3]^{1-}$ and Ynediolate and Enediolate Complexes from CO Reactions. *Chemical Science* **2020**, *11* (7), 2006–2014.

(12) Palumbo, C. T.; Halter, D. P.; Voora, V. K.; Chen, G. P.; Chan, A. K.; Fieser, M. E.; Ziller, J. W.; Hieringer, W.; Furche, F.; Meyer, K.; Evans, W. J. Metal versus Ligand Reduction in Ln^{3+} Complexes of a Mesitylene-Anchored Tris(Aryloxide) Ligand. *Inorganic Chemistry* **2018**, *57* (5), 2823–2833.

(13) Pividori, D.; Miehlich, M. E.; Kestel, B.; Heinemann, F. W.; Scheurer, A.; Patzschke, M.; Meyer, K. Uranium Going the Soft Way: Low-Valent Uranium(III) Coordinated to an Arene-Anchored Tris-Thiophenolate Ligand. *Inorganic Chemistry* **2021**, *60* (21), 16455–16465.

(14) Rekken, B. D.; Brown, T. M.; Fettinger, J. C.; Lips, F.; Tuononen, H. M.; Herber, R. H.; Power, P. P. Dispersion Forces and Counterintuitive Steric Effects in Main Group Molecules: Heavier Group 14 (Si-Pb) Dichalcogenolate Carbene Analogues with Sub-90 Interligand Bond Angles. *Journal of the American Chemical Society* **2013**, *135* (27), 10134–10148.

(15) Nguyen, T.; Panda, A.; Olmstead, M. M.; Richards, A. F.; Stender, M.; Brynda, M.; Power, P. P. Synthesis and Characterization of Quasi-Two-Coordinate Transition Metal Dithiolates $M(SAr^*)_2$ (M = Cr, Mn, Fe, Co, Ni, Zn; Ar* = C_6H_3-2,6(C_6H_2-2,4,6-Pr^i_3)$_2$. *Journal of the American Chemical Society* **2005**, *127* (23), 8545–8552.

(16) Niemeyer, M.; Power, P. P. Synthesis and Characterization of Some Group 1 and 2 Metal Derivatives of the Crowding Terphenyl Thiolate and Selenolate Ligands-EC_6H_3-2,6-$Trip_2$ (E = S or Se; Trip = 2,4,6-*i*-$Pr_3C_6H_2$-). *Inorganica Chimica Acta* **1997**, *263* (1–2), 201–207.

(17) Boynton, J. N.; Guo, J. D.; Fettinger, J. C.; Melton, C. E.; Nagase, S.; Power, P. P. Linear and Nonlinear Two-Coordinate Vanadium Complexes: Synthesis, Characterization, and Magnetic Properties of V(II) Amides. *Journal of the American Chemical Society* **2013**, *135* (29), 10720–10728.

(18) Boynton, J. N.; Merrill, W. A.; Reiff, W. M.; Fettinger, J. C.; Power, P. P. Two-Coordinate, Quasi-Two-Coordinate, and Distorted Three Coordinate, T-Shaped Chromium(II) Amido Complexes: Unusual Effects of Coordination Geometry on the Lowering of Ground State Magnetic Moments. *Inorganic Chemistry* **2012**, *51* (5), 3212–3219.

(19) Ni, C.; Rekken, B.; Fettinger, J. C.; Long, G. J.; Power, P. P. Two-Coordinate, Homoleptic Manganese(II) Primary Terphenyl Amido Complexes: The Effects of Secondary Coordination on Geometry and Lewis Base Complexation. *Dalton Transactions* **2009**, No. 39, 8349–8355.

(20) Merrill, W. A.; Stich, T. A.; Brynda, M.; Yeagle, G. J.; Fettinger, J. C.; De Hont, R.; Reiff, W. M.; Schulz, C. E.; Britt, R. D.; Power, P. P. Direct Spectroscopic Observation of Large Quenching of First-Order Orbital Angular Momentum with Bending in Monomeric, Two-Coordinate Fe(II) Primary Amido Complexes and the Profound Magnetic Effects of the Absence of Jahnand- and Renner-Teller Distortions in Rigorously Linear Coordination. *Journal of the American Chemical Society* **2009**, *131* (35), 12693–12702.

(21) Bryan, A. M.; Merrill, W. A.; Reiff, W. M.; Fettinger, J. C.; Power, P. P. Synthesis, Structural, and Magnetic Characterization of Linear and Bent Geometry Cobalt(II) and Nickel(II) Amido Complexes: Evidence of Very Large Spin-Orbit Coupling Effects in Rigorously Linear Coordinated Co^{2+}. *Inorganic Chemistry* **2012**, *51* (6), 3366–3373.

(22) Cofone, A.; Niemeyer, M. A Monomeric, Base-Free Samarium(II) Thiophenolate with a π-Encapsulated Rare-Earth Metal. In *Zeitschrift fur Anorganische und Allgemeine Chemie*; 2006; Vol. 632, pp 1930–1932.

(23) Angelkort, J.; Van Smaalen, S.; Hauber, S. O.; Niemeyer, M. Phase Transition and Crystal Structure of the Monomeric Europium(II) Thiolate $Eu(SC_{36}H_{49})_2$. *Zeitschrift fur Anorganische und Allgemeine Chemie* **2007**, *633* (7), 1031–1035.

(24) Niemeyer, M. σ-Donor versus η^6-π-Arene Interactions in Monomeric Europium(II) and Ytterbium(II) Thiolates - An Experimental and Computational Study. *European Journal of Inorganic Chemistry* **2001**, No. 8, 1969–1981.

(25) Niemeyer, M. A Sterically Crowded Ytterbium(II) Thiolate: Trans-Bis(2,4,6,2'',4'',6''-Hexaisopropyl-1,1':3',1''-Terphenyl-2'-Thiolato-S)Tetrakis(Tetrahydrofuran-O)Ytterbium(II). *Acta Crystallographica Section E Structure Reports Online* **2001**, *57* (9), m396–m398.

(26) Zhao, P.; Zhu, Q.; Fettinger, J. C.; Power, P. Characterization of a Monomeric, Homoleptic, Solvent-Free Samarium Bis(Aryloxide). *Inorganic Chemistry* **2018**, *57* (22), 14044–14046.

(27) Billow, B. S.; Livesay, B. N.; Mokhtarzadeh, C. C.; McCracken, J.; Shores, M. P.; Boncella, J. M.; Odom, A. L. Synthesis and Characterization of a Neutral U(II) Arene Sandwich Complex. *Journal of the American Chemical Society* **2018**, *140* (50), 17369–17373.

(28) Power, P. P.; Niemeyer, M. Donor-Free Alkali Metal Thiolates: Synthesis and Structure of Dimeric, Trimeric, and Tetrameric Complexes with Sterically Encumbered Terphenyl Substituents. *Inorganic Chemistry* **1996**, *35* (25), 7264–7272.

(29) Barnett, B. R.; Mokhtarzadeh, C. C.; Figueroa, J. S.; Lummis, P.; Wang, S.; Queen, J. D.; Gavenonis, J.; Schüwer, N.; Tilley, T. D.; Boynton, J. N.; Power, P. P. Terphenyl Ligands and Complexes; 2018; pp 85–122.

(30) Hauber, S. O.; Niemeyer, M. π-Bonding Encapsulation in Aryl-Substituted Lanthanide Selenolates: Monomeric Compounds with Apparent Low-Coordinate Metal Atoms. *Chemical Communications* **2007**, No. 3, 275–277.

(31) Shannon, R. D. Revised Effective Ionic Radii and Systematic Studies of Interatomic Distances in Halides and Chalcogenides. *Acta Crystallographica Section A* **1976**, *32* (5), 751–767.

(32) Bochkarev, M. N.; Fagin, A. A. A New Route to Neodymium(II) and Dysprosium(II) Iodides. *Chemistry - A European Journal* **1999**, *5* (10), 2990–2992.

(33) Evans, W. J.; Allen, N. T.; Workman, P. S.; Meyer, J. C. Large Scale Synthesis of Dysprosium and Neodymium Diiodides. *Inorganic Chemistry* **2003**, *42* (9), 3097–3099.

(34) Hitchcock, P. B.; Lappert, M. F.; Protchenko, A. V. The First Crystalline Alkali Metal Slat of a Benzenoid Radical Anion without a Stabilizing Substituent and of a Related Dimer: X-Ray

Structures of the Toluene Radical Anion and of the Benzene Radical Anion Dimer Potassium-Crown Ether Salts [9]. *Journal of the American Chemical Society* **2001**, *123* (1), 189–190.

(35) Boynton, J. N.; Guo, J. D.; Grandjean, F.; Fettinger, J. C.; Nagase, S.; Long, G. J.; Power, P. P. Synthesis and Characterization of the Titanium Bisamide Ti{N(H)Ar^{i}Pr$_6$}$_2$ (Ar^{i}Pr$_6$ = C$_6$H$_3$-2,6-(C$_6$H$_2$-2,4,6-^{i}Pr$_3$)$_2$ and Its TiCl{N(H)Ar^{i}Pr$_6$}$_2$ Precursor: Ti(II) → Ti(IV) Cyclization. *Inorganic Chemistry* **2013**, *52* (24), 14216–14223.

(36) Hubig, S. M.; Lindeman, S. V; Kochi, J. K. Charge-Transfer Bonding in Metal-Arene Coordination. *Coordination Chemistry Reviews* **2000**, *200–202* (2), 831–873.

(37) Rosokha, S. V.; Kochi, J. K. Modern Arene Chemistry; 2002; pp 435–478.

(38) Fedushkin, I. L.; Bochkarev, M. N.; Schumann, H.; Esser, L.; Kociok-K6hn, G. Binuclear Complexes of La(III) and Eu(II) with the Bridging Naphthalene. Synthesis and X-Ray Crystallographic analysis of [μ_2-η^4:η^4-C$_{10}$H$_8$][LaI$_2$(THF)$_3$]$_2$ and [μ_2-η^4:η^4-C$_{10}$H$_8$][EuI(DME)$_2$]$_2$. *Journal of Organometallic Chemistry* **1995**, *489*, 145–151.

(39) Straub, M. D.; Ouellette, E. T.; Boreen, M. A.; Britt, R. D.; Chakarawet, K.; Douair, I.; Gould, C. A.; Maron, L.; Del Rosal, I.; Villarreal, D.; Minasian, S. G.; Arnold, J. A Uranium(II) Arene Complex That Acts as a Uranium(I) Synthon. *Journal of the American Chemical Society* **2021**, *143* (47), 19748–19760.

(40) Boynton, J. N.; Guo, J.-D.; Grandjean, F.; Fettinger, J. C.; Nagase, S.; Long, G. J.; Power, P. P. Synthesis and Characterization of the Titanium Bisamide Ti{N(H)AriPr6}2 (AriPr6 = C6H3-2,6-(C6H2-2,4,6-IPr3)2 and Its TiCl{N(H)AriPr6}2 Precursor: Ti(II) → Ti(IV) Cyclization. *Inorganic Chemistry* **2013**, *52* (24), 14216–14223.

(41) Hubig, S. M.; Lindeman, S. V; Kochi, J. K. Charge-Transfer Bonding in Metal–Arene Coordination. *Coordination Chemistry Reviews* **2000**, *200–202*, 831–873.

(42) Rosokha, S. V; Kochi, J. K. Charge-Transfer Effects on Arene Structure and Reactivity. In *Modern Arene Chemistry*; 2002; pp 435–478.

(43) Fedushkin, I. L.; Bochkarev, M. N.; Schumann, H.; Esser, L. Binuclear Complexes of La(III) and Eu(II) with the Bridging Naphthalene Dianion. Synthesis and X-Ray Crystallographic Analysis of [M2-H4:H4-C10H8][LaI2(THF)3]2 and [M2-H4:H4-C10H8][EuI(DME)2]2. *Journal of Organometallic Chemistry* **1995**, *489* (1), 145–151.

(44) Straub, M. D.; Ouellette, E. T.; Boreen, M. A.; Britt, R. D.; Chakarawet, K.; Douair, I.; Gould, C. A.; Maron, L.; Del Rosal, I.; Villarreal, D.; Minasian, S. G.; Arnold, J. A Uranium(II) Arene Complex That Acts as a Uranium(I) Synthon. *Journal of the American Chemical Society* **2021**, *143* (47), 19748–19760.

(45) Stoll, S.; Schweiger, A. EasySpin, a Comprehensive Software Package for Spectral Simulation and Analysis in EPR. *Journal of Magnetic Resonance* **2006**, *178* (1), 42–55.

(46) Fieser, M. E.; Macdonald, M. R.; Krull, B. T.; Bates, J. E.; Ziller, J. W.; Furche, F.; Evans, W. J. Structural, Spectroscopic, and Theoretical Comparison of Traditional vs Recently Discovered Ln_{2+} Ions in the [K(2.2.2-Cryptand)][$(C_5H_4SiMe_3)_3Ln$] Complexes: The Variable Nature of Dy_{2+} and Nd_{2+}. *Journal of the American Chemical Society* **2015**, *137* (1), 369–382.

(47) Woen, D. H.; Huh, D. N.; Ziller, J. W.; Evans, W. J. Reactivity of Ln(II) Complexes Supported by $(C_5H_4Me)^{1-}$ Ligands with THF and $PhSiH_3$: Isolation of Ring-Opened, Bridging Alkoxyalkyl, Hydride, and Silyl Products. *Organometallics* **2018**, *37* (18), 3055–3063.

(48) Angadol, M. A.; Woen, D. H.; Windorff, C. J.; Ziller, J. W.; Evans, W. J. Tert-Butyl(Cyclopentadienyl) Ligands Will Stabilize Nontraditional +2 Rare-Earth Metal Ions. *Organometallics* **2019**, *38* (5), 1151–1158.

(49) Jenkins, T. F.; Woen, D. H.; Mohanam, L. N.; Ziller, J. W.; Furche, F.; Evans, W. J. Tetramethylcyclopentadienyl Ligands Allow Isolation of Ln(II) Ions across the Lanthanide Series in [K(2.2.2-Cryptand)][$(C_5Me_4H)_3Ln$] Complexes. *Organometallics* **2018**, *37* (21), 3863–3873.

(50) Kundu, K.; White, J. R. K.; Moehring, S. A.; Yu, J. M.; Ziller, J. W.; Furche, F.; Evans, W. J.; Hill, S. A 9.2-GHz Clock Transition in a Lu(II) Molecular Spin Qubit Arising from a 3,467-MHz Hyperfine Interaction. *Nature Chemistry* **2022**, *14* (4), 392–397.

(51) Evans, J. W.; Drummond, D. K. Samarium-Mediated Functionalization of N=N Bonds: Double Insertion of Carbon Monoxide into the N=N of Azobenzene. *Journal of the American Chemical Society* **1986**, *108* (1), 7440–7441.

(52) Evans, W. J.; Drummond, D. K.; Bott, S. G.; Atwood, J. L. Reductive Distortion of Azobenzene by an Organosamarium(II) Reagent To Form$[(C_5Me_5)_2Sm]_5(C_6H_5)_2N_2$: An X-Ray Crystallographic of an Agostic Hydrogen Complex on an Ortho-Metalation Reaction Coordinate. *Organometallics* **1986**, *5* (11), 2389–2391.

(53) Evans, W. J.; Drummond, D. K.; Chamberlain, L. R.; Doedens, R. J.; Bott, S. G.; Zhang, H.; Atwood2b, J. L. Synthetic, Structural, and Reactivity Studies of the Reduction and CO Derivatization of Azobenzene Mediated by Divalent Lanthanide Complexes. *J. Am. Chem. Soc* **1988**, *110*, 4983–4994.

(54) Evans, W. J.; Drummond, D. K. Reductive Coupling of Pyridazine and Benzaldehyde Azine and Reduction of Bipyridine by $(C_5Me_5)_2Sm(THF)_2$. *Journal of the American Chemical Society* **1989**, *111* (3), 3329–3335.

(55) La Pierre, H. S.; Scheurer, A.; Heinemann, F. W.; Hieringer, W.; Meyer, K. Synthesis and Characterization of a Uranium(II) Monoarene Complex Supported by δ Backbonding. *Angewandte Chemie International Edition* **2014**, *53* (28), 7158–7162.

(56) Pangborn, A. B.; Giardello, M. A.; Grubbs, R. H.; Rosen, R. K.; Timmers, F. J. Safe and Convenient Procedure for Solvent Purification. *Organometallics* **1996**, *15* (5), 1518–1520.

(57) Meyer, G.; Garcia, E.; Corbett, J. D. The Ammonium Chloride Route to Anhydrous Rare Earth Chlorides—The Example of YCl_3. In *Inorganic Syntheses*; 1989; pp 146–150.

(58) Bochkarev, M. N.; Fedushkin, I. L.; Fagin, A. A.; Petrovskaya, T. V.; Ziller, J. W.; Broomhall-Dillard, R. N. R.; Evans, W. J. Synthesis and Structure of the First Molecular Thulium(II) Complex: $[TmI_2(MeOCH_2CH_2OMe)_2]$. *Angewandte Chemie (International Edition in English)* **1997**, *36* (1–2), 133–135.

(59) Niemeyer, M.; Power, P. P. Donor-Free Alkali Metal Thiolates: Synthesis and Structure of Dimeric, Trimeric, And Tetrameric Complexes with Sterically Encumbered Terphenyl Substituents. *Inorganic Chemistry* **1996**, *13*, 7264–7272.

–Chapter 3–

The Variable Di(mesityl)boroxide Chemistry of the Lanthanide Metals

INTRODUCTION

Recent studies of reductive rare-earth metal chemistry have revealed that the sterically bulky oxygen-donor ligand $(OAr^*)^{1-}$ $(OC_6H_2Ad_2\text{-}2,6\text{-}^tBu\text{-}4)^{1-}$ (Ad = 1-adamantyl)$^{1-3}$ can stabilize both Ln(III) and Ln(II) complexes across the series, Scheme 3.1.

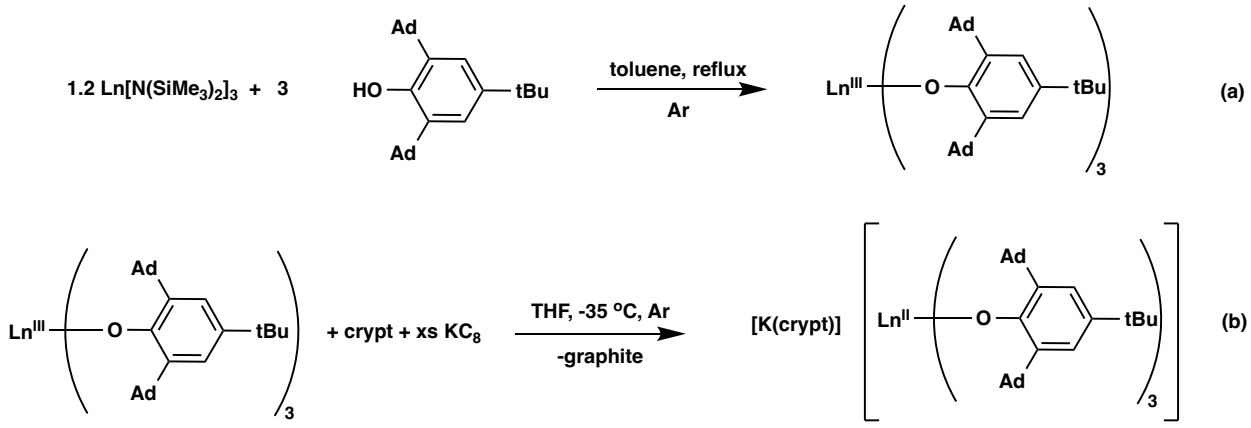

Ln = La, Ce, Pr, Nd, Gd, Tb, Dy, Ho, Yb, Lu
Ad = 1-adamantyl
crypt = 2.2.2-cryptand

Scheme 3.1. The synthesis of Ln(III) and Ln(II) complexes of the $(OC_6H_2Ad_2\text{-}2,6\text{-}^tBu\text{-}4)^{1-}$ ligand.

In search of other sterically bulky oxygen-donor atom ligands for the stabilization of lanthanide complexes, we have investigated the boroxide ligand, $(OBMes_2)^{1-}$ (Mes = $C_6H_2Me_3$-2,4,6),[4–11] which was identified as a surrogate alkoxide as early as 1987 by Power and co-workers.[4] Prior research indicated that the properties of this ligand can differ from those of alkoxide ligands because the low-lying empty p orbital of the boron atom of this sterically bulky oxygen-donor ligand can accept electron density from the oxygen atom, making the ligand less electron-donating overall, Figure 3.1.[4,8] It was of interest to determine if the electron-withdrawing character of the boroxide ligand would be useful in stabilizing new complexes of highly reducing Ln(II) ions .[12–20]

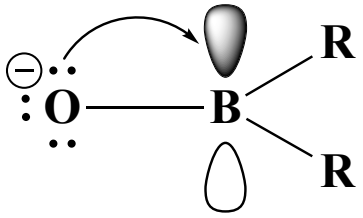

Boroxide

Figure 3.1. A boroxide ligand showing delocalization of oxygen electron density to boron.[8]

Although the $(OBMes_2)^{1-}$ ligand has been used with uranium to form dimeric $[U(OBMes_2)_3]_2$, [9,10] Figure 3.2, as well in complexes with a wide variety of transition metals and group 1 and 2 metals,[4,6–8] its use had not been explored with the lanthanide elements.[8] Uranium boroxide chemistry has also been reported with the $(OBTrip_2)^{1-}$ ligand (Trip = 2,4,6-triisopropylphenyl) as well as with the heterocyclic boroxide $[(HCNDipp)_2BO]^{1-}$ boroxide (Dipp = 2,6-di-isopropylphenyl), Figure 3.2.[21]

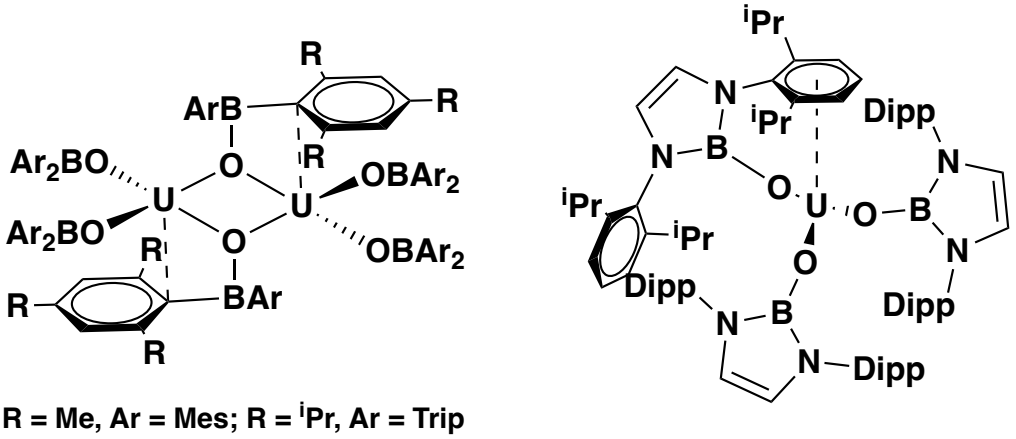

Figure 3.2. Uranium compounds featuring the di(mesityl)- and Trip-boroxide ligands[9] (left) and the $[(HCNDipp)_2BO]^{1-}$ boroxide ligand (right). [21]

Described in this Chapter is the reaction chemistry of $HOBMes_2$ and $KOBMes_2$ with Ln(III) amides and halides, respectively, as well as attempts to reduce these Ln(III) complexes to isolable Ln(II) complexes. Several types of representative reactions are presented to illustrate the diverse chemistry possible with this ligand. The reaction of $SmI_2(THF)_2$ with $KOBMes_2$ is also described, which led to an unusual Sm(II) cluster.

RESULTS

Bimetallic Ln(III) Boroxide Complexes. Since protonolysis was previously used successfully to ligate uranium with boroxide ligands[9], reactions between the Ln(III) amides $Ln(NR_2)_3$, (R = $SiMe_3$), and three equiv of di(mesityl)borinic acid, $HOBMes_2$, were examined. These reactions provided single crystals of the bimetallic bridged complexes $[(Mes_2BO)_2Ln(\mu\text{-}OBMes_2)]_2$, **3.1-Ln** (Ln =La, Ce, Nd**,** Gd), which could be separated from residual $HOBMes_2$ by crystallization. These compounds were found to crystallize as dimers in the solid state by X-ray crystallography, eq 3.1, Figure 3.3.

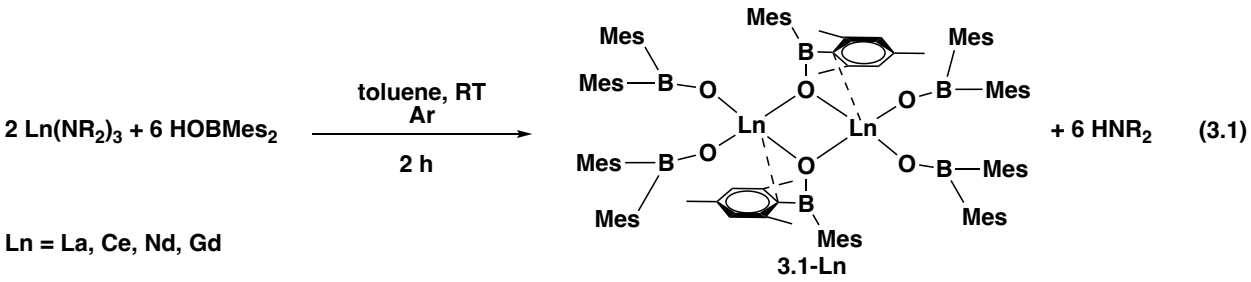

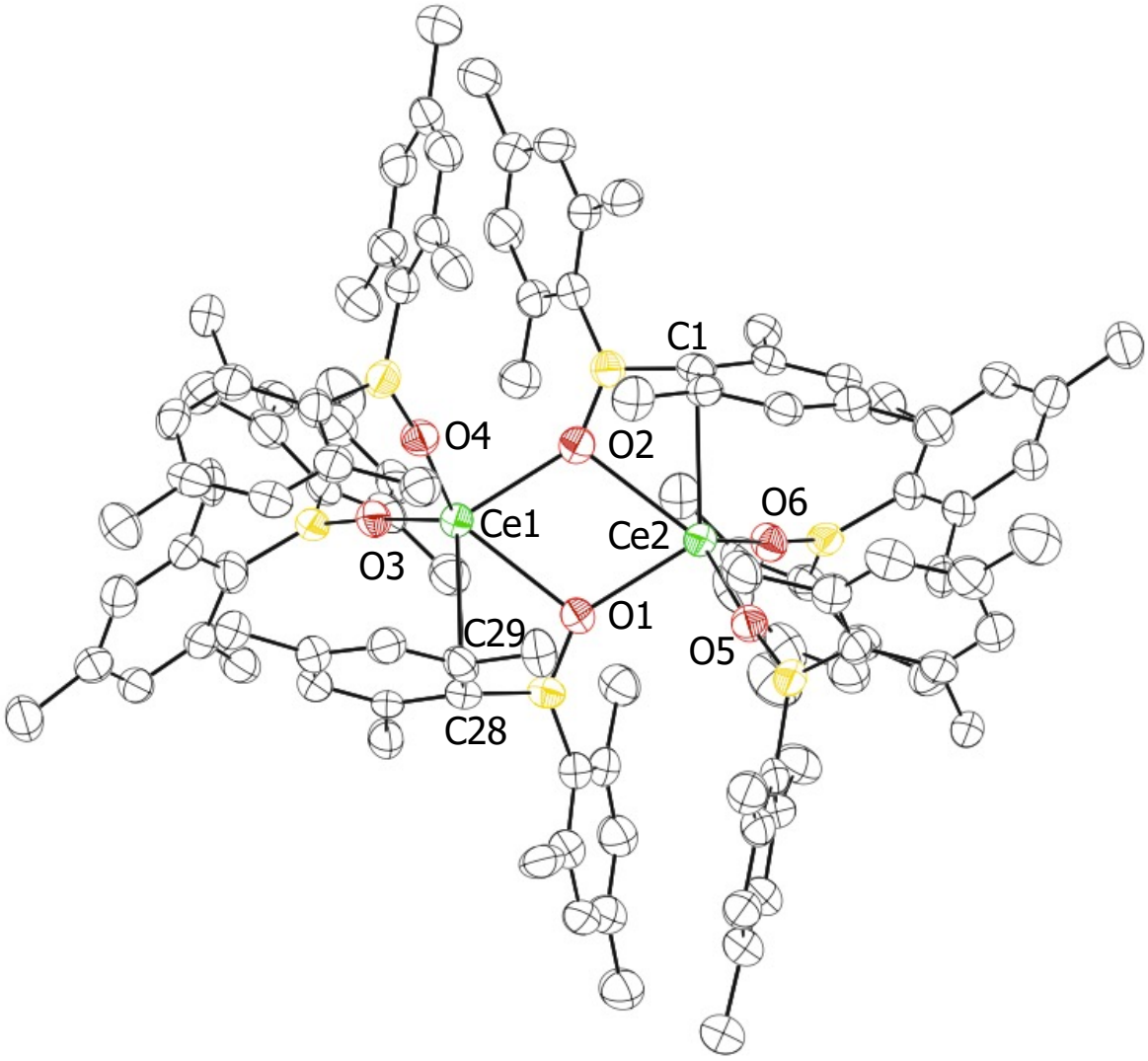

Figure 3.3. The molecular structure of $[(Mes_2BO)_2Ce(\mu\text{-}OBMes_2)]_2$, **3.1-Ce**. Thermal ellipsoids are drawn at the 50% probability level. Hydrogen atoms and toluene solvent molecules are not shown for clarity.

The four **3.1-Ln** complexes and $[(Mes_2BO)_2U(\mu\text{-}OBMes_2)]_2$[10] have similar structures in which each metal binds two terminal $(OBMes_2)^{1-}$ ligands and two bridging $(OBMes_2)^{1-}$ ligands. One ipso carbon of the flanking aryl ring of each bridging $(OBMes_2)^{1-}$ ligand is oriented toward the metal. However, these compounds are not isomorphous and the structures contain variable

amounts of co-crystallized solvent molecules. Complex **3.1-Ce** crystallizes in the $P2_1/c$ space group with 3.5 toluene molecules in the unit cell and the other **3.1-Ln** (Ln = La, Nd, Gd) compounds crystallize in the *Pnn*2 space group with a centrosymmetric inversion center lying along one Ln-O(bridging) bond, each with different amounts cocrystallized of solvent: **3.1-La** (11 hexane), **3.1-Nd** (5 hexane), and **3.1-Gd** (two toluene and one hexane). $[(Mes_2BO)_2U(\mu\text{-}OBMes_2)]_2$ crystallizes differently in the $P2/c$ space group with two hexane molecules in the lattice.

The metrical data on the **3.1-Ln** compounds are compared with those of $[(Mes_2BO)_2U(\mu\text{-}OBMes_2)]_2$, **3.1-U**, in Table 3.1. The B-O bonds in all five compounds fall in the range of 1.308(7)-1.393(6) Å. The B-O bond distances of the bridging ligands are numerically longer than those of the terminal ligands, but the difference is not significant within the error limits. The M–O(bridging) distances for each complex have different values, i.e. the bridging is not symmetrical. All of the Ln–O(bridging) distances are longer than the Ln–O(terminal) distances as expected. Each complex has an M–C(ipso aryl) bond that is approximately 0.2 Å shorter than any of the other M–C(aryl) distances.

Table 3.1. Selected Bond Distances(Å) of 3.1-Ln and $[(Mes_2BO)_2U(\mu\text{-}OBMes_2)]_2$

3.1-La		**3.1-Ce**			
La1-O1(bridging)	2.554(3)	Ce1-O1(bridging)	2.552(3)	Ce2-O1(bridging)	2.363(3)
La1-O1'(bridging)	2.375(3)	Ce1-O2(bridging)	2.366(3)	Ce2-O2(bridging)	2.549(3)
La1-O2(terminal)	2.230(4)	Ce1-O3(terminal)	2.194(3)	Ce2-O5(terminal)	2.204(3)
La1-O3(terminal)	2.205(4)	Ce1-O4(terminal)	2.194(3)	Ce2-O6(terminal)	2.192(3)

La1-C1	2.869(5)	Ce1-C1	2.870(5)	Ce2-C28	2.869(4)
La1-C6	3.040(5)	O1-B1(bridging)	1.371(6)	Ce2-C29	3.011(5)
O1-B1(bridging)	1.393(6)	O2-B2(bridging)	1.361(6)	O4-B4(terminal)	1.333(7)
O2-B2(bridging)	1.352(8)	O3-B3(terminal)	1.342(7)	O5-B5(terminal)	1.338(6)
O3-B3(terminal)	1.308(7)	–	–	O6-B6(terminal)	1.346(7)
3.1-Nd		**3.1-Gd**		$[(Mes_2BO)_2U(\mu\text{-}OBMes_2)]_2$	
Nd1-O1(bridging)	2.480(4)	Gd1-O1(bridging)	2.389(2)	U1-O1(bridging)	2.5518(2)
Nd1-O1'(bridging)	2.342(4)	Gd1-O1'(bridging)	2.282(2)	U1-O1'(bridging)	2.360(2)
Nd1-O2(terminal)	2.198(5)	Gd1-O2(terminal)	2.103(3)	U1-O2(terminal)	2.190(2)
Nd1-O3(terminal)	2.156(5)	Gd1-O3(terminal)	2.128(3)	U1-O3(terminal)	2.178(2)
Nd1-C1	2.814(7)	Gd1-C1	2.767(4)	U1-C1	2.811(3)
Nd1-C6	2.961(7)	Gd1-C2	2.960(4)	U1-C6	3.022(3)
O1-B1(bridging)	1.359(8)	O1-B1(bridging)	1.381(4)	O1-B1(bridging)	1.356(4)
O2-B2(bridging)	1.321(1)	O2-B2(bridging)	1.355(5)	O2-B2(bridging)	1.348(4)
O3-B3(terminal)	1.334(1)	O3-B3(terminal)	1.337(5)	O3-B3(terminal)	1.349(4)

The ^{1}H NMR spectrum of the **3.1-La** complex in deuterated toluene at room temperature down to 188 K did not show the number of resonances expected based on the solid-state structure

(Figure 3.4). Hence, dynamic processes likely occur in solution such that the aryl coordination of the bridging boroxide is not retained in solution.[22]

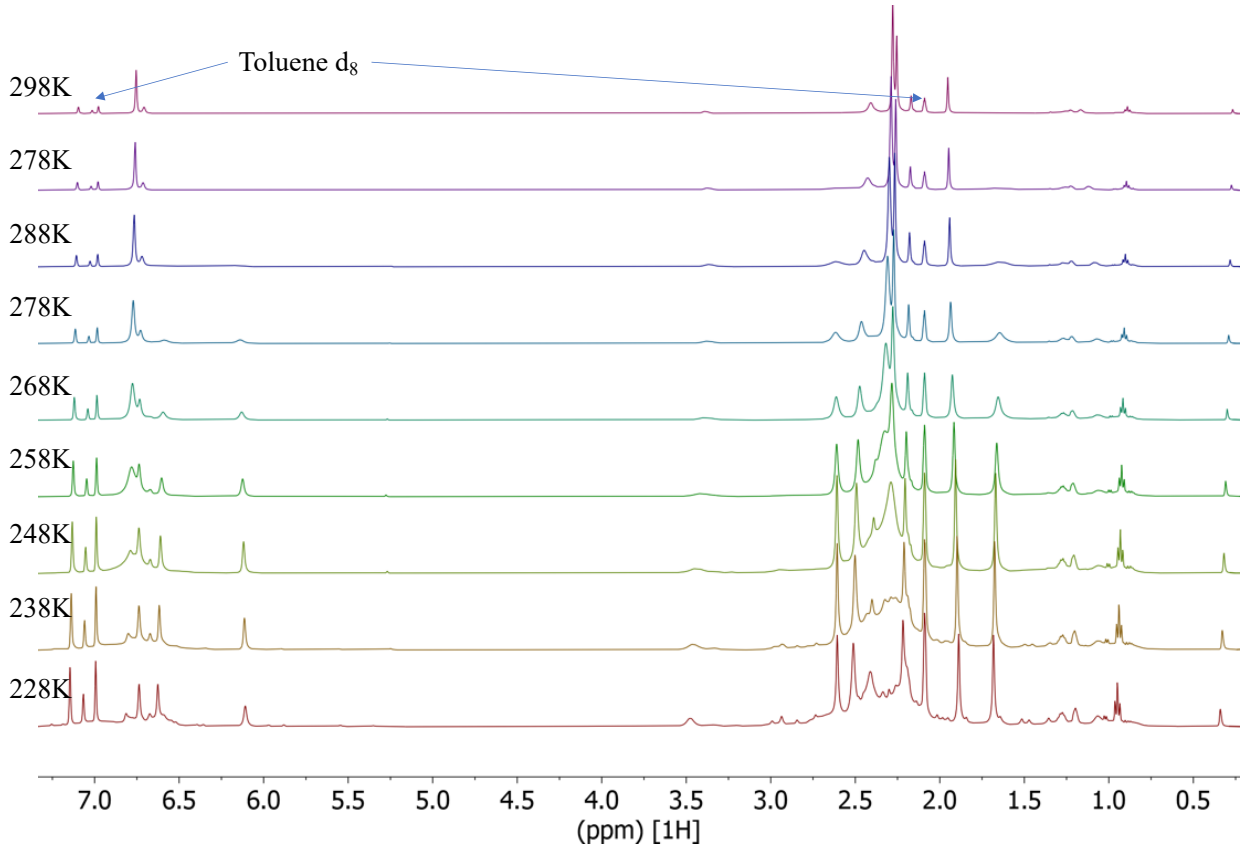

Figure 3.4. 1H NMR (498 MHz, C_7D_8, 228-298K) variable temperature spectra of $[(Mes_2BO)_2La(\mu\text{-}OBMes_2)]_2$, **3.1-La** in deuterated toluene.

At room temperature, two resonances assignable to aryl protons of $(OBMes_2)^{1-}$ ligands are observed at 6.80 and 6.40 ppm in a 2:1 ratio, respectively, which is consistent with a 2:1 terminal:bridging ligand ratio, but the methyl region between 2.58 and 1.96 ppm is more complicated (Figures 3.5 and 3.6).

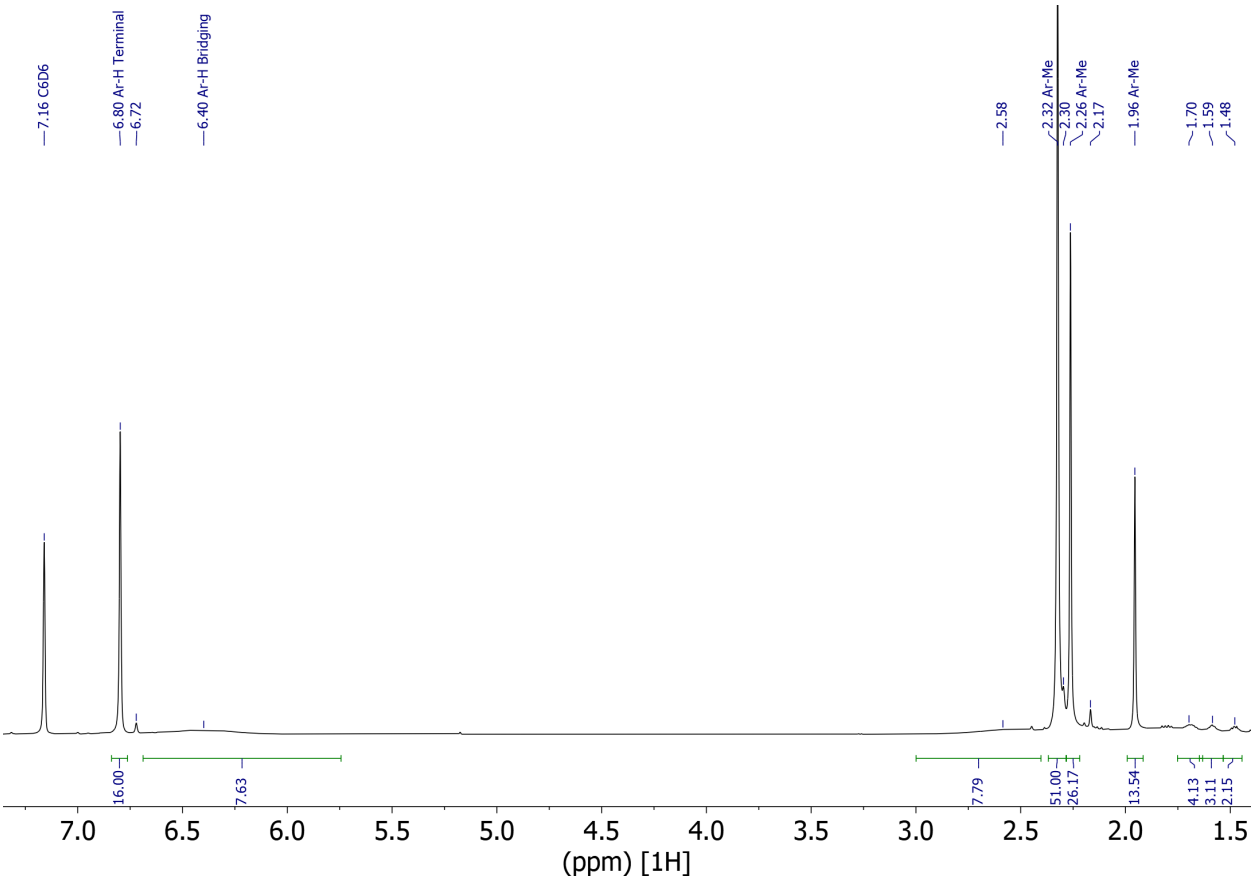

Figure 3.5. ^{1}H NMR (500 MHz, 298K) spectrum of $[(Mes_2BO)_2La(\mu\text{-}OBMes_2)]_2$**, 3.1-La** in deuterated benzene (residual proton signal marked at δ = 7.16 ppm). Note**:** Resonances of unreacted $HOBMes_2$ are present at δ = 6.72, 2.30 and 2.17.

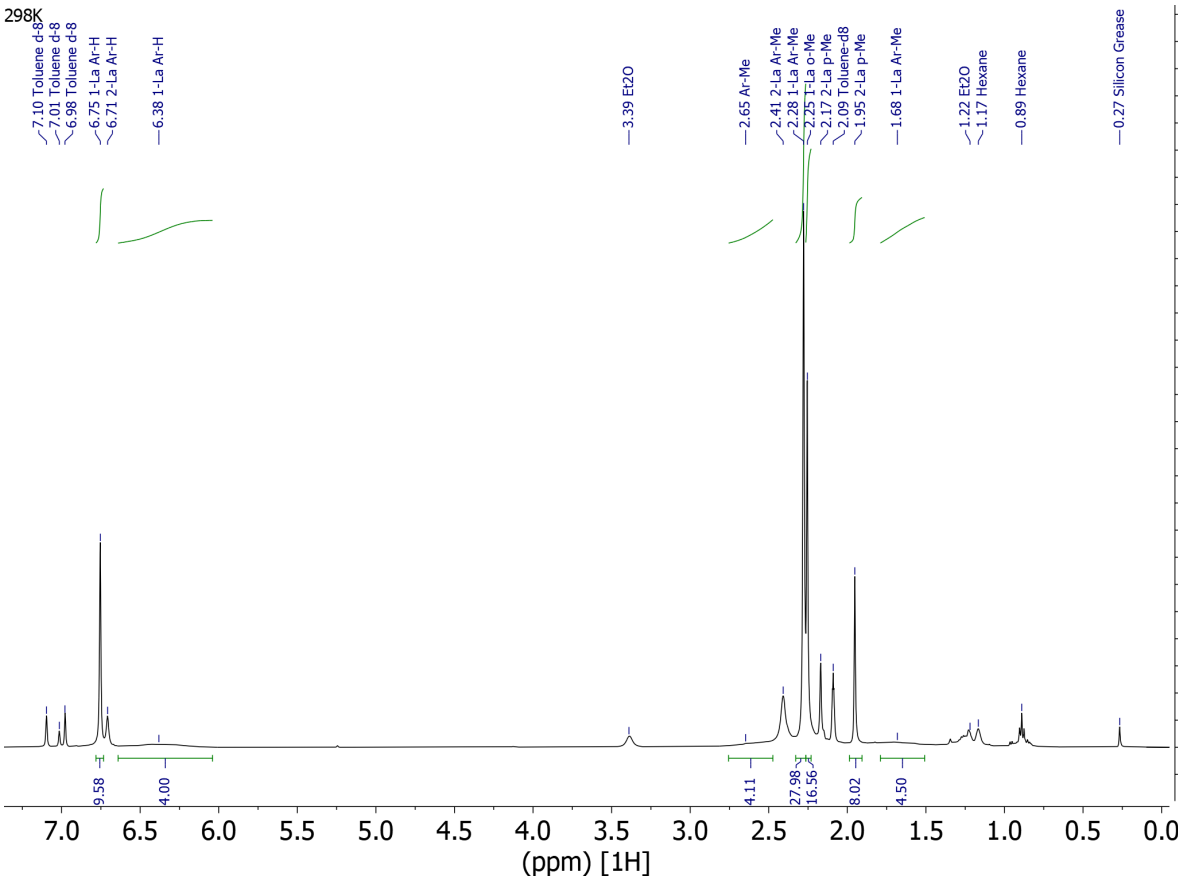

Figure 3.6. 1H NMR (498 MHz, C_7D_8, 298K) spectrum of $[(Mes_2BO)_2La(\mu\text{-}OBMes_2)]_2$, **3.1-La** in deuterated toluene (residual proton signal marked at δ = 7.10, 7.01, 6.98, and 2.09 ppm). Note**:** Resonances of **3.2-La**, Et_2O, hexane and silicon grease are marked on the spectrum.

Assignments of the NMR spectra of **3.1-Ce** and **3.1-Nd** complexes were more challenging due to the paramagnetism of the Ce(III) and Nd(III) ions (Figures 3.7 and 3.8).

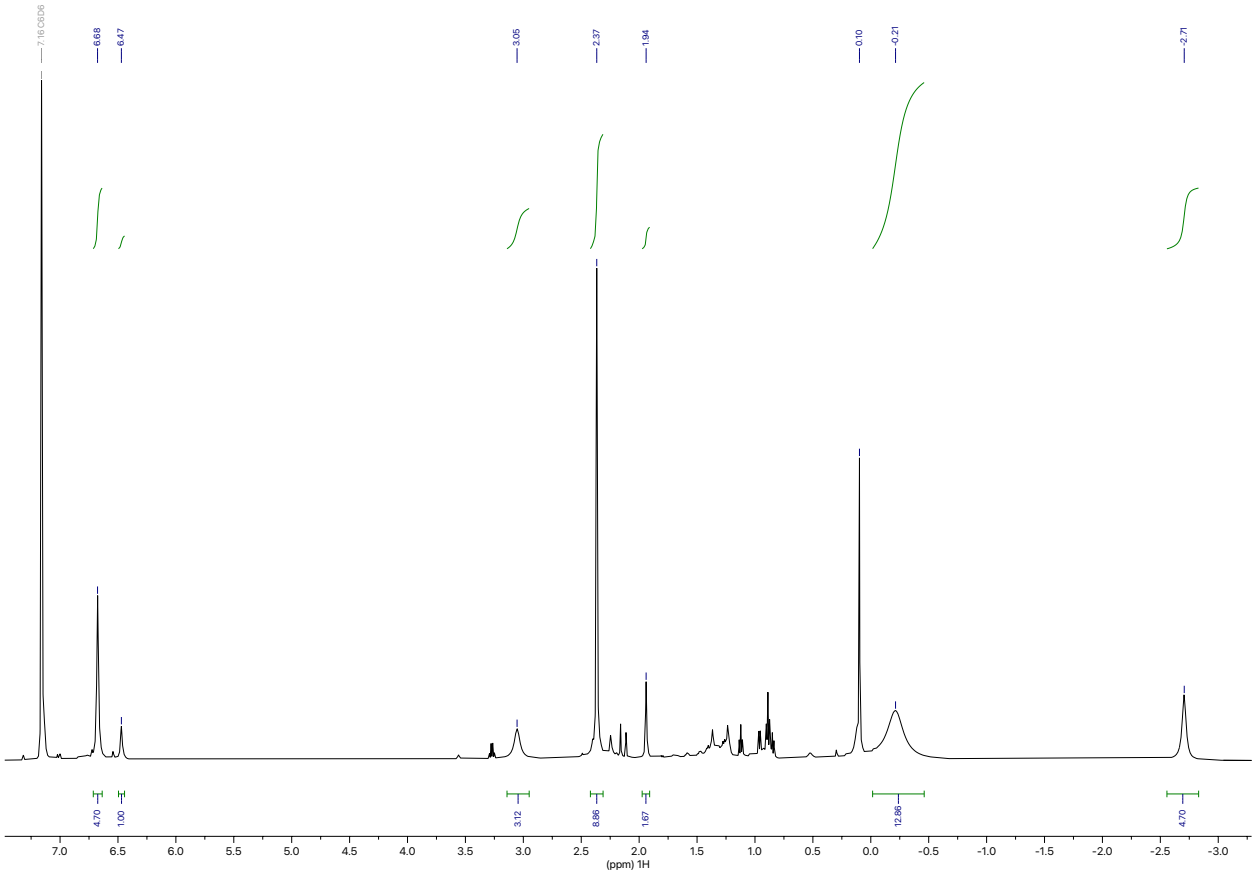

Figure 3.7. ^{1}H NMR (500 MHz, 298K) spectrum of $[(Mes_2BO)_2Ce(\mu\text{-}OBMes_2)]_2$, **3.1-Ce** in deuterated benzene (residual proton peak marked at δ = 7.16 ppm). Note**:** Resonance of side product HNR_2 appears at δ = 0.10 ppm.

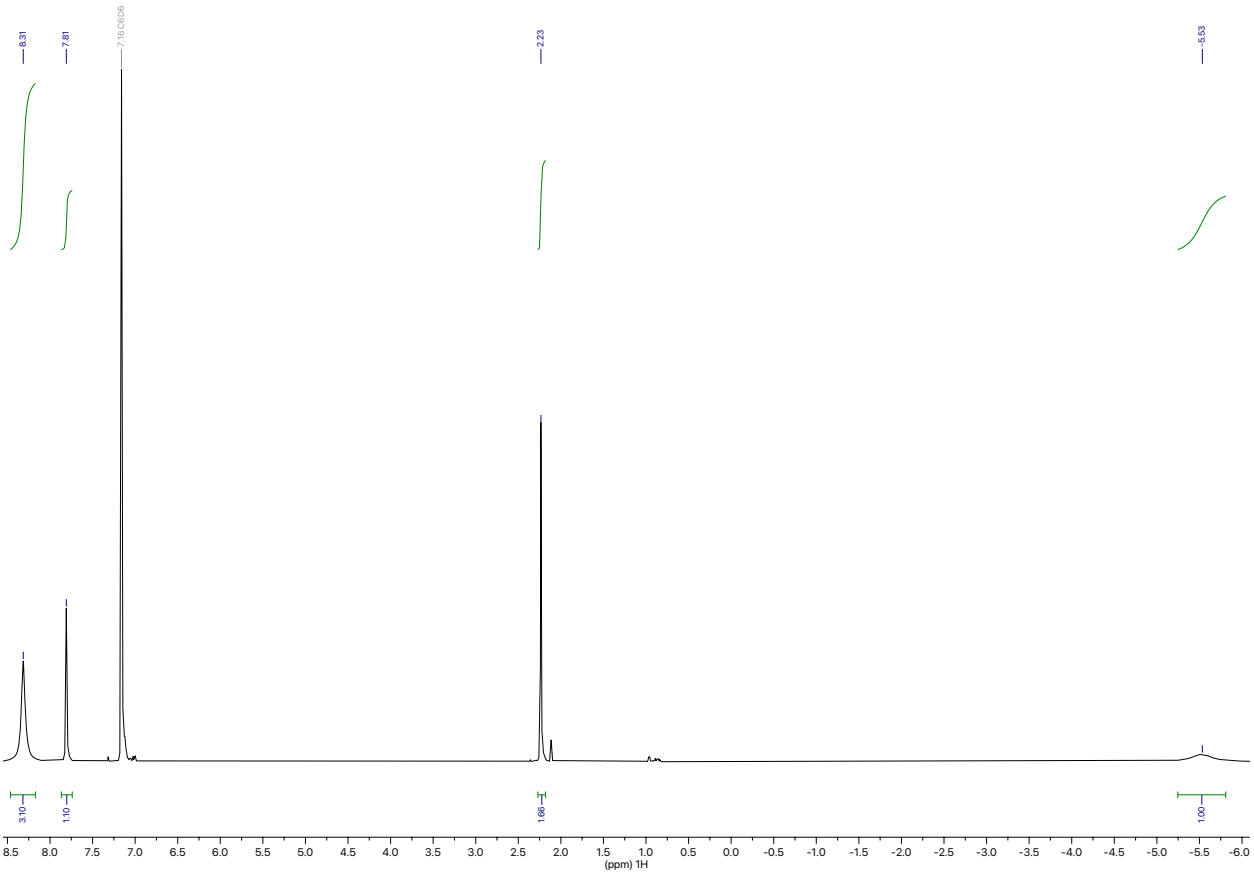

Figure 3.8. ^{1}H NMR (500 MHz, 298K) spectrum of $[(Mes_2BO)_2Nd(\mu\text{-}OBMes_2)]_2$, **3.1-Nd** in deuterated benzene (residual proton peak marked at δ = 7.16 ppm).

Monometallic Ln(III) Boroxide Complexes. Traditional ionic metathesis reactions between lanthanide halides and $KOBMes_2$, prepared from the reaction of $HOBMes_2$ and KH, were examined to determine if this common route to Ln(III) complexes would also be accessible using the $(OBMes_2)^{1-}$ ligand. Initial reactions with lanthanide trichlorides generated products that appeared to incorporate potassium and chloride ions and these structures were difficult to analyze due to large amounts of crystallographic disorder. These reactions were not pursued since the protonolysis route above was successful.

However, the protonolysis route, eq 3.1, repeatedly gave samples of **3.1-Ln** contaminated with $HOBMes_2$. It was found that treating the crude products of these protonolysis reactions with hexane and then with hexane/THF, the monometallic $Ln(OBMes_2)_3(THF)_3$, **3.2-Ln**, complexes

could be accessed. These could then be desolvated back to pure **3.1-Ln** by repeated addition of toluene, heating to 80 °C, and removal of solvent. The **3.1-Ln** complexes could be obtained in 35-45% yield by this method.

It was also found that $La(OBMes_2)_3(THF)_3$, **3.2-La**, could be obtained by ionic metathesis by using the iodide starting material, $LaI_3(THF)_{3.5}$, with $KOBMes_2$, eq 3.2. Complex **3.2-La** crystallizes as an incommensurately modulated structure in the superspace group *Pbca*(0β0)s0s.[23] The quality of data was suitable only to provide the connectivity of the structure, which involved a very distorted octahedral geometry around the La(III) ion.

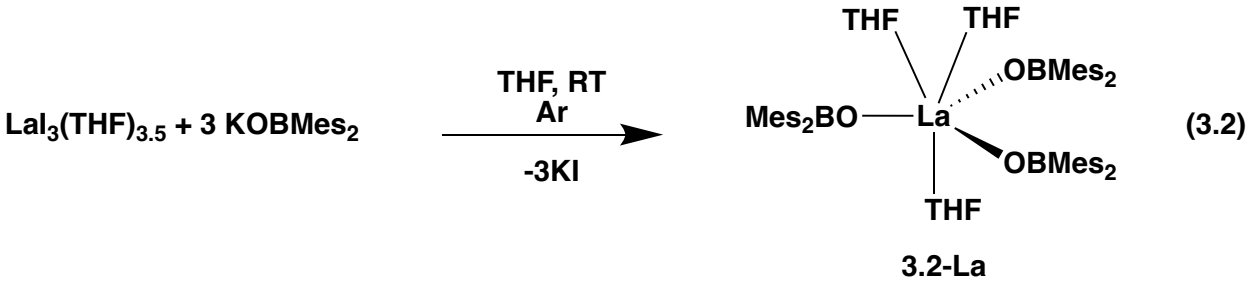

3.2-La

However, treatment of a toluene solution of **3.1-Nd** with an aliquot of THF and subsequent solvent removal under reduced pressure provided crystals of the neodymium analog, $Nd(OBMes_2)_3(THF)_3$, **3.2-Nd**, that were of higher quality than those of **3.2-La**. **3.2-Nd** crystallizes in the $P2_1/c$ space group with two molecules in the asymmetric unit and has a molecular structure, Figure 3.9, similar to that of **3.2-La,** Figure 3.10.

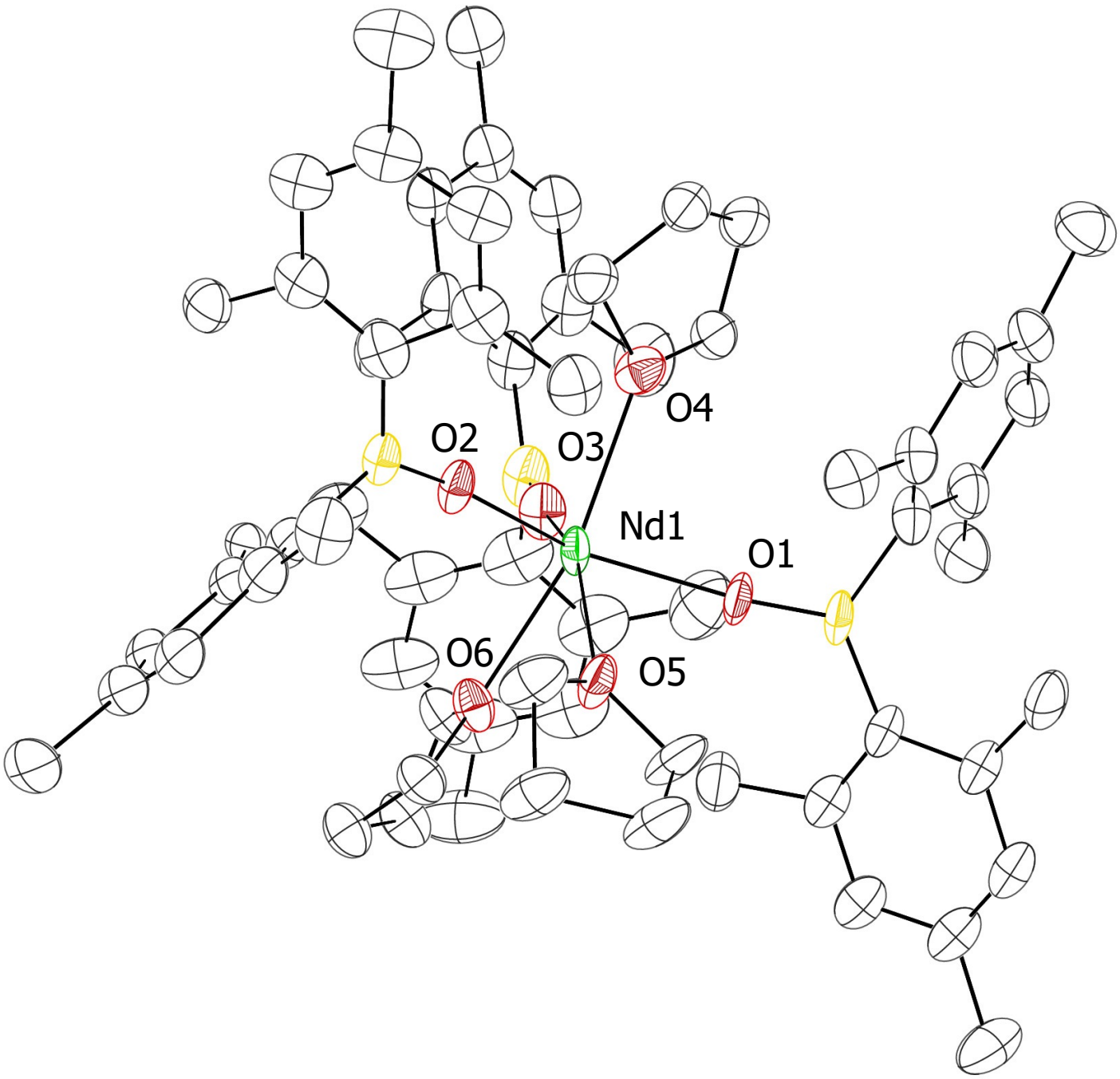

Figure 3.9. The molecular structure of $Nd(OBMes_2)_3(THF)_3$, **3.2-Nd**. Thermal ellipsoids are drawn at the 20% probability level. Atoms modeled with disorder, hydrogen atoms, and the second **3.2-Nd** molecule are not shown for clarity.

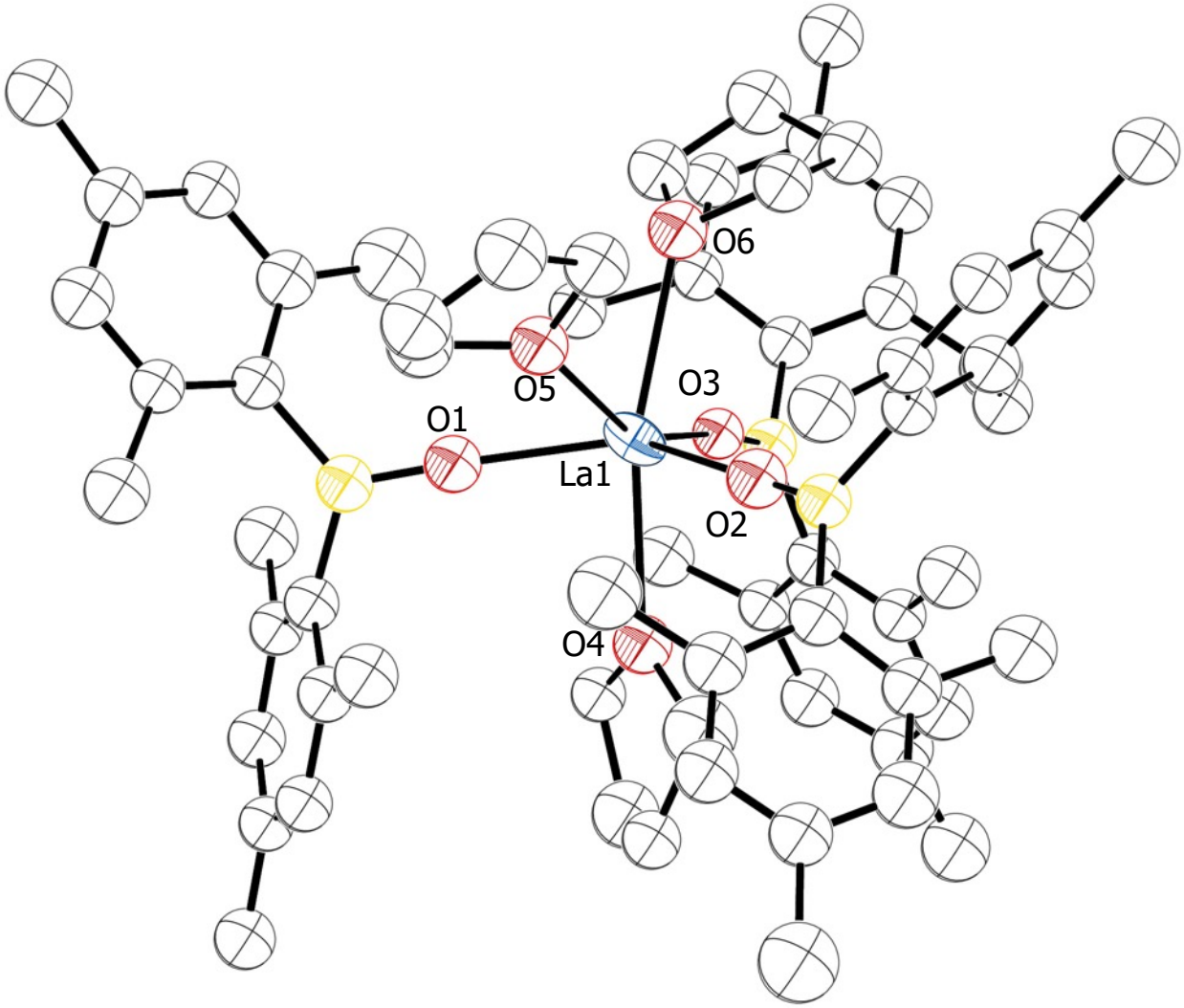

Figure 3.10. Molecular structure of $La(OBMes_2)_3(THF)_3$, **3.2-La**, drawn at the 30% probability level with selective atom labelling**.** Hydrogen atoms are not shown for clarity.

The metrical data of **3.2-Nd** are compared in Table 3.2 to other Nd boroxide complexes in this Chapter. The complex has a distorted octahedral structure as evidenced by the markedly different O(boroxide)–Nd–O(boroxide) angles of 107.3(3)°, 108.5(3)°, and 139.8(3)°. The O(THF)–Nd–O(THF) are even more disparate: 70.2(3)°, 123.1(3)°, and 166.0(3)°. The 2.202(6)–2.241(8) Å Nd–O(boroxide) distances are significantly shorter than the 2.478(9)–2.559(9) Å Nd–

O(THF) distances as expected for anionic versus neutral ligands. Only a few $NdX_3(THF)_3$ complexes are available for comparison in the Cambridge Structural Database (CSD) [$(X)^{1-}$ = unidentate monoanionic oxygen donor ligand], namely the thiophene-based ligand complexes $Nd[OC(C_{10}H_5S)_3]_3(THF)_3$,[24] $Nd[OC(C_4H_3S)_3]_3(THF)_3$,[24] $Nd[OCPh(C_4H_3S)_2]_3(THF)_3$,[25] and $Nd[OCPh_2(C_4H_3S)]_3(THF)_3$,[25] and the aryloxides, $Nd(OC_6H_3\text{-}2,6\text{-}^iPr_2)_3(THF)_3$,[26] and $Nd(OC_6H_3\text{-}2,4\text{-}^tBu_2)_3(THF)_3$.[27] Of these structures, only $Nd(OC_6H_3\text{-}2,4\text{-}^tBu_2)_3(THF)_3$[27] has the distorted octahedral structure of **3.2-Nd** with meridional anionic ligands. The lanthanum analog, $La(OC_6H_3\text{-}2,4\text{-}^tBu_2)_3(THF)_3$, [27] has a similar meridional geometry (Figure 3.11)

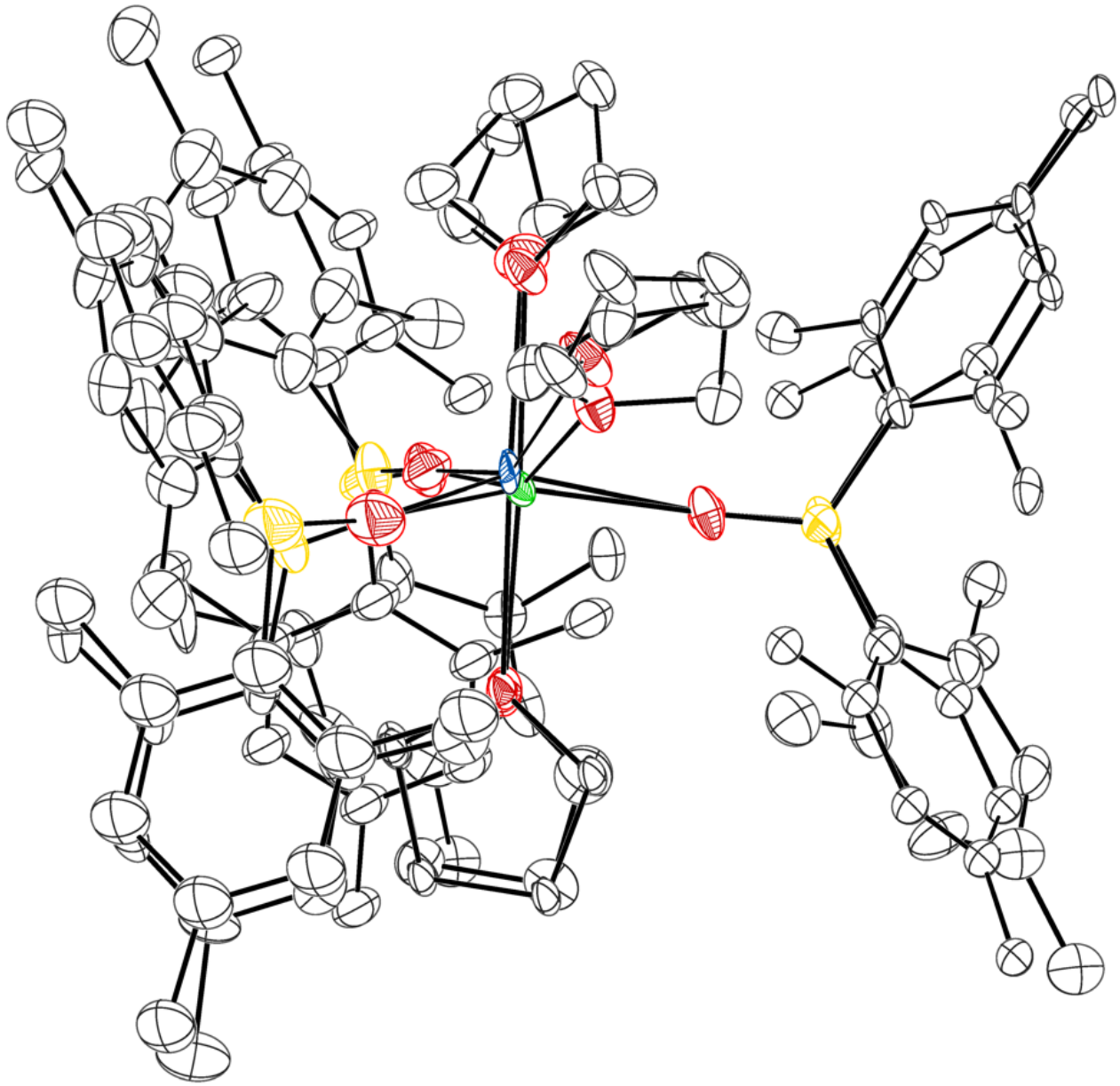

Figure 3.11. The overlapped structures of $La(OBMes_2)_3(THF)_3$, **3.2-La** and $Nd(OBMes_2)_3(THF)_3$, **3.2-Nd**, drawn at the 10% probability level**.** Hydrogen atoms and disordered atoms are not shown for clarity**.** The blue central atom is La and the green central atom is Nd.

Treatment of the Ln(III) Boroxides with Potassium Graphite (KC_8). Reductions of the $[(Mes_2BO)_2Ln(\mu\text{-}OBMes_2)]_2$ complexes, **3.1-La**, **3.1-Ce**, **3.1-Nd**, and **3.1-Gd**, as well as $La(OBMes_2)_3(THF)_3$, **3.2-La**, and with KC_8 at −35 °C in THF or Et_2O, were examined following the protocol that was successful for synthesizing $4f^n5d^1$ Ln(II) $[Ln^{II}(OAr^*)_3]^{1-}$ complexes for these metals, Scheme 1.[1–3] The reactions of **3.1-Ln** and **3.2-La** generated light orange-colored solutions in each case, which will be labelled **3.4-Ln**. Each shows a broad UV-visible absorbance near 325 nm (ϵ = 860-1270 $M^{-1}cm^{-1}$) that is absent in the spectra of **3.1-Ln** apart from the yellow **3.1-Ce** which has a broad absorbance at 337 nm (Figures 3.12 And 3.13).

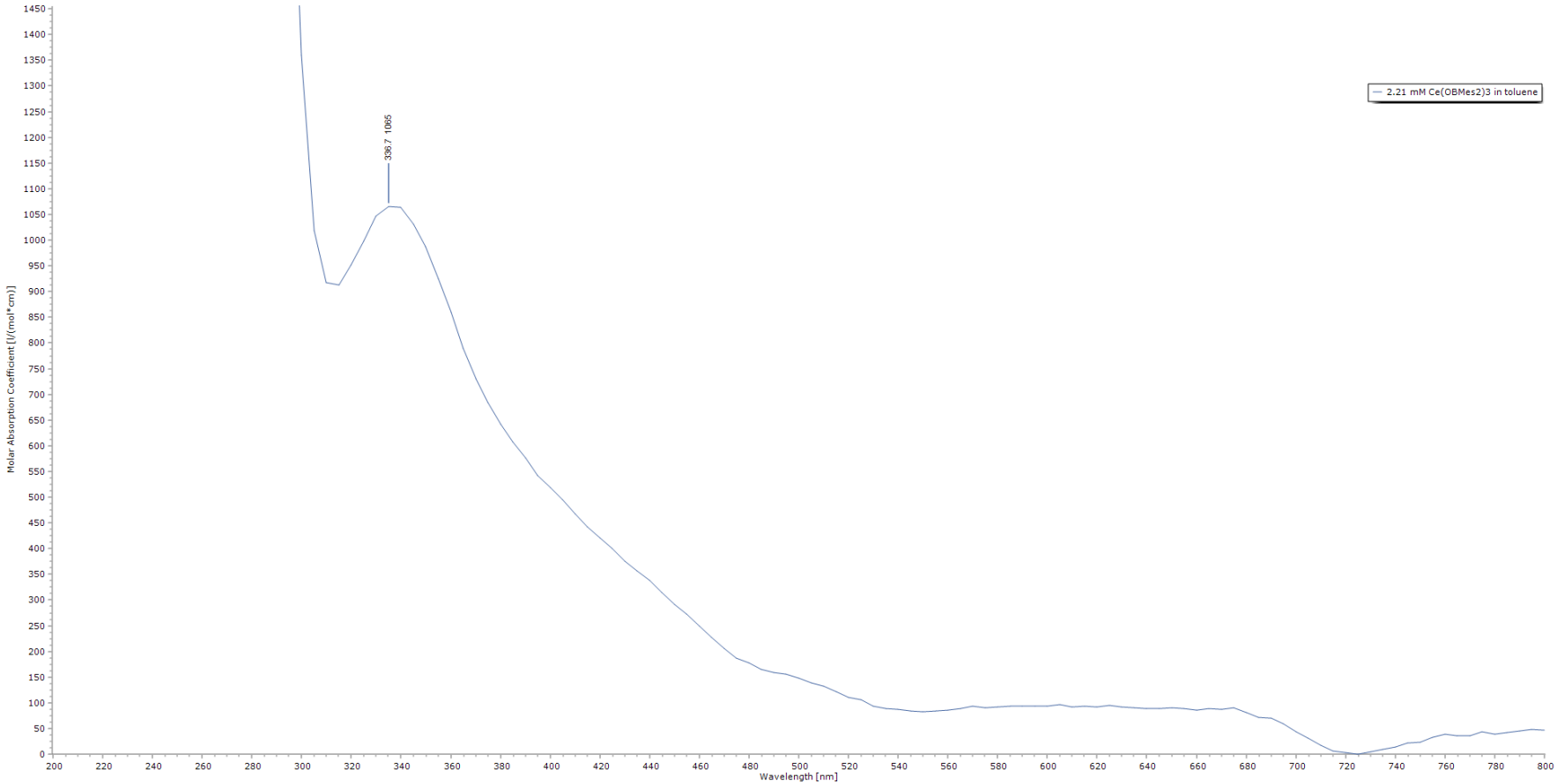

Figure 3.12. UV-Visible spectrum of a 2.2 mM toluene solution of $[(Mes_2BO)_2Ce(\mu\text{-}OBMes_2)]_2$, **3.1-Ce**

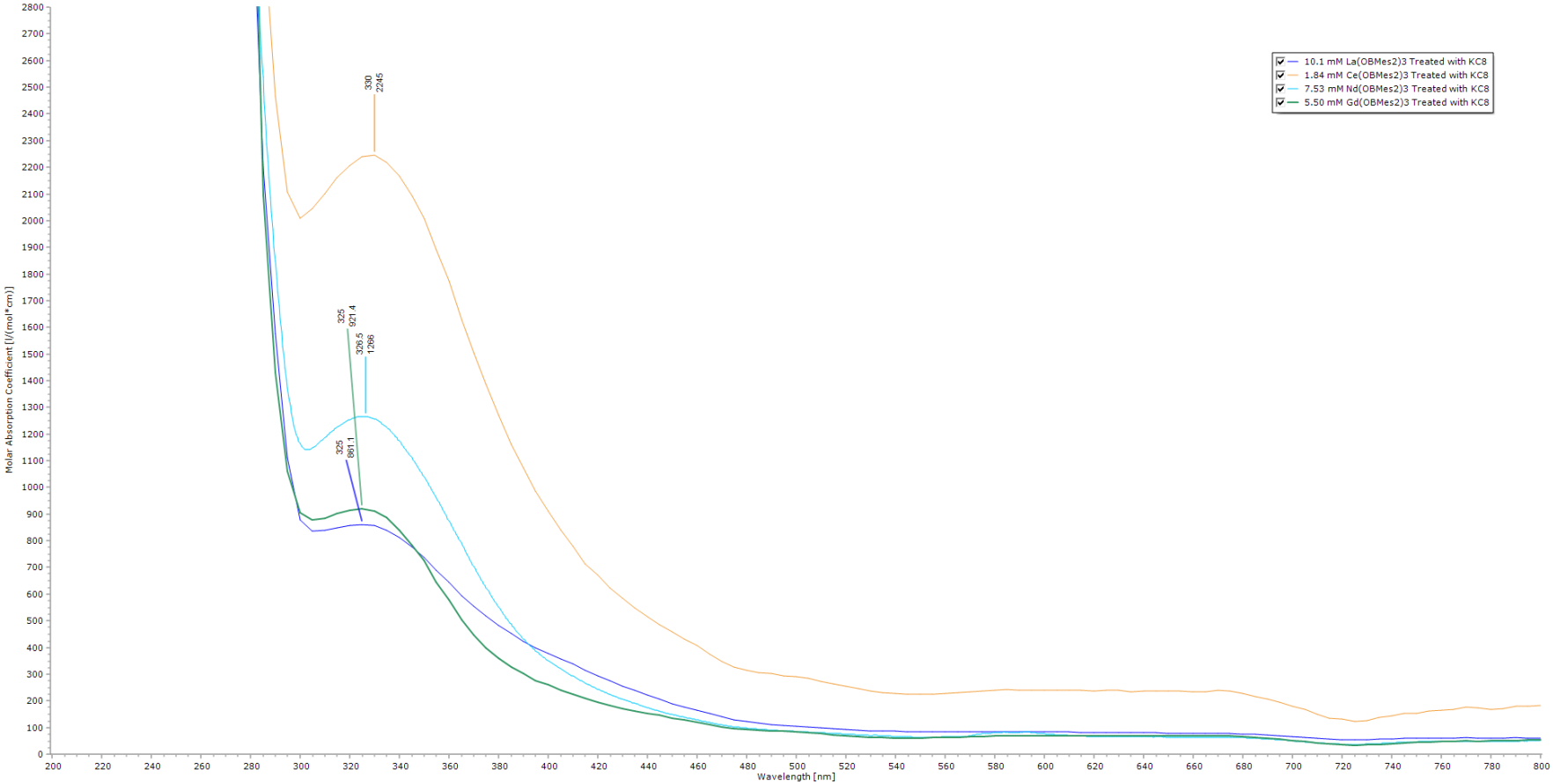

Figure 3.13. UV-Visible spectrum of toluene solution of **3.1-Ln** treated with KC_8 to produce **3.4-Ln** (Ln = La, Ce, Nd, Gd) in a 1 mm cuvette. Concentrations of each compound are given in the legend.

The color of the solutions of **3.4-Ln** is significantly different from the intense dark blue-black colors found for $[Ln^{II}(OAr^*)_3]^{1-}$ complexes of these metals, which have absorbances at 372 and 665 nm, 490 and 670 nm, 610 nm, and 570 nm for Ln=La, Ce, Nd, and Gd respectively, all of which have $\epsilon \geq 4500\ M^{-1}cm^{-1}$.[3–5] Moreover, the orange solutions did not change color with time as was even found for the remarkably stable $[(Ln^{II}(OAr^*)_3]^{1-}$ complexes. The **3.4-Ln** solutions also differed from the $(OAr^*)^{1-}$-ligated Ln(II) compounds in that they could also be generated at room temperature and in the nonpolar solvents toluene, benzene, and hexane. No evidence of an eight-line EPR pattern characteristic of the presence of an La(II) ion was observed in the reactions prepared from either **3.1-La** or **3.2-La,** Figure 3.14.

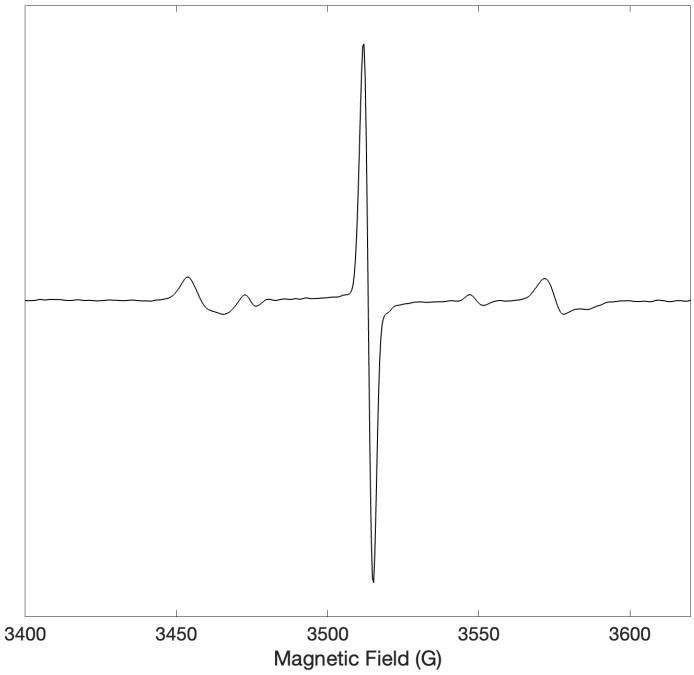

Figure 3.14. EPR spectrum of $[(Mes_2BO)_2La(\mu\text{-}OBMes_2)]_2$ treated with KC8, **3.4-La,** in toluene. Central peak $g_{iso} = 2.00$. Both sets of satellite peaks also have $g_{iso} = 2.00$ with splittings of 207.8 MHz (74.2 G) and 328.0 MHz (117.2 G).

The ^1H NMR spectrum of **3.4-La** was distinct from that of the starting material but was not informative of the identity of **3.4-La**, Figure 3.15.

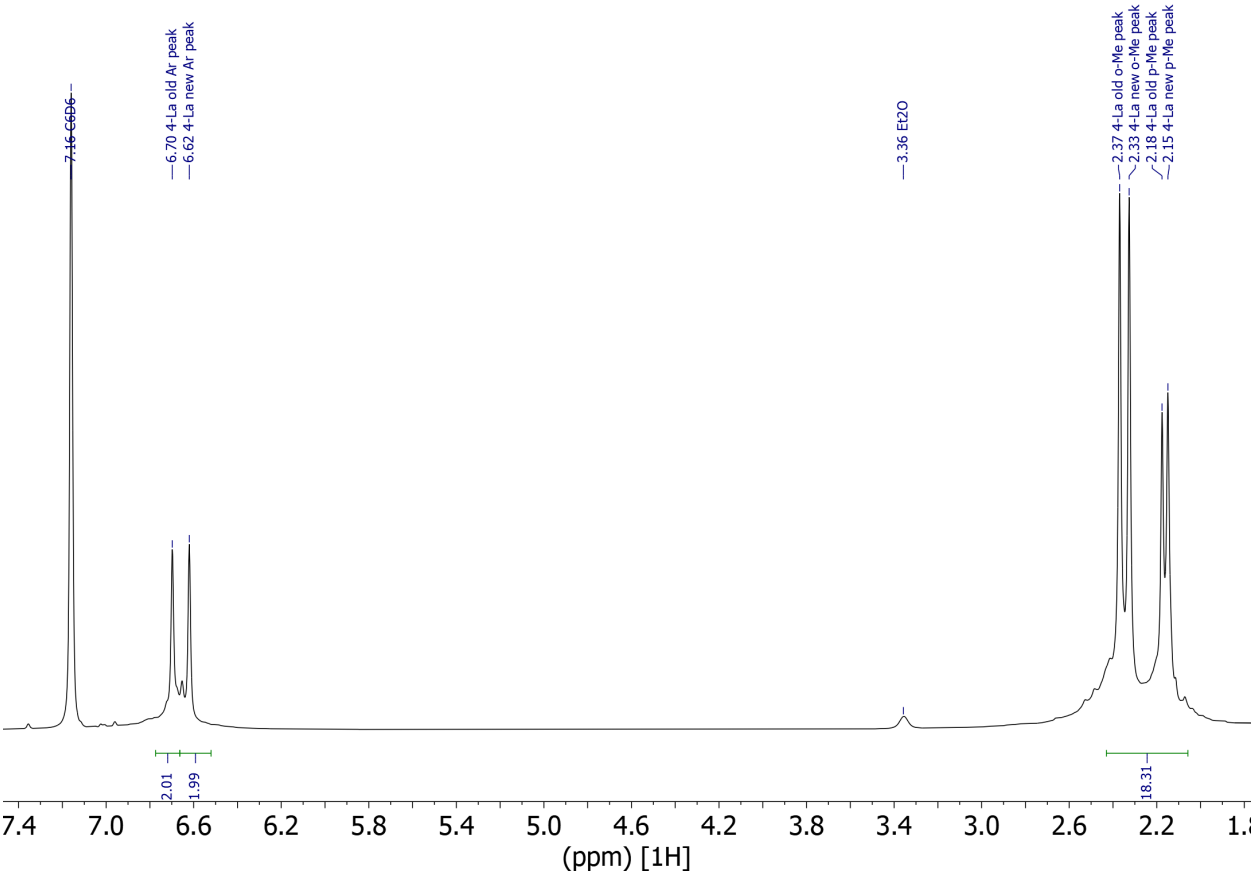

Figure 3.15. ^{1}H NMR (400 MHz, 298K) spectrum of **3.4-La** in deuterated benzene (residual proton peak marked at δ = 7.16 ppm). Note**:** Resonances of unreacted **3.1-La** appear at δ = 6.80, 2.32, 2.26, and 1.95 ppm. Residual solvent resonances for diethyl ether marked at δ = 3.36 ppm.

The KC_8 reactant was spent in these reactions, as indicated by the formation of black graphite, suggesting that reduction had occurred, but no evidence for Ln(II) products was observed. No crystallizable products were isolated from any of the reactions. Inclusion of one equivalent of 2.2.2-cryptand (crypt) during treatment of **3.1-La** with KC_8 provided a similar color change to orange, but again, no crystalline material was obtained, and ^{1}H NMR of this reaction was similar to that of **3.2-La** with new resonances of 2.2.2-cryptand present, Figure 3.16.

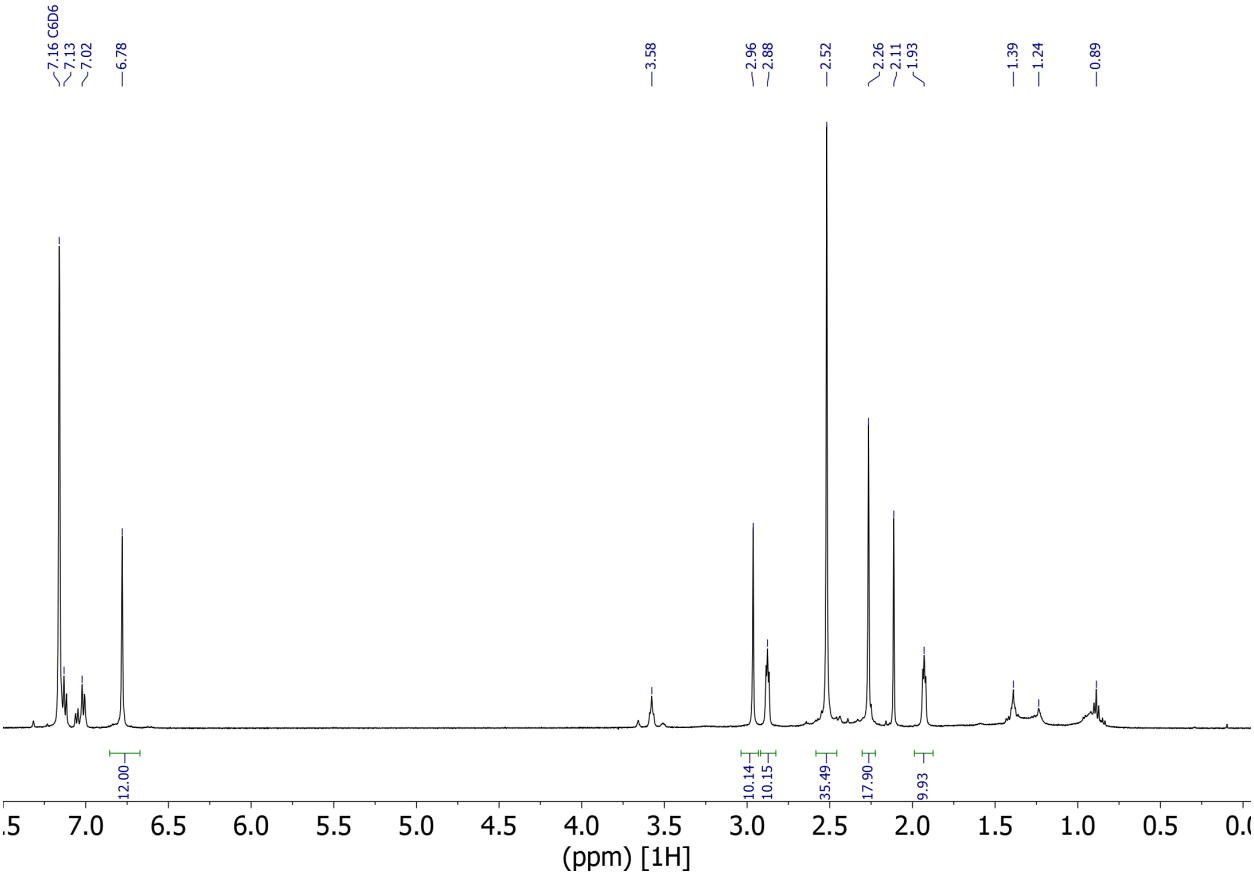

Figure 3.16. ^{1}H NMR (400 MHz, 298K) spectrum of **3.4-La/crypt** in deuterated benzene (residual proton peak marked at δ = 7.16 ppm). Note**:** Resonances of THF appear at δ = 3.58 and, 1.39, of toluene at δ = 7.13, 7.01 and 2.11, and of hexane at 1.24 and 0.89 ppm. Residual solvent resonances for diethyl ether marked at δ = 3.36 ppm.

The control reaction of $KOBMes_2$ with KC_8 did not consume the KC_8, i.e. no reduction of the ligand was observed. Hence, these boroxide complexes did not appear to be good precursors for Ln(II) compounds. This may be a result of the fact that the steric bulk of the $(OBMes_2)^{1-}$ ligand is oriented away from the metal. In contrast, with the stabilizing $(OC_6H_2Ad_2\text{-}2,6\text{-}^{t}Bu\text{-}4)^{1-}$ ligand, the bulky adamantyl groups at the 2 and 6 positions on the aryl ring are oriented to protect the metal center.[2,3] Previous studies have shown the importance of steric effects in stabilizing reduced metal centers.[2,3,28–32]

Heteroleptic Boroxide Complexes. The formation of heteroleptic boroxide complexes was explored in the reaction of $Nd(NR_2)_3$ with only one equiv of $HOBMes_2$, eq 3.3 . In this case, the heteroleptic monometallic Ln(III) boroxide complex $Nd(NR_2)_2(OBMes_2)(THF)$, **3.3**, was obtained and identified by X-ray crystallography, eq 3.3, Figure 3.17.

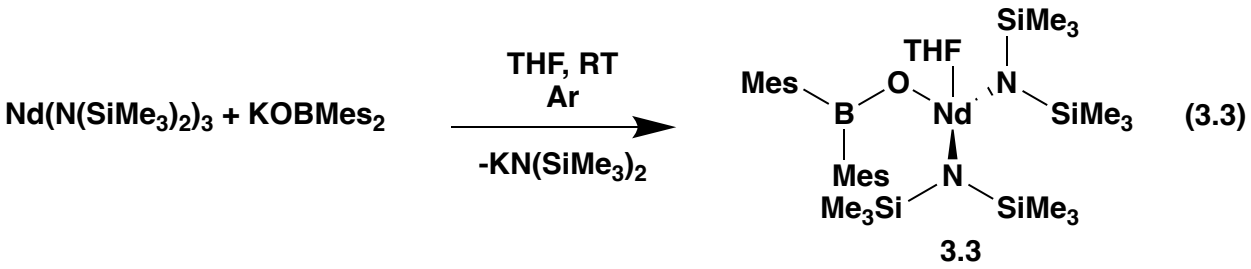

(3.3)

Complex **3.3** has a distorted tetrahedral structure with a τ_4 value of 0.80.[33] The Nd–N distances are 2.313(2) and 2.327(2) Å, Table 3.2, and are equivalent within experimental error with the analogous 2.29(2) Å Nd–N distances in $Nd(NR_2)_3$ (R = $SiMe_3$).[34]

Table 3.2. Selected Bond Distances (Å) and Angles [°] of $Nd(OBMes_2)_3(THF)_3$, 3.2-Nd, $Nd(OBMes_2)(NR_2)_2(THF)$, 3.3, and $K(\mu\text{-}OBMes_2)_2Nd(NR_2)_2$, 3.5-Nd

$Nd(OBMes_2)_3(THF)_3$, **3.2-Nd**					
Nd(1)-O(1)	2.202(6)	O(1)-Nd(1)-O(3)	108.5(3)	O(3)-Nd(1)-O(2)	139.8(3)
Nd(1)-O(2)	2.241(8)	O(1)-Nd(1)-O(4)	84.2(3)	O(3)-Nd(1)-O(4)	84.4(3)
Nd(1)-O(3)	2.232(9)	O(1)-Nd(1)-O(5)	82.6(3)	O(3)-Nd(1)-O(5)	104.4(4)
Nd(1)-O(4)	2.488(8)	O(1)-Nd(1)-O(6)	152.7(3)	O(3)-Nd(1)-O(6)	76.9(3)
Nd(1)-O(5)	2.478(9)	O(2)-Nd(1)-O(4)	82.6(3)	O(4)-Nd(1)-O(6)	123.1(3)

Nd(1)-O(6)	2.559(9)	O(2)-Nd(1)-O(5)	96.9(3)	O(5)-Nd(1)-O(4)	166.0(3)
O(1)-Nd(1)-O(2)	107.7(3)	O(2)-Nd(1)-O(6)	78.9(3)	O(5)-Nd(1)-O(6)	70.2(3)
$Nd(OBMes_2)(NR_2)_2(THF)$, **3.3**					
Nd(1)-O(1)	2.1768(2)	O(1)-Nd(1)-N(1)	109.07(6)	N(2)-Nd(1)-O(2)	132.22(5)
Nd(1)-O(2)	2.5399(2)	O(1)-Nd(1)-N(2)	105.74(6)	N(1)-Nd(1)-N(2)	115.17(6)
Nd(1)-N(1)	2.3152(2)	O(1)-Nd(1)-O(2)	95.38(6)		
Nd(1)-N(2)	2.3250(2)	N(1)-Nd(1)-O(2)	96.59(6)		
$K(\mu\text{-}OBMes_2)_2Nd(NR_2)_2$, **3.5-Nd**					
Nd(1)-O(1)	2.2655(1)	O(1)-Nd(1)-N(1)	107.45(6)	O(2)-Nd(1)-N(2)	106.24(6)
Nd(1)-O(2)	2.2297(2)	O(1)-Nd(1)-N(2)	107.58(6)	N(2)-Nd(1)-N(1)	128.18(6)
Nd(1)-N(1)	2.3718(2)	O(2)-Nd(1)-O(1)	97.53(5)		
Nd(1)-N(2)	2.3601(2)	O(2)-Nd(1)-N(1)	105.64(6)		

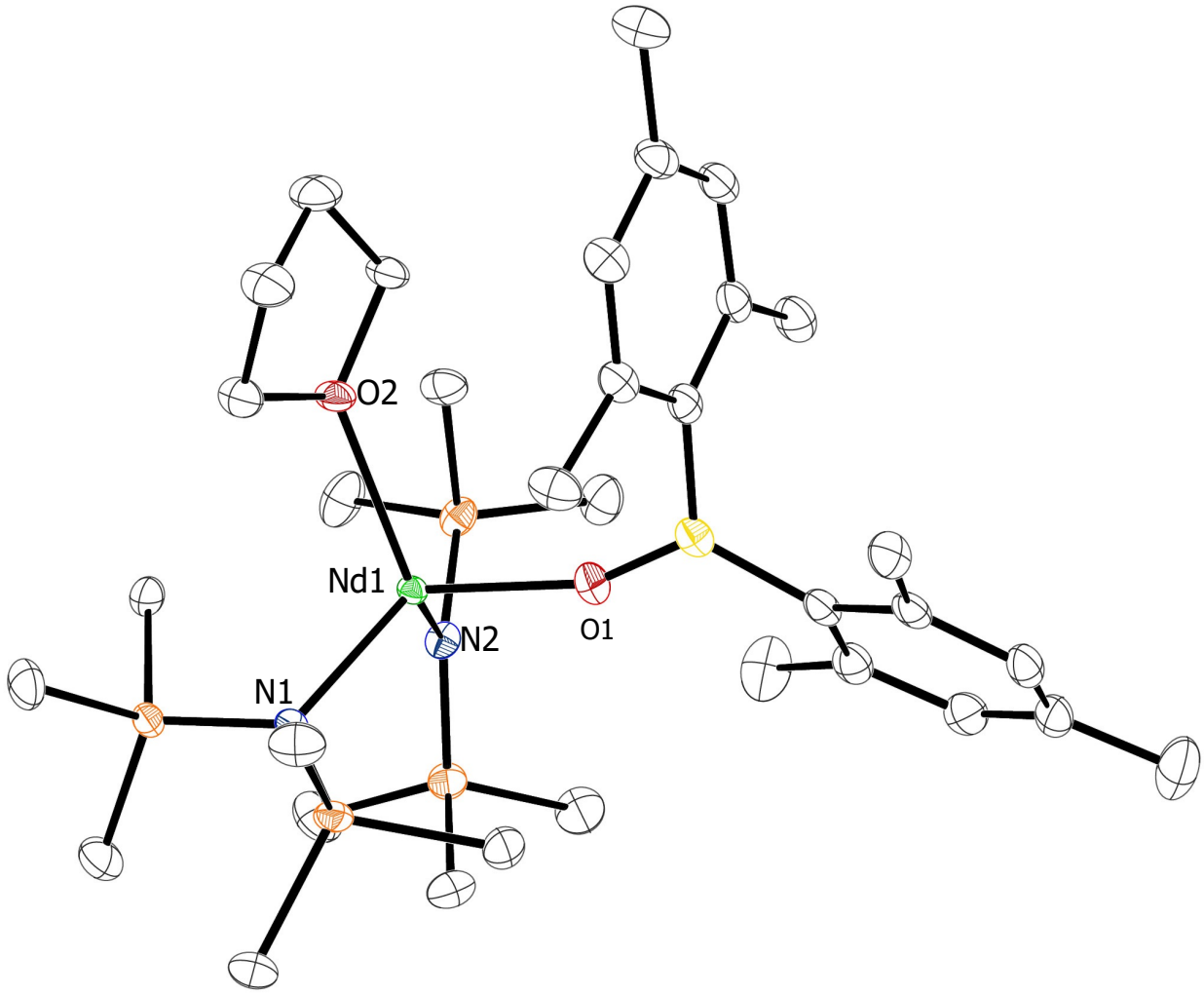

Figure 3.17. The molecular structure of $Nd(NR_2)_2(OBMes_2)(THF)$, **3.3**. Thermal ellipsoids are drawn at the 50% probability level. Hydrogen atoms are not shown for clarity.

Although $Nd(NR_2)_3$ can be reduced to form the intensely blue-colored $4f^35d^1$ Nd(II) complex $[Rb(crypt)][Nd^{II}(NR_2)_3]$,[35] reduction of the heteroleptic complex $Nd(NR_2)_2(OBMes_2)(THF)$, **3.3**, with KC_8 formed only an orange-colored solution similar to **3.4-Ln** as described above. The UV-visible spectrum of this reaction product contained only weak absorbances near 590 nm and 770 nm, like those of **3.3**, (Figure 3.18).

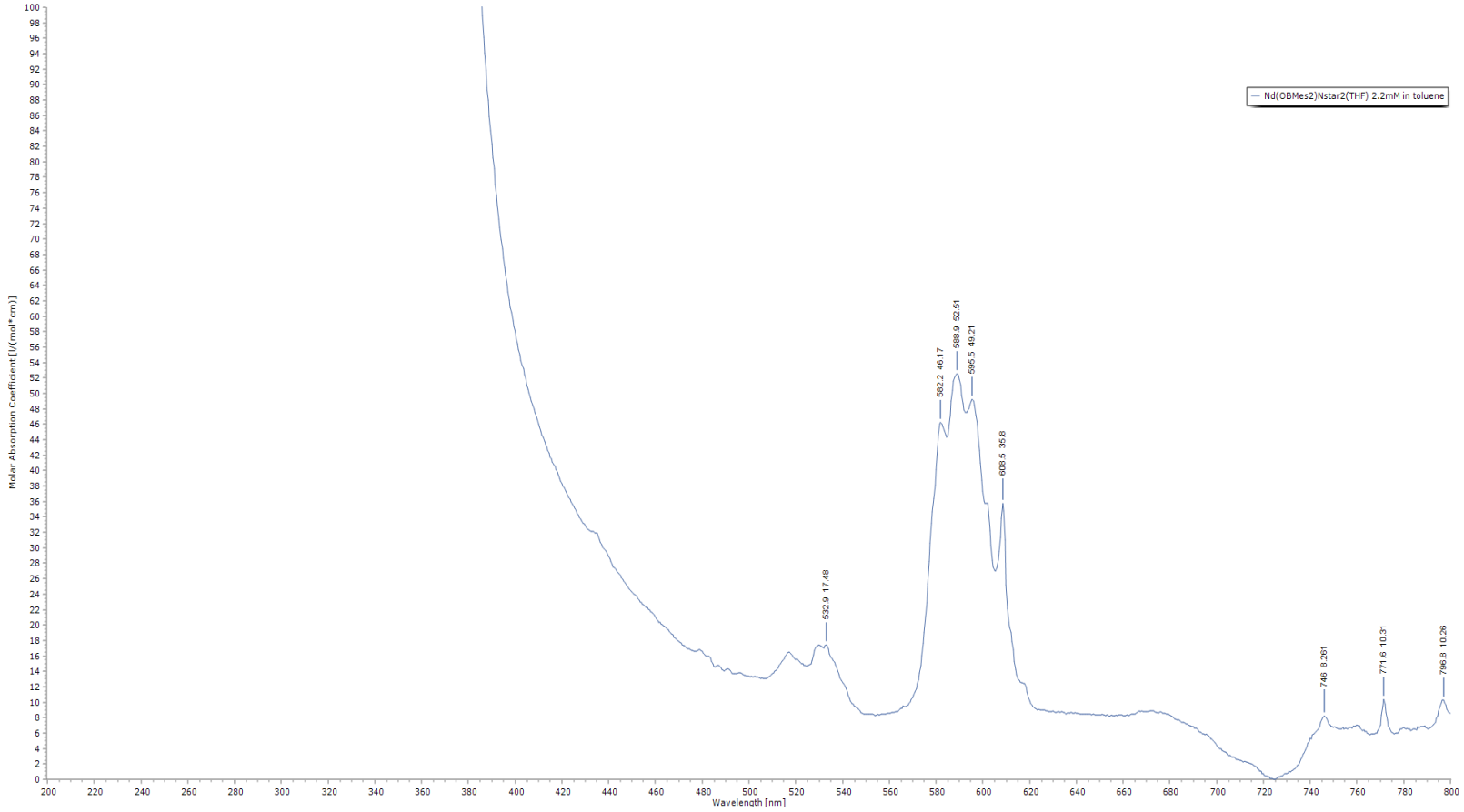

Figure 3.18. UV-Visible spectrum of a 2.2 mM toluene solution of $Nd(OBMes_2)(NR_2)_2(THF)$, **3.3**

As in the reactions above, the KC_8 was spent, which suggested that a reduction had occurred. In contrast to the reactions which generated **3.4-Ln**, a crystallographically characterizable product was isolated from this reduction reaction, the Ln(III) complex K(μ-$OBMes_2)_2Nd^{III}(NR_2)_2$, **3.5-Nd**, Figure 3.19.

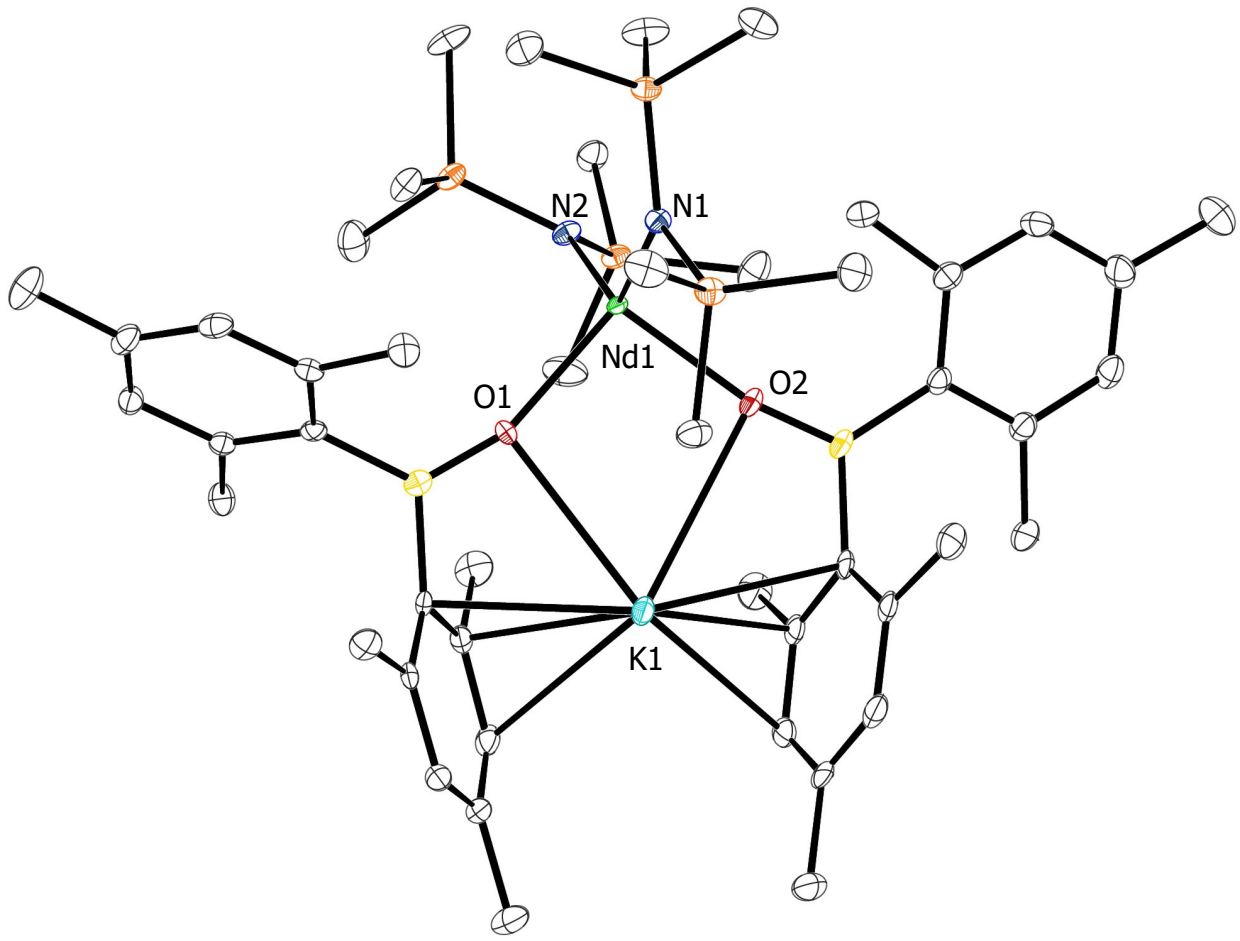

Figure 3.19. The molecular structure of K(μ-$OBMes_2)_2Nd(NR_2)_2$, **3.5-Nd**. Thermal ellipsoids are drawn at the 50% probability level. Hydrogen atoms and cocrystallized toluene solvent molecules are not shown for clarity.

Lanthanide reduction reactions of the type LnA_3/M/substrate [$(A)^{1-}$ = anion; M = alkali metal] that generate $(A_2Ln)_2$(substrate dianion) products often also lead to isolation of $(LnA_4)^{1-}$ byproducts since an $(A)^{1-}$ ligand lost by the LnA_3 starting material can combine with residual

LnA_3.[12,36–38] Complex **3.5-Nd** is a heteroleptic version of these $(LnA_4)^{1-}$ byproducts. Hence, the isolation of **3.5-Nd** is consistent with the occurrence of a reduction, but no reduced species have yet been identified. It should be noted here that a Ce(III) complex analogous to **3.5-Nd**, namely $K(\mu\text{-}OBMes_2)_2Ce(NR_2)_2$, **3.5-Ce**, was also obtained via treatment of $Ce(NR_2)_3$ with four equivalents of $KOBMes_2$ in THF (see Table 3.2 for structural comparisons).

Synthesis from NdI_2. When a mixture of 1.8 equivalents of $KOBMes_2$ and freshly prepared dark purple NdI_2[39] failed to react in toluene at room temperature overnight, the toluene was removed and the mixture was stirred in Et_2O. A light-yellow/blue solution developed that was separated from the white and purple solids from which light yellow crystals of a bridging species with an unknown central ligand was characterized, Figure 3.20.

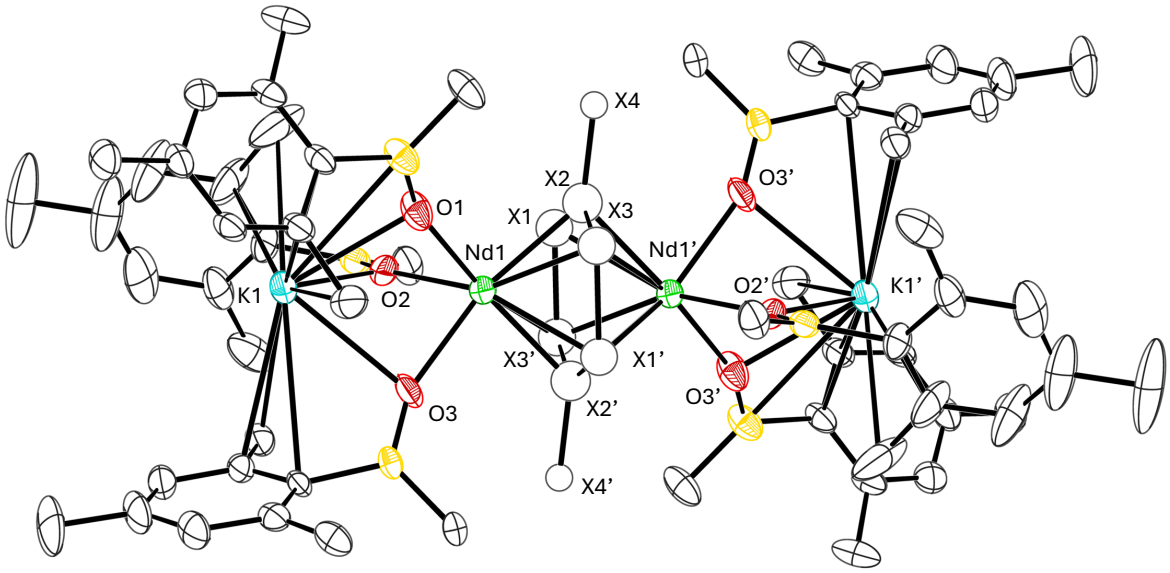

Figure 3.20. Molecular structure of **6**. Ellipsoids are drawn at the 50% probability level. Two hexane solvent molecules, hydrogen atoms, and non-ipso carbons surrounding the central ligand are not shown for clarity. Unknown atoms are given the label "X".

6 crystallizes in the $P2_1/n$ space group and only half of the molecule is present in the symmetry-independent unit cell with six unknown atoms in a ring (X1, X2, X3, X1', X2' and X3') located between two Nd ions. Each Nd is ligated by three boroxides (with O1, O2, and O3 donor

atoms) that bridge to K1. The Fourier difference map of the crystal structure data of this compound show electron densities for X1, X2, X3 and their primes of 5.27, 5.55, 5.84 e^- respectively, which is similar to the average electron density of 5.5 e^- for the rest of the carbon atoms in the molecule. This suggests that these atoms could be carbon. However, when the X atoms are refined as carbon atoms, the ring is centered between the two Nd ions at a Nd-Cnt_{X6} distance of 1.687 Å. This is much shorter than any reported Nd-centroid distance[40–43] In addition this refinement gives the unreasonable "C-C" bond lengths of 1.248(1), 1.579(1) and 1.949(1) Å and unusual "C-C-C" angles of 105.1(5), 120.6(7), and 130.7(7)°, Figure 3.21. Furthermore, X4 shows a density of 13.4 e^-, which could correspond to one Na atom or 0.5 of a K atom arising from half-occupancy. Hence, X4 is possibly a disordered alkali metal. Additionally, previous reports of complexes of doubly and quadruply reduced arene rings have an intense color and typically contain bond lengths different than those observed in the structure of **6**.[10] Atom X4 protrudes about 3.08° from the plane of the ring and is located at a distance of 1.741(8) Å from X2 with X1-X2-X4 and X3-X2-X4 angles of 102.7(5)° and 130.4(7)° respectively. This ring also exhibits a distortion with a torsion angle of 21.8(1)°.

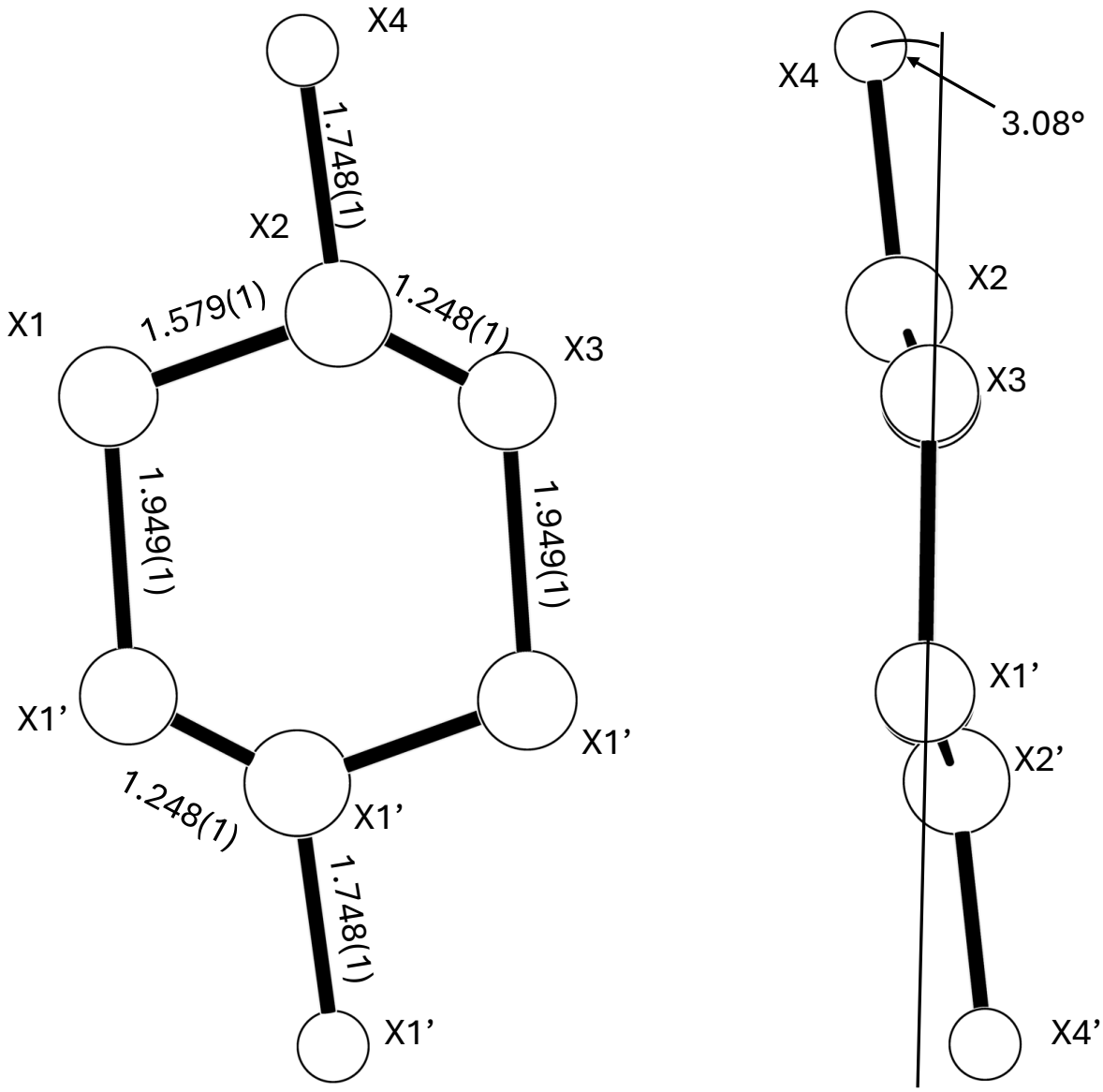

Figure 3.21. Graphical representation of the moiety found between Nd and Nd' in the crystal structure of **6**. Ellipsoids are drawn isotropically.

The Nd-O bonds in **3.6** are shorter than Shannon radii predicted lengths, ranging from 2.232(4) to 2.249(4) Å, but are not unusual when compared to Nd^{III}-$O_{boroxide}$ bonds found in complexes **3.1-Nd**, **3.3**, and **3.5-Nd,** which range from 2.156(5) (**3.1-Nd** terminal boroxide) to

2.651(1) Å (**3.5-Nd** bridging boroxide). Similarly, the O-B bond lengths of 1.309(9), 1.317(8) and 1.328(9) Å are similar to those in **3.5-Nd**.

At no time were benzene, sodium, nor any sodium compound intentionally included in this reaction. Any benzene present may have been extracted from the atmosphere of the glovebox. However similar chemistry deliberately including benzene has been seen in research in the Arnold group with $[(Mes_2BO)_2U(\mu\text{-}OBMes_2)]_2$.[10] These complexes, $[(OBMes_2)_3U]_2(\mu{-}\eta^6,\eta^6\text{-}C_6H_6)$ and $[(dmpm)(OBMes_2)_2U]_2$ $(\mu{-}\ \eta^6,\eta^6\text{-}C_6H_5R)$ (dmpm = bis(dimethylphosphino)methane; R = H or Me), both feature bound and reduced arene rings, but differ from **6** in that they do not contain bound countercations and require the addition of $P(C_6H_{11})_3$ as a catalyst or contain dmpm as a ligand, respectively. Moreover, the average $C\text{-}C_{bridging\ aryl}$ bond lengths in these complexes are equidistant at 1.412(2) Å (doubly reduced arene), 1.401(8) (triply reduced arene) and 1.434(2) (quadruply reduced arene).[10]

Additionally, from this reaction, light blue crystals of $[K(\mu\text{-}OBMes_2)_2][K(\mu\text{-}OBMes_2)_3]Nd$ were recovered, complex **3.7**, Figure 3.22. Complex **3.7** is a structural isomer of $[K(\mu\text{-}OBMes_2)_2]_2Nd(OBMes_2)$, **3.8**, that was also obtained separately and unexpectedly from the treatment of $NdCl_3$ with three equivalents of $KOBMes_2$ in THF. However, this structure features a different space group and the axial boroxide ligand forms a bridging bond via an oxygen atom with one of the potassium molecules, Figure 3.23. It is also worth mentioning that an isomorphous crystal of the Gd analog of compound **6** was collected, although crystallographic data for this compound was of poor quality and will not be discussed here.

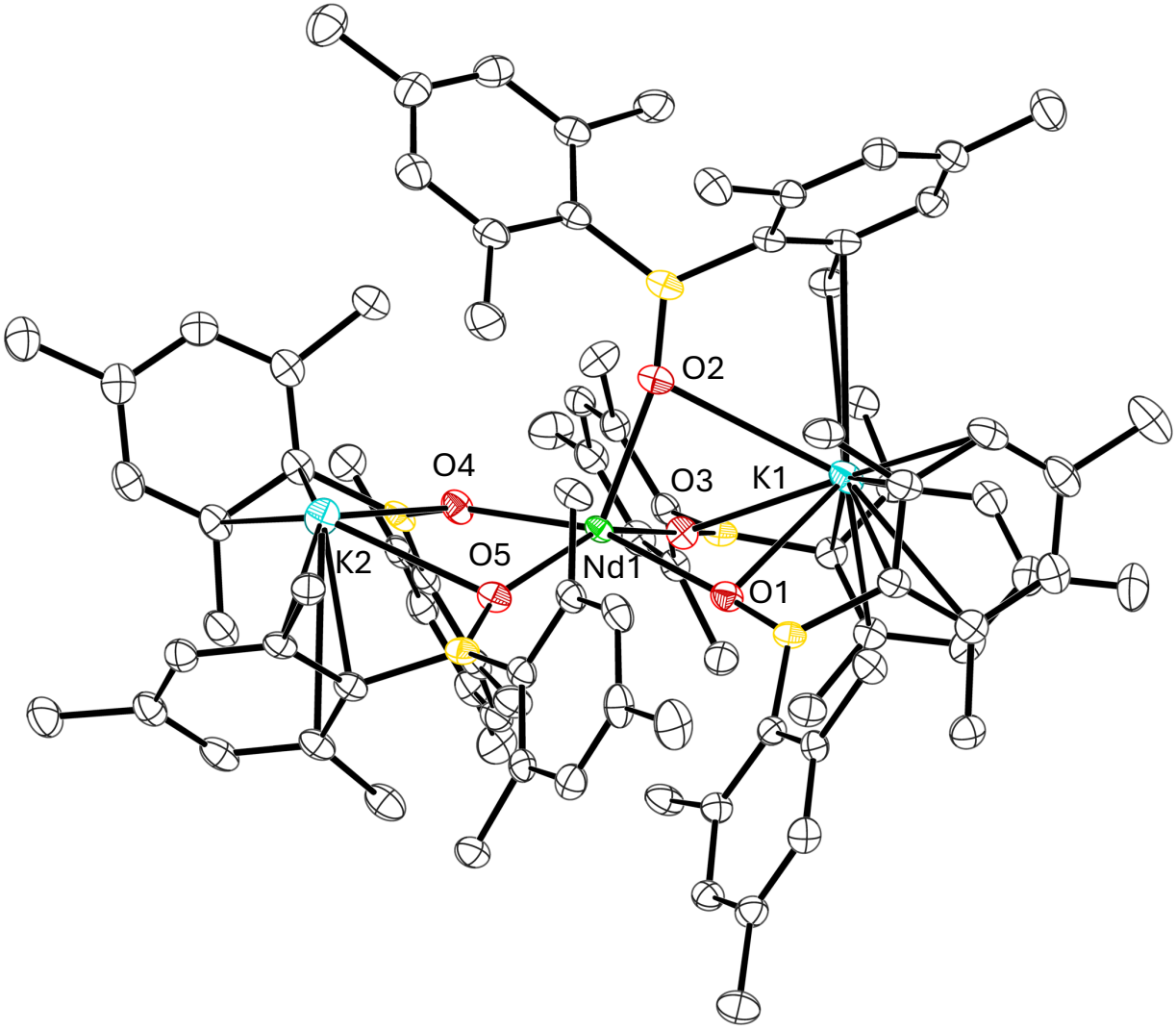

Figure 3.22. Molecular structure of [K(μ-OBMes$_2$)$_2$][K(μ-OBMes$_2$)$_3$]Nd, **3.7**, in the *P*-1 space group. Ellipsoids are drawn at the 50% probability level and a single hexane solvent molecule and all hydrogen atoms is not shown for clarity.

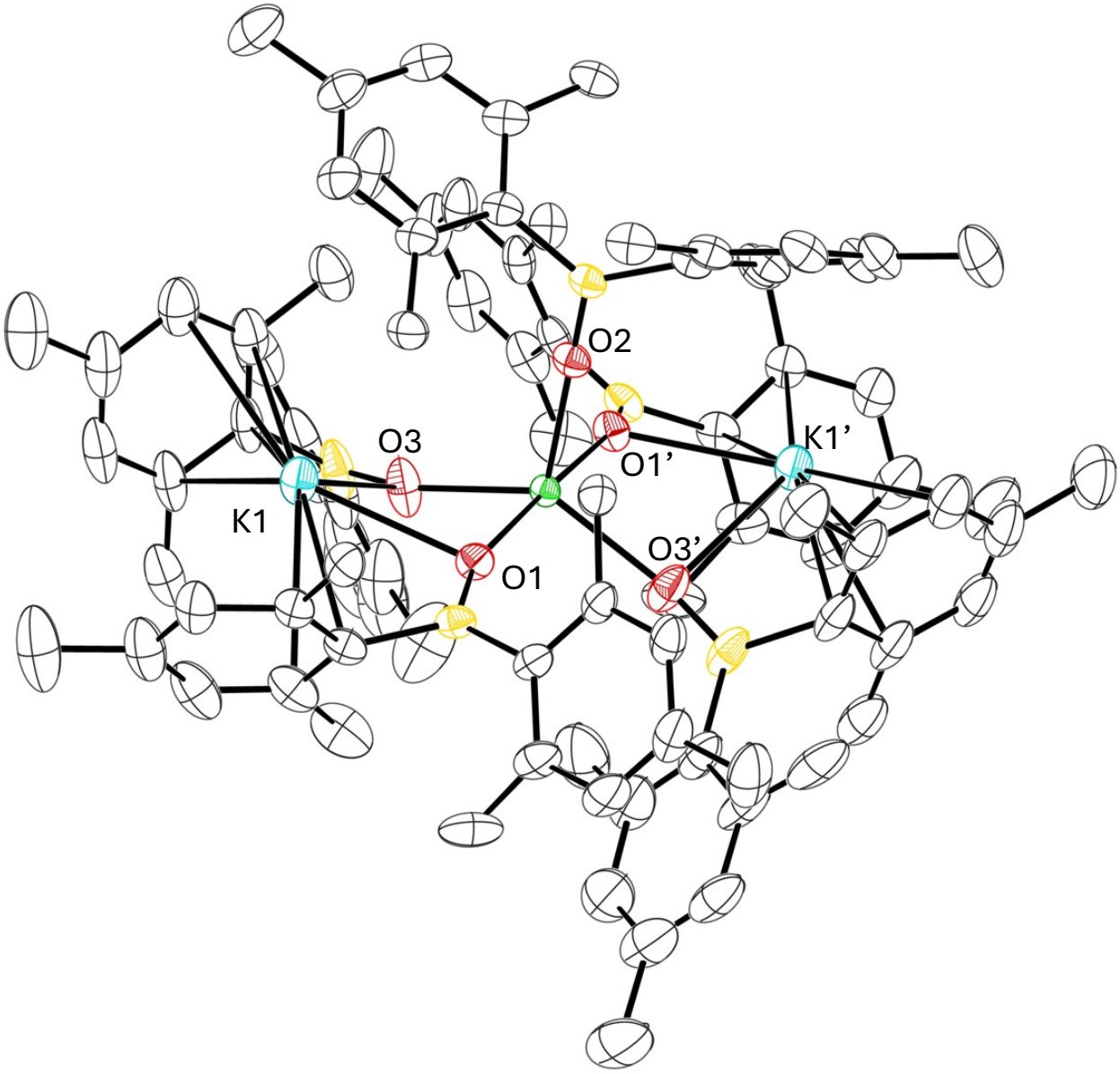

Figure 3.23. Molecular structure of $[K(\mu\text{-}OBMes_2)_2]_2Nd(OBMes_2)$, **3.8** in the *C*2/c space group. Ellipsoids are drawn at the 50% probability level and a single hexane solvent molecule and all hydrogen atoms is not shown for clarity.

Although occupying different space groups, both **3.7** and **3.8** feature five boroxide ligands bound to the central Nd atom and two encapsulated K ions. **3.8** is centrosymmetric about the Nd-($O_{terminal\ boroxide}$) axis and consists of O-B bonds of nearly identical lengths to **3.7** ranging from

1.333(3) (complex **3.8**) to 1.339(3) Å (complex **3.7**). The formation of **3.7** may have come from the higher solubility of $KOBMes_2$ in Et_2O compared to that of NdI_2, resulting in a higher concentration of ligand in solution than expected.

Synthesis From $SmI_2(THF)_2$. The reaction of $SmI_2(THF)_2$ with $KOBMes_2$ was examined to determine if Ln(II) boroxide complexes could be made directly from a Ln(II) precursor. When a deep blue solution of $SmI_2(THF)_2$ in THF was treated with two equivalents of light yellow $KOBMes_2$ in THF solution, it immediately turned black. Crystallization produced black solids of the oxo cluster, $Sm_4(OBMes_2)_6(\mu_4\text{-O})$, **3.9**, Figure 3.24, eq 3.4. In one reaction, a few colorless crystals of a Sm(III) complex, $[K(\mu\text{-}OBMes_2)_3Sm(OBMes_2)(THF)]$, **3.10**, Figure 3.25, were also isolated. This complex is included because it is another example of a lanthanide boroxide that has incorporated potassium as in **3.5-Ln**. Complex **3.9** has an intense absorption in the UV-visible spectrum at 422 nm with an extinction coefficient of 8000 $cm^{-1}M^{-1}$, Figure 3.26 .

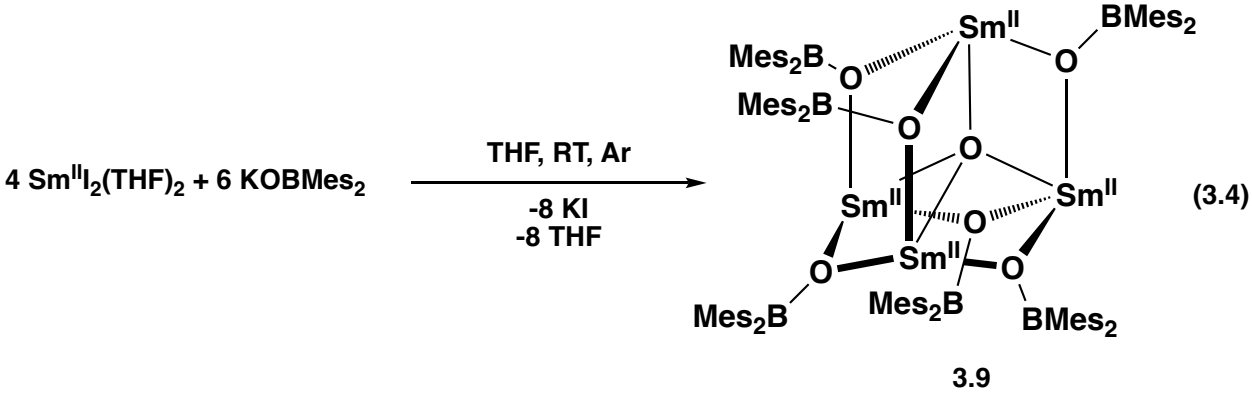

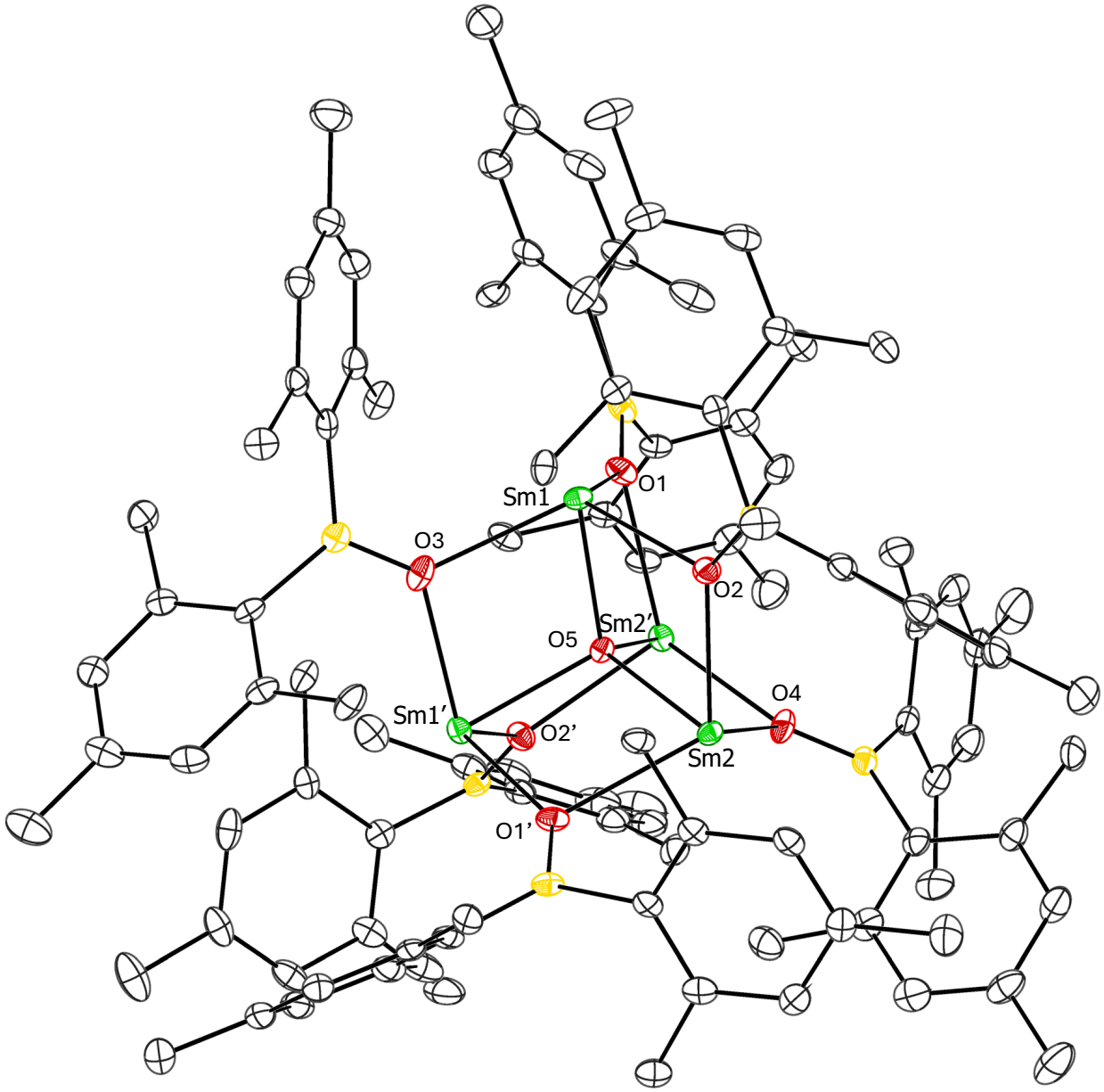

Figure 3.24. The molecular structure of $Sm_4(OBMes_2)_6(\mu_4\text{-}O)$, **3.9**. Thermal ellipsoids are drawn at the 30% probability level. Hydrogen atoms and the hexane solvent molecule are not shown for clarity.

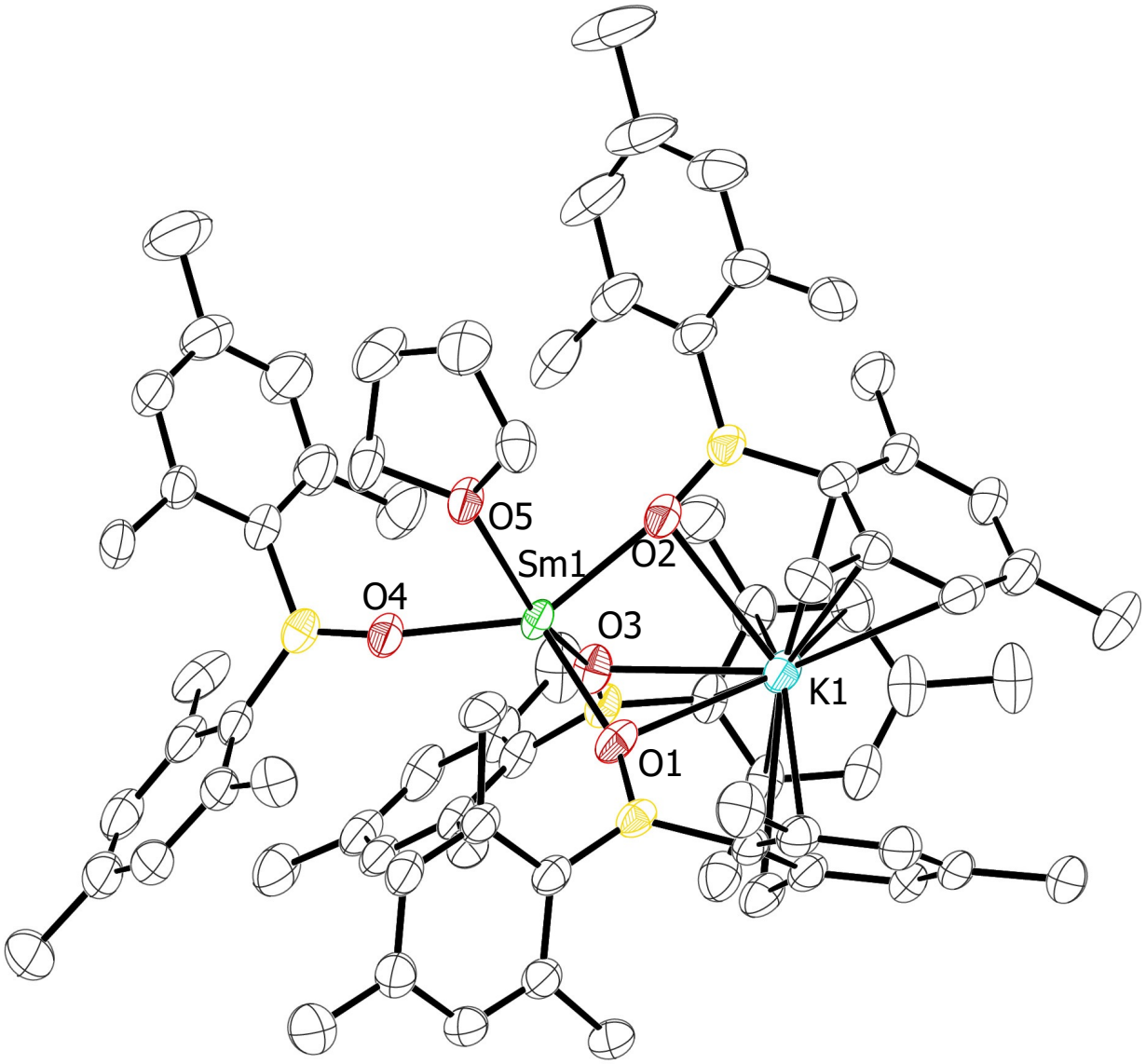

Figure 3.25. The molecular structure of [K(μ-OBMes$_2$)$_3$Sm(OBMes$_2$)(THF)], **3.10**. Thermal ellipsoids are drawn at the 30% probability level. Hydrogen atoms and the hexane solvent molecule are not shown for clarity.

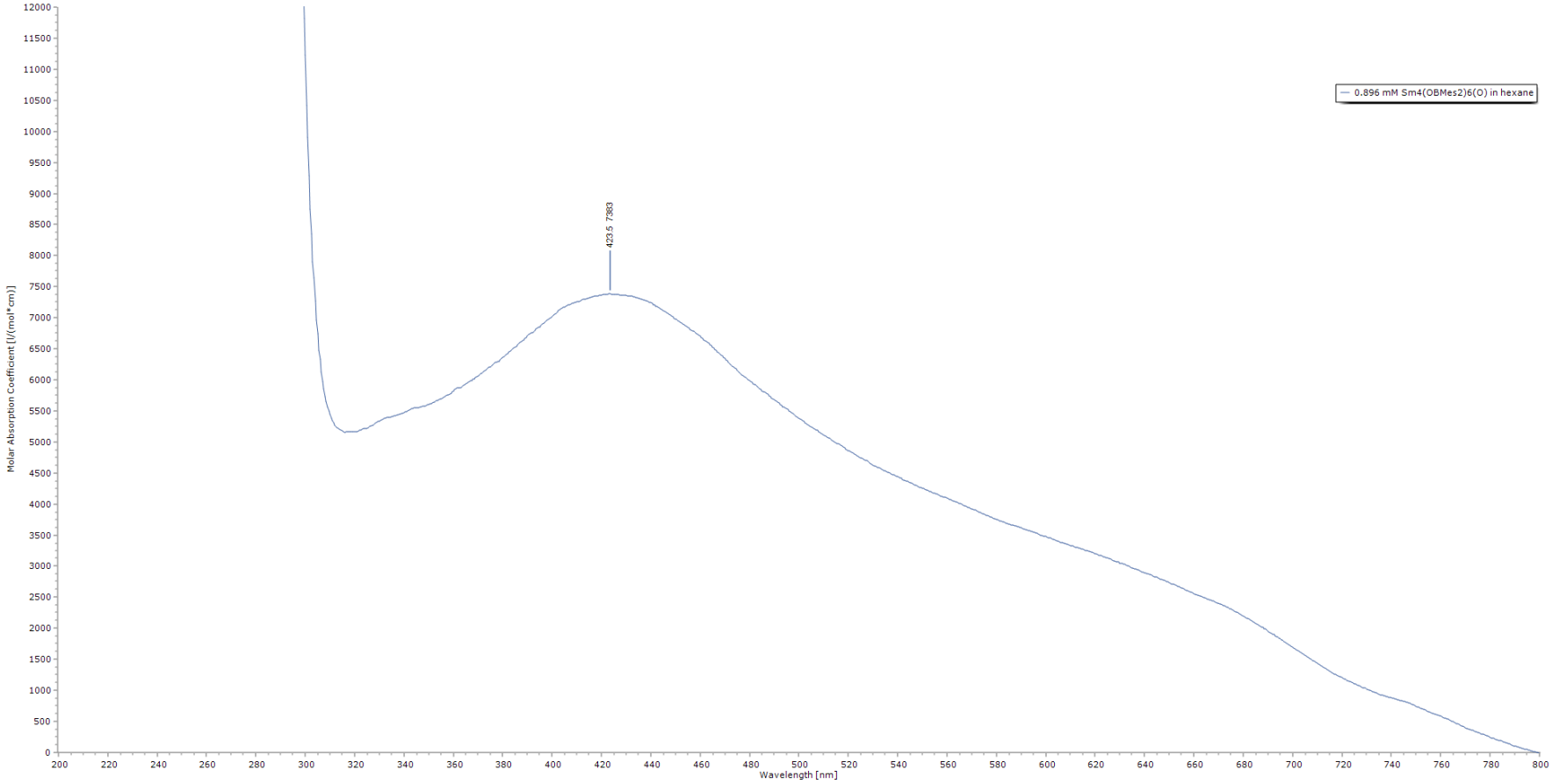

Figure 3.26. UV-Visible spectrum of a 0.90 mM hexane solution of $Sm_4(OBMes)_6(\mu_4\text{-}O)$, **3.9** in a 1 mm cuvette.

The $Sm_4(OBMes_2)_6(\mu_4\text{-}O)$ cluster crystallizes in the tetragonal space group $P4_32_12$ and its formulation is consistent with four Sm(II) ions that retain the oxidation state of the $SmI_2(THF)_2$ starting material. The isolation of a Sm(III) byproduct is consistent with the generation of the oxide from reduction by Sm(II), but the reaction stoichiometry is likely to be more complicated. It is also possible that the oxide could arise from condensation between $KOBMes_2$ ligands to form $Mes_2BOBMes_2$ and formally K_2O.[11]

The four Sm atoms in **3.9** are arranged in a tetrahedron. Each is ligated by three bridging $(OBMes_2)^{1-}$ anions and a bond to the central encapsulated O^{2-} dianion in an adamantane-like geometry with $\tau_{4[Sm(1)]} = 0.91$ and $\tau_{4[Sm(2)]} = 0.90$.[33] An analogous structure has been reported previously for $Ba_4(\mu\text{-}OBMes_2)_6(\mu_4\text{-}O)$,[11] although the barium compound is not isomorphous with **3.9**. This specific adamantane geometry with a caged $(O)^{2-}$ anion is also known for Pb(II)[44] and has been seen in other Ln(III) complexes (Table 3.3)[45–54] There are two sets of two symmetry equivalent Sm–(μ_4-O) bonds of lengths 2.313(3) and 2.320(5) Å and five unique Sm-O(bridging boroxide) bonds ranging from 2.449(4) to 2.526(5) Å. The complex features four very similar B–O bond lengths ranging from 1.323(8) to 1.345(10)Å, which fall in the range of analogs in **3.1-Ln** between the longest bridging B–O and shortest terminal B–O bonds of **3.1-Ln** (1.393 and 1.308 Å respectively).

Table 3.3. Complexes with O^{2-}-Encapsulated Adamantane-Like Structures
$\{Sc_4(\mu_4\text{-}O)(L_4H_{1.5})_3[L_4H(Na(NCMe)_{1.5})_{0.5}](NCMe)_3\}\cdot 19MeCN$ (L^4 = *p-tert*-butylcalix[4]arene)[54]
$[Ln_4(\mu_4\text{-}O)(\mu_2\text{-}OH)_2(\mu_2\text{-}L)_6][A]_2$ (Ln = Y, Eu-Lu, L = $[OC_6H_2\text{-}4\text{-}Me\text{-}2,6\text{-}(CHO)_2]^{1-}$, A = ClO_4, CF_3SO_4)[53]

$Dy_4(\mu_4\text{–}O)L_2(HL)_2(CH_3O)_4\bullet 4CH_3OH\bullet H_2O$ (L = 2-hydrazino benzothiazole)[47]
$La_4(\mu_4\text{-}O)(O_2CN^iPr_2)_{10}$[50]
$Yb_4(\mu_4\text{-}O)L_8(OH)_2$ (L= (benzothiazol2-yl)phenol)[51]
$Gd_4(\mu_4\text{-}O)L_5\bullet H_2O$ (L = 2-(Diphenylphosphinoylmethyl)tetrahydropyran-3,4-diol)[52]
$Ce_4(\mu_4\text{-}O)(\mu_2\text{-}O)_4(\mu_2\text{-}OH)_2(L)_4$ (L=$Co(\eta^5\text{-}C_5H_5)\{P(O)(OEt)_2\}_3$)[49]
La_4 (μ_4-O)L_{10} (L = acetylacetonate)[55]
$[Lu_4(\mu_4\text{-}O)(DBM)_6(L)_2]_2\bullet$ 6 C_7H_8 (DBM = dibenzoyl methane, L = 2-[{3-hydroxypropyl}methylamino]phenol)[46]
$[\{Ln(L)\}_4(\mu_2\text{-}OCH_3)_6(\mu_4\text{-}O)]$ (Ln = Pr-Tb, except Pm, L = 3-Nitrotrispyrazolylborates)[45]

The Sm(III) center in $[K(\mu\text{-}OBMes_2)_3Sm(OBMes_2)(THF)]$, **3.10,** is ligated by three boroxide ligands that bridge to the potassium cation through their oxygen atoms, one terminal boroxide, and one THF ligand. Additionally, aryl rings on each of the three bridging boroxide ligands are oriented toward potassium ion with K–C_{aryl} distances of 2.999(3), 3.029(3), and 3.066(3) Å for the closest carbons compared to the range of 3.113(3) to 4.993(3) Å for the rest of the K-C_{aryl} distances (see Table 3.4). As was seen with **3.5-Nd** and **3.5-Ce**, the potassium ion is encapsulated by the boroxide ligands. The four B–O distances in **3.10** are virtually identical and fall in the narrow range of 1.330(4)–1.335(4) Å.

Table 3.4. Selected Bond Lengths for $K(\mu\text{-}OBMes_2)_3Sm(OBMes_2)(THF)$, 3.10.

Atom	Atom	Length/Å
K1	O1	3.076(2)
K1	O2	2.903(2)

Table 3.4. Selected Bond Lengths for K(μ-OBMes$_2$)$_3$Sm(OBMes$_2$)(THF), 3.10.		
K1	O3	2.852(2)
K1	C6	3.234(3)
K1	C9	3.126(4)
K1	C19	3.029(3)
K1	C23	3.341(3)
K1	C24	2.999(3)
K1	C37	3.066(3)
K1	C38	3.430(3)
K1	C41	3.428(4)
K1	C42	3.113(3)

Reactivity of the Sm(II) Boroxide Cluster. To determine if the open spaces around the four Sm(II) ions in Sm$_4$(OBMes$_2$)$_6$(μ_4-O) would coordinate another ligand, complex **3.9** was treated with four equivalents of xylyl isocyanide, CNXyl (Xyl = 2,6-Me$_2$C$_6$H$_4$) in hexane. The black color changed to light yellow over about two h at room temperature and provided light yellow crystals. Although the crystallographic data are only of sufficient quality to discuss connectivity, they showed that these crystals, **3.11**, contained two co-crystallized Sm(III) complexes: Sm(OBMes$_2$)$_3$(CNXyl)$_3$, with central metals labeled Sm1 in Figure 3.27 and Sm(OBMes$_2$)$_3$(CNXyl)(Et$_2$O) labeled Sm2. The latter complex has a nearly trigonal bipyramidal geometry with the three boroxide ligands in the equatorial positions with a τ_5 value of 0.78.[56] The complex containing Sm(1) has a distorted six coordinate structure like that of **3.2-Ln**. These two co-crystallized complexes exhibit a π-stacking motif between the xylyl group of one of the

disocyanide ligands bound to Sm(1) with a xylyl isocyanide bound to Sm(2). Although the samarium ions were oxidized from +2 to +3, it is unclear what was reduced in this reaction.

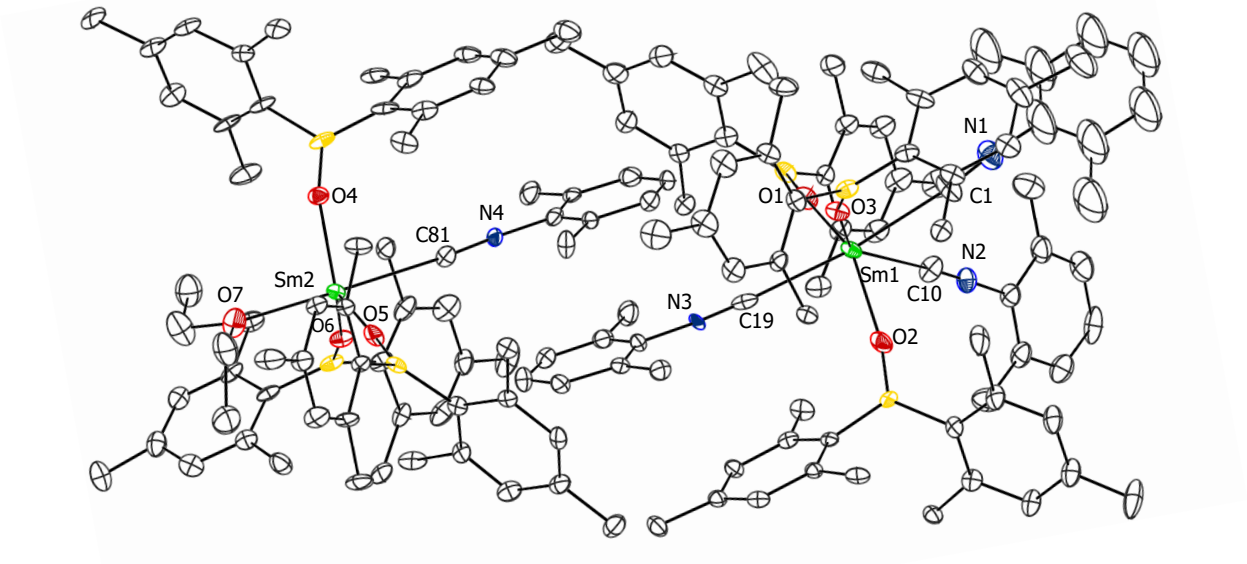

Figure 3.27. The molecular structure of $Sm(OBMes_2)_3(Et_2O)(CNXyl)\bullet Sm(OBMes_2)_3(CNXyl)_3$, **3.11**. Thermal ellipsoids are drawn at the 50% probability level. Atoms modeled with disorder and hydrogen atoms are not shown for clarity.

DISCUSSION

The coordination chemistry of the di(mesityl)boroxide ligand with the lanthanides has proven to be complicated. Initial salt metathesis reactions between lanthanide chlorides and $KOBMes_2$ gave complicated compositions that appeared to contain chloride and potassium in structures that were disordered and not resolvable. Reactions of the tris(silylamide) complexes, $Ln(NR_2)_3$ (R = $SiMe_3$), with $HOBMes_2$, generated crystalline products of $[(Mes_2BO)_2Ln^{III}(\mu\text{-}OBMes_2)]_2$, **3.1-Ln**, that demonstrated the propensity of the mesityl rings to coordinate metals since the bimetallic products contained Ln–aryl interactions. Single crystals of the four **3.1-Ln** complexes incorporated different amounts of lattice solvent, from one to eleven molecules of

hexane, such that none were isomorphous even though the metals were similar in size. In addition, none of the **3.1-Ln** compounds had a structure isomorphous to the previously reported $[(Mes_2BO)_2U(\mu\text{-}OBMes_2)]_2$.[10]

Monometallic complexes with simple terminally-bound boroxide ligands, $Ln(OBMes_2)_3(THF)_3$, **3.2-Ln**, could be obtained from $LaI_3(THF)_{3.5}$ and $KOBMes_2$, or from the reaction of **3.1-Nd** with THF to form **3.2-Nd**. Complex **3.2-La** was found to crystallize in an incommensurately modulated orthorhombic unit cell with a meridional octahedral molecular structure similar to that of **3.2-Nd** which crystallized in a monoclinic unit cell. A monometallic heteroleptic complex, $Nd^{III}(NR_2)_2(OBMes_2)(THF)$, **3**, was also isolated for comparison with readily reduced $Ln(NR_2)_3$ complexes.[35] This complex crystallized without the problems of **3.1-Ln** and **3.2-Ln** with no solvent molecules present in the crystal lattice.

While the reduction of these complexes with KC_8 did not provide the expected Ln(II) complexes that are readily accessible from other ligand systems, these reactions provided a variety of unusual structures. Likewise, the reduction of the heteroleptic $Nd(NR_2)_2(OBMes_2)(THF)$, **3.3**, did not give an isolable Ln(II) product although the closely related $Nd(NR_2)_3$ forms $[Nd(NR_2)_3]^{1-}$ complexes. However, the crystalline product isolated from this reduction, $K(\mu\text{-}OBMes_2)_2Nd(NR_2)_2$, showed the propensity of the mesityl rings to coordinate potassium as well as the lanthanide ions in **3.1-Ln**. This tendency to incorporate potassium was subsequently observed in attempts to make Ln(II) boroxide complexes from SmI_2: the side product $[K(\mu\text{-}OBMes_2)_3Sm(OBMes_2)(THF)]$, **3.10**, also incorporated potassium. Hence, in addition to the structural complexities of the potassium-free **3.1-Ln** and **3.2-Ln**, lanthanide boroxides can readily incorporate alkali metal cations. While it can be concluded that the structural chemistry of

lanthanide boroxides is quite complex, the tendency of the $(OBMes_2)^{1-}$ ligand to incorporate alkali metal ions proved to be useful in the reactions discussed in Chapter 4.

The Sm(II) boroxide chemistry was even more complicated. A Ln(II) boroxide compound was obtainable by reacting SmI_2 with $KOBMes_2$, but in this case no monometallic "$Sm(OBMes_2)_2$" was isolated. This suggests that the di(mesityl)boroxide ligand has insufficient steric bulk to stabilize such a complex and is consistent with the steric analysis above.[2,3,29–32] Instead, the tetrametallic cluster $Sm_4(OBMes_2)_6(\mu_4\text{-O})$, **3.9**, was found that contains three boroxides around each metal and has further ligation from a centrally incorporated oxide ligand. This could conceivably form from four "$Sm(OBMes_2)_2$" that condensed and eliminated $Mes_2BOBMes_2$ leaving the oxide ligand. However, it is likely that the reaction is more complicated since a Sm(III) complex containing potassium, $[K(\mu\text{-}OBMes_2)_3Sm(OBMes_2)(THF)]$, **3.10**, was also isolated from this reaction.

CONCLUSION

Protonolysis reactions of $HOBMes_2$ with $Ln(NR_2)_3$ complexes ($R = SiMe_3$) readily form bimetallic $[(Mes_2BO)_2Ln^{III}(\mu\text{-}OBMes_2)]_2$ complexes in which the $(OBMes_2)^{1-}$ ligand coordinates through both oxygen and the mesityl substituent. A $La(OBMes_2)_3(THF)_3$, complex can be isolated from LaI_3 and $KOBMes_2$, but ionic metathesis reactions tend to be more complicated than protonolysis. The mesityl groups can also coordinate potassium as demonstrated by the structures of $K(\mu\text{-}OBMes_2)_2Nd(NR_2)_2$, and $[K(\mu\text{-}OBMes_2)_3Sm(OBMes_2)(THF)]$. Although these Ln(III) boroxides appear to react with KC_8, no evidence for isolable Ln(II) complexes were obtained through this reductive route. Evidently, the boroxide is not a good ligand to support the Ln(II) ions of the metals studied. The reaction of SmI_2 did provide a Ln(II) boroxide, but surprisingly it

gave the Sm(II) oxo cluster, $Sm_4(\mu\text{-}OBMes_2)_6(\mu_4\text{-}O)$. The diverse chemistry exhibited by $(OBMes_2)^{1-}$ demonstrates that it has the capacity to support a greater variety of lanthanide coordination environments than would be expected from a simple sterically bulky oxygen donor ligand.

EXPERIMENTAL DETAILS

All manipulations and syntheses described below were conducted with the rigorous exclusion of air and water using standard Schlenk line and glovebox techniques under an argon or dinitrogen atmosphere. Solvents were sparged with UHP argon and dried by passage through columns containing Q-5 and molecular sieves prior to use. Deuterated NMR solvents were dried over NaK alloy or over molecular sieves, degassed by three freeze-pump-thaw cycles, vacuum transferred before use, and stored over molecular sieves. ^{1}H, ^{13}C and COSY [$^{13}C\{^{1}H\}$] NMR spectra were recorded on Bruker GN500, CRYO500, or AVANCE600 MHz spectrometers at 298 K unless otherwise stated and referenced internally to residual protio-solvent resonances. ^{11}B NMR are not reported, as the resonances of the ^{11}B nuclei in the lanthanide complexes could not be differentiated from ligand resonances. Electronic spectra were collected using an Agilent Cary 60 UV/Vis spectrophotometer with a quartz, air-free cuvette. Infrared spectra were collected on compressed solids using an Agilent Cary 630 ATR/FTIR instrument. EPR spectra were collected using the X-band frequency (9.3-9.8 GHz) on a Bruker EMX spectrometer equipped with an ER4119HS-W1 microwave bridge. Elemental analysis data were collected using a Thermo Scientific FlashSmart CHNS/O Elemental Analyzer at the UC Irvine Materials Research Institute's TEMPR facility in Irvine, CA. $KOB(C_6H_2Me_3\text{-}2,4,6)_2$ ($KOBMes_2$) was synthesized by treatment of $HOB(C_6H_2Me_3\text{-}2,4,6)_2$ ($HOBMes_2$) with one equiv of KH in THF, followed by filtration of the

resulting white solid, and washing with hexanes. $HOBMes_2$ was purchased from The Synnovator or synthesized via literature preparations.[11] KH in mineral oil (30%) was purchased from Sigma Aldrich and thoroughly rinsed with hexane before use. CNXyl (CNC_6H_3-2,6-Me_2) was purchased from Sigma Aldrich and used without further purification. $LaI_3(THF)_3$,[57] $SmI_2(THF)_2$,[58] and $Ln(NR_2)_3$[59] (R = $SiMe_3$; Ln = La, Ce, Nd, and Gd) starting materials were synthesized via literature procedures.

$KOBMes_2$. In an Ar filled glovebox with the blower turned off and the catalyst closed, a clear, colorless solution of $HOBMes_2$ (0.578 g, 2.17 mmol) in ca. 30 mL of THF was treated with white, powdered KH (0.077 g, 1.92 mmol) portionwise in a 150 mL round bottom flask. The reaction was stirred for 30 minutes while vigorous bubbling occurred and the solution became light yellow. One h after the bubbling stopped, the solvent was removed under reduced pressure. Toluene (ca. 30 mL) was added to the colorless, sticky solids and a white powder immediately precipitated. The white powder was isolated using a medium-porosity frit and dried under reduced pressure to yield $KOBMes_2$ (0.573 g, 1.90 mmol, 98%). ^{1}H NMR (500 MHz, THF-d_8) δ 6.56 (s, 4H, Ar-*Me*), 2.21, 2.14 (s, 12H, *o*-Me) 1.73 (s, 6H, *p*-Me). IR (cm^{-1}): 3018w, 2968w, 2945w, 2918w, 2855w, 1604m, 1546w, 1420s, 1407s, 1395s, 1372m, 1343w, 1284w, 1259w, 1233w, 1187m, 1129m, 1077w, 1027w, 1013w, 954w, 925w, 879w, 851s, 838m, 823s, 743m, 728w, 684w, 670m.

$[(Mes_2BO)_2La(\mu\text{-}OBMes_2)]_2$, 3.1-La. A solution of freshly prepared crystals of $La(NR_2)_3$ (0.332 g, 0.535 mmol) in ca. 5 mL toluene was added to a ca. 5 mL colorless solution of 3 equiv of $HOBMes_2$ (0.399 g, 1.49 mmol) in one portion at room temperature. The reaction was stirred for three h and remained clear. The solvent and the HNR_2 side product were then removed under reduced pressure. Hexane (ca. 10 mL) was added to the remaining solid to make a slurry of the

soluble **1** and any residual $HOBMes_2$, which is less soluble. The hexane was removed under reduced pressure and once again, ca. 10 mL of hexane was added to make a slurry of **1** . After stirring this mixture for 5 minutes, ca. 1 mL of THF was stirred into the slurry. This immediately dissolved all the species temporarily after which there was a sudden precipitation of the product $La(OBMes_2)_3(THF)_3$. The resulting slurry was stirred for 1 h, and then the mixture was centrifuged. The supernatant, containing unreacted $HOBMes_2$, was decanted away from the powdered solid pellet. The pellet containing $La(OBMes_2)_3(THF)_3$ was then dissolved in ca. 10 mL of toluene and heated with stirring to 80 °C under reduced pressure to remove coordinated THF from the product. The process of stirring the compound in heated toluene under reduced pressure was repeated, typically three times, until it could be verified that no resonances of THF were present in the NMR. The solid residue was then dissolved in minimal hexane and placed in the glovebox freezer at 0 °C, followed by setting the glovebox freezer to −35 °C for overnight crystallization via slow cooling. This afforded colorless crystals of $[(Mes_2BO)_2La(\mu\text{-}OBMes_2)]_2$, **3.1-La** (0.218 g, 0.233 mmol) in 43% yield. ^{1}H NMR (500 MHz, C_6D_6, 298K), δ 6.80 (s, 16H, terminal Ar-*H*), 6.40 (broad s, 8H, bridging Ar-*H*), 2.58 (broad s, 8H, Ar-*Me*), 2.32 (s, 51H, Ar-Me), 2.26 (s, 26H, Ar-*Me*), 1.96 (s, 14H, Ar-*Me*), 1.70 (s, 4H, Ar-*Me*), 1.59 (s, 3H, Ar-*Me*), 1.48 (s, 2H, Ar-*Me*). IR (cm^{-1}): 2946w, 2914m, 2855w, 1605s, 1548s, 1421s, 1373s, 1346m, 1318m, 1298m, 1280m, 1237w, 1025m, 956w, 926w, 834s, 742m, 671m. Anal. Calcd for $C_{108}H_{132}B_6La_2O_6$: C, 69.41; H, 7.12. Found: C, 70.44, H, 8.82. Elemental analytical data in this study routinely show high C and H values that we do not understand. They do not correspond to excess solvent present and differ from the usual problems in elemental analysis of lanthanide complexes in which incomplete combustion is observed [9,21,60,61]

[(Mes$_2$BO)$_2$Ce(μ-OBMes$_2$)]$_2$, 3.1-Ce. A yellow solution of Ce(NR$_2$)$_3$ (0.162 g, 0.261 mmol) in 10 mL toluene was treated with HOBMes$_2$ (0.202 g, 0.759 mmol) and the solution immediately turned a translucent light brown color. Workup proceeded in accordance with the synthesis of [(Mes$_2$BO)$_2$La(μ-OBMes$_2$)]$_2$, **3.1-La**. This afforded tan crystals of **3.1-Ce** (0.090 g, 0.096 mmol) in 38% yield. ^{1}H NMR (500 MHz, C$_6$D$_6$, 298K), δ 6.68 (32H, terminal Ar-*H*), 6.47 (s, 8H, bridging Ar-*H*), 3.05 (s, 24H, bridging *o-Me*), 2.37 (s, 58H terminal *p-Me*), 1.94 (s, 12H bridging *p-Me*), -0.22 (s, 94H terminal *o-Me*). Anal. Calcd for C$_{108}$H$_{132}$B$_6$Ce$_2$O$_6$: C, 69.32; H, 7.11. Found: C, 61.45, H, 7.92.

[(Mes$_2$BO)$_2$Nd(μ-OBMes$_2$)]$_2$, 3.1-Nd. A clear blue solution of Nd(NR$_2$)$_3$ (0.333 g, 0.532 mmol) in 10 mL of toluene was treated with solid HOBMes$_2$ (0.397 g, 1.49 mmol) in one portion and the solution remained a clear blue color. Workup proceeded in accordance with the synthesis of **3.1-La**. This afforded light blue crystals of **3.1-Nd** (0.227 g, 0.242 mmol, 45%). ^{1}H NMR (500 MHz, C$_6$D$_6$, 298K), δ 8.31, 7.81, 2.23, -5.53. IR (cm^{-1}): 2951w, 2915w, 2855w, 1606m, 1548w, 1422m, 1374w, 1346w, 1300s, 1280s, 1237m, 1206m, 1175w, 1146m, 1080w, 1022w, 958w, 927w, 844s, 832s, 743m, 672m. Anal. Calcd for C$_{108}$H$_{132}$B$_6$Nd$_2$O$_6$: C, 69.01; H, 7.08. Found: C, 70.15, H, 6.25.

[(Mes$_2$BO)$_2$Gd(μ-OBMes$_2$)]$_2$, 3.1-Gd. A colorless solution of Gd(NR$_2$)$_3$ (0.270 g, 0.423 mmol) in 10 mL toluene was treated with solid HOBMes$_2$ (0.338 g, 1.27 mmol) in one portion, which immediately turned an opaque light orange color. The solution was allowed to stir for 2 h and the solvent was then removed under vacuum. The resulting yellow residue was treated with toluene to make a yellow, cloudy mixture, and any remaining colorless solids were removed with a PTFE syringe filter. Solvent was removed and then the yellow solids were redissolved in minimal toluene. This was layered beneath hexanes and cooled to −35 °C, producing colorless X-

ray quality crystals of **3.1-Gd** (0.185 g, 0.19 mmol, 46%). IR (cm^{-1}): 3444w, 3429w, 3275w, 2951w, 2915w, 2854w, 1606m, 1548w, 1422m, 1374w, 1349w, 1299s, 1282s, 1258s, 1236m, 1204m, 1175w, 1146m, 1078m, 1062w, 1027m, 958w, 928w, 844s, 832s, 744w, 686w, 670m. Anal. Calcd for $C_{108}H_{132}B_6Gd_2O_6$: C, 68.07; H, 6.98. Found: C, 70.13, H, 8.72.

$La(OBMes_2)_3(THF)_3$, 3.2-La. THF (ca. 5 mL) was added to $LaI_3(THF)_{3.5}$ (0.147 g, 0.283 mmol) to form a grey slurry which was then treated with a light yellow solution of $KOBMes_2$ (0.251g, 0.825 mmol) in THF (ca. 5 mL) in one portion. The slurry became colorless and was stirred overnight. The colorless slurry was centrifuged to form a clear, colorless supernatant and a grey and white pellet. The supernatant was decanted from the pellet (presumably KI) and the solvent was removed from the supernatant to afford a light yellow solid. THF (ca. 1 mL) was added to the yellow solid to afford a colorless solution. Colorless crystals of 2 which were suitable for study by X-ray diffraction were recovered at −35 °C (0.226 g, 0.197 mmol, 72%). ^{1}H NMR (500 MHz, THF-d_8, 298K) δ 9.10 (s, 1H), 6.62 (s, 12H, Ar-*H*), 3.62 (m, 12H, O-CH_2 (THF)), 2.22 (s, 18H, *p-Me*), 2.18 (s, 36H, *o-Me*), 1.77 (s 12H, C-CH_2 (THF)). ^{1}H NMR (400 MHz, C_6D_6) δ 6.74 (s, 12H, Ar-*H*), 5.60 (s, 1H), 3.45 (m, 12H, O-CH_2 (THF)), 2.40 (s, 36H o-Me), 2.17 (s, 18H p-*Me*) 1.23 (m, 12H, C-CH_2 (THF)). IR (cm^{-1}): 2964w, 2929w, 2917w, 2875w, 1606w, 1471w, 1437w, 1407w, 1352s, 1326s, 1284m, 1259m, 1236w, 1200w, 1175w, 1161w, 1141w, 1070m, 1027m, 1006w, 975w, 949w, 914w, 873w, 844s, 829s, 743m, 707w, 672m.

$Nd(OBMes_2)_3(THF)_3$, 3.2-Nd. A clear, colorless solution of $HOBMes_2$ (0.397 g, 1.49 mmol) in toluene (ca. 10 mL) was treated with light blue powdered $Nd(NR_2)_3$ (0.333 g, 0.531 mmol) and was stirred for 3 h to make a clear, blue solution at room temperature. Solvent was removed under reduced pressure and the resulting light blue residue was dissolved in ca. 1 mL hexane and left to cool at −35 °C for 18 h to afford blue block crystals of **3.1-Nd**. The light blue

supernatant was extracted via pipette and the crystals were dissolved in ca. 7 mL hexane where they were treated with ca. 1 mL THF. Cooling the resulting solution to −35 °C for 18 h resulted in large, light blue crystals of **3.2-Nd** (0.227 g, 0.197 mmol, 37%). ^{1}H NMR (400 MHz, C_6D_6) δ = 8.53 (s, 36H, *o-Me*), 7.86 (s, 12H, Ar-*H*), 2.25 (s, 18H, *p-Me*), -5.97 (s, 12H, C-CH_2 (THF)), -11.36 (s, 12H, O-CH_2 (THF)).

$Nd(NR_2)_2(OBMes_2)(THF)$, 3.3. Blue, powdered $Nd(NR_2)_3$ (0.214 g, 0.345 mmol) was dissolved in 5 mL of THF to make a clear blue solution and treated with a clear, colorless solution of $HOBMes_2$ (0.093 g, 0.350 mmol) in 5 mL of THF. The clear blue solution was stirred for 18 h and volatiles were removed under reduced pressure to afford a blue solid residue. The blue solids were dissolved in hexane and volatiles were again removed under reduced pressure, leaving blue solids. Small blue crystals of **3.3** were recovered from a concentrated solution of **3.3** in ca. 1 mL of pentane after storage at −35 °C for 18 h (0.147 g, 0.212 mmol, 59%). Due to the paramagnetism of **3.3**, full assignment of the resonances of its ^{1}H NMR spectrum in C_6D_6 was not possible. ^{1}H NMR (600 MHz, C_6D_6, 298K) δ 10.80, 8.37, 7.81, 3.17, 2.91 , 2.23, -2.74, -5.09, -6.24. IR (cm^{-1}): 3020w, 2953m, 2922w, 2858w, 1605m, 1548w, 1422m, 1420m, 1377s, 1354s, 1318s, 1284m, 1242s, 1203m, 1177w, 1144m, 1113w, 1080w, 1049w, 993s, 958w, 934w, 829s, 764m, 736m, 672m. Anal. Calcd for $C_{34}H_{65}BN_2Nd_2O_2Si_4$: C, 50.96; H, 8.18; N: 3.50. Found: C, 52.14; H, 6.65; N, 0.91.

$K(\mu\text{-}OBMes_2)_2Nd(NR_2)_2$, 3.5-Nd. Blue powdered **3.3** (0.030 g, 0.038 mmol) was dissolved in 10 mL toluene to make a clear light blue solution. While stirring at room temperature, bronze powdered KC_8 (0.010 g, 0.073 mmol) was added which quickly made an opaque black mixture with a green hue. After 18 h, the mixture was filtered with a PTFE syringe filter to give an amber solution with a blue hue. This was cooled to −35 °C for 18 h and afforded blue X-ray

quality crystals of **3.5-Nd** (0.028 g, 0.026 mmol, 68%). ^{1}H NMR (500 MHz, C_6D_6, 298K) δ 5.09, 0.16, -0.39, -0.81, -1.82, -2.92. IR (cm^{-1}) : 2938m, 2854 w, 2728w, 1674w, 1604m, 1547w, 1419m, 1388m, 1366m, 1330m, 1310s, 1284m, 1239s, 1200m, 1142m, 1084s, 980s, 938m, 876m, 812s, 768m, 748s, 660m.

K(μ-OBMes$_2$)$_2$Ce(NR$_2$)$_2$, 3.5-Ce. A light yellow solution of Ce(NR$_2$)$_3$ (0.150 g, 0.241 mmol) in ca. 8 mL THF was treated with a colorless solution of KOBMes$_2$ (0.293 g, 963 mmol) in ca. 8 mL THF and stirred at room temperature for 4 h forming a light yellow solution. Solvent was removed under reduced pressure to leave beige sticky solids which were extracted into ca. 20 mL of hexane. This mixture was then centrifuged and the solvent was then removed from the yellow supernatant under reduced pressure. After repeating the extraction, centrifugation, and removal of solvent from the supernatant once more, the remaining yellow film was dissolved in minimal hexane (ca. 1 mL) and placed in the freezer at −35 °C for 18 h to yield yellow crystals of **3.5-Ce** (0.057 g, 0.055 mmol, 19%). ^{1}H NMR (500 MHz, C_6D_6, 298K) δ = 6.68, 6.47, 3.05, 2.37, 1.94, -0.22, -2.71.

[K$_2$(μ-(OBMes$_2$))$_3$ Nd]$_2$(X$_8$), 3.6 and [K(μ-OBMes$_2$)$_2$][K(μ-OBMes$_2$)$_3$]Nd, 3.7. A colorless slurry of 1.8 equiv KOBMes$_2$ (0.102 g, 0.335 mmol) in ca. 10 mL toluene was treated with one equiv dark purple NdI$_2$ (0.066 g, 0.165 mmol) and left to stir for 18 h. Solvent was removed and subsequently treated with ca. 10 mL Et$_2$O for 2 h. The purple mixture was centrifuged resulting in a purple and white pellet and a light blue/yellow dichroic supernatant. The solvent was concentrated from the supernatant under reduced pressure. Placement in the freezer at −35 °C for 18 h led to light blue crystals of **[K$_2$(μ-(OBMes$_2$))$_3$ Nd]$_2$(X$_8$), 3.6** and **[K(μ-OBMes$_2$)$_2$][K(μ-OBMes$_2$)$_3$]Nd, 3.7** in very low yield**.** IR **(3.7)** (cm^{-1}): 2954 w, 2918 m, 2854 w, 1604 w, 1548 w, 1438 m, 1421 m, 1407 m, 1351 s, 1322 s, 1284 m, 1261 m, 1235 m, 1197 m, 1176 w, 1140 m,

1103 w, 1079 m, 1026 w, 1007 w, 975 w, 950 w, 929 w, 876 w, 844 m, 828 s, 754 s, 742 m, 708 w, 672 m.

[K(μ-OBMes$_2$)$_2$]$_2$Nd(OBMes$_2$), 3.8. A light blue slurry of $NdCl_3$ (0.044 g, 0.176 mmol) in ca. 10 mL THF was treated with a light yellow solution of $KOBMes_2$ (0.146 g, 0.478 mmol) and stirred for 18 h. The resulting light blue mixture was centrifuged and a light blue supernatant was decanted away from a colorless pellet. Volatiles were removed from the supernatant under reduced pressure, resulting In light blue solids. Upon treatment with ca. 10 mL hexane, a colorless precipitate formed. This was centrifuged again and the resulting lighter blue supernatant was removed from the colorless pellet. The volume of the supernatant was reduced to ca. 1 mL and placed in the freezer at −35 °C to afford light blue crystals of **3.8** (0.070 g, 0.045 mmol 26% yield. IR (cm^{-1}): 2954 w, 2918 m, 2854 w, 1604 w, 1548 w, 1438 m, 1421 m, 1407 m, 1351 s, 1322 s, 1284 m, 1261 m, 1235 m, 1197 m, 1176 w, 1140 m, 1103 w, 1079 m, 1026 w, 1007 w, 975 w, 950 w, 929 w, 876 w, 844 m, 828 s, 754 s, 742 m, 708 w, 672 m.

Sm$_4$(OBMes$_2$)$_6$(μ_4-O), 3.9. A light yellow THF solution of $KOBMes_2$ (0.117 g, 0.385 mmol) was added to a stirred dark blue solution of $SmI_2(THF)_2$ (0.120 g, 0.220 mmol) in 10 mL of Et_2O to yield a grey suspension. The reaction was stirred for 1 h and then centrifuged to yield an opaque black supernatant and a white solid. The supernatant was decanted and solvent was removed under reduced pressure to yield a black powder, which was redissolved in minimal hexanes (ca. 1 mL) and placed in the freezer at −35 °C for 18 h to afford black crystalline blocks of **3.9** which were suitable for X-ray diffraction (0.110 g, 0.049 mmol, 89% based on Sm). With this 2:3 starting material ratio, no colorless crystals of [K(μ-OBMes$_2$)$_3$Sm(OBMes$_2$)(THF)], **3.10** were found. ^{1}H NMR (500 MHz, C_6D_6, 298K), δ 6.08 (s, 24H, *Ar*-H), 3.16 (s, 36H *p*-Me), 2.57 (s, 72H *o*-Me). IR (cm^{-1}): 2950w, 2915w, 2854w, 2725w, 1604m, 1547w, 1441m, 1420m, 1351m,

1320s, 1283m, 1236w, 1201m, 1176w, 1143m, 1098w, 1080m, 1057w, 1024m, 955w, 926w, 830s, 741w, 671m. Anal. Calcd for $C_{114}H_{146}B_6O_7Sm_4$ ($Sm_4(OBMes_2)_6(C_6H_{14})$) : C, 59.67; H, 6.41. Found: C, 60.85; H, 7.03.

When the $KOBMes_2$ reaction with $SmI_2(THF)_2$ was run with a 2:1 stoichiometry, a few colorless crystals of [K(μ-$OBMes_2$)$_3$Sm($OBMes_2$)(THF)], **3.10**, suitable for X-ray diffraction studies were manually separated from the majority product of black amorphous solids, presumably complex 6. ^{1}H NMR (THF-d_8): δ 6.69 (s, 16H, Ar-*H*), 3.62 (m, 4H, THF (O(C*H*$_2$)$_2$(CH$_2$)$_2$), 2.20 (s, 72H, *o*-C*H*$_3$, *p*-C*H*$_3$), 1.77 (m, 4H THF (O(CH$_2$)$_2$(C*H*$_2$)$_2$,). IR (cm^{-1}): 2951w, 2916m, 2856w, 1549w, 1420m, 1338s, 1284m, 1236m, 1205m, 1201m, 1143m, 1081w, 1025m, 956w, 926w, 834s, 742m, 671m.

Sm(OBMes$_2$)$_3$(Et$_2$O)(CNXyl)•Sm(OBMes$_2$)$_3$(CNXyl)$_3$, 3.11. Black crystals of 6 (0.100 g, 0.045 mmol) were dissolved in 5 mL of hexane to afford a black solution. Crystalline white CNXyl (0.022 g, 0.168 mmol) was added to this solution and after 30 minutes of stirring, green solids could be seen in a red/orange slurry. This green material was then filtered away from the red/orange solution using a pipette filter and solvent was removed under reduced pressure. The resulting orange solids were treated with minimal hexanes (ca. 1 mL) and heated to dissolution (ca. 50 °C). After cooling to room temperature for 18 h, orange crystals of 8 suitable for X-ray diffraction were collected in very low yield. ^{1}H NMR (500 MHz, C_6D_6, 298K), δ 6.88, 6.67, 6.49, 3.09, 2.19, 2.18, 1.87, 0.08.

General Procedures for Complex Reduction. A solution of freshly prepared crystals of a given complex were dissolved in 5 mL of an ethereal solvent such as THF, or Et_2O in a 20 mL scintillation vial and cooled to −35 °C for 30 minutes**.** To this, one to two equiv of KC_8 was portioned into the vial and the reaction was stirred at room temperature for 5 minutes for THF and

2 h for Et_2O. The resulting black solids were then filtered away from a dark orange solution through a glass pipette with a Kimwipe placed inside. The solvent was then removed under reduced pressure yielding orange hexane-insoluble solids.

Treatment of 3.1-La with KC_8, 3.4-La: A clear, colorless solution of **3.1-La** (0.200 g, 0.214 mmol) in 10 mL Et_2O was treated with KC_8 (0.058 g, 0.429 mmol) and workup proceeded in accordance with the general procedures for complex reduction to yield a yellow-orange product. IR (cm-1): 2949w, 2914w, 2855w, 1605s, 1548s, 1421s, 1373s, 1546s, 1318s, 1298s, 1280s, 1237s, 1205s, 1176s, 1146s, 1079s, 1057s, 1026s, 957s, 957s, 926s, 843s, 831s, 741s, 670s. ^1H NMR (400 MHz, C_6D_6, 298K) δ 6.70 (*H*-Ar) , 6.62 (*H*-Ar), 2.37 (*o*-Me) , 2.33 (*o*-Me), 2.18 (*p*-Me), 2.15(*p*-Me). Anal. Found: C, 65.94, H, 7.05.

Treatment of 3.1-Ce with KC_8, 4-Ce: A translucent light yellow solution of **3.1-Ce** (0.070 g, 0.075 mmol) in 10 mL Et_2O was treated with KC_8 (0.020 g, 0.148 mmol) and workup proceeded in accordance with the general procedures for complex reduction to yield a yellow-orange product. IR (cm^{-1}): 2916w, 2855w, 1603w, 1545w, 1531w, 1422m, 1419m, 1358s, 1330s, 1285m, 1259m, 1235m, 1197m, 1169w, 1141m, 1078m, 1015m, 956w, 920w, 881w, 847s, 829s, 741m, 692m, 673m.

Treatment of 3.1-Nd with KC_8, 4-Nd: A translucent light blue solution of **3.1-Nd** (0.150 g, 0.160 mmol) in 10 mL Et_2O was treated with 0.055 g (0.407 mmol) KC_8 and workup proceeded in accordance with the general procedures for complex reduction to yield a yellow-green product. IR (cm^{-1}): 2916 m, 2854w, 27225w, 1604m, 1547w, 1440w, 1419m, 1346m, 1316s, 1284m, 1262m, 1236m, 1201m, 1176w, 1144m, 1081m, 1025m, 957w, 926w, 877w, 830s, 742s, 673m.

^{1}H NMR (600 MHz, C_6D_6) δ 6.33 (*H*-Ar), 2.17 (*p*-Me), 0.20 (*o*-Me)**.** Anal. Found**:** C, 67.27; H, 7.59**.**

Table 3.5. Bridging and terminal O-B bond length (Å) of 3.1-Ln and [(Mes$_2$BO-μ)U(OBMes$_2$)$_2$]$_2$ for comparison

	3.1-La	**3.1-Ce**	**3.1-Nd**	**3.1-Gd**	[(Mes$_2$BO-μ)U(OBMes$_2$)$_2$]$_2$	Overall Average
Bridging B-O	1.393	1.371	1.359	1.379	1.356	
Bridging B-O		1.361				
Average Bridging	1.393	1.366	1.359	1.379	1.356	1.3706
Terminal B-O	1.352	1.342	1.335	1.343	1.349	
Terminal B-O	1.308	1.333	1.321	1.362	1.348	
Terminal B-O		1.346				
Terminal B-O		1.338				
Average Terminal	1.351	1.345	1.338	1.361	1.351	1.349

Treatment of 3.1-Gd with KC$_8$, 4-Gd: A translucent light blue solution of **3.1-Gd** (0.185 g, 0.194 mmol) in 10 mL Et_2O was treated with 0.053 g (0.392 mmol) KC_8 and workup proceeded in accordance with the general procedures for complex reduction to yield a yellow-orange product**.** IR (cm^{-1})**:** 2914w, 2855w, 1603w, 1575w, 1545w, 1492w, 1441w, 1418m, 1359s, 1330s, 1285m, 1260m, 1235m, 1196m, 1169w, 1140m, 1078m, 1027m, 956w, 924w, 884w, 846s, 827s, 727m, 693m, 673m.

Table 3.6. Selected bond lengths (Å) and angles [°] of 3.5-Ln for comparison

3.5-Ce		3.5-Nd	
Ce(1)-O(1)	2.2706(2)	Nd(1)-O(1)	2.2655(1)
Ce(1)-O(2)	2.2892(2)	Nd(1)-O(2)	2.2297(2)
Ce(1)-N(1)	2.3972(2)	Nd(1)-N(1)	2.3718(2)
Ce(1)-N(2)	2.3841(2)	Nd(1)-N(2)	2.3601(2)
O(1)-Ce(1)-O(2)	94.31(5)	O(1)-Nd(1)-N(1)	107.45(6)
O(1)-Ce(1)-N(1)	111.57(6)	O(1)-Nd(1)-N(2)	107.58(6)
O(1)-Ce(1)-N(2)	103.87(6)	O(2)-Nd(1)-O(1)	97.53(5)
O(2)-Ce(1)-N(1)	110.60(6)	O(2)-Nd(1)-N(1)	105.64(6)
O(2)-Ce(1)-N(2)	107.04(6)	O(2)-Nd(1)-N(2)	106.24(6)
N(2)-Ce(1)-N(1)	124.97(6)	N(2)-Nd(1)-N(1)	128.18(6)

Table 3.7. Selected bond lengths (Å) and angles [°] of 3.9 and 3.10 for comparison

3.9		3.10	
Sm(1)-O(1)	2.526(5)	Sm(1)-O(1)	2.204(3)
Sm(1)-O(2)	2.449(4)	Sm(1)-O(2)	2.245(4)
Sm(1)-O(3)	2.466(3)	Sm(1)-O(3)	2.184(3)
Sm(1)-O(5)	2.320(3)	Sm(1)-O(4)	2.204(3)
Sm(2)-O(1)	2.439(4)	Sm(1)-O(5)	2.512(3)
Sm(2)-O(2')	2.493(4)	O(1)-Sm(1)-O(2)	94.28(1)
Sm(2)-O(4)	2.449(4)	O(1)-Sm(1)-O(5)	113.65(1)
Sm(2)-O(5)	2.313(3)	O(2)-Sm(1)-O(5)	80.83(1)
O(1)-Sm(1)-O(2)	112.05(1)	O(4)-Sm(1)-O(1)	119.92(1)

O(3)-Sm(1)-O(2)	108.44(1)	O(4)-Sm(1)-O(2)	145.50(1)
O(1)-Sm(1)-O(3)	119.91(1)	O(4)-Sm(1)-O(3)	95.36(1)
O(1)-Sm(1)-O(5)	75.03(1)	O(4)-Sm(1)-O(5)	81.20(1)
O(2)-Sm(1)-O(5)	74.56(1)	O(3)-Sm(1)-O(1)	88.03(1)
O(3)-Sm(1)-O(5)	75.24(1)	O(3)-Sm(1)-O(2)	89.83(1)
O(1)-Sm(2)-O(2')	115.07(2)	O(3)-Sm(1)-O(5)	156.82(1)
O(1)-Sm(2)-O(4)	108.87(1)		
O(4)-Sm(2)-O(2')	117.31(1)		
O(5)-Sm(2)-O(1)	76.87(1)		
O(5)-Sm(2)-O(2')	73.85(1)		
O(5)-Sm(2)-O(4)	75.26(1)		

Table 3.8. Selected Bond Distances (Å) and angles [°] of $Nd(OBMes_2)_3(THF)_3$, 3.2-Nd, and $Nd(OC_6H_3\text{-}2,4\text{-}^tBu_2)_3(THF)_3$

3.2-Nd		Nd(OC6H3-2,4-tBu2)3(THF)3	
Nd(1)-O(boroxide)	2.241(8)	Nd(1)-O(aryloxide)	2.2070(2)
Nd(1)-O(boroxide)	2.232(9)	Nd(1)-O(aryloxide)	2.206(2)
Nd(1)-O(boroxide)	2.202(6)	Nd(1)-O(aryloxide)	2.194(2)
Nd(1)-O(THF)	2.559(9)	Nd(1)-O(THF)	2.580(2)
Nd(1)-O(THF)	2.488(8)	Nd(1)-O(THF)	2.535(2)
Nd(1)-O(THF)	2.478(9)	Nd(1)-O(THF)	2.500(2)
O(boroxide)-Nd(1)-O(boroxide)	139.8(3)	O(aryloxide)-Nd(1)-O(aryloxide)	135.40(8)
O(boroxide)-Nd(1)-O(boroxide)	108.5(3)	O(aryloxide)-Nd(1)-O(aryloxide)	112.60(8)

O(boroxide)-Nd(1)-O(boroxide)	107.7(3)	O(aryloxide)-Nd(1)-O(aryloxide)	106.35(8)
O(boroxide)-Nd(1)-O(THF)	84.4(3)	O(aryloxide)-Nd(1)-O(THF)	87.37(8)
O(boroxide)-Nd(1)-O(THF)	84.2(3)	O(aryloxide)-Nd(1)-O(THF)	82.64(7)
O(boroxide)-Nd(1)-O(THF)	82.6(3)	O(aryloxide)-Nd(1)-O(THF)	79.53(7)
O(boroxide)-Nd(1)-O(THF)	82.6(3)	O(aryloxide)-Nd(1)-O(THF)	78.99(7)
O(boroxide)-Nd(1)-O(THF)	78.9(3)	O(aryloxide)-Nd(1)-O(THF)	78.20(7)
O(boroxide)-Nd(1)-O(THF)	76.9(3)	O(aryloxide)-Nd(1)-O(THF)	76.72(7)
O(boroxide)-Nd(1)-O(THF)	152.7(3)	O(aryloxide)-Nd(1)-O(THF)	151.85(7)
O(boroxide)-Nd(1)-O(THF)	104.4(4)	O(aryloxide)-Nd(1)-O(THF)	106.81(7)
O(boroxide)-Nd(1)-O(THF)	96.9(3)	O(aryloxide)-Nd(1)-O(THF)	100.71(7)
O(THF)-Nd(1)-O(THF)	70.2(3)	O(THF)-Nd(1)-O(THF)	72.47(7)
O(THF)-Nd(1)-O(THF)	166.0(3)	O(THF)-Nd(1)-O(THF)	166.02(7)
O(THF)-Nd(1)-O(THF)	123.1(3)	O(THF)-Nd(1)-O(THF)	120.22(7)

X-ray Data Collection, Structure Solution and Refinement for complexes, **3.1-Ln**, **3.2-Ln**, **3.3**, **3.5-Ln**, **3.6**, **3.7**, **3.8, 3.9** and **3.10.** More metrical data can be found in the CCDC.

$[(Mes_2BO)_2La(\mu\text{-}OBMes_2)]_2$, 3.1-La. A colorless crystal of approximate dimensions 0.221 x 0.229 x 0.334 mm was mounted in a cryoloop and transferred to a Bruker SMART APEX II diffractometer system. The APEX2[62] program package was used to determine the unit-cell parameters and for data collection (90 sec/frame scan time). The raw frame data was processed using SAINT[63] and SADABS[64] to yield the reflection data file. Subsequent calculations were carried out using the SHELXTL[65] program package. The diffraction symmetry was *mmm* and the

systematic absences were consistent with the orthorhombic space groups *Pnn*2 and *Pnnm*. It was later determined that space group *Pnn2* was correct. The structure was solved by direct methods and refined on F^2 by full-matrix least-squares techniques. The analytical scattering factors[66] for neutral atoms were used throughout the analysis. Hydrogen atoms were included using a riding model. The molecule was located about a two-fold rotation axis. Least-squares analysis yielded wR2 = 0.0752 and Goof = 1.035 for 569 variables refined against 115827 data (0.76 Å), R1 = 0.0282 for those 14028 data with $I > 2.0\sigma(I)$. The complex was refined as a two-component inversion twin, BASF = 0.29(01). There were high residuals present in the final difference-Fourier map. It was not possible to determine the nature of the residuals although it was probable hexane and toluene solvents were present based on the crystallization method used. A solvent accessible void of 2310 $Å^3$ was found to contain 1082 electrons. This was consistent with the presence of approximately four hexane and six toluene molecules. The SQUEEZE[67] routine in the PLATON[68] program package was used to account for the electrons in the solvent accessible voids.

$[(Mes_2BO)_2Ce(\mu\text{-}OBMes_2)]_2$, 3.1-Ce. A colorless crystal of approximate dimensions 0.061 x 0.086 x 0.117 mm was mounted in a cryoloop and transferred to a Bruker X8 Prospector diffractometer system**.** The APEX3[69] program package was used to determine the unit-cell parameters and for data collection (10sec/frame scan time)**.** The raw frame data was processed using SAINT[70] and SADABS[64] to yield the reflection data file**.** Subsequent calculations were carried out using the SHELXTL[65] program package**.** The diffraction symmetry was 2/*m* and the systematic absences were consistent with the monoclinic space group $P2_1/c$ that was later determined to be correct. The structure was solved by direct methods and refined on F^2 by full-matrix least-squares techniques**.** The analytical scattering factors[66] for neutral atoms were used throughout the analysis**.** Hydrogen atoms were included using a riding model**.** There were 3.5

molecules of toluene solvent present**.** One solvent molecule was located about an inversion center and was refined using partial site-occupancy factors and geometric restraints. Least-squares analysis yielded wR2 = 0.1375 and Goof = 1.038 for 1355 variables refined against 21551 data (0.83 Å), R1 = 0.0549 for those 17195 data with I > 2.0σ(I)**.**

[(Mes$_2$BO)$_2$Nd(μ-OBMes$_2$)]$_2$, 3.1-Nd. A blue crystal of approximate dimensions 0.061 x 0.086 x 0.177 mm was mounted in a cryoloop and transferred to a Bruker X8 Prospector APEX II diffractometer system. The APEX3[69] program package was used to determine the unit-cell parameters and for data collection (10 sec/frame scan time). The raw frame data was processed using SAINT[70] and SADABS[64] to yield the reflection data file. Subsequent calculations were carried out using the SHELXTL[65] program package. The diffraction symmetry was *mmm* and the systematic absences were consistent with the orthorhombic space groups *Pnn*2 and *Pnnm*. It was later determined that space group *Pnn2* was correct. The structure was solved by direct methods and refined on F^2 by full-matrix least-squares techniques. The analytical scattering factors[66] for neutral atoms were used throughout the analysis. Hydrogen atoms were included using a riding model. The molecule was located about a two-fold rotation axis. Least-squares analysis yielded wR2 = 0.0766 and Goof = 1.049 for 569 variables refined against 10906 data (0.83Å), R1 = 0.0292 for those 9595 data with I > 2.0σ(I). The complex was refined as a two-component inversion twin, BASF = 0.177(4). There were high residuals present in the final difference-Fourier map. It was not possible to determine the nature of the residuals although it was probable hexane and toluene solvents were present based on the crystallization method used. A solvent accessible void of 2316 $Å^3$ was found to contain 543 electrons. This was consistent with the presence of approximately three hexane and two toluene molecules. The SQUEEZE[67] routine in the PLATON[68] program package was used to account for the electrons in the solvent accessible voids.

$[(Mes_2BO)_2Gd(\mu\text{-}OBMes_2)]_2$, 3.1-Gd.. A colorless crystal of approximate dimensions 0.286 x 0.330 x 0.376 mm was mounted in a cryoloop and transferred to a Bruker APEX II diffractometer system. The APEX2[62] program package was used to determine the unit-cell parameters and for data collection (30 sec/frame scan time). The raw frame data was processed using SAINT[63] and SADABS[64] to yield the reflection data file. Subsequent calculations were carried out using the SHELXTL[65] program package. The diffraction symmetry was *mmm* and the systematic absences were consistent with the orthorhombic space groups *Pnn*2 and *Pnnm*. It was later determined that space group *Pnn2* was correct. The structure was solved by direct methods and refined on F^2 by full-matrix least-squares techniques. The analytical scattering factors[66] for neutral atoms were used throughout the analysis. Hydrogen atoms were included using a riding model. The molecule was located about a two-fold rotation axis. Disordered atoms were included using multiple components, partial site-occupancy-factors and isotropic displacement parameters. Least-squares analysis yielded wR2 = 0.0605 and Goof = 1.037 for 568 variables refined against 19827 data (0.70Å), R1 = 0.0261 for those 16612 data with $I > 2.0\sigma(I)$. The absolute structure was assigned by refinement of the Flack parameter.[71] There were high residuals present in the final difference-Fourier map. It was not possible to determine the nature of the residuals although it was probable hexane and toluene solvents were present based on the crystallization method used. A solvent accessible void of 2266 $Å^3$ was found to contain 533 electrons. This was consistent with the presence of approximately three hexane and two toluene molecules. The SQUEEZE[67] routine in the PLATON[68] program package was used to account for the electrons in the solvent accessible voids.

Table 3.9. Crystal data and structure refinement for $[(Mes_2BO)_2Ln(\mu\text{-}OBMes_2)]_2$, 3.1-Ln.				
	3.1-La	3.1-Ce	3.1-Nd	3.1-Gd
Identification code	kgb39 (Kito Gilbert-Bass)	kgb34 (Kito Gilbert-Bass)	kgb33	kgb28 (Kito Gilbert-Bass)
Empirical formula	$C_{174}H_{236}B_6La_2O_6$	$C_{132.5}H1_{60}B_6O_6Ce_2$	$C_{140}H_{190}B_6O_6Nd_2$	$C_{140}H_{190}B_6O_6Gd_2$
Formula weight	2766.29	2193.7	2322.25	2348.27
Temperature/K	93.15	92.85	93(2)	133(2)
Crystal system	orthorhombic	monoclinic	orthorhombic	orthorhombic
Space group	Pnn2	$P2_1/c$	Pnn2	Pnn2
a/Å	24.727(2)	13.9609(3)	24.7097(10)	24.717(3)
b/Å	13.9228(12)	26.8054(7)	14.0999(6)	14.1913(18)
c/Å	19.2943(16)	31.4550(7)	19.1069(8)	18.768(2)
α/°	90	90	90	90

Table 3.9. Crystal data and structure refinement for $[(Mes_2BO)_2Ln(\mu\text{-}OBMes_2)]_2$, 3.1-Ln.				
β/°	90	96.6057(13)	90	90
γ/°	90	90	90	90
Volume/Å^3	6642.5(10)	11693.2(5)	6656.9(5)	6582.9(14)
Z	2	4	2	2
ρ_{calc}g/cm^3	1.383	1.246	1.159	1.185
μ/mm^{-1}	0.698	6.345	6.261	1.05
F(000)	2944	4596	2456	2472
Crystal size/mm^3	0.344 × 0.229 × 0.221	0.117 × 0.086 × 0.061	0.271 × 0.264 × 0.188	0.376 × 0.33 × 0.286
Radiation	MoKα (λ = 0.71073)	CuKα (λ = 1.54178)	CuKα (λ = 1.54178)	MoKα (λ = 0.71073)
2Θ range for data collection/°	3.608 to 56.632	4.344 to 137.814	5.846 to 137.748	2.724 to 61.224
Index ranges	-33 ≤ h ≤ 32, -18 ≤ k ≤ 18, -17 ≤ l ≤ 25	-16 ≤ h ≤ 16, -31 ≤ k ≤ 32, -38 ≤ l ≤ 32	-29 ≤ h ≤ 29, -17 ≤ k ≤ 17, -23 ≤ l ≤ 19	-34 ≤ h ≤ 35, -20 ≤ k ≤ 20, -26 ≤ l ≤ 26

Table 3.9. Crystal data and structure refinement for $[(Mes_2BO)_2Ln(\mu\text{-}OBMes_2)]_2$, 3.1-Ln.				
Reflections collected	58304	121114	55771	156414
Independent reflections	14950 [R_{int} = 0.0599, R_{sigma} = 0.0582]	21551 [R_{int} = 0.0942, R_{sigma} = 0.0611]	10759 [R_{int} = 0.0447, R_{sigma} = 0.0435]	19827 [R_{int} = 0.0481, R_{sigma} = 0.0351]
Data/restraints/parameters	14950/271/569	21551/15/1355	10759/1/569	19827/1/568
Goodness-of-fit on F^2	0.948	1.035	1.049	1.037
Final R indexes [I>=2σ (I)]	R_1 = 0.0431, wR_2 = 0.1089	R_1 = 0.0549, wR_2 = 0.1268	R_1 = 0.0292, wR_2 = 0.0737	R_1 = 0.0261, wR_2 = 0.0564
Final R indexes [all data]	R_1 = 0.0544, wR_2 = 0.1136	R_1 = 0.0737, wR_2 = 0.1375	R_1 = 0.0345, wR_2 = 0.0766	R_1 = 0.0378, wR_2 = 0.0605

Table 3.9. Crystal data and structure refinement for $[(Mes_2BO)_2Ln(\mu\text{-}OBMes_2)]_2$, 3.1-Ln.				
Largest diff. peak/hole / e $Å^{-3}$	1.27/-0.46	2.40/-0.66	0.66/-0.45	1.49/-0.66

$La(OBMes_2)_3(THF)_3$, 3.2-La (modulated and non-modulated structural data). A colorless crystal of approximate dimensions 0.212 x 0.182 x 0.143 mm was mounted in a cryoloop and transferred to a Bruker SMART APEX II diffractometer system. The APEX3[69] program package was used to determine the unit-cell parameters and for data collection (20sec/frame scan time, 1.5 degree frame angle). The raw frame data was processed using SAINT[70] and SADABS[64] to yield the reflection data file. Subsequent calculations were carried out using the Jana2020software package.[72] The diffraction symmetry of the modulated structure was assigned to the nonstandard Pbca(0b0)s0s superspace group based on systematic absences. The structure was solved using Superflip[73] charge flipping methods and refined on F^2 using least squares techniques. The analytical scattering factors[66] for neutral atoms were used throughout the analysis. Significant spot overlap due to poor data collection parameters led to the requirement of significant restraints and constraints in the data refinement leading to poor refinement quality. La1 was refined as an anisotropic ellipsoid. All C, O, and B atoms were refined as isotropic spheres. The displacement parameters of each mesityl group, each pair of boron and oxygen, and each THF molecule were constrained to the same value. All aromatic sp2 C—C bonds were restrained to the same value, all methyl C—C bonds were restrained to the same value, all B—C bonds were restrained to the same value, and all B—O bonds were restrained to the same value. THF C—C bonds were restrained to 1.54 A, and THF C—O bonds were restrained to 1.45 A. All C—C—C bond angles and B—C—C bond angles were restrained to 120 degrees. All mesityl groups, including boron atoms were constrained to a plane and modulated as a rigid group. All hydrogen atoms were refined along riding positions.

$Nd(OBMes_2)_3(THF)_3$, 3.2-Nd. A blue crystal of approximate dimensions 0.282 x 0.351 x 0.357 mm was mounted in a cryoloop and transferred to a Bruker SMART APEX II diffractometer

system. The APEX2[62] program package was used to determine the unit-cell parameters and for data collection (10 sec/frame scan time). The raw frame data was processed using SAINT[63] and SADABS[64] to yield the reflection data file. Subsequent calculations were carried out using the SHELXTL[65] program package. The diffraction symmetry was 2/*m* and the systematic absences were consistent with the monoclinic space group $P2_1/c$ that was later determined to be correct. The structure was solved by direct methods and refined on F^2 by full-matrix least-squares techniques. The analytical scattering factors[66] for neutral atoms were used throughout the analysis. Hydrogen atoms were included using a riding model. The data were refined as an inversion twin with BASF [0.3206(19)] using the twin command in OLEX2. Disordered atoms were included using multiple components, partial site-occupancy-factors, and displacement (SIMU, ISOR, DFIX, EADP) constraints. An extinction coefficient (EXTI) of 0.0052(3) was also implemented. There were several high residuals present in the final difference-Fourier map. It was not possible to determine the nature of the residuals although it was probable that 3 THF solvent molecules were present. A solvent mask was calculated and 452 electrons were found in a volume of 1212\%A^3^ in 2 voids per unit cell. This is consistent with the presence of 1.5[C4H8O], 1.5[C4H8O] per formula unit which account for 480 electrons per unit cell. The SQUEEZE[67] routine in the PLATON[68] program package was used to account for the electrons in the solvent accessible voids. Least-squares analysis yielded wR2 = 0.4141 and Goof = 1.042 for 1653 variables refined against 40732 data (0.70 Å), R1 = 0.1415 for those 26758 data with $I > 2.0\sigma(I)$.

Table 3.10. Crystal data and structure refinement for 3.2-Ln.			
	3.2-La (modulated)	**3.2-La (non-modulated)**	**3.2-Nd**
Identification code	kgb16_0m (Kito Gilbert-Bass)	kgb16b (Kito Gilbert-Bass)	kgb66 (Kito Gilbert-Bass)
Empirical formula	$C_{66}H_{90}B_3LaO_6$	$C_{66}H_{90}B_3LaO_6$	$C_{144.57}H_{204.9}B_6Nd_2O_{15}$
Formula weight	1150.8	1150.71	2536.12
Temperature/K	90	93(2)	93.15
Crystal system	Orthorhombic,	orthorhombic	monoclinic
Space group	*Pbca*(0β0)*s*0*s*†	$P2_12_12_1$	$P2_1/c$
a/Å	16.6351(8)	16.6501(10)	16.521(2)
b/Å	18.3261(6)	18.3268(9)	18.728(3)
c/Å	44.1081(17)	44.0965(19)	42.885(6)

α/°	90	90	90
β/°	90	90	91.355(3)
γ/°	90	90	90
Volume/Å^3	13446.6(9)	13455.7(12)	13265(3)
Z	8	8	4
ρ_{calc}g/cm^3	1.1369	1.136	1.27
μ/mm^{-1}	5.25	5.246	0.836
F(000)	4848	4848	5369
Crystal size/mm^3	0.212 × 0.182 × 0.143	0.212 × 0.182 × 0.143	0.357 × 0.351 × 0.282
Radiation	Cu Kα (λ = 1.54184)	CuKα (λ = 1.54178)	MoKα (λ = 0.71073)
2Θ range for data collection/°	3.74 to 138.6	4.008 to 133.532	1.9 to 61.766

Index ranges	$-20 \leq h \leq 18$, $-22 \leq k \leq 22$, $-53 \leq l \leq 50$	$-19 \leq h \leq 18$, $-21 \leq k \leq 21$, $-52 \leq l \leq 50$	$-23 \leq h \leq 23$, $0 \leq k \leq 26$, $0 \leq l \leq 61$
Reflections collected	159370	167942	40732
Independent reflections	37013 [$R_{int} = 0.0902$, $R_{sigma} = ?$]	23476 [$R_{int} = 0.1307$, $R_{sigma} = 0.0709$]	40732 [$R_{int} = ?$, $R_{sigma} = 0.0745$]
Data/restraints/parameters	37013/152/733	23476/1656/393	40732/676/1653
Goodness-of-fit on F^2	9.844	2.233	1.042
Final R indexes [$I>=2\sigma(I)$]	$R_1 = 0.3544$, $wR_2 = 0.6060$	$R_1 = 0.1924$, $wR_2 = 0.4876$	$R_1 = 0.1415$, $wR_2 = 0.3859$
Final R indexes [all data]	$R_1 = 0.3808$, $wR_2 = 0.6117$	$R_1 = 0.2122$, $wR_2 = 0.5144$	$R_1 = 0.1816$, $wR_2 = 0.4141$
Largest diff. peak/hole / e $Å^{-3}$	17.90/-10.35	9.01/-3.49	4.71/-3.63

Nd(OBMes$_2$)(NR$_2$)$_2$(THF), 3. A colorless crystal of approximate dimensions 0.075 x 0.138 x 0.237 mm was mounted in a cryoloop and transferred to a Bruker X8 Prospector diffractometer system. The APEX3[69] program package was used to determine the unit-cell parameters and for data collection (10sec/frame scan time). The raw frame data was processed using SAINT[70] and SADABS[64] to yield the reflection data file. Subsequent calculations were carried out using the SHELXTL[65] program package. There were no systematic absences nor any diffraction symmetry other than the Friedel condition. The centrosymmetric triclinic space group $P\bar{1}$ was assigned and later determined to be correct. The structure was solved by direct methods and refined on F^2 by full-matrix least-squares techniques. The analytical scattering factors[66] for neutral atoms were used throughout the analysis. Hydrogen atoms were included using a riding model. Least-squares analysis yielded wR2 = 0.0514 and Goof = 1.031 for 415 variables refined against 7745 data (0.83 Å), R1 = 0.0200 for those 7595 data with I > 2.0σ(I).

Table 3.11. Crystal data and structure refinement for Nd(OBMes$_2$)(NR$_2$)$_2$(THF), 3.3.	
Identification code	kgb31 (Kito Gilbert-Bass)
Empirical formula	$C_{34}H_{66}BN_2O_2Si_4Nd$
Formula weight	802.29
Temperature/K	92.85
Crystal system	triclinic
Space group	P-1
a/Å	8.7359(18)
b/Å	12.228(2)
c/Å	20.228(4)

α/°	89.06(3)
β/°	85.55(3)
γ/°	76.54(3)
Volume/Å^3	2095.1(8)
Z	2
ρ_{calc}g/cm^3	1.272
μ/mm^{-1}	10.766
F(000)	842.0
Crystal size/mm^3	0.237 × 0.138 × 0.075
Radiation	CuKα (λ = 1.54184)
2Θ range for data collection/°	4.382 to 137.994
Index ranges	-10 ≤ h ≤ 10, -14 ≤ k ≤ 14, -24 ≤ l ≤ 24
Reflections collected	49988
Independent reflections	7734 [R_{int} = 0.1410, R_{sigma} = 0.0672]
Data/restraints/parameters	7734/0/415
Goodness-of-fit on F^2	1.027
Final R indexes [I>=2σ (I)]	R_1 = 0.0374, wR_2 = 0.0942
Final R indexes [all data]	R_1 = 0.0384, wR_2 = 0.0950
Largest diff. peak/hole / e Å^{-3}	2.69/-1.62

K(μ-(Mes$_2$BO)$_2$Ce(N(SiMe$_3$)$_2$)$_2$, 3.5-Ce. A colorless crystal of approximate dimensions 0.196 x 0.224 x 0.364 mm was mounted in a cryoloop and transferred to a Bruker SMART APEX II diffractometer system. The APEX2[62] program package was used to determine the unit-cell

parameters and for data collection (30 sec/frame scan time). The raw frame data was processed using SAINT[63] and SADABS[64] to yield the reflection data file. Subsequent calculations were carried out using the SHELXTL[65] program package. The diffraction symmetry was *mmm* and the systematic absences were consistent with the orthorhombic space group *Pbca* that was later determined to be correct. The structure was solved by direct methods and refined on F^2 by full-matrix least-squares techniques. The analytical scattering factors[66] for neutral atoms were used throughout the analysis. Hydrogen atoms were included using a riding model. Least-squares analysis yielded wR2 = 0.0811 and Goof = 1.137 for 565 variables refined against 261814 data (0.70 Å), R1 = 0.0334 for those 13071 data with I > 2.0σ(I).

Table 3.12. Crystal data and structure refinement for K(μ-(Mes_2BO)$_2$Ce($N(SiMe_3)_2$)$_2$, 3.5-Ce.

Identification code	dlc2 (Domonic Caruth)
Empirical formula	$C_{48}H_{80}B_2CeKN_2O_2Si_4$
Formula weight	1030.34
Temperature/K	93.15
Crystal system	orthorhombic
Space group	Pbca
a/Å	21.5672(17)
b/Å	22.7025(17)
c/Å	23.0768(18)
α/°	90
β/°	90
γ/°	90

Volume/Å^3	11299.1(15)
Z	8
ρ_{calc}g/cm^3	1.211
μ/mm^{-1}	0.999
F(000)	4328.0
Crystal size/mm^3	0.364 × 0.224 × 0.196
Radiation	MoKα (λ = 0.71073)
2Θ range for data collection/°	3.146 to 61.122
Index ranges	-30 ≤ h ≤ 30, -32 ≤ k ≤ 31, -32 ≤ l ≤ 32
Reflections collected	261814
Independent reflections	17266 [R_{int} = 0.0611, R_{sigma} = 0.0269]
Data/restraints/parameters	17266/0/565
Goodness-of-fit on F^2	1.137
Final R indexes [I>=2σ (I)]	R_1 = 0.0334, wR_2 = 0.0681
Final R indexes [all data]	R_1 = 0.0574, wR_2 = 0.0811
Largest diff. peak/hole / e Å^{-3}	2.31/-0.88

K(μ-OBMes$_2$)$_2$(N(SiMe$_3$)$_2$)$_2$• 1.5 (C$_7$H$_8$), 3.5-Nd. A blue prism of approximate dimensions 0.200 x 0.202 x 0.239 mm was mounted in a cryoloop fiber and transferred to a Bruker X8 Prospector diffractometer system. The APEX3[69] program package was used to determine the unit-cell parameters and for data collection (10 sec/frame scan time). The raw frame data was processed using SAINT[63] and SADABS[64] to yield the reflection data file. Subsequent calculations were carried out using the SHELXTL[65] program package. There were no systematic absences. The

centrosymmetric triclinic space group $P\bar{1}$ was assigned and later determined to be correct. The structure was solved by direct methods and refined on F^2 by full-matrix least-squares techniques.[65] The analytical scattering factors[66] for neutral atoms were used throughout the analysis. Hydrogen atoms were included using a riding model. There were 1.5 molecules of toluene solvent present. One molecule was disordered about an inversion center and included with partial site-occupancy-factors. Least-squares analysis yielded wR2 = 0.0653 and Goof = 1.034 for 666 variables refined against 11562 data (0.83Å), R1 = 0.0257 for those 11373 data with I > 2.0σ(I).

Table 3.13. Crystal data and structure refinement for $K(\mu\text{-}OBMes_2)_2(N(SiMe_3)_2)_2 \bullet 1.5(C_7H_8)$, 3.5-Nd.	
Identification code	kgb35 (Kito Gilbert-Bass)
Empirical formula	$C_{58.5}H_{91.5}B_2KN_2NdO_2Si_4$
Formula weight	1172.15
Temperature/K	92.85
Crystal system	triclinic
Space group	P-1
a/Å	11.5741(7)
b/Å	12.0148(7)
c/Å	23.2986(14)
α/°	81.019(2)
β/°	88.121(2)
γ/°	79.023(2)
Volume/Å^3	3141.6(3)

Z	2
ρ_{calc}g/cm^3	1.239
μ/mm^{-1}	7.922
F(000)	1235.0
Crystal size/mm^3	0.239 × 0.202 × 0.2
Radiation	CuKα (λ = 1.54178)
2Θ range for data collection/°	3.84 to 138.056
Index ranges	-13 ≤ h ≤ 13, -14 ≤ k ≤ 14, -28 ≤ l ≤ 28
Reflections collected	49575
Independent reflections	11526 [R_{int} = 0.0391, R_{sigma} = 0.0309]
Data/restraints/parameters	11526/0/666
Goodness-of-fit on F^2	1.034
Final R indexes [I>=2σ (I)]	R_1 = 0.0257, wR_2 = 0.0650
Final R indexes [all data]	R_1 = 0.0261, wR_2 = 0.0653
Largest diff. peak/hole / e Å^{-3}	0.47/-0.95

[K$_2$(μ-(OBMes$_2$))$_3$Nd]$_2$(X$_8$)•(C$_6$H$_{14}$), 3.6, **X$_8$ modeled as isotropic carbons.** A light blue crystal of approximate dimensions 0.214 x 0.313 x 0.0.336 mm was mounted in a cryoloop / on a glass fiber and transferred to a Bruker X8 Prospector diffractometer system. The APEX3[69] program package was used to determine the unit-cell parameters and for data collection (10 sec/frame scan time). The raw frame data was processed using SAINT[63] and SADABS[64] to yield the reflection data file. Subsequent calculations were carried out using the SHELXTL[65] program package. The diffraction symmetry was 2/*m* and the systematic absences were consistent with the

monoclinic space group $P2_1/n$ that was later determined to be correct. The structure was solved by direct methods and refined on F^2 by full-matrix least-squares techniques. The analytical scattering factors[66] for neutral atoms were used throughout the analysis. Hydrogen atoms were included using a riding model. Hydrogen atoms were included using a riding model. Least-squares analysis yielded wR2 = 0.1581 and Goof = 1.075 for 653 variables refined against 10871 data (0.83 Å), R1 = 0.0556 for those 8878 data with $I > 2.0\sigma(I)$.

Table 3.14. Crystal data and structure refinement for $[K_2(\mu\text{-}(OBMes_2))_3Nd]_2(X_8)\bullet(C_6H_{14})$, 3.6, X_8 modeled as isotropic carbons.	
Identification code	kgb62_k
Empirical formula	$C_{129.12}H_{160}B_6K_2Nd_2O_6$
Formula weight	2239.48
Temperature/K	92.85
Crystal system	monoclinic
Space group	$P2_1/n$
a/Å	15.3982(7)
b/Å	20.1823(11)
c/Å	19.4907(9)
α/°	90
β/°	102.445(2)
γ/°	90
Volume/Å^3	5914.8(5)

Z	2
ρ_{calc}g/cm^3	1.257
μ/mm^{-1}	7.648
F(000)	2341.0
Crystal size/mm^3	0.336 × 0.313 × 0.214
Radiation	CuKα (λ = 1.54178)
2Θ range for data collection/°	6.382 to 136.756
Index ranges	-13 ≤ h ≤ 18, -24 ≤ k ≤ 24, -23 ≤ l ≤ 23
Reflections collected	114666
Independent reflections	10850 [R_{int} = 0.1228, R_{sigma} = 0.0605]
Data/restraints/parameters	10850/0/653
Goodness-of-fit on F^2	1.075
Final R indexes [I>=2σ (I)]	R_1 = 0.0556, wR_2 = 0.1375
Final R indexes [all data]	R_1 = 0.0741, wR_2 = 0.1581
Largest diff. peak/hole / e Å^{-3}	1.27/-1.79

[K(μ-OBMes$_2$)$_2$][K(μ-OBMes$_2$)$_3$]Nd, 3.7. A light blue crystal of approximate dimensions 0.072 x 0.131 x 0.177 mm was mounted in a cryoloop and transferred to a Bruker SMART APEX II diffractometer system. The APEX2[62] program package was used to determine the unit-cell parameters and for data collection (60 sec/frame scan time). The raw frame data was processed using SAINT[63] and SADABS[64] to yield the reflection data file. Subsequent calculations were carried out using the SHELXTL[65] program package. There were no systematic

absences nor any diffraction symmetry other than the Friedel condition. The centrosymmetric triclinic space group $P\bar{1}$ was assigned and later determined to be correct. The structure was solved by direct methods and refined on F^2 by full-matrix least-squares techniques. The analytical scattering factors[66] for neutral atoms were used throughout the analysis. Hydrogen atoms were included using a riding model. Least-squares analysis yielded wR2 = 0.0887 and Goof = 1.017 for 986 variables refined against 25261 data (0.7 Å), R1 = 0.0401 for those 20023 data with I > 2.0σ(I).

Table 3.15. Crystal data and structure refinement for [K(*μ*-OBMes$_2$)$_2$][K(*μ*-OBMes$_2$)$_3$]Nd, 3.7.	
Identification code	kgb63_k_K2NdOBMes5
Empirical formula	$C_{93}H_{117}B_5K_2NdO_5$
Formula weight	1591.35
Temperature/K	93.15
Crystal system	triclinic
Space group	P-1
a/Å	12.2813(15)
b/Å	12.9074(15)
c/Å	28.541(3)
α/°	93.573(2)
β/°	93.200(2)
γ/°	111.952(2)

Volume/Å^3	4172.8(9)
Z	2
ρ_{calc}g/cm^3	1.267
μ/mm^{-1}	0.773
F(000)	1676.0
Crystal size/mm^3	0.177 × 0.131 × 0.072
Radiation	MoKα (λ = 0.71073)
2Θ range for data collection/°	3.978 to 61.22
Index ranges	-17 ≤ h ≤ 17, -18 ≤ k ≤ 18, -40 ≤ l ≤ 40
Reflections collected	108315
Independent reflections	25261 [R_{int} = 0.0653, R_{sigma} = 0.0673]
Data/restraints/parameters	25261/0/986
Goodness-of-fit on F^2	1.017
Final R indexes [I>=2σ (I)]	R_1 = 0.0401, wR_2 = 0.0825
Final R indexes [all data]	R_1 = 0.0600, wR_2 = 0.0887
Largest diff. peak/hole / e Å^{-3}	0.66/-0.80

K(μ-OBMes$_2$)$_2$]$_2$Nd(OBMes$_2$), **3.8**. A light blue crystal of approximate dimensions 0.245 x 0.257 x 0.316 mm was mounted in a cryoloop / on a glass fiber and transferred to a Bruker SMART APEX II diffractometer system. The APEX2[62] program package was used to determine the unit-cell parameters and for data collection (60sec/frame scan time). The raw frame data was processed using SAINT[63] and SADABS[64] to yield the reflection data file. Subsequent calculations were

carried out using the SHELXTL[65] program package. The diffraction symmetry was 2/*m* and the systematic absences were consistent with the monoclinic space groups *Cc* and *C*2/*c*. It was later determined that space group *C*2/*c* was correct. The structure was solved by direct methods and refined on F^2 by full-matrix least-squares techniques. The analytical scattering factors[66] for neutral atoms were used throughout the analysis. Hydrogen atoms were included using a riding model. Least-squares analysis yielded wR2 = 0.0827 and Goof = 1.041 for 481 variables refined against 16956 data (0.7 Å), R1 = 0.0329 for those 13867 data with $I > 2.0\sigma(I)$. There were several high residuals present in the final difference-Fourier map. It was not possible to determine the nature of the residuals although it was probable that two hexane solvent was present. The S SQUEEZE[67] routine in the PLATON[68] program package was used to account for the electrons in the solvent accessible voids.

Table 3.16. Crystal data and structure refinement for $K(\mu\text{-}OBMes_2)_2]_2Nd(OBMes_2)$, 3.8.	
Identification code	kgb12monocc
Empirical formula	$C_{57}H_{83}B_{2.5}KNd_{0.5}O_{2.5}$
Formula weight	946.47
Temperature/K	133.15
Crystal system	monoclinic
Space group	C2/c
a/Å	24.370(2)
b/Å	28.331(3)
c/Å	16.5349(15)

α/°	90
β/°	99.230(2)
γ/°	90
Volume/Å^3	11268.4(18)
Z	8
ρ_{calc}g/cm^3	1.116
μ/mm^{-1}	0.583
F(000)	4052.0
Crystal size/mm^3	0.316 × 0.257 × 0.245
Radiation	MoKα (λ = 0.71073)
2Θ range for data collection/°	3.132 to 61.178
Index ranges	-34 ≤ h ≤ 34, -40 ≤ k ≤ 40, -23 ≤ l ≤ 22
Reflections collected	98928
Independent reflections	16956 [R_{int} = 0.0481, R_{sigma} = 0.0395]
Data/restraints/parameters	16956/0/481
Goodness-of-fit on F^2	1.041
Final R indexes [I>=2σ (I)]	R_1 = 0.0329, wR_2 = 0.0788
Final R indexes [all data]	R_1 = 0.0447, wR_2 = 0.0827
Largest diff. peak/hole / e Å^{-3}	0.61/-0.29

$Sm_4(\mu$-OBMes$)_6(\mu_4$-O)•C_6H_{14}, **3.9**. A black crystal of approximate dimensions 0.105 x 0.132 x 0.145 mm was mounted in a cryoloop and transferred to a Bruker X8 Prospector

diffractometer system. The APEX5[74] program package was used to determine the unit-cell parameters and for data collection (10 to 60 sec/frame variable scan time). The raw frame data was processed using SAINT[75] and SADABS[76] to yield the reflection data file. Subsequent calculations were carried out using the SHELXTL[65] program package. The diffraction symmetry was 4/*mmm* and the systematic absences were consistent with the tetragonal space group $P4_32_12$ or $P4_12_12$. Space group $P4_32_12$ was later determined to be correct.

The structure was solved by direct methods and refined on F^2 by full-matrix least-squares techniques. The analytical scattering factors[66] for neutral atoms were used throughout the analysis. Hydrogen atoms were included using a riding model. There was one molecule of *n*-hexane solvent present. The solvent molecule was located about a two-fold rotation axis and was disordered. Disordered atoms were included using multiple components with partial site-occupancy factors. Least-squares analysis yielded wR2 = 0.0776 and Goof = 1.012 for 621 variables refined against 9745 data (0.83 Å), R1 = 0.0317 for those 8963 data with I > 2.0σ(I). The absolute structure was assigned by refinement of the Flack parameter[6].

Table 3.17. Crystal data and structure refinement for $Sm_4(\mu\text{-}OBMes)_6(\mu_4\text{-}O)\bullet C_6H_{14}$, 3.9.	
Identification code	kgb60 (Kito Gilbert-Bass)
Empirical formula	$C_{114}H_{146}B_6O_7Sm_4$
Formula weight	2294.56
Temperature/K	92.85
Crystal system	tetragonal
Space group	$P4_32_12$

a/Å	16.2359(5)
b/Å	16.2359(5)
c/Å	40.5064(13)
α/°	90
β/°	90
γ/°	90
Volume/Å^3	10677.7(7)
Z	4
ρ_{calc}g/cm^3	1.427
μ/mm^{-1}	16.660
F(000)	4656.0
Crystal size/mm^3	0.145 × 0.132 × 0.105
Radiation	CuKα (λ = 1.54178)
2Θ range for data collection/°	5.864 to 137.054
Index ranges	-19 ≤ h ≤ 19, -18 ≤ k ≤ 19, -48 ≤ l ≤ 43
Reflections collected	62690
Independent reflections	9745 [R_{int} = 0.0756, R_{sigma} = 0.0463]
Data/restraints/parameters	9745/0/621
Goodness-of-fit on F^2	1.012
Final R indexes [I>=2σ (I)]	R_1 = 0.0317, wR_2 = 0.0758
Final R indexes [all data]	R_1 = 0.0360, wR_2 = 0.0776
Largest diff. peak/hole / e Å^{-3}	0.90/-0.51
Flack parameter	-0.006(2)

K(μ-OBMes$_2$)$_3$Sm(OBMes$_2$)(THF), **3.10**. A colorless crystal of approximate dimensions 0.270 x 0.402 x 0.423 mm was mounted in a cryoloop and transferred to a Bruker SMART APEX II diffractometer system. The APEX2[62] program package was used to determine the unit-cell parameters and for data collection (60sec/frame scan time). The raw frame data was processed using SAINT[63] and SADABS[64] to yield the reflection data file. Subsequent calculations were carried out using the SHELXTL[65] program package. The diffraction symmetry was 2/*m* and the systematic absences were consistent with the monoclinic space groups *Cc*, and *C*2/*c*. It was later determined that space group *C*2*c* was correct. The structure was solved by direct methods and refined on F^2 by full-matrix least-squares techniques. The analytical scattering factors[66] for neutral atoms were used throughout the analysis. Hydrogen atoms were included using a riding model. Least-squares analysis yielded wR2 = 0.0953 and Goof = 1.154 for 808 variables refined against 18324 data (0.78 Å), R1 = 0.0457 for those 15326 data with I > 2.0σ(I). There were several high residuals present in the final difference-Fourier map. It was probable that a mixture of hexanes solvent was present. The SQUEEZE[67] routine in the PLATON[68] program package was used to account for the electrons in the solvent accessible voids.

Table 3.18. Crystal data and structure refinement for K(μ-OBMes$_2$)$_3$Sm(OBMes$_2$)(THF), 3.10.	
Identification code	kgb9 (Kito Gilbert-Bass)
Empirical formula	$C_{76}H_{96}B_4O_5KSm$
Formula weight	1322.21

Temperature/K	133.15
Crystal system	monoclinic
Space group	C2/c
a/Å	29.639(3)
b/Å	33.518(3)
c/Å	17.3806(17)
α/°	90
β/°	105.8721(15)
γ/°	90
Volume/Å^3	16608(3)
Z	8
ρ_{calc}g/cm^3	1.058
μ/mm^{-1}	0.798
F(000)	5544.0
Crystal size/mm^3	0.423 × 0.402 × 0.27
Radiation	MoKα (λ = 0.71073)
2Θ range for data collection/°	2.43 to 54.206
Index ranges	-37 ≤ h ≤ 37, -42 ≤ k ≤ 42, -22 ≤ l ≤ 22
Reflections collected	171396
Independent reflections	18324 [R_{int} = 0.0301, R_{sigma} = 0.0146]
Data/restraints/parameters	18324/0/808
Goodness-of-fit on F^2	1.154
Final R indexes [I>=2σ (I)]	R_1 = 0.0457, wR_2 = 0.0838

Final R indexes [all data]	$R_1 = 0.0599$, $wR_2 = 0.0953$
Largest diff. peak/hole / e Å^{-3}	2.73/-1.38

$Sm(OBMes_2)_3(Et_2O)(CNXyl)•Sm(OBMes_2)_3(CNXyl)_3•2(Et_2O)$, **3.11.** A yellow crystal of approximate dimensions 0.062 x 0.223 x 0.344 mm was mounted in a cryoloop and transferred to a Bruker X8 Prospector diffractometer system. The APEX3[69] program package was used to determine the unit-cell parameters and for data collection (10 sec/frame scan time). The raw frame data was processed using SAINT[63] and SADABS[64] to yield the reflection data file. Subsequent calculations were carried out using the SHELXTL[65] program package. The diffraction symmetry was 2/*m* and the systematic absences were consistent with the monoclinic space group $P2_1/n$ that was later determined to be correct. The structure was solved by direct methods and refined on F^2 by full-matrix least-squares techniques. The analytical scattering factors[66] for neutral atoms were used throughout the analysis. Hydrogen atoms were located from a difference-Fourier map and refined (x,y,z and U_{iso}). There were two different molecular species present in than asymmetric unit and two molecules of diethyl ether solvent. Least-squares analysis yielded wR2 = 0.3500 and Goof = 1.134 for 1542 variables refined against 26570 data (0.83 Å), R1 = 0.1358 for those 21127 data with $I > 2.0\sigma(I)$. The quality of the data led to a poorly resolved model; however, the molecular connectivity has been established.

Table 3.19. Crystal data and structure refinement for $Sm(OBMes_2)_3(Et_2O)(CNXyl)•Sm(OBMes_2)_3(CNXyl)_3•2(Et_2O)$, 3.11.	
Identification code	kgb61 (Kito Gilbert-Bass)
Empirical formula	$C_{156}H_{198}B_6N_4O_9Sm_2$

Formula weight	2638.73
Temperature/K	93(2)
Crystal system	monoclinic
Space group	$P2_1/n$
a/Å	27.4079(17)
b/Å	15.4937(10)
c/Å	34.804(2)
α/°	90
β/°	101.173(4)
γ/°	90
Volume/Å^3	14499.5(16)
Z	4
ρ_{calc}g/cm^3	1.209
μ/mm^{-1}	6.451
F(000)	5552.0
Crystal size/mm^3	0.344 × 0.223 × 0.062
Radiation	CuKα (λ = 1.54178)
2Θ range for data collection/°	6.264 to 137.966
Index ranges	$-32 \leq h \leq 33$, $-18 \leq k \leq 18$, $-40 \leq l \leq 42$
Reflections collected	336696
Independent reflections	26570 [R_{int} = 0.1815, R_{sigma} = 0.0707]
Data/restraints/parameters	26570/0/1542
Goodness-of-fit on F^2	1.134

Final R indexes [I>=2σ (I)]	R_1 = 0.1358, wR_2 = 0.3360
Final R indexes [all data]	R_1 = 0.1604, wR_2 = 0.3500
Largest diff. peak/hole / e Å^{-3}	5.75/-3.69

REFERENCES

(1) Moehring, S. A.; Beltrán-Leiva, M. J.; Páez-Hernández, D.; Arratia-Pérez, R.; Ziller, J. W.; Evans, W. J. Rare-Earth Metal(II) Aryloxides: Structure, Synthesis, and EPR Spectroscopy of [K(2.2.2-Cryptand)][Sc($OC_6H_2{}^tBu_2$-2,6-Me-4)$_3$]. *Chemistry - A European Journal* **2018**, *24* (68), 18059–18067.

(2) Moehring, S. A.; Miehlich, M.; Hoerger, C. J.; Meyer, K.; Ziller, J. W.; Evans, W. J. A Room-Temperature Stable Y(II) Aryloxide: Using Steric Saturation to Kinetically Stabilize Y(II) Complexes. *Inorganic Chemistry* **2020**, *59* (5), 3207–3214.

(3) Anderson-Sanchez, L. M.; Yu, J. M.; Ziller, J. W.; Furche, F.; Evans, W. J. Room-Temperature Stable Ln(II) Complexes Supported by 2,6-Diadamantyl Aryloxide Ligands. *Inorganic Chemistry* **2023**, *62* (2), 706–714.

(4) Weese, K. J.; Bartlett, R. A.; Murray, B. D.; Olmstead, M. M.; Power, P. R. Synthesis and Spectroscopic and Structural Characterization of Derivatives of the Quasi-Alkoxide Ligand [$OBMes_2$]$^-$ (Mes = 2,4,6-$Me_3C_6H_2$). *Inorganic Chemistry* **1987**, *26* (15), 2409–2413.

(5) Beck, G.; Hitchcock, P. B.; Lappert, M. F.; Mackinnon, A. Lipophilic Lithium Alkoxides or Dialkylboroxides; X-Ray Structures of [Li(μ-OR')]$_2$ and Li(OBR_2)(Tmeda), [Tmeda =

($Me_2NCH_2)_2$, R = $CH(SiMe_3)_2$, R' = CBu^t_3 or BR_2]. *Journal of the American Chemical Society, Chemical Communications* **1989**, 1312–1314.

(6) Cole, S. C.; Coles, M. P.; Hitchcock, P. B. Boroxide Complexes of the Group 4 Metals: A "Noninnocent" Ligand in Olefin Polymerization. *Ogranometallics* **2005**, *24* (13), 3279–3289.

(7) Cole, S. C.; Coles, M. P.; Hitchcock, P. B. Sodium Boroxide Containing an Unusual Na_4O_4 Ladder Core. *Inorganic Chemistry Communications* **2010**, *13* (10), 1163–1165.

(8) Coles, M. P. Metal Compounds of Boron-Substituted Alkoxide ('Boroxide') Ligands. *Coordination Chemistry Reviews* **2016**, *323*, 52–59.

(9) Arnold, P. L.; Puig-Urrea, L.; Wells, J. A. L.; Yuan, D.; Cruickshank, F. L.; Young, R. D. Applications of Boroxide Ligands in Supporting Small Molecule Activation by U(III) and U(IV) Complexes. *Dalton Transactions* **2019**, *48* (15), 4894–4905.

(10) Arnold, P. L.; Halliday, C. J. V.; Puig-Urrea, L.; Nichol, G. S. Instantaneous and Phosphine-Catalyzed Arene Binding and Reduction by U(III) Complexes. *Inorganic Chemistry* **2021**, *60* (6), 4162–4170.

(11) Le Coz, E.; Hammoud, J.; Roisnel, T.; Cordier, M.; Dorcet, V.; Kahlal, S.; Carpentier, J. F.; Saillard, J. Y.; Sarazin, Y. Bonding in Barium Boryloxides, Siloxides, Phenoxides and Silazides: A Comparison with the Lighter Alkaline Earths. *Chemistry - A European Journal* **2021**, *27* (46), 11966–11982.

(12) Evans, W. J. Tutorial on the Role of Cyclopentadienyl Ligands in the Discovery of Molecular Complexes of the Rare-Earth and Actinide Metals in New Oxidation States. *Organometallics* **2016**, *35* (18), 3088–3100.

(13) Kamenskaya, A. N.; Mikheev, N. B. Complex Formation of the Lanthanides and Actinides in Lower Oxidation States. *Coordination Chemistry Reviews* **1991**, *109*, 1–59.

(14) Hitchcock, P. B.; Lappert, M. F.; Maron, L.; Protchenko, A. V. Lanthanum Does Form Stable Molecular Compounds in the +2 Oxidation State. *Angewandte Chemie International Edition* **2008**, *47* (8), 1488–1491.

(15) MacDonald, M. R.; Bates, J. E.; Fieser, M. E.; Ziller, J. W.; Furche, F.; Evans, W. J. Expanding Rare-Earth Oxidation State Chemistry to Molecular Complexes of Holmium(II) and Erbium(II). *Journal of the American Chemical Society* **2012**, *134* (20), 8420–8423.

(16) Corbey, J. F.; Woen, D. H.; Palumbo, C. T.; Fieser, M. E.; Ziller, J. W.; Furche, F.; Evans, W. J. Ligand Effects in the Synthesis of Ln^{2+} Complexes by Reduction of Tris(Cyclopentadienyl) Precursors Including C-H Bond Activation of an Indenyl Anion. *Organometallics* **2015**, *34* (15), 3909–3921.

(17) Gilbert-Bass, K.; Stennett, C. R.; Grotjahn, R.; Ziller, J. W.; Furche, F.; Evans, W. J. Exploring Sulfur Donor Atom Coordination Chemistry with La(II), Nd(II), and Tm(II) Using a Terphenylthiolate Ligand. *Chemical Communications* **2024**, *60* (34), 4601–4604.

(18) Huh, D. N.; Darago, L. E.; Ziller, J. W.; Evans, W. J. Utility of Lithium in Rare-Earth Metal Reduction Reactions to Form Nontraditional Ln^{2+} Complexes and Unusual [Li(2.2.2-Cryptand)]$^{1+}$ Cations. *Inorganic Chemistry* **2018**, *57* (4), 2096–2102.

(19) Kotyk, C. M.; MacDonald, M. R.; Ziller, J. W.; Evans, W. J. Reactivity of the Ln^{2+} Complexes [K(2.2.2-Cryptand)][$(C_5H_4SiMe_3)_3Ln$]: Reduction of Naphthalene and Biphenyl. *Organometallics* **2015**, *34* (11), 2287–2295.

(20) Palumbo, C. T.; Halter, D. P.; Voora, V. K.; Chen, G. P.; Chan, A. K.; Fieser, M. E.; Ziller, J. W.; Hieringer, W.; Furche, F.; Meyer, K.; Evans, W. J. Metal versus Ligand Reduction in Ln^{3+} Complexes of a Mesitylene-Anchored Tris(Aryloxide) Ligand. *Inorganic Chemistry* **2018**, *57* (5), 2823–2833.

(21) Dan, X.; Du, J.; Zhang, S.; Seed, J. A.; Perfetti, M.; Tuna, F.; Wooles, A. J.; Liddle, S. T. Arene-, Chlorido-, and Imido-Uranium Bis- and Tris(Boryloxide) Complexes. *Inorganic Chemistry* **2024**, *63* (21), 9588–9601.

(22) Fetrow, T. V.; Zgrabik, J.; Bhowmick, R.; Eckstrom, F. D.; Crull, G.; Vlaisavljevich, B.; Daly, S. R. Quantifying the Influence of Covalent Metal-Ligand Bonding on Differing Reactivity of Trivalent Uranium and Lanthanide Complexes. *Angewandte Chemie - International Edition* **2022**, *61* (45), e202211145.

(23) Janssen, T.; Janner, A.; Looijenga-Vos, A.; de Wolff, P. M. *International Tables for Crystallography Volume C: 9.8 Incommensurate and Commensurate Modulated Structures*; Prince, E., Ed.; 2006; Vol. C.

(24) Veith, M.; Belot, C.; Guyard, L.; Huch, V.; Knorr, M.; Zimmer, M. Synthesis and Crystal Structure Investigations of Trivalent Rare Earth (Y^{3+}, Nd^{3+}, Er^{3+}) Thienyl-Substituted Methoxides. *European Journal of Inorganic Chemistry* **2008**, *2008* (15), 2397–2406.

(25) Veith, M.; Belot, C.; Huch, V.; Cui, H. L.; Guyard, L.; Knorr, M.; Wickleder, C. Synthesis, Crystal Structure and Physico-Chemical Studies of Neodymium and Erbium Methoxides Containing Thienyl Substituents. *European Journal of Inorganic Chemistry* **2010**, *2010* (6), 879–889.

(26) Hamidi, S.; Deacon, G. B.; Junk, P. C.; Neumann, P. Direct Reaction of Iodine-Activated Lanthanoid Metals with 2,6-Diisopropylphenol. *Dalton Transactions* **2012**, *41* (12), 3541–3552.

(27) Lawrence Clark; Glen B. Deacon; Craig M. Forsyth; Peter C. Junk; Philip Mountford; Josh P. Townley. Low-Coordinate Rare-Earth Complexes of the Asymmetric,4-Di-Tert-Butylphenolate Ligand Prepared by Redox/Protolysis Reactions, and Their Reactivity Towards Ring-Opening Polymerisation. *Dalton Transactions* **2010**, *39* (29), 6693–6704.

(28) Witzke, R. J.; Hait, D.; Head-Gordon, M.; Tilley, T. D. Two-Coordinate Iron(I) Complexes on the Edge of Stability: Influence of Dispersion and Steric Effects. *Organometallics* **2021**, *40* (11), 1758–1764.

(29) Queen, J. D.; Anderson-Sanchez, L. M.; Stennett, C. R.; Rajabi, A.; Ziller, J. W.; Furche, F.; Evans, W. J. Synthesis of Crystallographically Characterizable Bis(Cyclopentadienyl) Sc(II) Complexes: $(C_5H_2TBu_3)_2Sc$ and $\{[C_5H_3(SiMe_3)_2]_2ScI\}^{1-}$. *Journal of the American Chemical Society* **2024**, *146* (5), 3279–3292.

(30) Cloke, F. G. N.; Khan, K.; Perutzb, R. N. η-Arene Complexes of Scandium(0) and Scandium(II). *Journal of the Chemical Society, Chemical Communications* **1991**, No. 19, 1372–1373.

(31) Anderson, D. M.; Cloke, F. G. N.; Cox, P. A.; Edelstein, N.; Green, J. C.; Pang, T.; Sameh, A. A.; Shalimoff, G. On the Stability and Bonding in Bis(η-Arene)Lanthanide Complexes. *Journal of the Chemical Society, Chemical Communications* **1989**, No. 1, 53–55.

(32) Brennan, J. G.; Cloke, F. G. N.; Sameh, A. A.; Zalkin Allan. Synthesis of Bis(η-1,3,5-Tri-t-Butylbenzene) Sandwich Complexes of Yttrium(0) and Gadolinium(0); the X-Ray Crystal Structure of the First Authentic Lanthanide(0) Complex, $[Gd(\eta\text{-}Bu^t{}_3C_6H_3)_2]$. *Journal of the Chemical Society, Chemical Communications* **1987**, No. 21, 1668–1669.

(33) Yang, L.; Powell, D. R.; Houser, R. P. Structural Variation in Copper(I) Complexes with Pyridylmethylamide Ligands: Structural Analysis with a New Four-Coordinate Geometry Index, T4. *Journal of the Chemical Society. Dalton Transactions* **2007**, No. 9, 955–964.

(34) Andersen, R. A.; Templeton, D. H.; Zalkin, A. Structure of Tris(Bis(Trimethylsilyl)Amido)Neodymium(III), $Nd[N(Si(CH_3)_3)_2)]_3$. *Inorganic Chemistry* **1978**, *17* (8), 2317–2319.

(35) Ryan, A. J.; Darago, L. E.; Balasubramani, S. G.; Chen, G. P.; Ziller, J. W.; Furche, F.; Long, J. R.; Evans, W. J. Synthesis, Structure, and Magnetism of Tris(Amide) $[Ln\{N(SiMe_3)_2\}_3]^{1-}$ Complexes of the Non-Traditional +2 Lanthanide Ions. *Chemistry - A European Journal* **2018**, *24* (30), 7702–7709.

(36) Evans, W. J.; Kozimor, S. A.; Brady, J. C.; Davis, B. L.; Nyce, G. W.; Seibel, C. A.; Ziller, J. W.; Doedens, R. J. Metallocene Allyl Reactivity in the Presence of Alkenes Tethered to Cyclopentadienyl Ligands. *Organometallics* **2005**, *24* (10), 2269–2278.

(37) Evans, W. J.; Rego, D. B.; Ziller, J. W. Synthesis, Structure, and 15N NMR Studies of Paramagnetic Lanthanide Complexes Obtained by Reduction of Dinitrogen. *Inorganic Chemistry* **2006**, *45* (26), 10790–10798.

(38) Evans, W. J.; Perotti, J. M.; Kozimor, S. A.; Champagne, T. M.; Davis, B. L.; Nyce, G. W.; Fujimoto, C. H.; Clark, R. D.; Johnston, M. A.; Ziller, J. W. Synthesis and Comparative η^1-Alkyl and Sterically Induced Reduction Reactivity of $(C_5Me_5)_3Ln$ Complexes of La, Ce, Pr, Nd, and Sm. *Organometallics* **2005**, *24* (16), 3916–3931.

(39) Evans, W. J.; Allen, N. T.; Workman, P. S.; Meyer, J. C. Large Scale Synthesis of Dysprosium and Neodymium Diiodides. *Inorganic Chemistry* **2003**, *42* (9), 3097–3099.

(40) Huang, W.; Diaconescu, P. L. Rare Earth Arene-Bridged Complexes Obtained by Reduction of Organometallic Precursors; 2014; pp 261–329.

(41) Cassani, M. C.; Gun'ko, Y. K.; Hitchcock, P. B.; Lappert, M. F.; Laschi, F. Synthesis and Characterization of Organolanthanidocene(III) (Ln = La, Ce, Pr, Nd) Complexes Containing the 1,4-Cyclohexa-2,5-Dienyl Ligand (Benzene 1,4-Dianion): Structures of $[K([18]\text{-Crown-}6)][Ln\{\eta^5\text{-}C_5H_3(SiMe_3)_2\text{-}1,3\}2(C_6H_6)]$. *Organometallics* **1999**, *18* (26), 5539–5547.

(42) Arliguie, T.; Lance, M.; Nierlich, M.; Ephritikhine, M. *Inverse Cycloheptatrienyl Sandwich Complexes of Uranium and Neodymium*; 1997.

(43) Cassani, M. C.; Gun'ko, Y. K.; Hitchcock, P. B.; Hulkes, A. G.; Khvostov, A. V; Lappert, M. F.; Protchenko, A. V. Mini Review Aspects of Non-Classical Organolanthanide Chemistry. *Journal of Organometallic Chemistry* **2002**, *647*, 71–83.

(44) Christine Gaffney, B.; Harrison, P. G.; King, T. J. The Crystal and Molecular Structure of Adamanta-(μ_4-Oxo-Hexakis(μ-Triphenylsiloxy)-Tetralead(II). *Journal of the American Chemical Society, Chemical Communications* **1980**, No. 24, 1251–1252.

(45) Hossack, C. H.; Butcher, R. J.; Cahill, C. L.; Besson, C. Structural Diversity of Lanthanide 3-Nitrotrispyrazolylborates: Tunable Nuclearity and Intra-Ligand Charge Transfer Sensitization of Visible and NIR Ln^{3+}Emission. *Inorganic Chemistry* **2021**, *60* (20), 15724–15743.

(46) Kumar Jami, A.; Prangya Behera, S.; Mondal, S.; Baskar, V. Lutetium Oxo Clusters Utilizing Mixed Ligand System: Isolation of a Rare Lu_4 Oxo Cluster in a Tetrahedral Architecture. *Inorganic Chemistry Communications* **2022**, *143*, 109784.

(47) Yang, Q.; Ungur, L.; Chibotaru, L. F.; Tang, J. Toroidal *versus* Centripetal Arrangement of the Magnetic Moment in a Dy_4 Tetrahedron. *Chemical Communications* **2022**, *58* (11), 1784–1787.

(48) Tamang, S. R.; Singh, A.; Bedi, D.; Bazkiaei, A. R.; Warner, A. A.; Glogau, K.; McDonald, C.; Unruh, D. K.; Findlater, M. Polynuclear Lanthanide–Diketonato Clusters for the Catalytic Hydroboration of Carboxamides and Esters. *Nature Catalysis* **2020**, *3* (2), 154–162.

(49) Wang, G. C.; So, Y. M.; Wong, K. L.; Au-Yeung, K. C.; Sung, H. H. Y.; Williams, I. D.; Leung, W. H. Synthesis, Structure, and Reactivity of a Tetranuclear Cerium(IV) Oxo Cluster Supported by the Kläui Tripodal Ligand $[Co(\eta^5\text{-}C_5H_5)\{P(O)(OEt)_2\}_3]^-$. *Chemistry - A European Journal* **2015**, *21* (45), 16126–16135.

(50) Belli Dell'Amico, D.; Biagini, P.; Chiaberge, S.; Falchi, L.; Labella, L.; Lezzerini, M.; Marchetti, F.; Samaritani, S. Partial and Exhaustive Hydrolysis of Lanthanide N,N-Dialkylcarbamato Complexes. A Viable Access to Lanthanide Mixed Oxides. *Polyhedron* **2015**, *102*, 452–461.

(51) Balashova, T. V.; Ilichev, V. A.; Grishin, I. D.; Rumyantcev, R. V.; Fukin, G. K.; Bochkarev, M. N. Lanthanide Complexes with Oxygen Bridges as Models for Potential Up-Conversion Materials. *Inorganica Chimica Acta* **2018**, *483*, 379–385.

(52) Kato, N.; Mita, T.; Kanai, M.; Therrien, B.; Kawano, M.; Yamaguchi, K.; Danjo, H.; Sei, Y.; Sato, A.; Furusho, S.; Shibasaki, M. Assembly State of Catalytic Modules as Chiral Switches in Asymmetric Strecker Amino Acid Synthesis. *Journal of the American Chemical Society* **2006**, *128* (21), 6768–6769.

(53) Singh-Wilmot, M. A.; Kahwa, I. A.; White, A. J. P.; Williams, D. J.; Lough, A. J. Tunable Electronic Interactions in Small Lanthanide(III) Nanoclusters: The Comparative Effects of OH^- and O^{2-} Supramolecular Glues on Europium(III)-to-Dysprosium(III) Energy Transfer. *Polyhedron* **2010**, *29* (1), 270–279.

(54) Alshamrani, A. F. A.; Santoro, O.; Prior, T. J.; Alamri, M. A.; Stasiuk, G. J.; Elsegood, M. R. J.; Redshaw, C. Scandium Calix[n]Arenes (N= 4, 6, 8): Structural, Cytotoxicity and Ring Opening Polymerization Studies. *Dalton Transactions* **2021**, *50* (24), 8302–8306.

(55) Gordon, R. G.; Barry, S.; R Broomhall-Dillard, R. N.; Teff, D. J. *Synthesis and Solution Decomposition Kinetics of Flash-Vaporizable Liquid Barium Beta-Diketonates*; 2000.

(56) Addison, A. W.; Nageswara Rao, T.; Reedijk, J.; van Rijn, J.; Verschoor, G. C. Synthesis, Structure, and Spectroscopic Properties of Copper(II) Compounds Containing Nitrogen-Sulphur Donor Ligands; the Crystal and Molecular Structure of Aqua[1,7-Bis(N-Methylbenzimidazol-2'-

Yl)-2,6-Dithiaheptane]Copper(II) Perchlorate. *Journal of the Chemical Society, Dalton Transactions* **1984**, No. 7, 1349–1356.

(57) Izod, K.; Liddle, S. T.; Clegg, W. A Convenient Route to Lanthanide Triiodide THF Solvates. Crystal Structures of $LnI_3(THF)_4$ [Ln = Pr] and $LnI_3(THF)_{3.5}$ [Ln = Nd, Gd, Y]. *Inorganic Chemistry* **2004**, *43* (1), 214–218.

(58) Girard, P.; Namy, J. L.; Kagan, B. Divalent Lanthanide Derivatives in Organic Synthesis. 1. Mild Preparation of SmI_2 and YbI_2 and Their Use as Reducing or Coupling Agents. *Journal of the American Chemical Society* **1980**, *8* (102), 2693–2698.

(59) Bradley, D. C.; Ghotra, J. S.; Hart, F. A. Low Co-Ordination Numbers in Lanthanide and Actinide Compounds. Part 1. The Preparation and Characterization of Tris{bis(Trimethylsilyl)-Amido}lanthanides. *Journal of the Chemical Society, Dalton Transactions* **1973**, 1021–1023.

(60) Gabbaï, F. P.; Chirik, P. J.; Fogg, D. E.; Meyer, K.; Mindiola, D. J.; Schafer, L. L.; You, S. L. An Editorial about Elemental Analysis. *Organometallics* **2016**, *35* (19), 3255–3256.

(61) Kuveke, R. E. H.; Barwise, L.; Van Ingen, Y.; Vashisth, K.; Roberts, N.; Chitnis, S. S.; Dutton, J. L.; Martin, C. D.; Melen, R. L. An International Study Evaluating Elemental Analysis. *ACS Central Science* **2022**, *8* (7), 855–863.

(62) APEX2, Version 2014.11-0. Bruker AXS, Inc.: Madison, WI 2014.

(63) SAINT, Version 8.34a. Bruker AXS, Inc.: Madison, WI 2013.

(64) Sheldrick, G. M. SADABS, Version 2014/5. Bruker AXS, Inc.: Madison, WI 2014.

(65) Sheldrick, G. M. SHELXTL, Version 2014/7. Bruker AXS, Inc.: Madison, WI 2014.

(66) International Tables for Crystallography. *Dordrecht: Kluwer Academic Publishers*. 1992.

(67) Spek, A. L. PLATON SQUEEZE: A Tool for the Calculation of the Disordered Solvent Contribution to the Calculated Structure Factors. *Acta Crystallographica* **2015**, *C71*, 9–19.

(68) Spek, A. L. Structure Validation in Chemical Crystallography. *Acta Crystallographica* **2009**, *D65* (2), 148–155.

(69) APEX3, Version 2018.1-0. Bruker AXS Inc.: Madison, WI 2018.

(70) SAINT, Version 8.38a. Bruker AXS inc. : Madison, WI 2013.

(71) Parsons, S.; Flack, H. D.; Wagner, T. Use of Intensity Quotients and Differences in Absolute Structure Refinement. *Acta Crystallographica* **2013**, *B69*, 249–259.

(72) Petříček, V.; Palatinus, L.; Plášil, J.; Dušek, M. Jana2020 – a New Version of the Crystallographic Computing System Jana. *Zeitschrift für Kristallographie - Crystalline Materials* **2023**, *238* (7–8), 271–282.

(73) Palatinus, L.; Chapuis, G. SUPERFLIP – a Computer Program for the Solution of Crystal Structures by Charge Flipping in Arbitrary Dimensions. *Journal of Applied Crystallography* **2007**, *40* (4), 786–790.

(74) APEX5 Version 2023.9-2. Bruker AXS, Inc.: Madison, WI 2023.

(75) SAINT Version 8.40b. Bruker AXS, Inc: Madison, WI 2013.

(76) Sheldrick, G. M. SADABS, Version 2016/2. Bruker AXS, Inc: Madison, WI 2016.

–Chapter 4–

Using the Di(mesityl)boroxide Ligand, $(OBMes_2)^{1-}$, to Generate a Ce(IV) Complex (Mes = C_6H_2-2,4,6-Me_3)

INTRODUCTION

Since their discovery, most coordination complexes of the lanthanides contain the lanthanide metals in the 3+ oxidation state. Within the past thirty years or so, the window of available oxidation states has been expanded to include 0,[1,2] 2+, [3–13] 4+,[4,7,14,15]and even 5+[16] via significant discoveries in the reduction and oxidation chemistries of these complexes. Recently, as described in Chapter 3, the use of the di(mesityl)boroxide ligand, $(OBMes_2)^{1-}$ (Mes = C_6H_2-2,4,6-Me_3), as an electron-deficient alkoxide analog has been studied for its ability to stabilize lanthanides in the 2+ oxidation state through reduction with KC_8. These studies revealed quite complicated chemistry and resulted in the formation of various "ate" complexes, $[M^+][LnA_4]^{1-}$ (M = alkali metal; Ln = La, Ce, Pr, Nd, Tb; A = anionic ligand), in which more than three negatively charged anionic ligands are bound to the Ln(III) center and charge-balanced with an alkali metal countercation. In all of these (dimesityl)boroxide examples, the alkali metal was chelated by the arene rings and the oxygen donor atoms of the boroxide ligands. Although this ligand did not seem suitable for reduction of the lanthanides to the 2+ oxidation state, the encapsulation of alkali metals is reminiscent of the potassium-encapsulated $K(\mu\text{-}Ph_3SiO)_3Ln^{III}(OSiPh_3)(THF)$[3,4] (Ln = Pr, Tb), $(THF)K(\mu\text{-}^t BuO)_3SiO)_3Tb^{III}(OSi(O^tBu)_3)(THF)$[3,14] and $K\{\mu\text{-}[(NEt_2)(R)PN]\}_2Tb[NP(R)(NEt_2)]_2$[7] (R = 1,2-bis-^{t}Bu-diamidoethane) siloxide and imidophosphorane complexes that were the precursors to the first Pr(IV) and Tb(IV) molecular structures, $Ln^{IV}(OSiPh_3)_4$, $Tb^{IV}(OSi(O^tBu)_3)_4$,

and $Tb^{IV}[NP(R)(NEt_2)]_4$.[15] In these complexes, the oxidation of the lanthanide may have been facilitated by the fact that four ligands were already bound to it, Scheme 4.1. To investigate the extension of this approach to the (dimesityl)boroxide ate salts, oxidation reactions were pursued to evaluate the compatibility of Ce(IV) with boroxide ligands.

Scheme 4.1. Previously isolated molecular complexes of Pr(IV) and Tb(IV) using the (a)

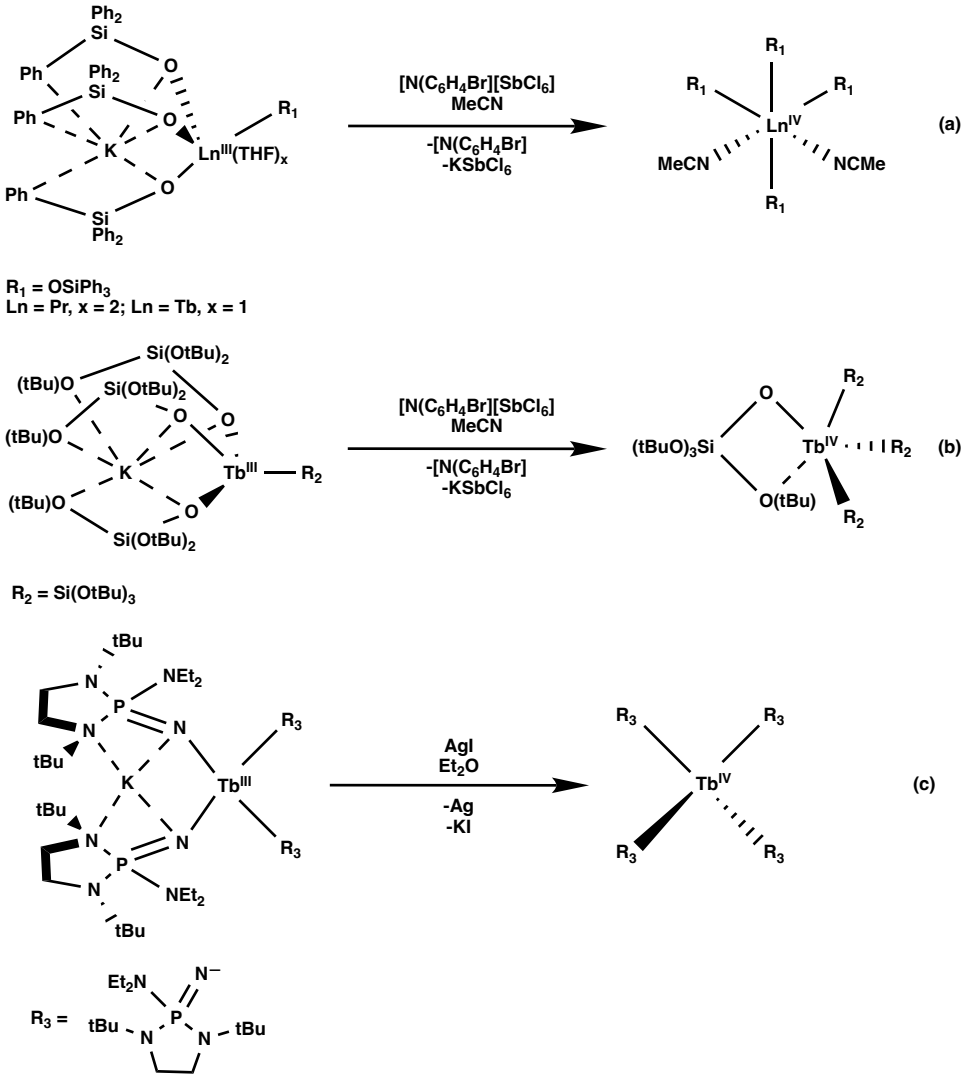

triphenylsiloxide,[3,4] (b) tris(*tert*-butoxy)siloxide[14] and (c) the tris(amidyl)imidophosphorane[7] ligands, formed from "ate" salts.[15]

RESULTS

To explore the stability of Ce(IV) with di(mesityl)boroxide ligands, a yellow slurry of $Ce(OTf)_4$ in ca. 10 mL of MeCN at 80 °C was treated with a solution of four equiv of $KOBMes_2$ in ca. 1 mL of THF at 25 °C. Over the span of 15 minutes, the slurry changed to a dark orange/yellow color while it was left to cool to room temperature. Stirring continued for 18 h, and after extraction away from colorless solids into ca. 5 mL of toluene, the resulting orange solution was placed in the freezer at −35 °C to produce dark red crystals of **4.1**, $Ce(OBMes_2)_4(THF)_2$, eq 4.1, Figure 4.1.

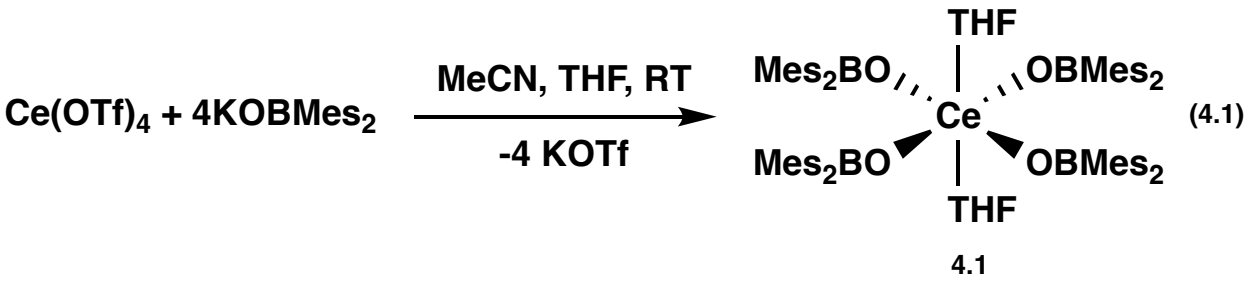

4.1

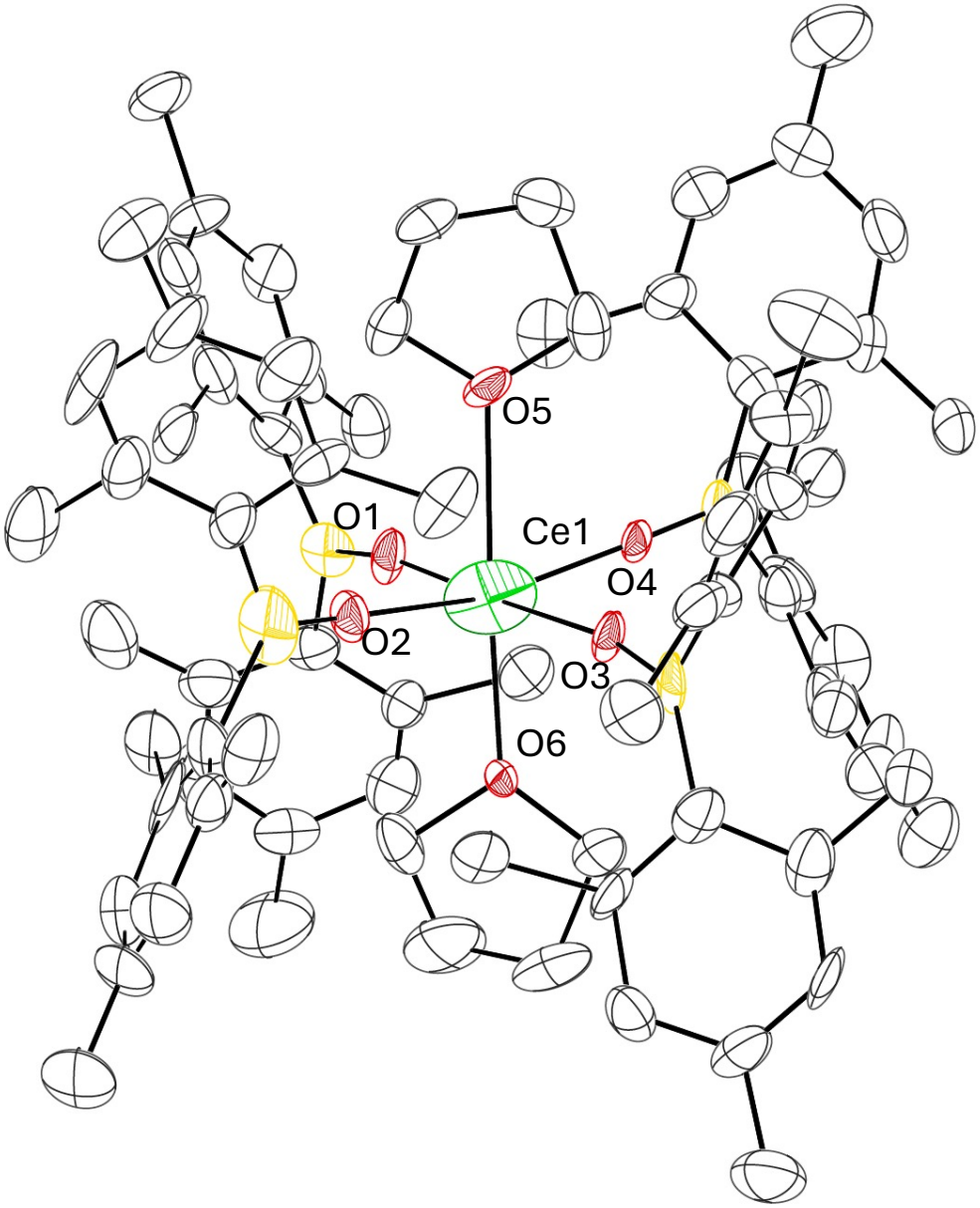

Figure 4.1. Graphical representation of $Ce^{IV}(OBMes_2)_4(THF)_2$, **4.1.** Thermal ellipsoids are drawn at the 50% probability level and hydrogen atoms are not shown for clarity.

Complex **4.1** crystallizes in the rhombohedral space group R3 and features a distorted octahedral geometry with four $(OBMes_2)^{1-}$ ligands in an equatorial plane and axial THF ligands. The O(boroxide)-Ce-O(boroxide) angles are 88.3(5) to 91.7(5)° and the O(THF)-Ce-O(boroxide) angles are 85.4(5) to 94.9(5)°.

The ^{1}H NMR spectrum of **4.1** shows three resonances at δ = 6.48, 2.28 and 0.28 in a 2:3:6 integration ratio, which is stoichiometrically consistent for the Ar-H, *p*-Me, and *o*-Me proton ratios of the di(mesityl)boroxide ligand respectively, Figure 4.2. Although these resonances are distinct from those of $HOBMes_2$ and $[(Mes_2BO)_2Ce(\mu\text{-}OBMes_2)]_2$, similar diamagnetic species like $La(OBMes_2)_3(THF)_3$ show a downfield shift of the *p*-Me hydrogen resonances in comparison with the *o*-Me resonances (Table 4.1).

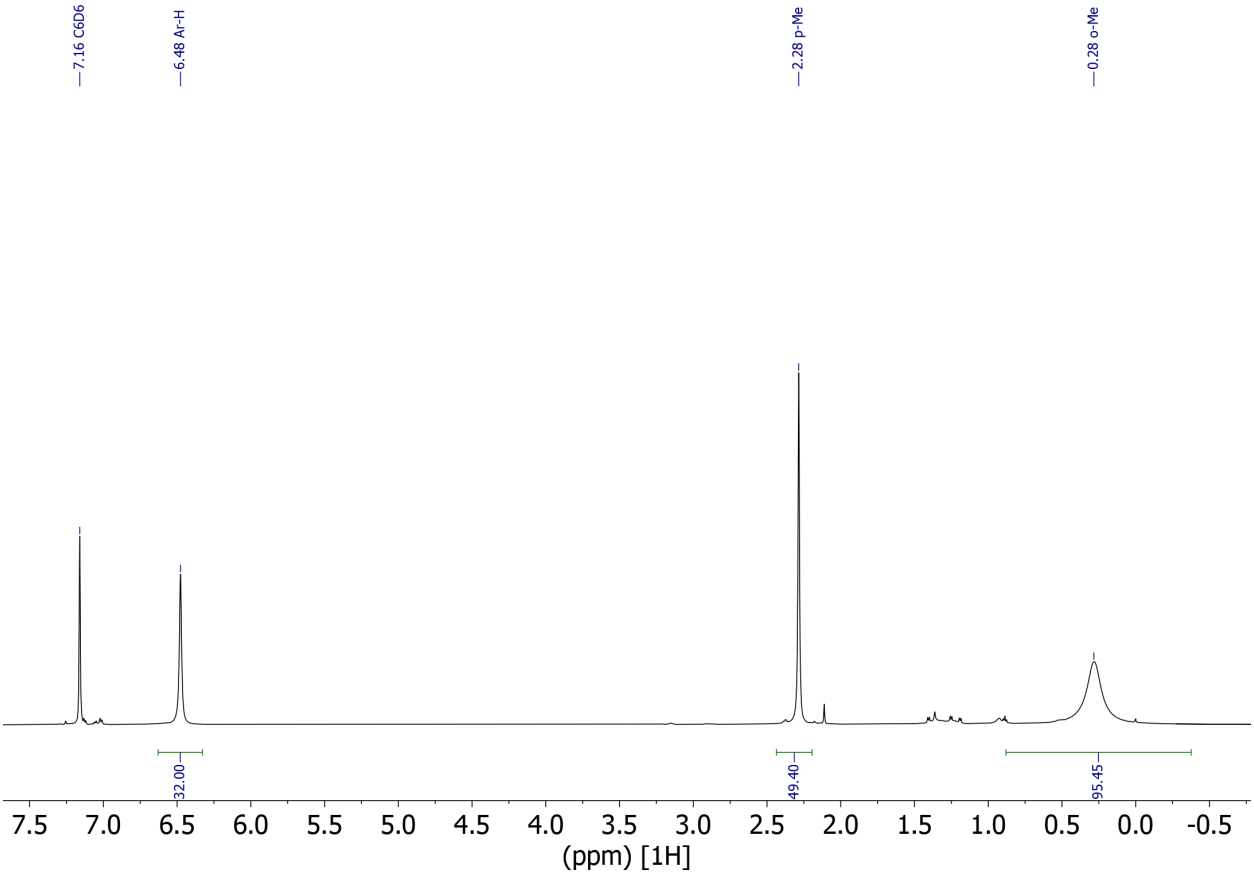

Figure 4.2. ^{1}H NMR (500 MHz, 298K) spectrum of **4.1** in deuterated benzene (residual proton peak marked at δ = 7.16 ppm). Note**:** Resonances of side product HNR_2 at 0.10 ppm. Residual solvent resonances for hexane marked at δ = 1.24 and 0.98, and for THF at 3.46 and 1.39 ppm.

Table 4.1. ^{1}H NMR shifts for selected complexes in C_6D_6 (δ ppm)

	4.1	$La(OBMes_2)_3(THF)_3$	$[(Mes_2BO)_2Ce(\mu\text{-}OBMes_2)]_2$	$HOBMes_2$
Ar-H (terminal)	6.48	6.74	6.68	6.73
Ar-H (bridging)	–	–	6.47	–
o-Me (terminal)	2.28	2.4	0.22	2.26
o-Me (bridging)	–	–	3.05	–
p-Me (terminal)	0.28	1.23	2.37	2.17
p-Me (bridging)	–	–	1.94	–

Surprisingly, resonances for THF are not present in the spectrum of **1** which, suggests that coordinated THF ligands were lost during solvent removal in preparation of the NMR sample.

After it was established that the Ce(IV) cation could be supported by the (dimesityl)boroxide ligand, the prospect of oxidation of a Ce(III) complex was addressed. Attempts to synthesize the "$K(\mu\text{-}Mes_2BO)_3Ce^{III}(OBMes_2)(THF)$" ate complex from $CeCl_3$ and four equiv of $KOBMes_2$ resulted in colorless precipitates. No crystallographically characterizable material could be collected and after treatment of the precipitates with AgI, the ^1H NMR spectrum of the product was difficult to interpret and was inconsistent with resonances found in that of **4.1**. However, treatment of $Ce(NR_2)_3$ with four equiv of $KOBMes_2$ did lead to the isolation of crystals of the heteroleptic ate salt, $K(\mu\text{-}Mes_2BO)_2Ce(NR_2)_2$, **4.2-Ce**. This complex could be reliably

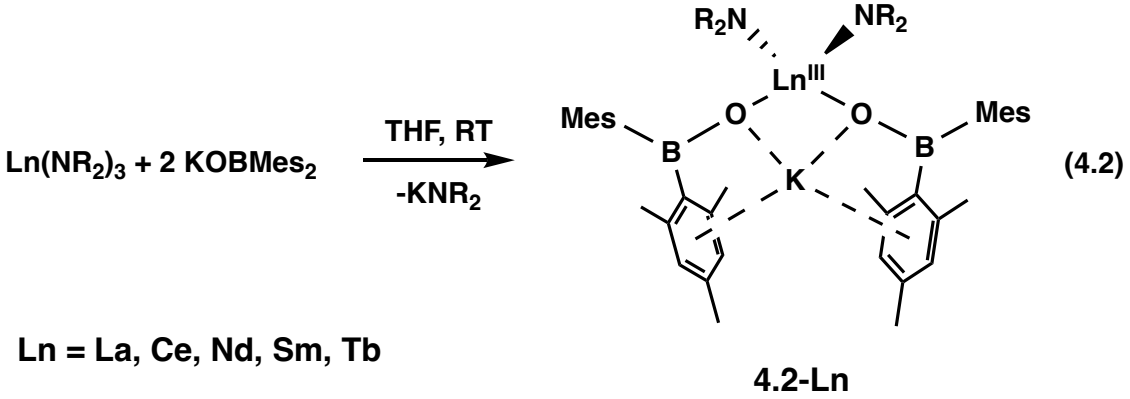

formed in 60% yield from the treatment of $Ce(NR_2)_3$ with two equiv $KOBMes_2$ in THF, eq 4.2, Figure 4.3.

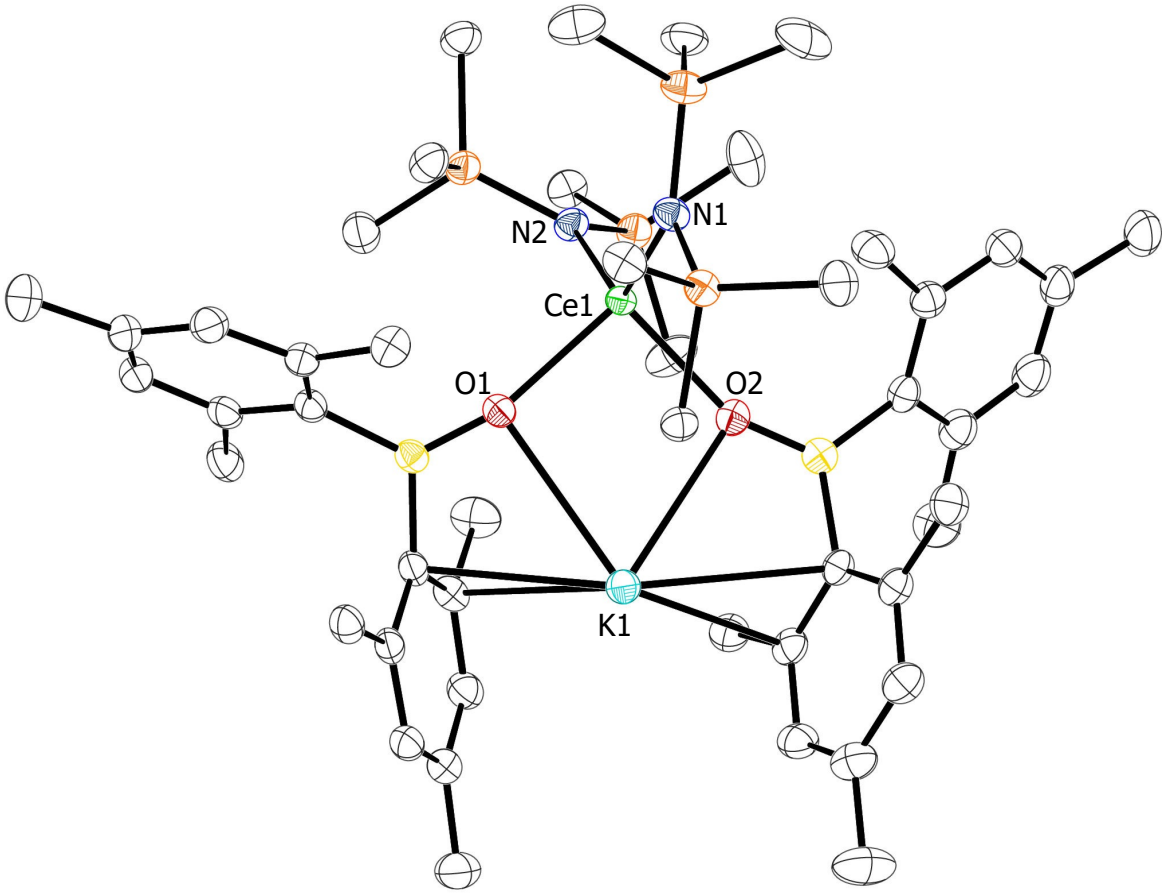

Figure 4.3. Graphical representation of $K(\mu\text{-}Mes_2BO)_2Ce(NR_2)_2$, **4.2-Ce**. Thermal ellipsoids are drawn at the 50% probability level and hydrogen atoms are not shown for clarity.

Complex **4.2-Ce** crystallizes in the orthorhombic space group *Pbca* and has two $(NR_2)^{1-}$ ligands and two $(OBMes_2)^{1-}$ ligands bound to the central Ce(III) metal in a distorted tetrahedral arrangement with a τ_4 value of 0.88 (where $\tau_4 = 1$ is tetrahedral and $\tau_4 = 0$ is square planar). A potassium countercation is encapsulated by the two $(OBMes_2)^{1-}$ ligands and is coordinated through the oxygen atoms of the boroxides as well as the mesityl rings through an η^2 interaction with one

ring and an η^3 interaction with the other, Table 4.2. These rings are canted at a Cnt1-K-Cnt2 angle of 129.7° (Cnt = centroid of the arene ring).

The ^{1}H NMR spectrum of this complex shows only one set of resonances for the *o*-Me, *p*-Me, Ar-*H* and Si*Me*$_3$ hydrogens in the ratio of 2:6:3:9 which suggests that the solid state structure is not maintained in solution. The spectrum does not show a distinction between aryl hydrogens, suggesting labile coordination of the arenes to the metal center, Figure 4.4.

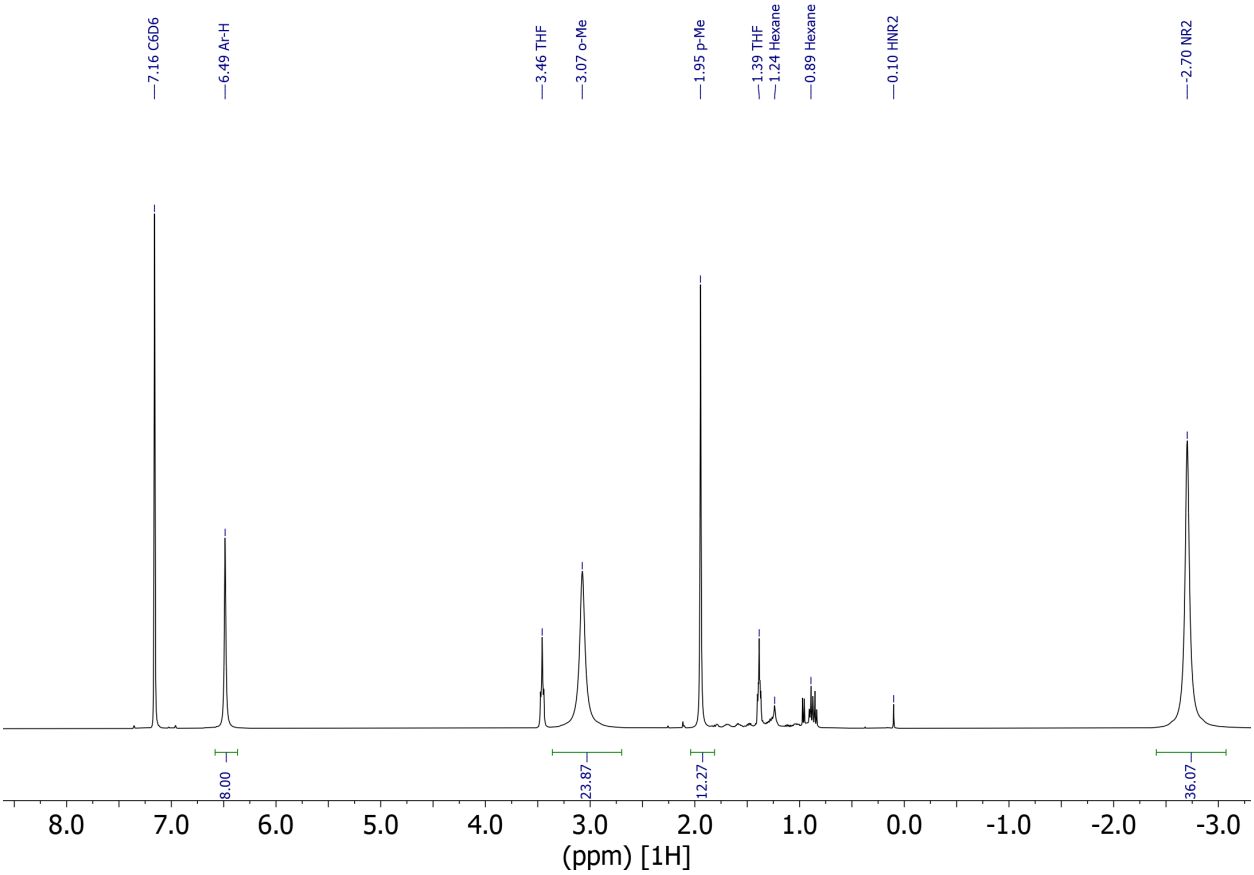

Figure 4.4. ^{1}H NMR (500 MHz, 298K) spectrum of **4.2-Ce** in deuterated benzene (residual proton peak marked at δ = 7.16 ppm). Note**:** Resonances of side product HNR_2 at 0.10 ppm. Residual solvent resonances for hexane marked at δ = 1.24 and 0.98, and for THF at 3.46 and 1.39 ppm.

UV-visible spectroscopy of a yellow solution of **4.2-Ce** in toluene shows two absorbances of similar molar extinction at 326 nm and 361 nm (ϵ = 523 and 512 L•M^{1-}•cm^{1-}, respectively).

These values are similar to the single absorbance at 336 nm (ϵ = 1,065 L•M^{1-}•cm^{1-}) of the homoleptic and dimeric complex [(Mes$_2$BO)$_2$Ce(OBMes$_2$)]$_2$, described in Chapter 3, although with an absorption coefficient of about half as much.

Following the methods used to isolate **4.2-Ce**, crystallographically characterizable compounds of K(μ-Mes$_2$BO)$_2$Ln(NR$_2$)$_2$ [Ln = Nd (**4.2-nd)**, Pr (**4.2-Pr)**, Sm (**4.2-Sm)**, Tb (**4.2-Tb)**] were also obtained in comparable yields. **4.2-Pr** and **4.2-Tb** are isomorphous with **4.2-Ce**. Complexes **4.2-nd** and **4.2-Sm** are structurally similar to these three, but they crystallize with two toluene molecules present in the triclinic *P*–1 unit cell and are isomorphous. Metrical parameters are given in Table 4.2.

Table 4.2. Select bond lengths (Å) and angles [°] for 4.2-Ln and 4.4

4.2-Ce				**4.2-Pr**				**4.2-Tb**			
Ce1	O1	2.2706(2)		Pr1	O1	2.2747(2)		Tb	O1	2.173(2)	
Ce1	O2	2.2892(2)		Pr1	O2	2.2540(2)		Tb	O2	2.177(2)	
Ce1	N1	2.3972(2)		Pr1	N1	2.375(2)		Tb	N1	2.299(3)	
Ce1	N2	2.3841(2)		Pr1	N2	2.364(2)		Tb	N2	2.285(3)	
K1	O1	2.9257(2)		K1	O1	3.0073(2)		K	O1	2.985(2)	
K1	O2	2.9921(2)		K1	O2	2.9365(2)		K	O2	3.117(2)	
O1	Ce1	O2	94.31(6)	O1	Pr1	O2	94.87(6)	O1	Tb	O2	98.78(8)
O1	Ce1	N1	111.57(6)	O1	Pr1	N1	110.14(7)	O1	Tb	N1	111.73(9)
O1	Ce1	N2	103.87(6)	O1	Pr1	N2	106.88(7)	O1	Tb	N2	103.97(9)
O2	Ce1	N1	110.60(6)	O2	Pr1	N1	111.32(7)	O2	Tb	N1	108.97(9)
O2	Ce1	N2	107.04(6)	O2	Pr1	N2	103.76(7)	O2	Tb	N2	106.65(9)
N2	Ce1	N1	124.97(6)	N2	Pr1	N1	125.45(7)	N2	Tb	N1	123.79(1)

O1	K1	O2	68.79(4)	O1	K1	O2	68.26(5)	O1	K	O2	65.48(6)
B1	O1	Ce1	160.81(1)	B1	O1	Pr1	158.75(2)	B1	O1	Tb1	162.6(2)
B2	O2	Ce1	158.23(2)	B2	O2	Pr1	160.94(2)	B2	O2	Tb1	163.2(2)
4.2-Nd				**4.2-Sm**				**4.4**			
Nd1	O1	2.2653(1)		Sm1	O1	2.2296(1)		Ce1	O1	2.1123(1)	
Nd1	O2	2.2310(1)		Sm1	O2	2.1977(1)		Ce1	O2	2.1312(1)	
Nd1	N1	2.3716(2)		Sm1	N1	2.3445(1)		Ce1	N1	2.2220(2)	
Nd1	N2	2.3603(2)		Sm1	N2	2.3382(1)		Ce1	N2	2.2301(2)	
K1	O1	2.9726(2)		K1	O1	3.0067(1)		O1	Ce1	O2	109.58(5)
K1	O2	3.3708(2)		K1	O2	3.4270(1)		O1	Ce1	N1	98.99(6)
O1	Nd1	O2	97.53(5)	O1	Sm1	O2	99.24(4)	O1	Ce1	N2	106.32(6)
O1	Nd1	N1	107.45(6)	O1	Sm1	N1	107.56(4)	O2	Ce1	N1	114.42(6)
O1	Nd1	N2	107.58(6)	O1	Sm1	N2	107.62(4)	O2	Ce1	N2	102.38(6)
O2	Nd1	N1	105.63(6)	O2	Sm1	N1	105.17(4)	N1	Ce1	N2	124.44(6)
O2	Nd1	N2	106.23(6)	O2	Sm1	N2	105.45(4)	B1	O1	Ce1	176.43(1)
N2	Nd1	N1	128.19(6)	N2	Sm1	N1	128.08(5)	B2	O2	Ce1	170.57(1)
O1	K1	O2	64.06(4)	O1	K1	O2	62.83(3)				
B1	O1	Nd1	159.96(1)	B1	O1	Sm1	160.80(1)				
B2	O2	Nd1	168.62(2)	B2	O2	Sm1	170.14(1)				

Although "K(μ-$Mes_2BO)_3Ce^{III}(OBMes_2)$(THF)" was not obtained, the similar complex, Cs(μ-$Mes_2BO)_2Pr^{III}(OBMes_2)_2$(THF), **4.3,** Figure 4.5, could be obtained in 67% yield by treatment of PrI_3 with the cesium boroxide cluster, $[Cs(OBMes_2)]_4(THF)_4$, Figures 4.14 and 4.15, in THF.

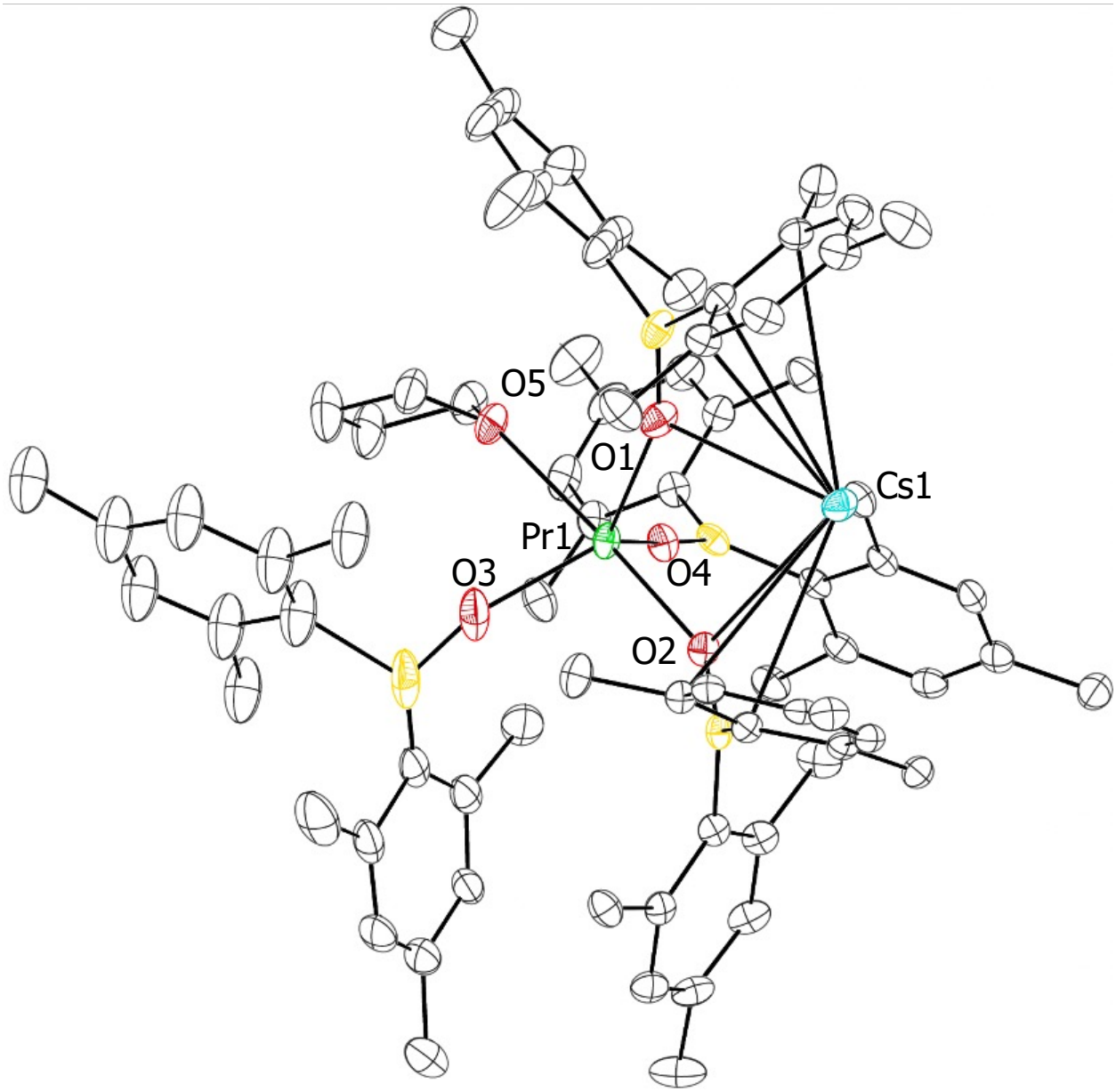

Figure 4.5. Graphical representation of Cs(μ-Mes$_2$BO)$_2$Pr^{III}(OBMes$_2$)$_2$(THF), **4.3**. Thermal ellipsoids are drawn at the 50% probability level and hydrogen atoms are not shown for clarity.

Cs(μ-Mes$_2$BO)$_2$Pr^{III}(OBMes$_2$)$_2$(THF), **4.3**, crystallizes in the $P2_1/c$ space group in a distorted trigonal bipyramidal geometry around the Pr(III) center. Three di(mesityl)boroxide ligands with donor atoms O1, O3, and O4 are arranged equatorially with a sum of O$_{boroxide}$–Pr–

$O_{boroxide}$ angles of 356°. The axial positions are occupied by one bridging di(mesityl)boroxide with donor atom O2 and one THF ligand with the O5 donor atom such that there is a O_{THF}–Pr–$O_{boroxide}$ angle of 175.36(8)° which contributes to a τ_5 value of 0.86 (where $\tau_5 = 1$ is trigonal bipyramidal and $\tau_5 = 0$ is square pyramidal). The Cs^+ ion is encapsulated by the aryl rings and oxygen atoms of one terminal and one axial di(mesityl)boroxide with the closest carbon atoms, C1, C6, C19 and C24 (Figure 4.6) at a range of 3.302(8) to 3.456(16) Å. It is also at a comparable distance with two carbons with a neighboring aryl ring of a nearby molecule of **4.3.** The closest carbon atoms of the aryl ring of the neighboring molecule, $C13^1$ and $C14^1$, are at a distance of only about 0.2 Å further away than the closest carbons of the original **4.3** molecule, essentially forming a polymeric structure, Figure 4.6.

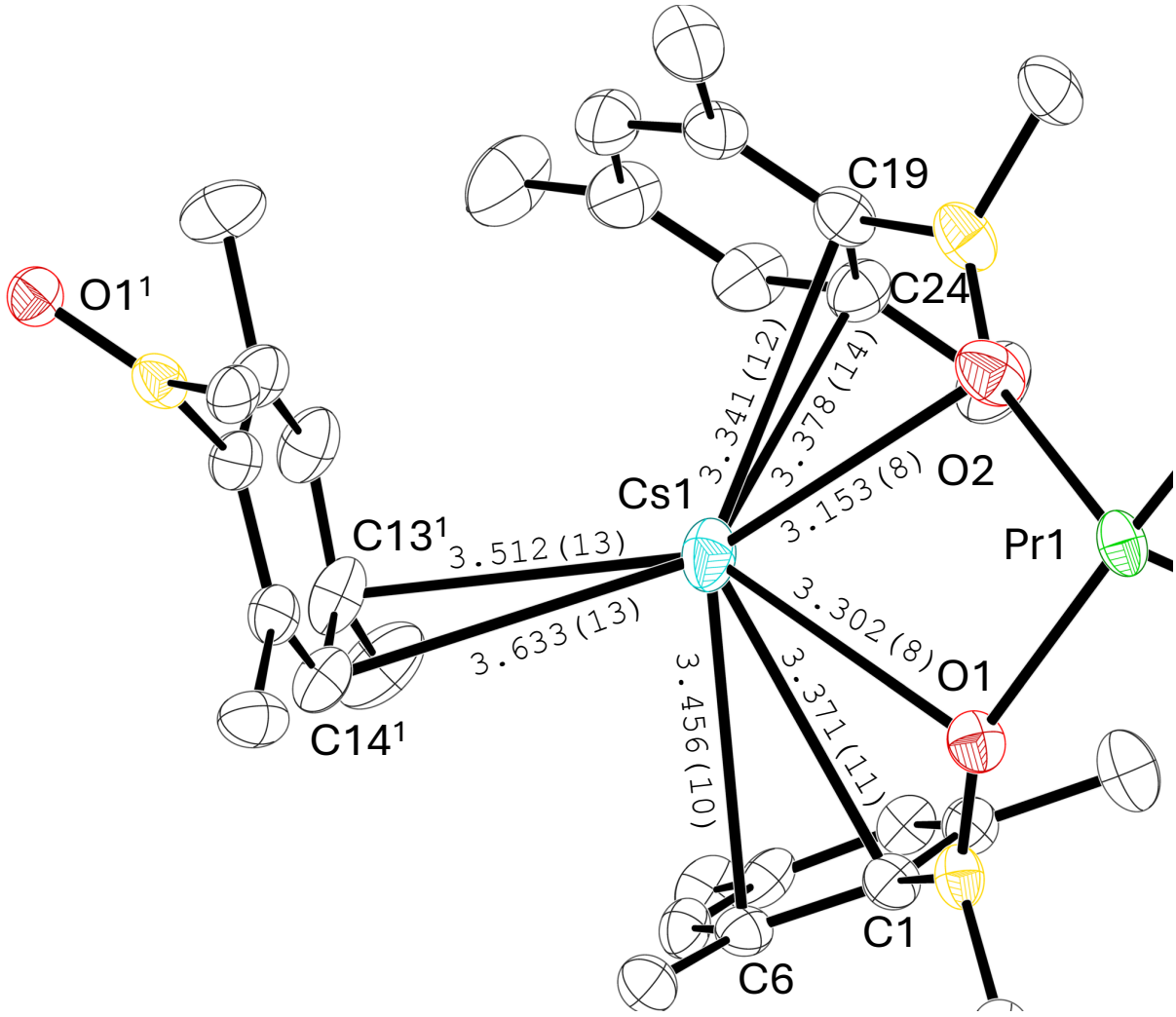

Figure 4.6. Graphical representation of Cs(μ-Mes$_2$BO)$_2$Pr^{III}(OBMes$_2$)$_2$(THF), **4.3**, highlighting the proximity of neighboring **4.3** aryl rings (denoted with (atom)^1 annotation) to the Cs^+ cation. Distances are measured in Å. Thermal ellipsoids are drawn at the 50% probability level and hydrogen atoms are not shown for clarity.

Oxidation of 4.2-Ce. Treatment of a yellow solution of **4.2-Ce** in diethyl ether with 1 equiv of AgI led to a dark red solution after filtration away from grey precipitates. Crystallization from ca. 1 mL of hexane by slow cooling from 0° C to −35 °C yielded red crystals of $Ce^{IV}(OBMes_2)_2(NR_2)_2$, **4.4**, suitable for X-ray diffraction, Figure 4.7, eq 4.

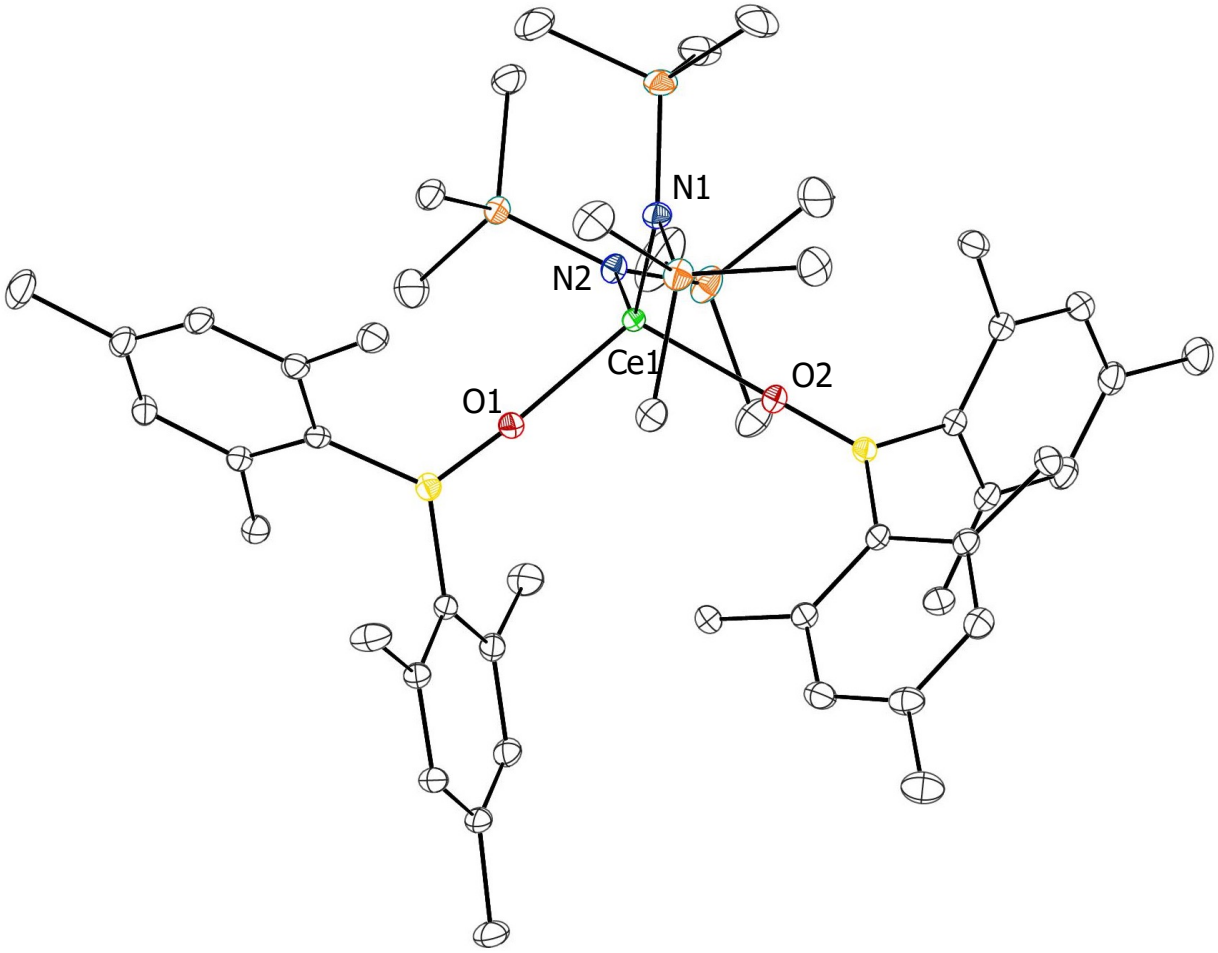

Figure 4.7. Graphical representation of $Ce^{IV}(OBMes_2)_2(NR_2)_2$, **4.4**. Thermal ellipsoids are drawn at the 50% probability level and hydrogen atoms are not shown for clarity.

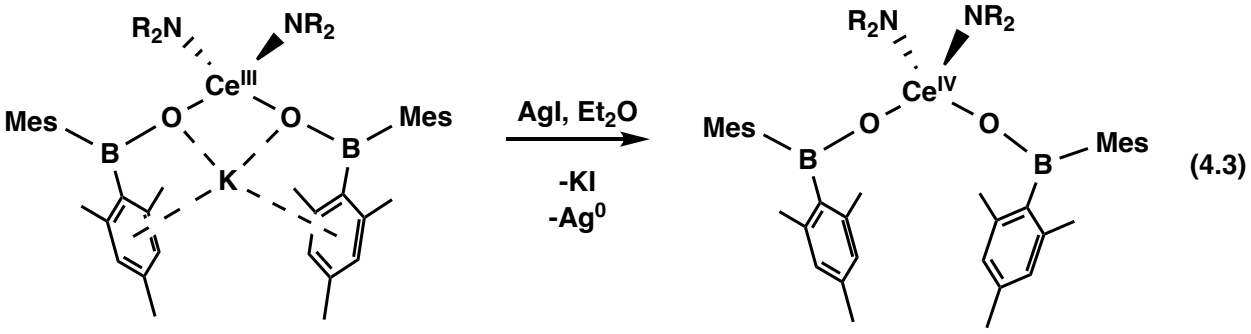

(4.3)

4.4

Complex **4.4** crystallizes in the $P2_1/n$ space group with ligands in a distorted tetrahedral geometry with a τ_4 value of 0.86. This is similar to the 0.88 value of **4.2-Ce**, but the 94.31(6)° O–Ce–O angle in **4.2-Ce** has opened to 109.58(5)° in **4.4**, which does not have the bridging potassium countercation. In comparison, the N–Ce–N angles of **4.2-Ce** and **4.4** are virtually identical at 124.97(6)° and 124.44(6)°, respectively. Complexes **4.2-Ce** and **4.4** differ in that the O–B–Ce angles are 176.43(1)° and 170.57(1)° in **4.4** and 160.81(1)° and 158.23(2)° in **4.2-Ce,** which are typical angles when compared to other lanthanide di(mesityl)boroxide complexes. There is also a significant difference in bond distances between **4.2-Ce** and **4.3**. In **4.3**, both the Ce-N and Ce-O distances are ca. 0.161 Å on average shorter than in **4.2-Ce**. This is close to the 0.14 Å difference between Ce(III) and Ce(IV) ionic radii for coordination number IV.[17] Similarly, the Ce-N(1) bond lengths of 2.3972(2) for **4.2-Ce** and 2.2220(2) for **4.4** differ by ca. 0.175 Å.

The ^{1}H NMR spectrum of **4.4** exhibits much sharper resonances than that of **4.2-Ce** which is consistent with the presence of diamagnetic Ce(IV). The 2:6:3:9 ratio of proton resonances as found for **4.2-Ce**, indicates that the structure is not rigid in solution, Figure 4.8

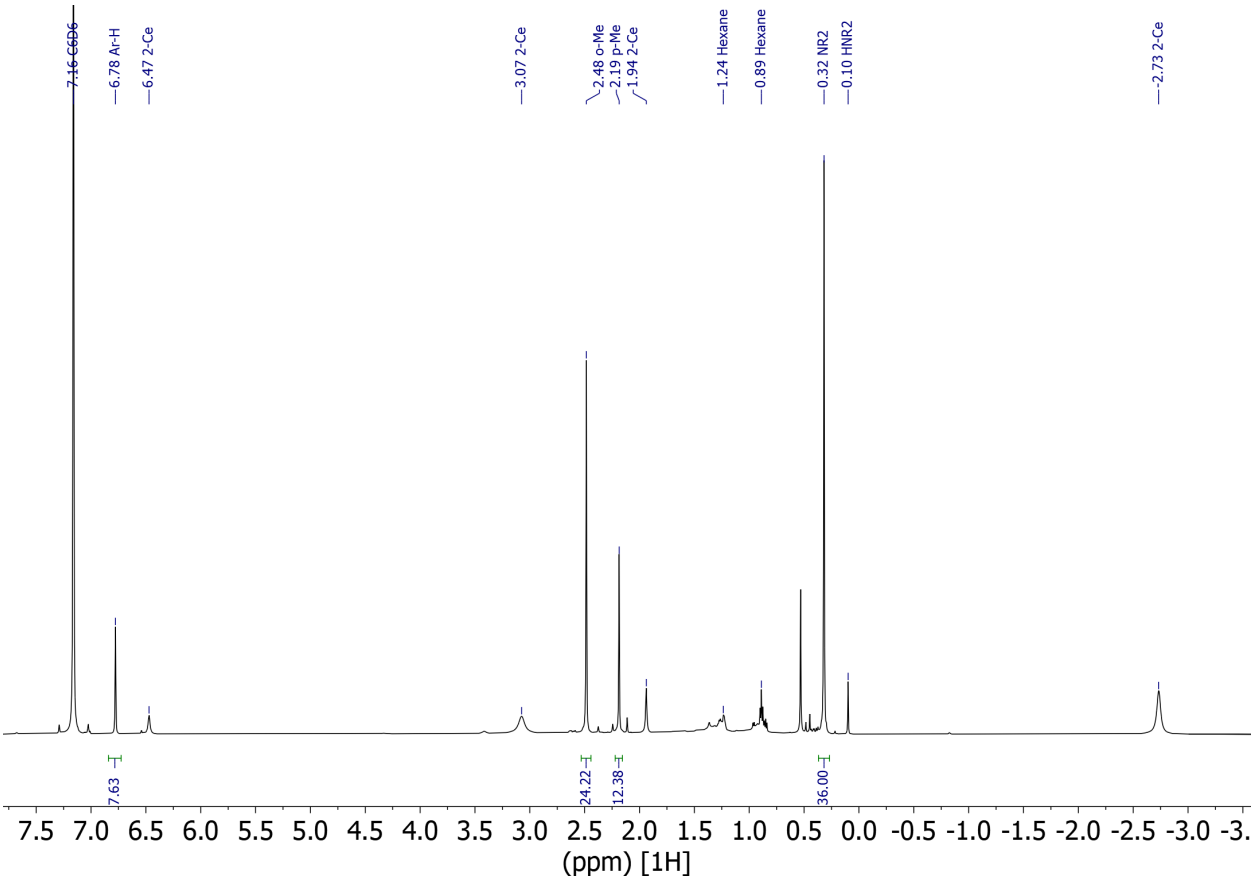

Figure 4.8. ^{1}H NMR (500 MHz, 298K) spectrum of **4.4** in deuterated benzene (residual proton peak marked at δ = 7.16 ppm). Note**:** Resonances of unreacted **4.2-Ce** marked at δ = 6.47, 3.07, and -2.73; and side product HNR_2 at 0.10 ppm. Residual solvent resonances for hexane marked at δ = 1.24 and 0.98.

To assess the capacity of this system to form Ln(IV) complexes with the two other lanthanides known to support the Ln(IV) oxidation state, oxidations of **4.2-Pr**, **4.2-Tb**, and **4.4** were examined. When either **4.2-Pr** or **4.2-Tb** were treated with one equiv of yellow powdered AgI or [Ag][BPh_4] at −35 °C, an immediate precipitation of grey solids appeared, presumably Ag(0) and KI or $KBPh_4$. When filtered away, a deep red solution remained. Removal of solvent under reduced pressure and subsequent workup of the red-brown solids did not produce crystals of $Pr^{IV}(OBMes_2)_2(NR_2)_2$ nor of $Tb^{IV}(OBMes_2)_2(NR_2)_2$. However, from both reactions, crystallization from toluene at −35 °C provided crystals of the known complex $AgNR_2$[18] in high

yield, as expected due to its low solubility in most organic solvents. This suggested that ligand transfer rather than oxidation to the Ln(IV) oxidation state had occurred. Attempts to oxidize **4.3** with AgI or Magic Blue led to a change in color from light green to dark red, but no crystallographically characterizable material was obtained.

A yellow solution of **4.2-Tb** in toluene shows a UV-visible absorbance at $\lambda = 351$ nm ($\epsilon = 483$ $L*M^{-1}*cm^{-1}$). When treated with [Ag][BPh_4], a new absorbance at $\lambda = 418$ nm is present with a molar absorptivity value close to three times its starting value ($\epsilon = 1178$ $L*M^{-1}*cm^{-1}$), Figures 4.9 and 4.10. Although integration of ^{1}H NMR of Tb(III) complexes is challenging due to the large paramagnetism of **4.2-Tb**, adjusting the data collection parameters for paramagnetic species revealed paramagnetic resonances at $\delta = -5.63, -18.14, -32.63, -62.12$ ppm which is consistent with the number of resonances expected for the complex, Figure 4.11.[19] Collection of a ^{1}H NMR of **4.2-Tb** after treatment with $AgBPh_4$ revealed no resonances besides that of residual proton resonances of the C_6D_6 solvent. Evans method calculations were not successful due to the tendency for the elimination of KNR_2 upon addition of solvent, leading to a varying concentration of **4.2-Tb**. This concentration could not be accurately measured due to the difficulty of integration of ^{1}H NMR resonances of **4.2-Tb**.

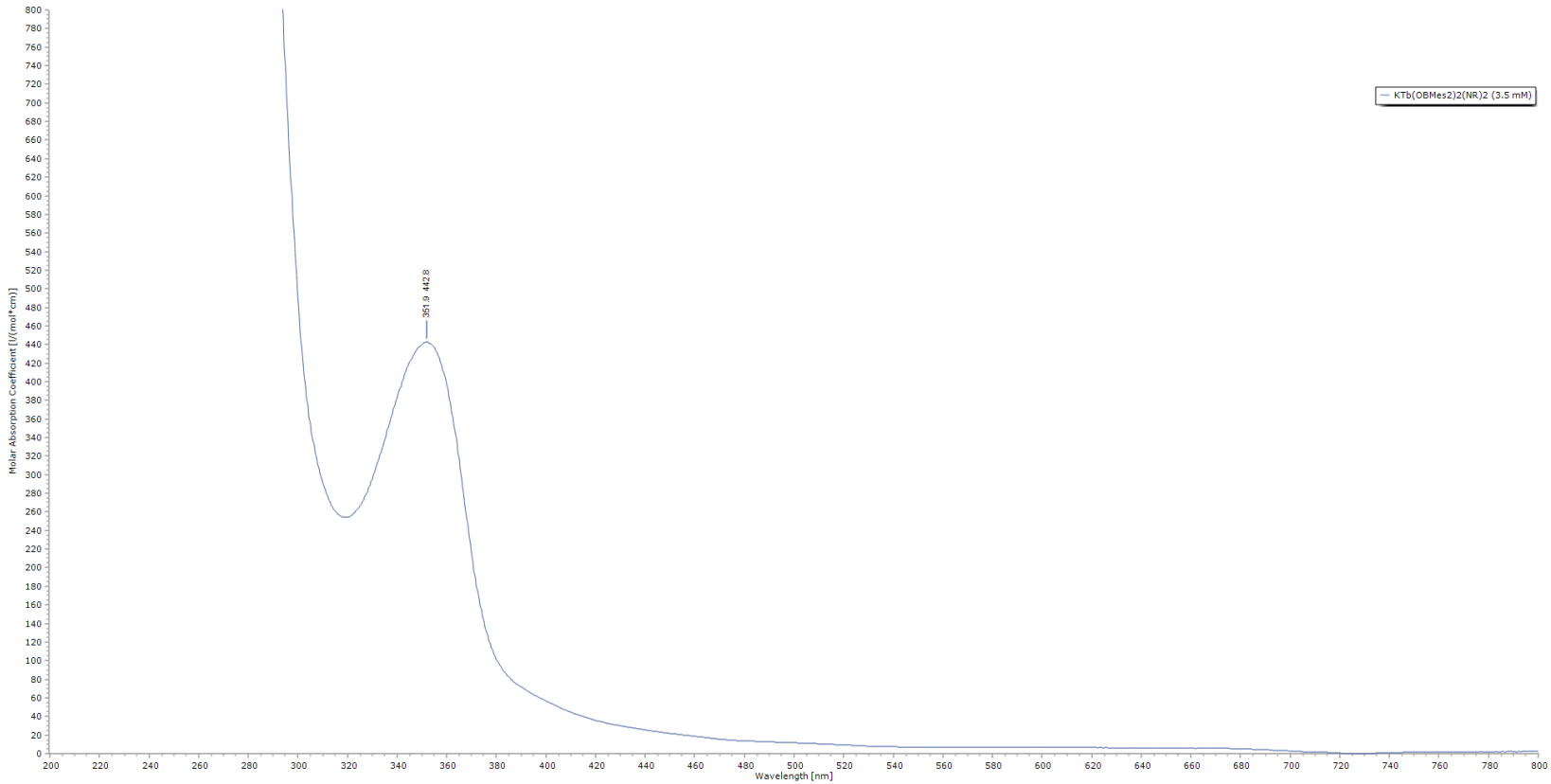

Figure 4.9. UV-Visible spectrum of **4.2-Tb** at 3.5 mM in toluene.

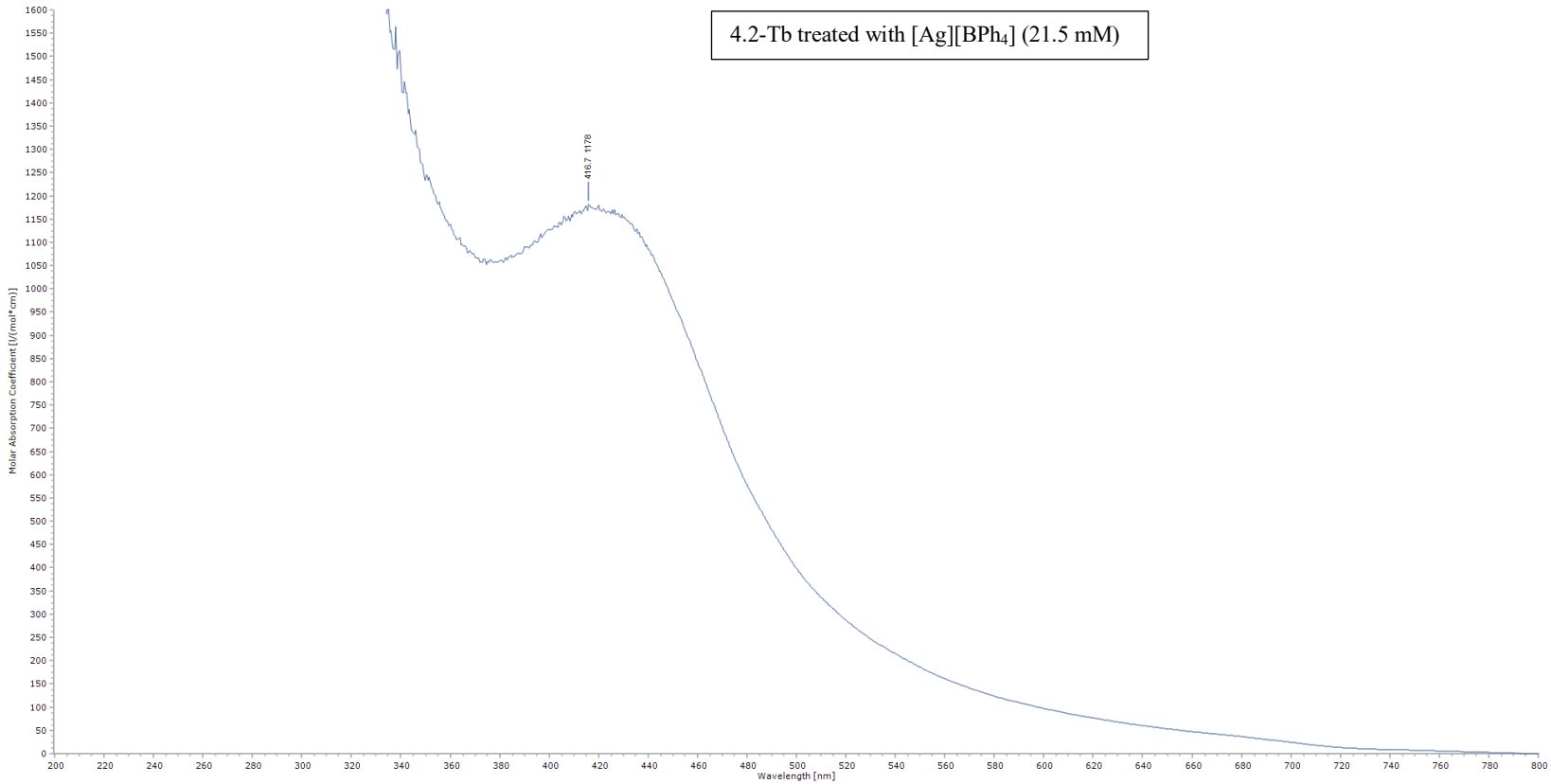

Figure 4.10. UV-Visible spectrum of **4.2-Tb** treated with [Ag][BPh_4] at 3.5 mM in toluene.

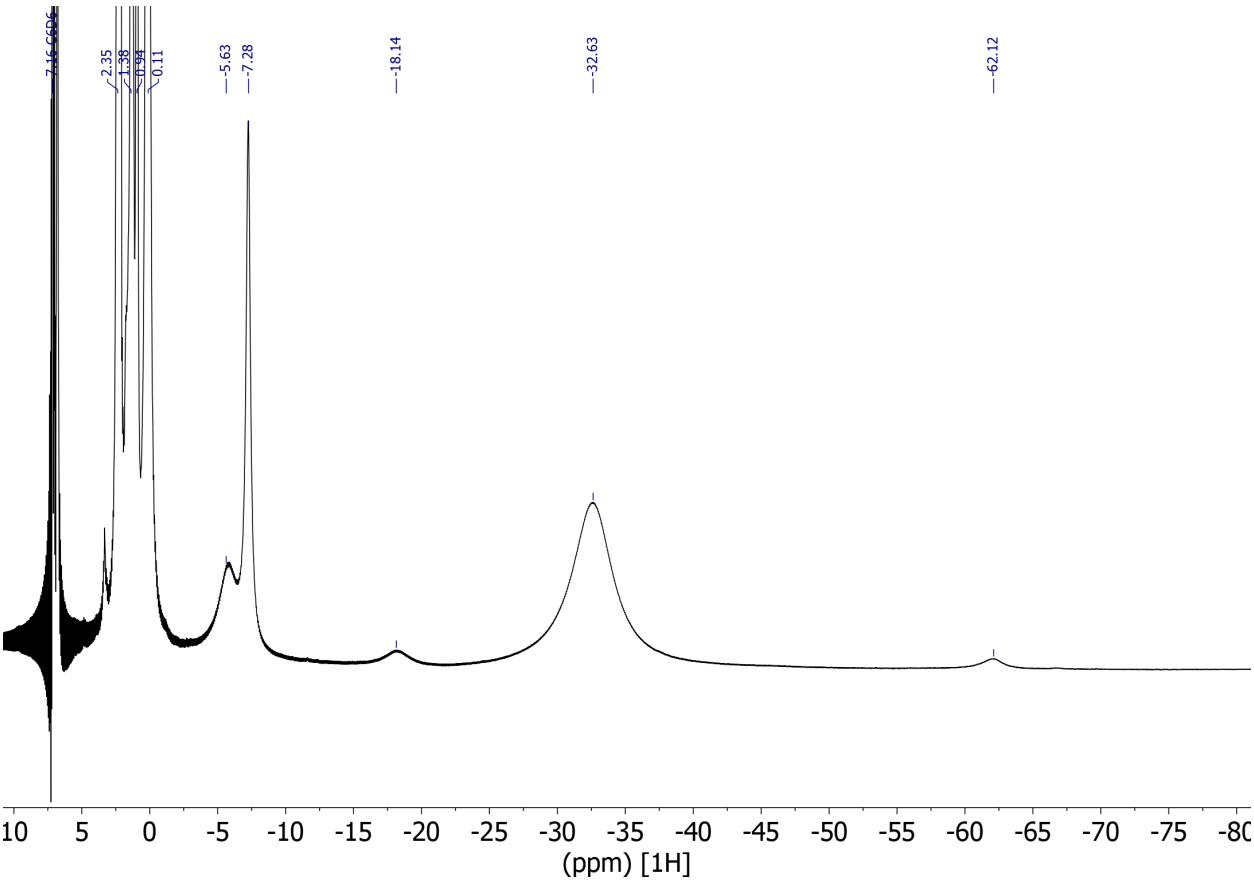

Figure 4.11. ^{1}H NMR (400 MHz, 298K) spectrum of **4.2-Tb** in deuterated benzene (residual proton peak marked at δ = 7.16 ppm). Residual solvent resonances for $HOBMes_2$ at δ 2.35, for hexane at δ = 1.38 and 0.94, for KNR_2 at 0.11, and for unreacted $Pr(NR_2)_3$ at -7.28 ppm. Acquisition time was set to 0.04 s, D1 to 1 ms. An ablative baseline correction and gaussian apodization of 15 Hz were applied.

When **4.2-Pr** and **4.2-Tb** were treated with one equiv of the intensely colored strong oxidant $[N(C_6H_4\text{-Br-}4)_3][SbCl_6]$, commonly referred to as "Magic Blue", in MeCN, an immediate color change to deep reddish brown with a darkly red-colored precipitate occurred suggesting oxidation. Crystallization from toluene provided brown crystals of $N(C_6H_4\text{-Br-}4)_3$, one of the expected products of oxidation with Magic Blue.[20]

Out of interest to see if lanthanides could support the Ln(IV) oxidation state other than those already in the literature, a light yellow solution of **4.2-Sm** in MeCN was treated with Magic Blue and an immediate color change to a brown slurry was observed. Workup in toluene revealed a red solution. Concentration and cooling to −35 °C did not yield an oxidation product, rather it afforded colorless triangular prismatic crystals of the unexpected product $Sb^{III}(OBMes_2)_3$, **4.5,** Figure 4.12.

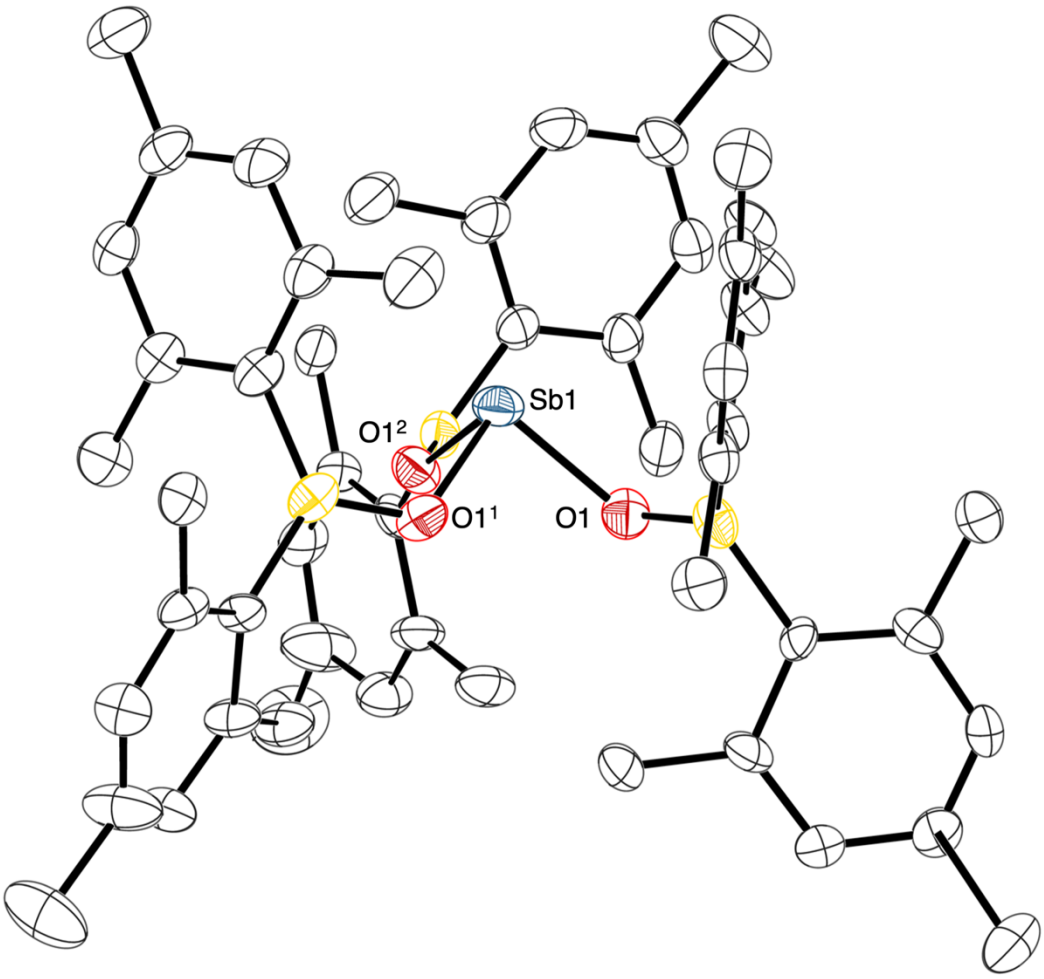

Figure 4.12. Graphical representation of $Sb(OBMes_2)_3$, **4.5**. Thermal ellipsoids are drawn at the 50% probability level and hydrogen atoms and one toluene molecule are not shown for clarity.

Complex **4.5** crystallizes in the rhombohedral *R*3 space group with one toluene molecule in the crystal lattice with three-fold symmetry about the Sb center. As is typical of molecular, monometallic $Sb(A)_3$ A-Sb-A bonds (A = monodentate anionic ligand), the O-Sb-O angles of **4.5** are close to 90° at 90.57(9)°.[18,20–23] The Sb-O bond lengths of 1.976(2) Å are within the expected range for ~~a~~ Sb^{III}-O bonds.[22,24,25] The ^{1}H NMR spectrum of **4.5** shows a 2:6:3 ratio of proton resonances expected for this complex and is indicative of free rotation about the B-O bond, Figure 4.13. Complex **4.4** is isomorphous with the bismuth analog, $Bi(OBMes_2)_3$, Appendix A, Figure A1.

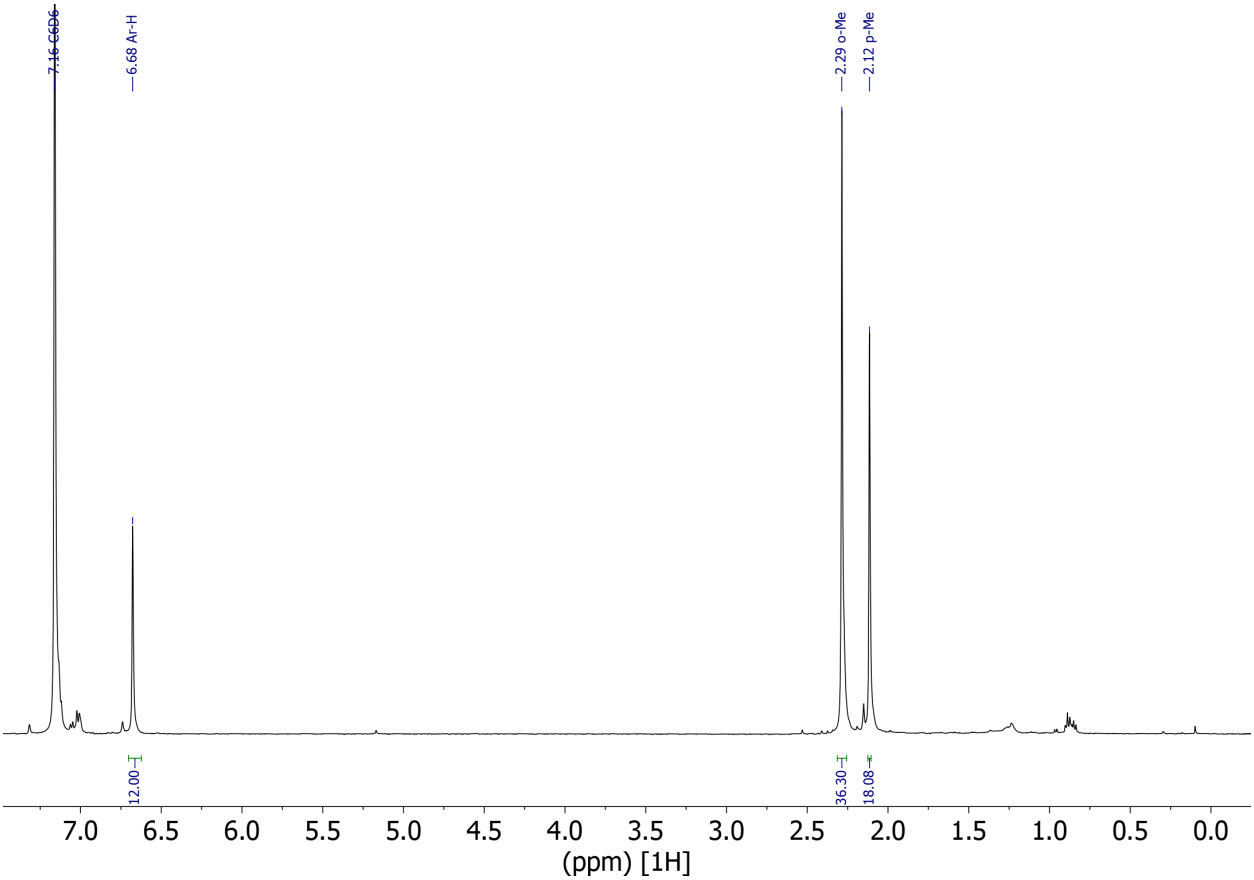

Figure 4.13. ^{1}H NMR (500 MHz, 298K) spectrum of **4.4** in deuterated benzene (residual proton peak marked at δ = 7.16 ppm). Residual solvent resonances for hexane at δ = 1.24 and 0.98.

DISCUSSION

The di(mesityl)boroxide ligand has been shown here to support the Ce(IV) oxidation state in two ligand environments. Initial studies to address the stability of the di(mesityl)boroxide ligand with a Ce(IV) cation led to salt metathesis with $Ce^{IV}(OTf)_4$ and four equiv $KOBMes_2$ to form $Ce(OBMes_2)_4(THF)_2$, **1**. The synthesis of a natural Ce(III) precursor to **1**, "K(μ-$Mes_2BO)_3Ce(OBMes_2)$", which has previously been formed with Sm (see Chapter 3) and Pr (with Cs instead of K), was found to be challenging and no crystal structure was acquired. This proved to complicate studying oxidation of the Ce(III) cation to obtain the Ce(IV) compound in the manner that has been successful for previous Ln(IV) complex syntheses.[3,4,7,14,15]

However, metathesis reactions with the tris(silylamide) complexes, $Ln(NR_2)_3$ (Ln = Ce, Pr, Nd, Sm, Tb; R = $SiMe_3$), when treated with two equiv $KOBMes_2$ routinely form the potassium-encapsulated compounds, K(μ-$Mes_2BO)_2Ln(NR_2)_2$, **4.2-Ln**, via elimination of one equiv KNR_2. Single crystals of each of these compounds were isolated, showing similar bond angles and lengths and can be categorized into two groups of crystallographic isomorphism. **4.2-Ce**, **4.2-Pr**, and **4.2-Tb** crystallize in the *Pbca* space group, and **4.2-nd** and **4.2-Sm** crystallize in the *P*–1 space group.

Attempts to oxidize **4.2-Ln** were made with AgI, $AgBPh_4$, and $[N(C_6H_4\text{-Br-}4)_3][SbCl_6]$ (Magic Blue). Each of these reactions resulted in color changes for each compound and the precipitation of side products. AgI and $AgBPh_4$ oxidations resulted in a color change to deep red, but the only crystals recovered from these reactions were those of $AgNR_2$. The use of Magic Blue also resulted in the disappearance of the oxidant's intense blue color and the formation of a brown solution with colorless precipitate, but the only recovered crystals were those of the reduced species $N(C_6H_4\text{-Br-}4)_3$ and $Sb(OBMes_2)_3$, **4.4**. The presence of a Sb(III) complex coming from a Sb(V) precursor indicates the transfer of electrons to the Sb cation, although it is unclear what was oxidized in this reaction.

Treatment of **4.2-Ce** with AgI, however, did result in the isolation of the heteroleptic $Ce^{IV}(OBMes_2)_2(NR_2)_2$, **4** as bright red crystals. This again shows that the Ce(IV) cation can be isolated with di(mesityl)boroxide ligands, even with a heteroleptic ligand environment. It also suggests that the elimination of the encapsulated potassium countercation is a feasible means to obtain a heteroleptic Ln(IV) complex. However, the inability to isolate crystals of the other Ln(IV) complexes through oxidation suggests that this ligand system may be unsuitable for metals other than cerium.

CONCLUSION

Four di(mesityl)boroxide ligands can coordinate to a Ce(IV) cation, as shown by the synthesis of $Ce(OBMes_2)_4(THF)$, **1**, by way of salt metathesis with $Ce(OTf)_4$ and $KOBMes_2$. Similarly, metathesis reactions of $Ln(NR_2)_3$ and $KOBMes_2$ readily form the heteroleptic complexes $K(\mu\text{-}Mes_2BO)_2Ln(NR_2)_2$, **4.2-Ln** (Ln = Ce, Pr, Nd, Sm, Tb; R = $SiMe_3$), in which the potassium ion is coordinated to the arenes and oxygen atoms of the di(mesityl)boroxide ligands. For **4.2-Ce**, with the treatment of AgI, this encapsulation provides the opportunity for the oxidation of the Ce(III) metal center to the Ce(IV) oxidation state via the elimination of KI and formation of Ag metal. Although this oxidation is available with **4.2-Ce**, similar oxidation techniques of the other **4.2-Ln** complexes did not result in crystallographically characterizable Ln(IV) complexes.

EXPERIMENTAL DETAILS

All manipulations and syntheses described below were conducted with the rigorous exclusion of air and water using standard Schlenk line and glovebox techniques under an argon or dinitrogen atmosphere. Solvents were sparged with UHP argon and dried by passage through columns containing Q-5 and molecular sieves prior to use. Deuterated NMR solvents were dried over NaK alloy, degassed by three freeze-pump-thaw cycles, and vacuum transferred before use. ^1H, NMR

spectra were recorded on Bruker GN500, CRYO500, or AVANCE600 MHz spectrometers at 298 K unless otherwise stated and referenced internally to residual protio-solvent resonances. ^{11}B NMR are not reported, as the resonances of the ^{11}B nuclei in the lanthanide complexes could not be differentiated from ligand resonances. Electronic spectra were collected using an Agilent Cary 60 UV/Vis spectrophotometer with a quartz, air-free cuvette. Infrared spectra were collected on compressed solids using an Agilent Cary 630 ATR/FTIR instrument. Elemental analysis data were collected using a Thermo Scientific FlashSmart CHNS/O Elemental Analyzer at the UC Irvine Materials Research Institute's TEMPR facility in Irvine, CA. $KOB(C_6H_2Me_3\text{-}2,4,6)_2$ ($KOBMes_2$) was synthesized in accordance with the process described in chapter 3. $[CsOBMes_2]_5(THF)_4$ was synthesized by treatment of $HOBMes_2$ with one equiv Cs metal in THF, followed by washing with hexane. $HOBMes_2$ was purchased from The Synnovator or synthesized via literature preparations.[26] KH in mineral oil (30%) was purchased from Sigma Aldrich and thoroughly rinsed with hexane before use. Cs was purchased from Sigma Aldrich and used without further purification. $Ce(OTf)_4$ was purchased from Fischer Scientific, tested by FTIR for water, and used without further purification. LnI_3 (Ln = Pr, Nd, Tb),[27] $SmI_3(THF)_{3.5}$[28] and $Ln(NR_2)_3$[29] ($R = SiMe_3$; Ln = La, Ce, Nd, and Gd) starting materials were synthesized via literature procedures.

$Ce(OBMes_2)_4(THF)_2$, 4.1. Yellow $Ce(OTf)_4$ (0.126 g, 0.171 mmol) was added to 10 mL of MeCN at ca. 80 °C to make a yellow slurry. A solution of $KOBMes_2$ (0.221 g, 0.725 mmol) in ca. 2 mL of THF at 25 °C was added all at once to the slurry. The resulting yellow mixture was stirred for 30 min while cooling to room temperature and it gradually turned orange after about 5 min. After the mixture was stirred for 15 h, solvent was removed under reduced pressure. Treatment of the resulting off-white solids with ca. 20 mL of toluene yielded a light yellow slurry. The slurry was centrifuged and the resulting yellow supernatant was decanted away from a light

brown pellet. Removal of solvent from the supernatant resulted in yellow solids. The solids were dissolved in minimal toluene (ca. 1 mL) and placed in a freezer at −35 °C for 1 year, producing light yellow crystals suitable for X-ray diffraction in very low yield. ^{1}H NMR (600 MHz, C_6D_6) δ 6.48 (16H, s, Ar-*H)*, 2.28 (24H, s, p-*Me*), 0.28 (48H, s, o-*Me*).

K(μ-Mes$_2$BO)$_2$Ce(NR$_2$)$_2$, 4.2-Ce. Yellow Ce(NR$_2$)$_3$ (x g, x mmol) and colorless KOBMes$_2$ (x g, x mmol) powders were combined in ca. 15 mL of THF. The clear colorless solution was allowed to stir at room temperature for 15 h and the solvent was then removed under reduced pressure. The mixed yellow-brown and colorless solids were dissolved in cold toluene (ca x mL) and the cloudy yellow-brown mixture was filtered. The resultant yellow-brown clear solution was reduced in volume until saturation and placed in a –35 °C freezer to yield crystals of **4.2-Ce** (x g, x % yield) suitable for X-ray diffraction. ^{1}H NMR (400 MHz, C_6D_6) δ 6.49(8H, s, Ar-*H*), 3.07 (24H, s, o-*Me*), 1.95 (12H, s, p-*Me*), -2.70 (36H, s, N(Si*Me*$_3$).

K(μ-Mes$_2$BO)$_2$Pr(N(SiMe$_3$)$_2$)$_2$, 4.2-Pr. A light green solution of Pr(NR$_2$)$_3$ (0.462 g, 0.742 mmol) in ca. 10 mL THF was treated with KOBMes$_2$ (0.448 g, 1.472 mmol) and stirred for 15 h to produce a light green slurry. Workup proceeded in accordance with the experimental procedure of **4.2-Ce** and cooling to −35 °C yielded light yellow X-ray quality crystals of **4.2-Pr** (0.341 g, 0.286 mmol, 45% yield).

K(μ-Mes$_2$BO)$_2$Nd(N(SiMe$_3$)$_2$)$_2$, 4.2-Nd. A light blue solution of Nd(NR$_2$)$_3$ (0.0743 g, 0.119 mmol) in ca. 10 mL THF was treated with KOBMes$_2$ (0.075 g, 0.246 mmol) and stirred for 15 h to produce a light blue slurry. Workup proceeded in accordance with the experimental procedure of **4.2-Ce** and cooling to −35 °C yielded light blue X-ray quality crystals of **4.2-nd** (0.0610 g, 0.051 mmol, 49% yield).

K(μ-Mes$_2$BO)$_2$Sm(N(SiMe$_3$)$_2$)$_2$, 4.2-Sm. A yellow solution of Sm(NR$_2$)$_3$ (0.465 g, 0.722 mmol) in ca. 10 mL THF was treated with KOBMes$_2$ (0.457 g, 1.502 mmol) and stirred for 15 h to produce a light brown slurry. Workup proceeded in accordance with the experimental procedure of **4.2-Ce** and cooling to −35 °C yielded pale yellow X-ray quality crystals of **4.2-Sm** (0.409 g, 0.341 mmol, 53% yield). ^{1}H NMR (400 MHz, C_6D_6) δ 6.59 (8H, s, Ar-*H*), 2.55 (24H, s, *o*-*Me*), 2.05 (12H, s, *p*-*Me*), -0.39 (36H, s, N(Si*Me*$_3$)$_2$).

K(μ-Mes$_2$BO)$_2$Tb(N(SiMe$_3$)$_2$)$_2$, 4.2-Tb. A clear, colorless solution of Tb(NR$_2$)$_3$ (0.054 g, 0.084 mmol) in ca. 10 mL THF was treated with KOBMes$_2$ (0.051 g, 0.167 mmol) and stirred for 15 h to produce a light yellow slurry. Workup proceeded in accordance with the experimental procedure of **4.2-Ce** and cooling to −35 °C yielded light colorless X-ray quality crystals of **4.2-Tb** (0.051 g, 0.042 mmol, 58% yield).

Cs(μ-Mes$_2$BO)$_2$Pr^{III}(OBMes$_2$)$_2$(THF), 4.3. A pale green slurry of PrI$_3$ (0.139 g, 0.266 mmol) in ca. 7 mL THF was treated with a colorless solution of [Cs(OBMes)$_2$]$_5$(THF)$_4$ (0.500 g, 0.220 mmol) in ca. 7 mL THF at room temperature. The resulting pale green mixture was stirred for 2.5 h and then the clear, colorless supernatant was centrifuged away from a colorless pellet. The solvent of the supernatant was removed under reduced pressure to yield pale green solids. Treatment of the solids with ca. 1 mL hexane and cooled to −35 °C to yield light green crystals of **4.3** (0.253 g, 0.180 mmol, 67% yield)^{1}H NMR (600 MHz, C_6D_6) δ 6.86 (16H, s, Ar-*H*), 2.47 (24H, s, *p*-*Me*), -0.71 (48H, s, *o*-*Me*).

Ce^{IV}(OBMes$_2$)$_2$(NR$_2$)$_2$, 4.4. Addition of yellow, powdered AgI (0.0618 g, x mmol) to a clear yellow solution of **4.1** (0.1904 g, x mmol) in ca. 15 mL of diethyl ether immediately generated a dark red slurry. The slurry was stirred overnight in the dark and filtered through a glass pipette containing a Kimwipe to remove grey precipitates. The solvent of the filtrate was removed under

reduced pressure and the resulting dark red solid was dissolved in minimal hexane (ca. 1 mL). Cooling in a glovebox freezer from 0 to -35 °C overnight at the rate of about nine degrees per h formed red crystals of **4.2-Ce** that were suitable for X-ray diffraction in very low yield. ^{1}H NMR (600 MHz, C_6D_6) δ 6.78 (8H, s, Ar-*H*), 2.48 (24H, s, o-*Me*), 2.19 (12H, s, p-*Me*), 0.32 (36H, s, N(Si*Me*$_3$).

[Cs(OBMes$_2$)]$_5$(THF)$_4$. Note: These procedures were conducted in an argon atmosphere. Cesium reacts violently in the presence of air, take caution when conducting this synthesis. Cesium metal can be sticky, be cautious that it does not unintentionally stick to objects removed from the inert atmosphere. In a glovebox, Cs metal (0.800 g, 6.02 mmol) was heated to melting at ca. 75 °C and then pipetted into a 150 mL reaction flask with a screw-on Teflon stopper. A solution of HOBMes$_2$ (1.34 g, 5.03 mmol) in ca. 50 mL THF was added to the flask portionwise. Immediately, the Cs metal, now cooled, became coated in white, cloudy solids and was subsequently removed from the glovebox to a Schlenk line to be stirred under flow of argon gas. Upon heating to 60 °C, the mixture began to bubble and a cloudy mixture formed. This was stirred for 2 h, at which time the solution became clear and colorless with Cs metal visible. Ca. 30 min after this, the solution turned yellow, followed by a transition to a cloudy green mixture after 30 more min. The reaction was cooled to room temperature and stirred for 14 h. Volatiles of the resulting yellow solution were removed under reduced pressure and the resulting yellow solids were washed with hexane over a medium frit. Crystallization from concentrated THF solution resulted in large, colorless crystals of [Cs(OBMes$_2$)]$_5$(THF)$_4$, (1.417 g, 0.623 mmol, 53% yield). ^{1}H NMR (498 MHz, THF-d$_8$) δ 6.56 (16H, s, Ar-*H*), 3.62 (6H, m, OC*H*$_2$CH$_2$), 2.25 (48H, s, *o-Me*), 2.14 (24H, s, *p-Me*), 1.77 (6H, m, OCH$_2$C*H*$_2$).

X-ray Crystallographic Data.

$Ce(OBMes_2)_4(THF)_2$, 4.1. A yellow crystal of approximate dimensions 0.228 x 0.394 x 0.535 mm was mounted in a cryoloop and transferred to a Bruker SMART APEX II diffractometer system. The APEX3[30] program package was used to determine the unit-cell parameters and for data collection (60 sec/frame scan time). The raw frame data was processed using SAINT[31] and SADABS[32] to yield the reflection data file. Subsequent calculations were carried out using the SHELXTL[33] program package. The systematic absences were consistent with the hexagonal space groups $R3c$ and $R\bar{3}c$. The centrosymmetric space group $R\bar{3}c$ was assigned and later determined to be correct. The structure was solved by direct methods and refined on F^2 by full-matrix least-squares techniques. The analytical scattering factors[34] for neutral atoms were used throughout the analysis. Hydrogen atoms were included using a riding model. Least-squares analysis yielded wR2 = 0.4969 and Goof = 1.039 for 710 variables refined against 16345 data (0.7 Å), R1 = 0.2025 for those 11198 data with $I > 2.0\sigma(I)$. Disordered atoms were included using multiple components, partial site-occupancy-factors, constraints, and restraints. The absolute structure could not be fully determined and this model is for connectivity only. There were several high residuals present in the final difference-Fourier map. It was not possible to determine the nature of the residuals although it was probable that four THF and one toluene molecule was present. The SQUEEZE[35] routine in the PLATON[35] program package was used to account for the electrons in the solvent accessible voids.

Table 4.3. Crystal data and structure refinement for $Ce(OBMes_2)_4(THF)_2$, 4.1.	
Identification code	kgb64_rhombohedral_R3
Empirical formula	$C_{252}H_{358}B_8Ce_2O_{27}$
Formula weight	4186.08

Temperature/K	93.15
Crystal system	trigonal
Space group	R-3c:r
a/Å	25.146(9)
b/Å	25.146(9)
c/Å	25.146(9)
α/°	86.602(5)
β/°	86.602(5)
γ/°	86.602(5)
Volume/Å^3	15820(17)
Z	3
ρ_{calc}g/cm^3	1.318
μ/mm^{-1}	0.498
F(000)	6726.0
Crystal size/mm^3	0.535 × 0.394 × 0.228
Radiation	MoKα (λ = 0.71073)
2Θ range for data collection/°	2.232 to 61.326
Index ranges	-35 ≤ h ≤ 35, -34 ≤ k ≤ 35, -35 ≤ l ≤ 26
Reflections collected	148378
Independent reflections	15922 [R_{int} = 0.1304, R_{sigma} = 0.0755]
Data/restraints/parameters	15922/0/710

Goodness-of-fit on F^2	1.039
Final R indexes [I>=2σ (I)]	R_1 = 0.2025, wR_2 = 0.4594
Final R indexes [all data]	R_1 = 0.2445, wR_2 = 0.4969
Largest diff. peak/hole / e $Å^{-3}$	5.79/-5.06

K(μ-Mes$_2$BO)$_2$Ce(NR$_2$)$_2$, 4.2-Ce. Data is already reported in Chapter 3.

K(μ-Mes$_2$BO)$_2$Pr(N(SiMe$_3$)$_2$)$_2$, 4.2-Pr. A yellow crystal of approximate dimensions 0.082 x 0.083 x 0.217 mm was mounted in a cryoloop and transferred to a Bruker APEX DUO diffractometer system. The APEX4[36] program package was used to determine the unit-cell parameters and for data collection (45 sec/frame scan time). The raw frame data was processed using SAINT[31] and SADABS[32] to yield the reflection data file. Subsequent calculations were carried out using the SHELXTL[33] program package. The diffraction symmetry was *mmm* and the systematic absences were consistent with the orthorhombic space group *Pbca* that was later determined to be correct. The structure was solved by direct methods and refined on F^2 by full-matrix least-squares techniques. The analytical scattering factors[34] for neutral atoms were used throughout the analysis. Hydrogen atoms were included using a riding model. Least-squares analysis yielded wR2 = 0.0831 and Goof = 1.061 for 565 variables refined against 17092 data (0.70 Å), R1 = 0.0378 for those 12112 data with I > 2.0σ(I).

Table 4.4. Crystal data and structure refinement for K(μ-Mes$_2$BO)$_2$Pr(N(SiMe$_3$)$_2$)$_2$, 4.2-Pr.	
Identification code	dlc10

Empirical formula	$C_{48}H_{80}B_2KN_2O_2PrSi_4$
Formula weight	1031.13
Temperature/K	100(2)
Crystal system	orthorhombic
Space group	Pbca
a/Å	21.5624(12)
b/Å	22.6422(13)
c/Å	23.0936(13)
α/°	90
β/°	90
γ/°	90
Volume/Å^3	11274.8(11)
Z	8
ρ_{calc}g/cm^3	1.215
μ/mm^{-1}	1.058
F(000)	4336.0
Crystal size/mm^3	0.217 × 0.083 × 0.082
Radiation	MoKα (λ = 0.71073)
2Θ range for data collection/°	3.148 to 61.068
Index ranges	$-30 \leq h \leq 30$, $-31 \leq k \leq 32$, $-32 \leq l \leq 31$
Reflections collected	182623

Independent reflections	17092 [R_{int} = 0.0838, R_{sigma} = 0.0467]
Data/restraints/parameters	17092/0/565
Goodness-of-fit on F^2	1.061
Final R indexes [I>=2σ (I)]	R_1 = 0.0378, wR_2 = 0.0733
Final R indexes [all data]	R_1 = 0.0715, wR_2 = 0.0831
Largest diff. peak/hole / e Å^{-3}	1.07/-0.66

K(μ-Mes$_2$BO)$_2$Nd(N(SiMe$_3$)$_2$)$_2$, 4.2-Nd. Data is already reported in Chapter 3.

K(μ-Mes$_2$BO)$_2$Sm(N(SiMe$_3$)$_2$)$_2$, 4.2-Sm. A colorless crystal of approximate dimensions 0.100 x 0.151 x 0.205 mm was mounted in a cryoloop and transferred to a Bruker APEX DUO diffractometer system. The APEX4[36] program package was used to determine the unit-cell parameters and for data collection (20 sec/frame scan time). The raw frame data was processed using SAINT[31] and SADABS[32] to yield the reflection data file. Subsequent calculations were carried out using the SHELXTL[33] program package. There were no systematic absences nor any diffraction symmetry other than the Friedel condition. The centrosymmetric triclinic space group $P\bar{1}$ was assigned and later determined to be correct. The structure was solved by direct methods and refined on F^2 by full-matrix least-squares techniques. The analytical scattering factors[34] for neutral atoms were used throughout the analysis. Hydrogen atoms were included using a riding model. There are two toluene solvent present in the outer-sphere. One of the toluene molecules is situated about an inversion center and was modeled as a fragment with half occupancy and restraints. Least-squares analysis yielded wR2 = 0.0574 and Goof = 1.040 for 693 variables refined against 18591 data (0.70 Å), R1 = 0.0254 for those 16464 data with I > 2.0σ(I).

Table 4.5. Crystal data and structure refinement for K(μ-Mes$_2$BO)$_2$Sm(N(SiMe$_3$)$_2$)$_2$, 4.2-Sm.	
Identification code	dlc11
Empirical formula	$C_{58.5}H_{92}B_2KN_2O_2Si_4Sm$
Formula weight	1178.77
Temperature/K	100(2)
Crystal system	triclinic
Space group	P-1
a/Å	11.5598(5)
b/Å	12.0017(5)
c/Å	23.2986(10)
α/°	81.0680(10)
β/°	88.2150(10)
γ/°	78.9980(10)
Volume/Å^3	3134.5(2)
Z	2
ρ_{calc}g/cm^3	1.249
μ/mm^{-1}	1.119
F(000)	1240.0
Crystal size/mm^3	0.205 × 0.151 × 0.1
Radiation	MoKα (λ = 0.71073)

2Θ range for data collection/°	3.498 to 61.056
Index ranges	$-16 \leq h \leq 16$, $-17 \leq k \leq 16$, $-32 \leq l \leq 32$
Reflections collected	78515
Independent reflections	18591 [$R_{int} = 0.0336$, $R_{sigma} = 0.0321$]
Data/restraints/parameters	18591/59/693
Goodness-of-fit on F^2	1.040
Final R indexes [I>=2σ (I)]	$R_1 = 0.0254$, $wR_2 = 0.0552$
Final R indexes [all data]	$R_1 = 0.0327$, $wR_2 = 0.0574$
Largest diff. peak/hole / e $Å^{-3}$	0.54/-0.41

K(μ-Mes$_2$BO)$_2$Tb(N(SiMe$_3$)$_2$)$_2$, 4.2-Tb. A yellow crystal of approximate dimensions 0.026 x 0.043 x 0.125 mm was mounted in a cryoloop and transferred to a Bruker D8 Advance Photon III diffractometer system. The APEX5[37] program package was used to determine the unit-cell parameters and for data collection (60 sec/frame scan time). The raw frame data was processed using SAINT[31] and SADABS[32] to yield the reflection data file. Subsequent calculations were carried out using the SHELXTL[33] program package. The diffraction symmetry was *mmm* and the systematic absences were consistent with the orthorhombic space group *Pbca* that was later determined to be correct. The structure was solved by direct methods and refined on F^2 by full-matrix least-squares techniques. The analytical scattering factors[34] for neutral atoms were used throughout the analysis. Hydrogen atoms were included using a riding model. Least-squares analysis yielded wR2 = 0.0999 and Goof = 1.012 for 565 variables refined against 16966 data (0.70 Å), R1 = 0.398 for those 9967 data with $I > 2.0\sigma(I)$.

Table 4.6. Crystal data and structure refinement for K(μ-Mes$_2$BO)$_2$Tb(N(SiMe$_3$)$_2$)$_2$, 4.2-Tb.	
Identification code	kgb73
Empirical formula	$C_{48}H_{80}B_2N_2O_2Si_4KTb$
Formula weight	1049.14
Temperature/K	100.00
Crystal system	orthorhombic
Space group	Pbca
a/Å	21.4475(6)
b/Å	22.4582(7)
c/Å	23.0407(7)
α/°	90
β/°	90
γ/°	90
Volume/Å^3	11098.1(6)
Z	8
ρ_{calc}g/cm^3	1.256
μ/mm^{-1}	1.471
F(000)	4384.0
Crystal size/mm^3	0.125 × 0.043 × 0.026
Radiation	MoKα (λ = 0.71073)
2Θ range for data collection/°	3.798 to 61.086

Index ranges	$-30 \leq h \leq 28$, $-32 \leq k \leq 31$, $-25 \leq l \leq 32$
Reflections collected	152393
Independent reflections	16966 [$R_{int} = 0.1162$, $R_{sigma} = 0.0710$]
Data/restraints/parameters	16966/0/565
Goodness-of-fit on F^2	1.012
Final R indexes [I>=2σ (I)]	$R_1 = 0.0398$, $wR_2 = 0.0776$
Final R indexes [all data]	$R_1 = 0.1035$, $wR_2 = 0.0999$
Largest diff. peak/hole / e $Å^{-3}$	1.27/-0.69

Cs(μ-$Mes_2BO)_2Pr^{III}(OBMes_2)_2(THF)$, 4.3. A green crystal of approximate dimensions 0.045 x 0.095 x 0.150 mm was mounted in a cryoloop /and transferred to a Bruker D8 Advance Photon III diffractometer system. The APEX5[37] program package was used to determine the unit-cell parameters and for data collection (30 sec/frame scan time). The raw frame data was processed using SAINT[2] and SADABS[3] to yield the reflection data file. Subsequent calculations were carried out using the SHELXTL[4] program package. The diffraction symmetry was 2/*m* and the systematic absences were consistent with the monoclinic space group $P2_1/c$ that was later determined to be correct. The structure was solved by direct methods and refined on F^2 by full-matrix least-squares techniques. The analytical scattering factors[34] for neutral atoms were used throughout the analysis. Hydrogen atoms were included using a riding model. Disordered atoms were included using multiple components, partial site-occupancy-factors, constraints, and restraints. Least-squares analysis yielded wR2 = 0.1357 and Goof = 1.045 for 928 variables refined against 25230 data (0.70 Å), R1 = 0.0516 for those 18553 data with $I > 2.0\sigma(I)$. There were several high residuals

present in the final difference-Fourier map. It was not possible to determine the nature of the residuals although it was probable that hexane solvent was present. The SQUEEZE[35] routine in the PLATON[35] program package was used to account for the electrons in the solvent accessible voids.

Table 4.7. Crystal data and structure refinement for $Cs(\mu\text{-}Mes_2BO)_2Pr^{III}(OBMes_2)_2(THF)$, 4.3.	
Identification code	dlc4
Empirical formula	$C_{91}H_{131}B_4CsO_5Pr$
Formula weight	1622.01
Temperature/K	100.00
Crystal system	monoclinic
Space group	$P2_1/c$
a/Å	21.3081(10)
b/Å	14.4720(6)
c/Å	27.7799(12)
α/°	90
β/°	104.687(2)
γ/°	90
Volume/Å^3	8286.6(6)
Z	4
ρ_{calc}g/cm^3	1.300
μ/mm^{-1}	1.071

F(000)	3404.0
Crystal size/mm^3	0.15 × 0.095 × 0.045
Radiation	MoKα (λ = 0.71073)
2Θ range for data collection/°	3.196 to 61.036
Index ranges	-30 ≤ h ≤ 30, -20 ≤ k ≤ 20, -39 ≤ l ≤ 39
Reflections collected	193817
Independent reflections	25230 [R_{int} = 0.0665, R_{sigma} = 0.0435]
Data/restraints/parameters	25230/278/928
Goodness-of-fit on F^2	1.045
Final R indexes [I>=2σ (I)]	R_1 = 0.0516, wR_2 = 0.1218
Final R indexes [all data]	R_1 = 0.0777, wR_2 = 0.1357
Largest diff. peak/hole / e Å^{-3}	1.38/-1.21

$Ce^{IV}(OBMes_2)_2(NR_2)_2$, 4.4. A red crystal of approximate dimensions 0.0264 x 0.0268 x 0.0288 mm was mounted in a cryoloop and transferred to a Bruker SMART APEX II diffractometer system. The APEX2[38] program package was used to determine the unit-cell parameters and for data collection (15 sec/frame scan time). The raw frame data was processed using SAINT[31] and SADABS[32] to yield the reflection data file. Subsequent calculations were carried out using the SHELXTL[33] program package. The diffraction symmetry was 2/*m* and the systematic absences were consistent with the monoclinic space group $P2_1/n$ that was later determined to be correct. The structure was solved by direct methods and refined on F^2 by full-matrix least-squares techniques. The analytical scattering factors[34] for neutral atoms were used throughout the analysis. Hydrogen atoms were included using a riding model. Disordered atoms

were included using multiple components, partial site-occupancy-factors, and constraints. Least-squares analysis yielded wR2 = 0.0807 and Goof = 1.025 for 564 variables refined against 16378 data (0.70 Å), R1 = 0.0321 for those 12847 data with I > 2.0σ(I).

Table 4.8. Crystal data and structure refinement for $Ce^{IV}(OBMes_2)_2(NR_2)_2$, 4.4.	
Identification code	dlc1
Empirical formula	$C_{48}H_{80}B_2CeN_2O_2Si_4$
Formula weight	991.24
Temperature/K	93(2)
Crystal system	monoclinic
Space group	$P2_1/n$
a/Å	20.103(2)
b/Å	12.8498(12)
c/Å	22.542(2)
α/°	90
β/°	112.589(2)
γ/°	90
Volume/$Å^3$	5376.2(9)
Z	4
$\rho_{calc}g/cm^3$	1.225
μ/mm^{-1}	0.972
F(000)	2088.0

Crystal size/mm^3	0.288 × 0.268 × 0.264
Radiation	MoKα (λ = 0.71073)
2Θ range for data collection/°	3.726 to 61.084
Index ranges	-28 ≤ h ≤ 28, -18 ≤ k ≤ 18, -32 ≤ l ≤ 31
Reflections collected	136955
Independent reflections	16378 [R_{int} = 0.0578, R_{sigma} = 0.0361]
Data/restraints/parameters	16378/0/564
Goodness-of-fit on F^2	1.025
Final R indexes [I>=2σ (I)]	R_1 = 0.0321, wR_2 = 0.0731
Final R indexes [all data]	R_1 = 0.0489, wR_2 = 0.0807
Largest diff. peak/hole / e Å^{-3}	1.43/-0.59

[Cs(OBMes$_2$)]$_5$(THF)$_4$. A colorless crystal of approximate dimensions 0.136 x 0.164 x 0.390 mm was mounted in a cryoloop / on a glass fiber and transferred to a Bruker APEX DUO diffractometer system. The APEX4[36] program package was used to determine the unit-cell parameters and for data collection (20 sec/frame scan time). The raw frame data was processed using SAINT[31] and SADABS[32] to yield the reflection data file. Subsequent calculations were carried out using the SHELXTL[33] program package. The diffraction symmetry was 2/*m* and the systematic absences were consistent with the monoclinic space groups *Cc* and *C*2/*c*. It was later determined that space group *C*2/*c* was correct. The structure was solved by direct methods and refined on F^2 by full-matrix least-squares techniques. The analytical scattering factors[34] for neutral atoms were used throughout the analysis. Hydrogen atoms were included using a riding model. Least-squares analysis yielded wR2 = 0.1464 and Goof = 1.162 for 654 variables refined against

18289 data (0.7 Å), R1 = 0.0530 for those 13908 data with I > 2.0σ(I). There were several high residuals present in the final difference-Fourier map. It was not possible to determine the nature of the residuals although it was probable that two THF molecules were present. The SQUEEZE[35] routine in the PLATON[35] program package was used to account for the electrons in the solvent accessible voids.

Table 4.9. Crystal data and structure refinement for $[Cs(OBMes_2)]_5(THF)_4$.	
Identification code	mo_kgb65_K_c2c
Empirical formula	$C_{122}H_{170}B_5Cs_5O_{13}$
Formula weight	2563.17
Temperature/K3	93.15
Crystal system	monoclinic
Space group	C2/c
a/Å	29.810(9)
b/Å	12.671(4)
c/Å	31.871(9)
α/°	90
β/°	101.486(5)
γ/°	90
Volume/Å^3	11797(6)
Z	4
ρ_{calc}g/cm^3	1.443
μ/mm^{-1}	1.589

F(000)	5224.0
Crystal size/mm^3	0.39 × 0.164 × 0.136
Radiation	MoKα (λ = 0.71073)
2Θ range for data collection/°	2.788 to 61.362
Index ranges	$-42 \leq h \leq 41$, $-18 \leq k \leq 18$, $-45 \leq l \leq 44$
Reflections collected	137584
Independent reflections	17662 [R_{int} = 0.0401, R_{sigma} = 0.0278]
Data/restraints/parameters	17662/37/607
Goodness-of-fit on F^2	1.107
Final R indexes [I>=2σ (I)]	R_1 = 0.0472, wR_2 = 0.0967
Final R indexes [all data]	R_1 = 0.0660, wR_2 = 0.1053
Largest diff. peak/hole / e Å^{-3}	2.35/-1.68

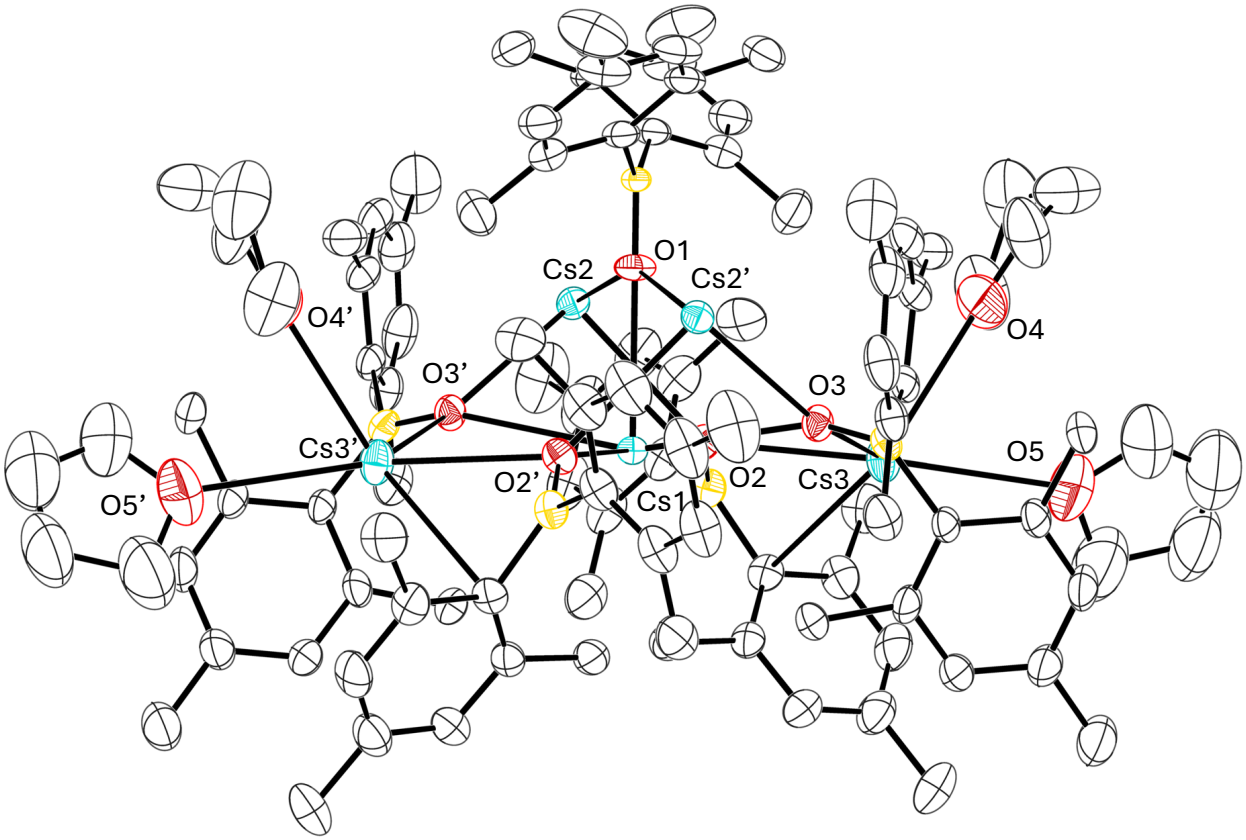

Figure 4.14. Graphical representation of $[Cs(OBMes_2)]_5(THF)_4$. cluster Thermal ellipsoids are drawn at the 50% probability level and hydrogen atoms are not shown for clarity.

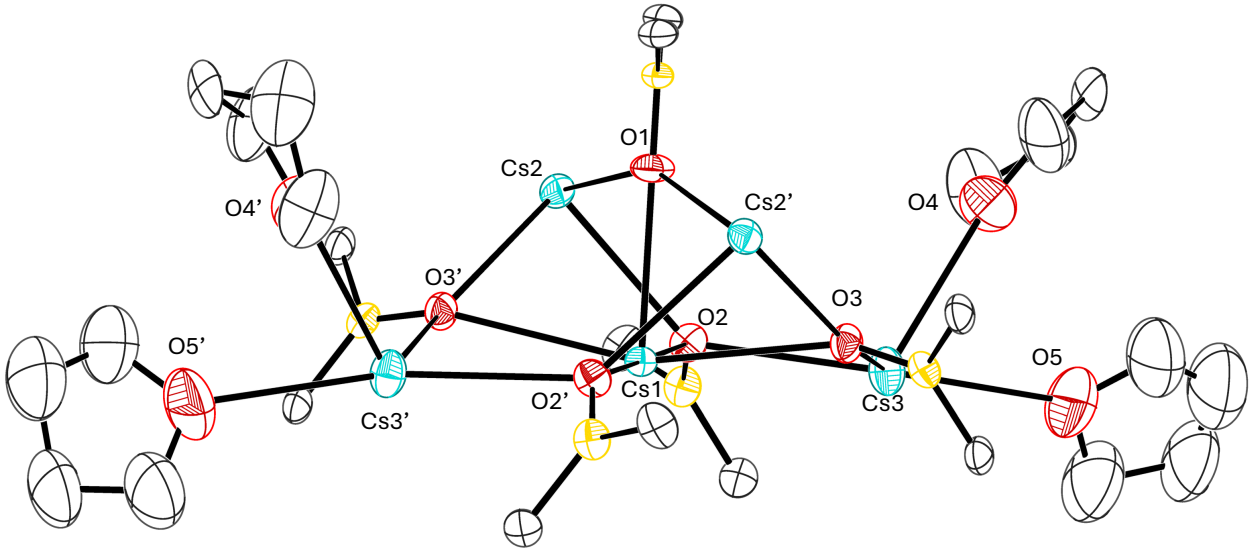

Figure 4.15. Graphical representation of $[Cs(OBMes_2)]_5(THF)_4$. cluster Thermal ellipsoids are drawn at the 50% probability level and hydrogen atoms and aryl groups are not shown for clarity.

REFERENCES

(1) Cloke, F. G. N. Zero Oxidation State Compounds of Scandium, Yttrium, and the Lanthanides. *Chem Soc Rev* **1993**, *22* (1), 17–24.

(2) Arnold, P. L.; Cloke, F. G. N.; Hitchcock, P. B. The First Structurally Authenticated Zerovalent Heteroarene Complex of a Lanthanide; Synthesis and X-Ray Structure of Bis(2,4,6-Tri-Tert-Butyl-Phosphorin)Holmium(0). *Chemical Communications* **1997**, 481–482.

(3) Willauer, A. R.; Palumbo, C. T.; Scopelliti, R.; Zivkovic, I.; Douair, I.; Maron, L.; Mazzanti, M. Stabilization of the Oxidation State +IV in Siloxide-Supported Terbium Compounds. *Angewandte Chemie - International Edition* **2020**, *59* (9), 3549–3553.

(4) Willauer, A. R.; Palumbo, C. T.; Fadaei-Tirani, F.; Zivkovic, I.; Douair, I.; Maron, L.; Mazzanti, M. Accessing the +IV Oxidation State in Molecular Complexes of Praseodymium. *J Am Chem Soc* **2020**, *142* (12), 5538–5542.

(5) Evans, W. J.; Deming, T. J.; Ziller, J. W. The Utility of Ceric Ammonium Nitrate Derived Alkoxide Complexes in the Synthesis of Organometallic Cerium(IV) Complexes: Synthesis and First X-Ray Crystallographic Determination of a Tetravalent Cerium Cyclopentadienide Complex, $(C_5H_5)_3Ce(OCMe_3)$. *Organometallics* **1989**, *8* (6), 1581–1584.

(6) Ma, C. G.; Brik, M. G.; Liu, D. X.; Feng, B.; Tian, Y.; Suchocki, A. Energy Level Schemes of FN Electronic Configurations for the Di-, Tri-, and Tetravalent Lanthanides and Actinides in a Free State. *J Lumin* **2016**, *170*, 369–374.

(7) Rice, N. T.; Popov, I. A.; Russo, D. R.; Gompa, T. P.; Ramanathan, A.; Bacsa, J.; Batista, E. R.; Yang, P.; La Pierre, H. S. Comparison of Tetravalent Cerium and Terbium Ions in a Conserved, Homoleptic Imidophosphorane Ligand Field. *Chem Sci* **2020**, *11* (24), 6149–6159.

(8) Evans, W. J. Tutorial on the Role of Cyclopentadienyl Ligands in the Discovery of Molecular Complexes of the Rare-Earth and Actinide Metals in New Oxidation States. *Organometallics* **2016**, *35* (18), 3088–3100.

(9) Hitchcock, P. B.; Lappert, M. F.; Maron, L.; Protchenko, A. V. Lanthanum Does Form Stable Molecular Compounds in the +2 Oxidation State. *Angewandte Chemie International Edition* **2008**, *47* (8), 1488–1491.

(10) Kamenskaya, A. N.; Mikheev, N. B. Complex Formation of the Lanthanides and Actinides in Lower Oxidation States. *Coord Chem Rev* **1991**, *109*, 1–59.

(11) Windorff, C. J.; Chen, G. P.; Cross, J. N.; Evans, W. J.; Furche, F.; Gaunt, A. J.; Janicke, M. T.; Kozimor, S. A.; Scott, B. L. Identification of the Formal +2 Oxidation State of Plutonium:

Synthesis and Characterization of $\{Pu^{II}[C_5H_3(SiMe_3)_2]_3\}^-$. *J Am Chem Soc* **2017**, *139* (11), 3970–3973.

(12) Su, J.; Windorff, C. J.; Batista, E. R.; Evans, W. J.; Gaunt, A. J.; Janicke, M. T.; Kozimor, S. A.; Scott, B. L.; Woen, D. H.; Yang, P. Identification of the Formal +2 Oxidation State of Neptunium: Synthesis and Structural Characterization of $\{Np^{II}[C_5H_3(SiMe_3)_2]_3\}^{1-}$. *J Am Chem Soc* **2018**, *140* (24), 7425–7428.

(13) Macdonald, M. R.; Bates, J. E.; Ziller, J. W.; Furche, F.; Evans, W. J. Completing the Series of +2 Ions for the Lanthanide Elements: Synthesis of Molecular Complexes of Pr^{2+}, Gd^{2+}, Tb^{2+}, and Lu^{2+}. *J Am Chem Soc* **2013**, *135* (26), 9857–9868.

(14) Palumbo, C. T.; Zivkovic, I.; Scopelliti, R.; Mazzanti, M. Molecular Complex of Tb in the +4 Oxidation State. *J Am Chem Soc* **2019**, *141* (25), 9827–9831.

(15) Gompa, T. P.; Ramanathan, A.; Rice, N. T.; La Pierre, H. S. The Chemical and Physical Properties of Tetravalent Lanthanides: Pr, Nd, Tb, and Dy. *Dalton Transactions* **2020**, *49* (45), 15945–15987.

(16) Boggiano, A. C.; Studvick, C. M.; Roy Chowdhury, S.; Niklas, J. E.; Tateyama, H.; Wu, H.; Leisen, J. E.; Kleemiss, F.; Vlaisavljevich, B.; Popov, I. A.; La Pierre, H. S. Praseodymium in the Formal +5 Oxidation State. *Nat Chem* **2025**.

(17) Shannon, R. D. Revised Effective Ionic Radii and Systematic Studies of Interatomic Distances in Halides and Chalcogenides. *Acta Cryst* **1976**, *32*, 751.

(18) Hitchcock, P. B.; Lappert, M. F.; Pierssens, L. J.-M. Synthesis and X-Ray Molecular Structures of the Silver (I) Amides $[\{Ag[\mu\text{-}N(SiMe_3)_2]\}_4$ and$[\{Ag[\mu\text{-}NCMe_2(CH_2)_3CMe_2]\}_4]$. *Chem. Commun* **1996**, No. 2.

(19) Lehr, M.; Paschelke, T.; Trumpf, E.; Vogt, A. M.; Näther, C.; Sönnichsen, F. D.; McConnell, A. J. A Paramagnetic NMR Spectroscopy Toolbox for the Characterisation of Paramagnetic/Spin-Crossover Coordination Complexes and Metal–Organic Cages. *Angewandte Chemie - International Edition* **2020**, *59* (43), 19344–19351.

(20) A Bell, B. F.; Ledwith, A.; Sherrington, D. C.; H Bawn, C. E.; Bell, F. A.; Hagopian, L.; Kohler, G.; Walter, R. I. Cation-Radicals: Tris-(*p*-Bromophenyl)Amminium Perchlorate and Hexa-Chloroantimonate. *Journal of the American Chemical Society C: Organic* **1969**, 2719–2720.

(21) Reimers, J. R.; McKemmish, L. K.; McKenzie, R. H.; Hush, N. S. Bond Angle Variations in XH_3 [X = N, P, As, Sb, Bi]: The Critical Role of Rydberg Orbitals Exposed Using a Diabatic State Model. *Physical Chemistry Chemical Physics* **2015**, *17* (38), 24618–24640.

(22) Brym, M.; Jones, C.; Junk, P. C. Rare Examples of Mononuclear, Homoleptic Antimony(III) and Bismuth(III) Aryloxides. *Main Group Chemistry* **2006**, *5* (1), 13–19.

(23) Lipkowski, J.; Fonari, M. S.; Kravtsov, V. C.; Simonov, Y. A.; Ganin, E. V; Gelmboldt, V. O. Antimony(III) Fluoride: Inclusion Complexes with Crown Ethers. *J Chem Crystallogr* **1996**, *26* (12).

(24) Ensinger, U.; Schwarz, W.; Schrutz, B.; Sommer, K.; Schmidt, A. Methoxostibanes. Structure and Vibrational Spectra. *Journal of Inorganic and General Chemistry* **1987**, *544* (1), 181–191.

(25) Moaven, S.; Yu, J.; Yasin, J.; Unruh, D. K.; Cozzolino, A. F. Precise Steric Control over 2D versus 3D Self-Assembly of Antimony(III) Alkoxide Cages through Strong Secondary Bonding Interactions. *Inorg Chem* **2017**, *56* (14), 8372–8380.

(26) Le Coz, E.; Hammoud, J.; Roisnel, T.; Cordier, M.; Dorcet, V.; Kahlal, S.; Carpentier, J. F.; Saillard, J. Y.; Sarazin, Y. Bonding in Barium Boryloxides, Siloxides, Phenoxides and Silazides:

A Comparison with the Lighter Alkaline Earths. *Chemistry - A European Journal* **2021**, *27* (46), 11966–11982.

(27) Stennett, C. R.; Luevano, M. R.; Queen, J. D.; Nguyen, J. Q.; Moore, W. N. G.; Evans, W. J. Large- and Small-Scale Syntheses of Donor-Free Rare-Earth Triiodides from the Metals and Ammonium Iodide. *Inorg Chem* **2024**, *63* (36), 16855–16860.

(28) Windorff, C. J.; Dumas, M. T.; Ziller, J. W.; Gaunt, A. J.; Kozimor, S. A.; Evans, W. J. Small-Scale Metal-Based Syntheses of Lanthanide Iodide, Amide, and Cyclopentadienyl Complexes as Analogues for Transuranic Reactions. *Inorg Chem* **2017**, *56* (19), 11981–11989.

(29) Bradley, D. C.; Ghotra, J. S.; Hart, F. A. Low Co-Ordination Numbers in Lanthanide and Actinide Compounds. Part 1. The Preparation and Characterization of Tris{bis(Trimethylsilyl)-Amido}lanthanides. *Journal of the Chemical Society, Dalton Transactions* **1973**, 1021–1023.

(30) APEX3, Version 2018.1-0. Bruker AXS Inc.: Madison, WI 2018.

(31) SAINT, Version 8.34a. Bruker AXS, Inc.: Madison, WI 2013.

(32) Sheldrick, G. M. SADABS, Version 2014/5. Bruker AXS, Inc.: Madison, WI 2014.

(33) Sheldrick, G. M. SHELXTL, Version 2014/7. Bruker AXS, Inc.: Madison, WI 2014.

(34) International Tables for Crystallography. *Dordrecht: Kluwer Academic Publishers*. 1992.

(35) Spek, A. L. PLATON SQUEEZE: A Tool for the Calculation of the Disordered Solvent Contribution to the Calculated Structure Factors. *Acta Crystallogr* **2015**, *C71*, 9–19.

(36) APEX4 Version 2021.4-0. Bruker ZXS Inc.: Madison, WI 2021.

(37) APEX5 Version 2023.9-2. Bruker AXS, Inc.: Madison, WI 2023.

(38) APEX2, Version 2014.11-0. Bruker AXS, Inc.: Madison, WI 2014.

–Chapter 5–

Investigating a Di-*tert*-butylmethyl Silanide Ligand, $(SiMe^tBu_2)^{1-}$ for the Stabilization of Ln(II) Molecular Complexes

INTRODUCTION

Structures of rare-earth complexes in the Ln(II) oxidation state are dominated by the use of first-row main group donor atom ligands, i.e. those that bind through O, N and C.[1,2] Relatively few coordination environments stabilize the $4f^n5d^1$ electron configurations of the non-traditional Ln(II) complexes defined in the introduction of this dissertation due to their high reactivity and the number of complexes of second-row main-group donor atoms is even more scarce. To further emphasize this point, a search of the Cambridge Crystal Database for any non-traditional rare-earth metals (Ln = Y, Sc, and the lanthanides excluding Sm, Eu, Yb and Tm, and radioactive Pm) that form complexes with at least one bond to silicon resulted in just 83 results, none of which consisted of Ln(II) compounds. Comparatively, changing the identity of the bound atom from silicon to carbon resulted in 2,921 structures, many of which include non-traditional metals in the 2+ oxidation state.

The compatibility of Ln(III) ions and first-row p-block donor atoms is most likely due to the hard Lewis acid nature of these metals that complement the hard Lewis base nature of these first row donor atoms.[3,4] However as a Ln(III) ion is reduced to the 2+ oxidation state, logically it can be considered softer than Ln(III) as it is less positively charged with a larger ionic radius,[5] and may be stabilized more successfully with the heavier p block elements. Silicon, being a softer congener of the carbon atom, was a natural choice to explore for Ln(II) compatibility.[2,4] Previously, it has been used to stabilize numerous transition metals, although through the availability of d-

orbital interactions, these complexes tend to be much simpler.[6–8] That being said, silicon donor atoms have been shown to stabilize the traditional $4f^{n+1}$ Ln(II) ions (Ln = Sm, Eu, Yb, Tm) in numerous examples, with alkylsilanide ligands like $(Si^tBu_3)^{1-}$ [9] and $(SiPh_3)^{1-}$ [10,11]and some hypersilylated ligands such as $[Si(SiMe_3)_3]^{1-}$[12–15] and the bidentate $[SiMe_2(Si\{SiMe_3\}_2)_2]^{1-}$,[13] to name a few. [16–21] Perhaps most relevant to this Chapter, the $[Si(H_2Ph)]^{1-}$ ligand has coordinated to an Y(II) atom in the complex $[K(crypt)][(C_5H_4CH_3)_3Y(SiH_2Ph)]$.[22]

One notable alkylsilanide is the di-*tert*-butylmethylsilyl ligand used by Liddle to form the complexes $Ln^{II}(SiMe^tBu_2)_3(THF)_3$ (Ln = Sm, Eu, Yb).[9] While these traditional rare-earth elements form generally stable divalent complexes,[23,24] the use of this ligand is reminiscent of the work of Sekiguchi who developed this ligand for the stabilization of Si and Ge radicals[25] and also used it to isolate radical anions of Al and Ga by use of potassium and 2.2.2 cryptand (crypt), namely $[K(crypt)][M(SiMe^tBu_2)_3]$ (M = Al, Ga).[26] Given these previous results, $(SiMe^tBu_2)^{1-}$, despite the difficulty of its synthesis,[27] was chosen to assess its ability to stabilize the 2+ oxidation state of the non-traditional rare-earth metals, [27] To begin this study, yttrium was used due to its similarity in ionic radius to that of the lanthanide holmium. This resulted in the first crystallographically characterized complex containing three Y–Si bonds, namely $(THF)_3Na(\mu{-}Cl)Y(SiMe^tBu_2)_3(THF)$, **5.1**.

RESULTS

The $NaSiMe^tBu_2$ ligand was synthesized via literature procedures in the three-step process, Scheme 5.1.

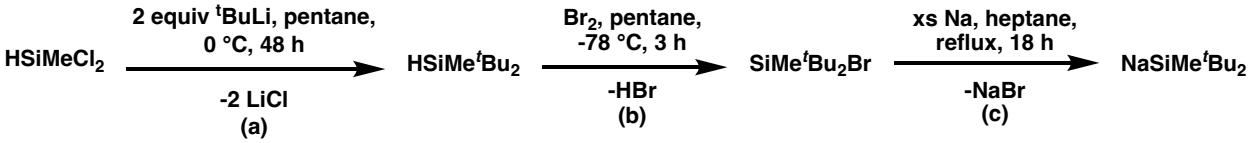

Scheme 5.1. The *tert*-butylation (a), bromination (b) and metalation (c) steps for the synthesis of the $NaSiMe^tBu_2$ ligand.

In a reaction flask under flow of argon gas, a pentane solution of dichloromethylsilane was treated with a dropwise addition of *tert*-butyllithium over thirty minutes and left to stir for 48 h, Scheme 5.1, reaction (a). This was followed by removal of the solvent to leave a di-*tert*-butylmethylsilane as a colorless oil. Subsequent treatment of this oil with elemental bromine in a dry ice and isopropanol bath, reaction for three h and removal of volatiles under reduced pressure yielded bromo-di-*tert*-butylmethylsilane as a colorless powder, reaction (b). Finally, this product was dissolved in heptane and treated with sodium metal, yielding the final product, sodium di-*tert*-butylmethylsilane in 46% overall yield, reaction (c).

To prepare a precursor for reduction to a +2 complex, a colorless slurry of YCl_3 in ca.10 mL THF was treated with three equivalents of dark yellow crystalline $NaSiMe^tBu_2$ at −35°C in an effort to synthesize the homoleptic complex "$Y(SiMe^tBu_2)_3$." The reaction immediately became an opaque light-yellow color and the mixture was then stirred for 3 h while it warmed to room temperature. The reaction mixture was centrifuged, and the yellow supernatant was decanted away from a light-yellow pellet. About half of the solvent was removed under reduced pressure and the solution was placed in the freezer for 16 h. Crystallization of the yellow solution at ca. −35°C yielded thin yellow crystals of $(THF)_3Na(\mu{-}Cl)Y(SiMe^tBu_2)_3(THF)$, **5.1**, in low yield, identified by X-ray crystallography, Figure 5.1, eq 5.1.

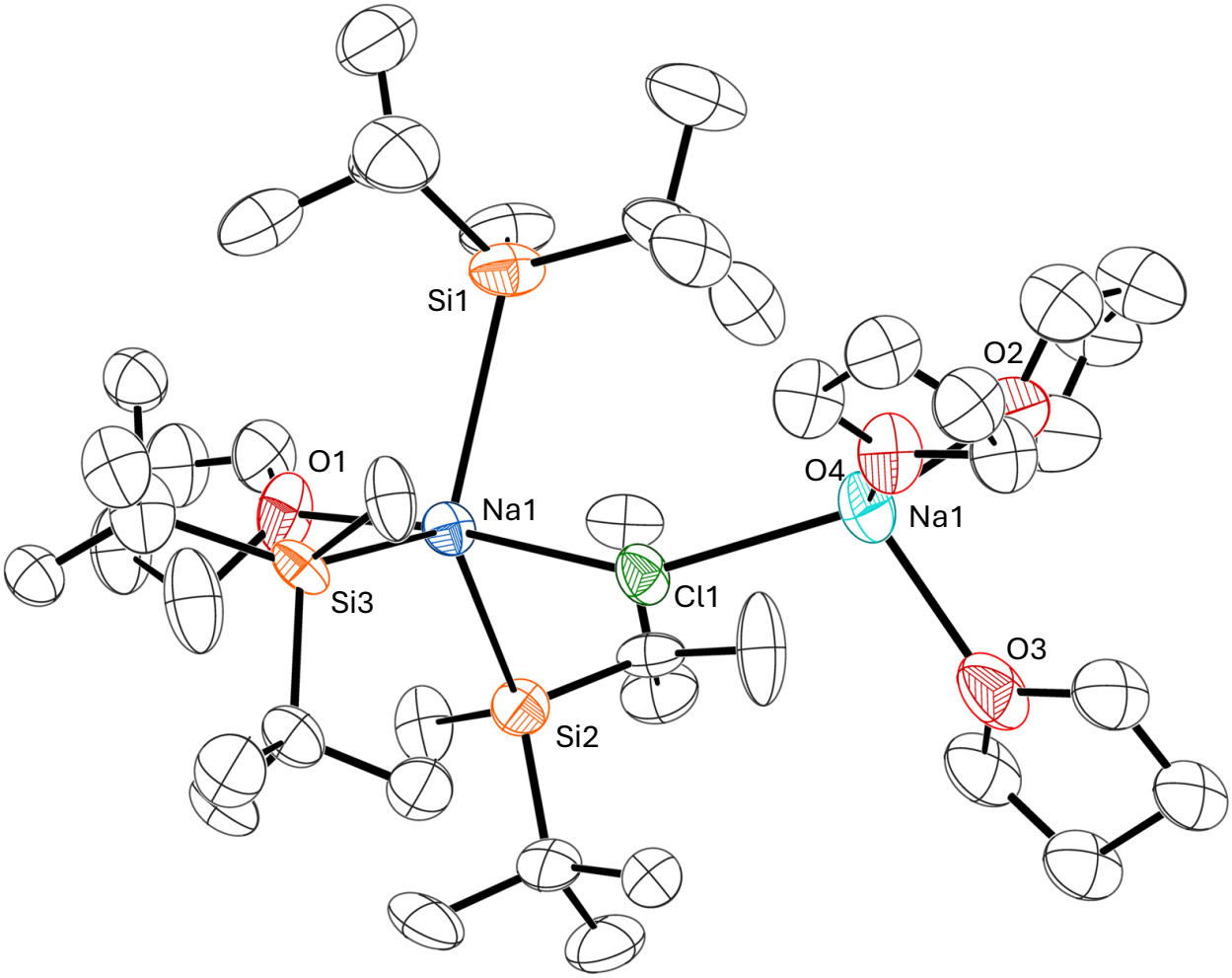

Figure 5.1. Graphical representation of $(THF)_3Na(\mu-Cl)Y(SiMe^tBu_2)_3(THF)$, **5.1**, with displacement ellipsoids drawn at the 50% probability level. Hydrogen atoms are omitted for clarity.

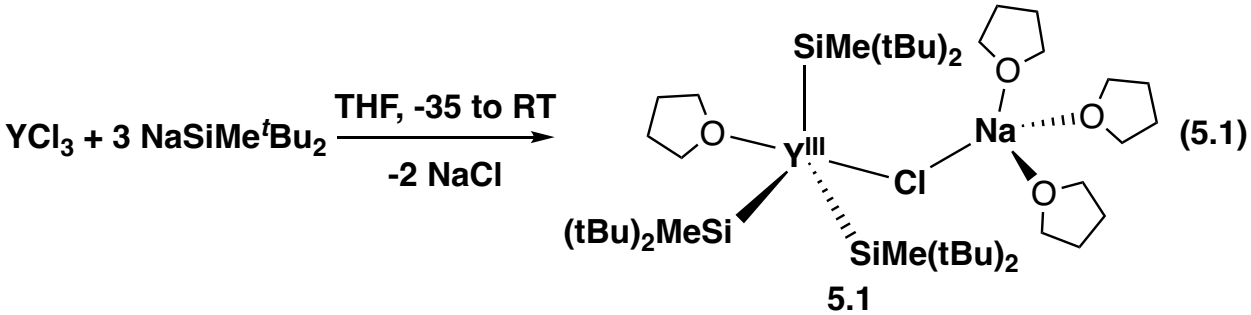

This complex is similar to many of the di(mesityl)boroxide $[Ln(A)_4(THF)]^{1-}$ "ate" complexes (A = anionic ligand in Chapters 3 and 4 in that it has four anionic ligands, a THF coordinating the Y(III) metal center and a countercation bound in some way to the anionic

lanthanide moiety. In this case, a bridging chloride ligand links the cation and the anion. The five coordinate yttrium has a distorted trigonal bipyramidal coordination geometry with τ_5 = 0.73 (where τ_5 = 1 is trigonal bipyramidal and τ_5 = 0 is square pyramidal) and Si-Y-Si angles ranging from 112.77(10) to 127.38(10)°.[28] The SiMe^{t}Bu ligands are bound through the silicon atom at Y–Si distances of 3.0832(2), 3.0424(1), and 3.077 Å, the latter of which is the average of the Y1–Si3/3A distances where atom Si3 is disordered in two parts (Y–Si3 = 2.956(6) and Y–Si3A = 3.197(5) Å). These distances are comparable to other Y^{III}–Si bonds found in the literature, specifically in the compounds $YI_2[Si(SiMe_3)_3](THF)_3$ (2.979(3) Å),[29] $YI_2[Si(SiMe_3)_2(Et)](THF)_3$ (2.9661(2) Å),[29] $Y\{N(SiHMe_2)_2\}_2(L^NSi)$ (L^N = PhC(2-(methylamido)pyridine)^{t}Bu); (3.0134(5) Å),[30] and the ate-salts $[K(2.2.2\text{-cryptand})][(C_5H_4CH_3)_3Y(SiH_2Ph)]$ (2.953 Å), $K_2Y[Si(SiHMe_2)_3]_2Cl(OEt_2)_3$ (3.039(1) and 3.030(1) Å),[16] $[(DME)_4K]\{(DME)YCl_2[Si(SiMe_3)_2SiMe_2]_2O\}$ (3.064(2) and 3.057(1) Å).[31] The ligands surrounding the metal center in **5.1** exhibit a high Guzei solid *G* value (a measurement of steric crowding about the metal, given in percentages) of 89%.[32]

The ^{1}H NMR spectrum of **5.1** shows two distinct singlets for the ^{t}Bu and Me substituents on the silyl ligands at δ 0.99 (54 H) and 0.00 (9 H) ppm respectively, which are similar to but distinct from the δ 1.17 (18H) and 0.01 (3H) ppm resonances of NaSiMe^{t}Bu$_2$ for the analogous hydrogens, Figures 5.2 and 5.3.

In the presence of 2.2.2 cryptand, two equiv of KC_8 was added to a yellow solution of **5.1** in ca. 5 mL THF at −35 °C. After allowing the reaction to stir for 1 h, eventually warming to room temperature, no change was seen and the KC_8 retained its bronze color, suggesting that no reduction event occurred.

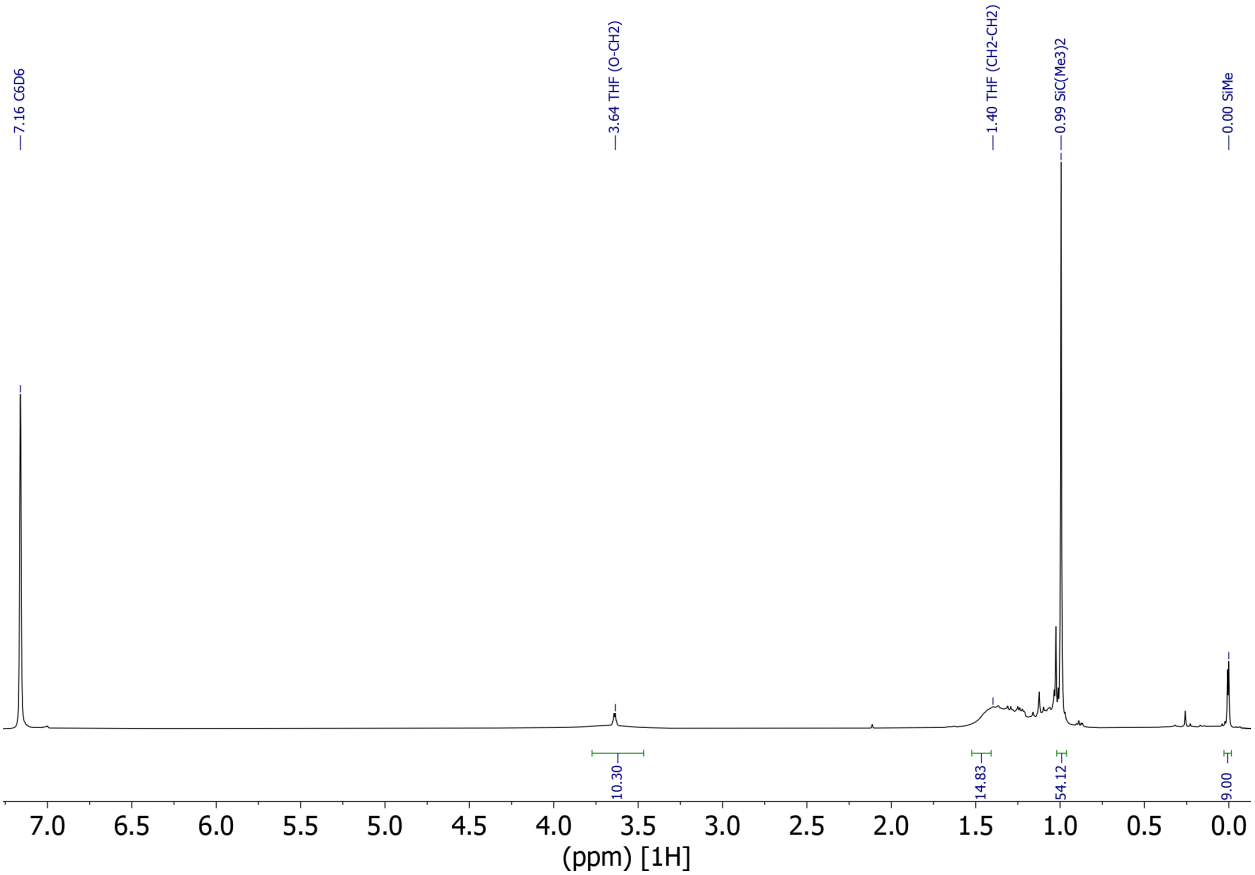

Figure 5.2. ^{1}H NMR (500 MHz, 298K) spectrum of **5.1** in deuterated benzene (residual proton peak marked at δ = 7.16 ppm). Note**:** Residual solvent resonances for hexane present at δ = 1.24 and 0.98.

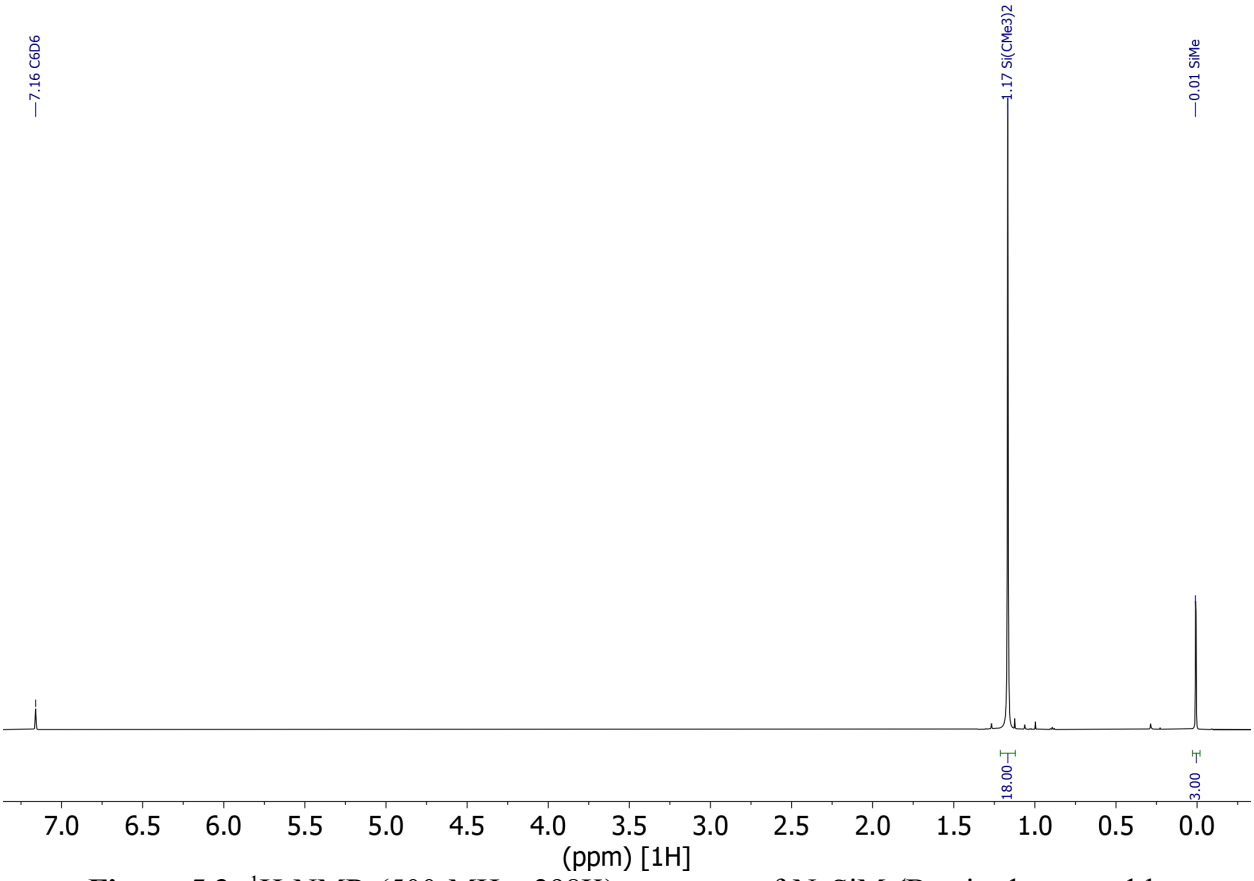

Figure 5.3. ^{1}H NMR (500 MHz, 298K) spectrum of NaSiMe^{t}Bu$_2$ in deuterated benzene (residual proton peak marked at δ = 7.16 ppm).

Attempted Syntheses of Ln(SiMe^{t}Bu$_2$)$_2$Cl. To assess the compatibility of the (SiMe^{t}Bu$_2$)$^{-}$ ligand with other lanthanide metals for reduction and subsequent loss of KCl, salt metathesis reactions with LnCl$_3$ (Ln = La, Sm) were conducted with two equiv of NaSiMe^{t}Bu$_2$. When white LaCl$_3$ was stirred into a yellow solution of NaSiMe^{t}Bu$_2$ in ca. 10 mL of Et$_2$O at room temperature, a colorless precipitate and a yellow supernatant were formed. Workup was conducted in hexane and cooling to −35 °C in minimal hexane (ca. 1 mL) led to small hexagonal colorless crystals of the previously reported [Na(μ-SiMe^{t}Bu$_2$)]$_4$ in a new unit cell, Figure 5.4.[25]

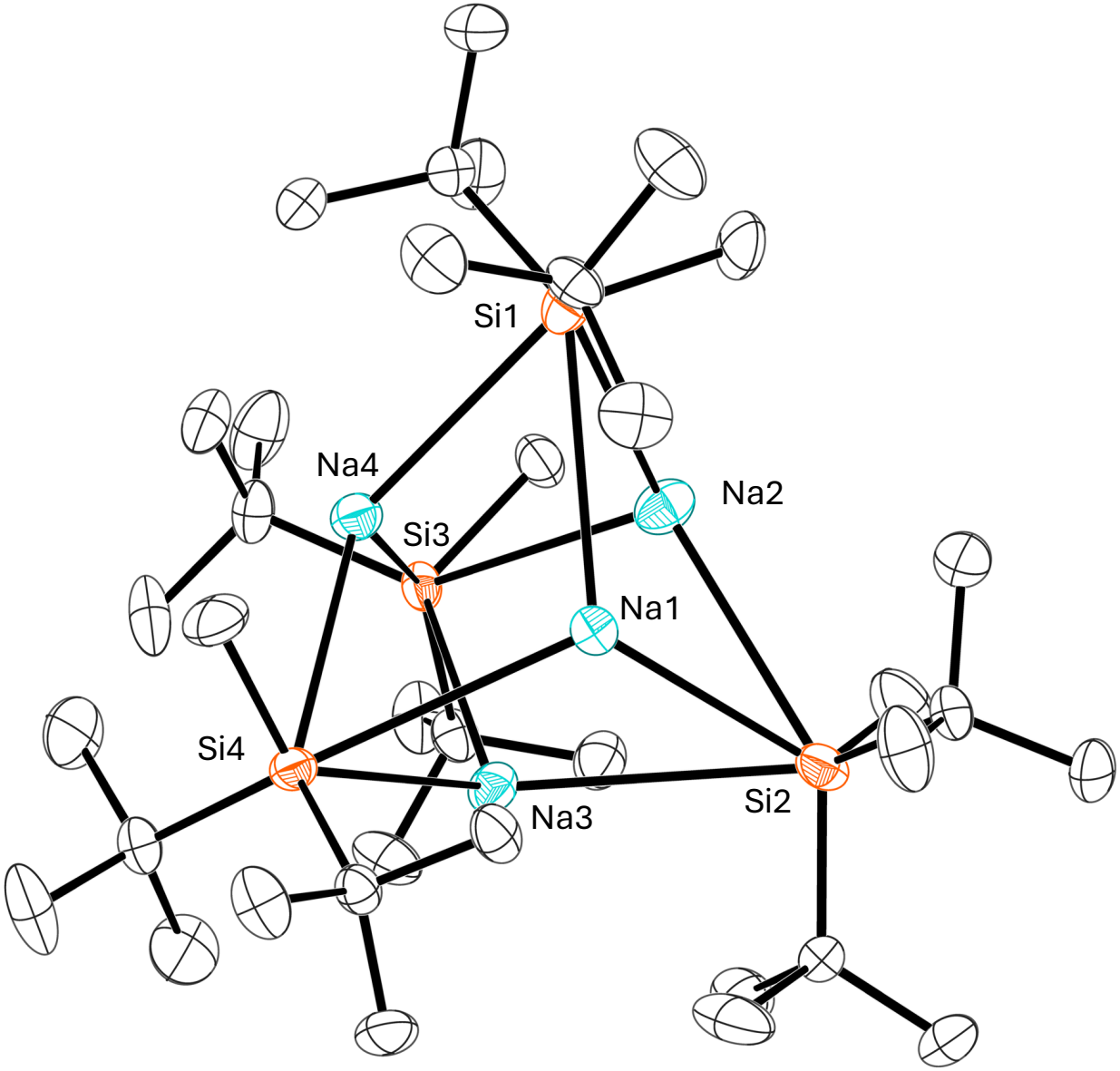

Figure 5.4. Graphical representation of $[Na(\mu\text{-}SiMe^tBu_2)]_4$, with displacement ellipsoids drawn at the 50% probability level. Hydrogen atoms are omitted for clarity.

The ^1H NMR spectrum in C_6D_6 of the yellow product of this reaction showed major resonances at δ 1.22 and 0.13 ppm in a 6:1 ratio that correspond to Me and ^{t}Bu resonances and are not overlapping with literature values of $NaSiMe^tBu$[9,25] or resonances of **5.1**. Interestingly, resonances consistent with the multiplicity of THF and Et_2O appear, but they are shifted upfield

from the standards provided in the literature,[33] suggesting that these may be ligated to a metal center, Figure 5.4. Additionally, three sets of resonances with the same 6:1 ratio are also found shifted upfield from the largest resonances, denoted as "unknown products [resonant hydrogen atoms] [corresponding product]" in the expansion window of Figure 5.5.

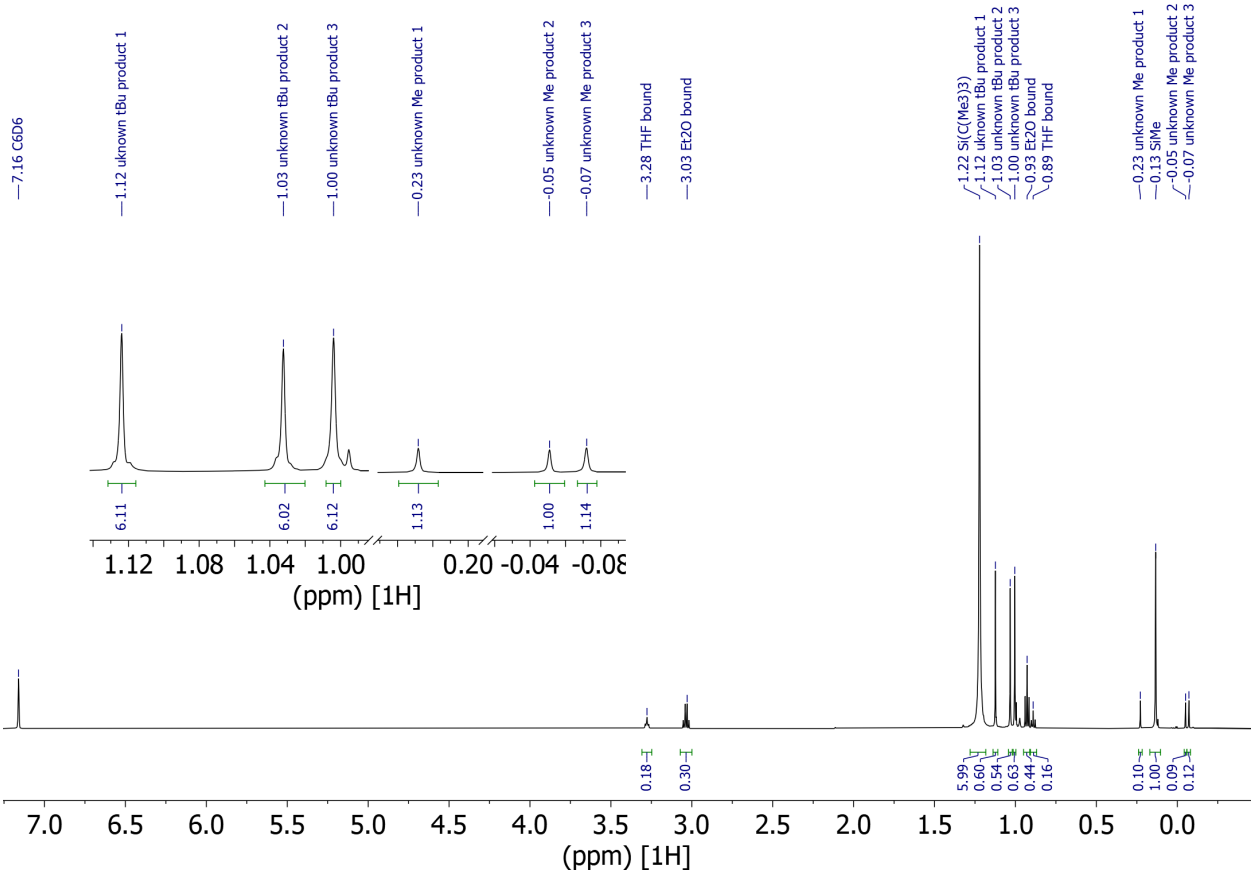

Figure 5.5. ^{1}H NMR (500 MHz, 298K) spectrum of "La(SiMe^{t}Bu$_2$)$_3$" in deuterated benzene (residual proton peak marked at δ = 7.16 ppm). Note**:** The expansion window contains resonances that have been removed for clarity between δ 0.98-0.24 and 0.19 and -0.02 ppm.

Another reaction run with $SmCl_3$ under similar conditions led to a nearly identical NMR, suggesting that the resonances observed are most likely from unreacted ligand and that no reaction occurred.

DISCUSSION

As stated, complex **5.1** is the first example of a coordination complex with three Y–Si bonds present in the CCDC. The crystal structure exhibits excellent shielding of the Y(III) metal center, as evidenced by the Solid *G* value of 89%, which is thought to aid in the stabilization of Ln(II) species.[34–36] This is comparable to the *G* values of other Ln(II) complexes with high thermal stability, such as $Sc^{II}(C_5H_2\,{}^tBu_3\text{-}1,3,4\text{-})_2$ at 87%,[36,37] and $Ln^{II}(OAr^*)_2(THF)_2$ (Ar* = $C_6H_2Ad_2$-2,6-^{t}Bu-4; Ad = 1-adamantyl) (Ln = Sm, Yb),[34] $Ln^{II}(OAr^*)_2$ (Sm = Eu)[34] and $[Ln^{II}(OAr^*)_3]^-$ (Ln = La, Ce, Nd, Gd, Dy, Y, Yb and Lu) at 85-92.[35,38] However, after manipulation of the model of **5.1** and removing the THF and $(THF)_3NaCl$ substituents that are bound to the Y(III) metal in **5.1** to better simulate the $[Al(SiMe^tBu_2)_3]^-$ structure that this work was inspired by,[25,26] the *G* value calculation drops to 66%, suggesting poor steric crowding.

With less steric crowding around the metal center, the ligation of THF may be necessary for an isolable $4f^n5d^1$ Ln(II) complex. Additionally, the use of a chelated potassium may be mandatory, as an $Ln^{II}(SiMe^tBu_2)_2$ complex would presumably have even further decreased steric crowding. Furthermore, as the trivalent ionic radius of the smallest of the rare earth metals, scandium, is 0.75 Å[5] and is larger than that of Al(III) (0.54 Å) or Ga(III) (0.62 Å)[5] under similar coordination conditions, the rare earth metals may be too large in general to be isolable in homoleptic nontraditional Ln(II) complexes.

Interestingly, when calculated, the *G* value for $[Al(SiMe^tBu_2)_3]^-$ is 80%. This is a much smaller *G* value than found for 1 and other stable Ln(II) complexes.. However, as reduction of an Al(III) ion would lead to the population of a 3s orbital, the *G* value calculation for elements other than rare earth metals may not be analogous.

CONCLUSION

Complex **5.1** is the first crystallographically characterized rare-earth metal complex to coordinate three monodentate silyl ligands based on Cambridge Crystallographic Data Centre searches. Silyl ligands have been used in the past with these metals, but usually with only one or two silyl ligands per metal. Additionally, they are typically stabilized by aryl ligands or only involve Si-C or Si-H interactions suggesting unique stability in the ligand system of **5.1**.[39–42]

EXPERIMENTAL DETAILS

All manipulations and syntheses described below were conducted with the rigorous exclusion of air and water using standard Schlenk line and glovebox techniques under an argon or atmosphere. Solvents were sparged with UHP argon and dried by passage through columns containing Q-5 and molecular sieves prior to use. Deuterated NMR solvents were dried over NaK alloy or over molecular sieves, degassed by three freeze-pump-thaw cycles, vacuum transferred before use, and stored over molecular sieves. ^{1}H, ^{13}C and COSY [$^{13}C\{^{1}H\}$] NMR spectra were recorded on Bruker GN500, CRYO500, or AVANCE600 MHz spectrometers at 298 K unless otherwise stated and referenced internally to residual protio-solvent resonances. ^{29}Si NMR are not reported, as the resonances of the ^{29}Si nuclei in the yttrium complex could not be differentiated from NMR tube resonances. Infrared spectra were collected on compressed solids using an Agilent Cary 630 ATR/FTIR instrument. $NaSiMe^{t}Bu_2$ was synthesized via literature procedures.[9,25,26] $YCl_3(H_2O)_x$ was purchased from Sigma Aldrich and water was removed under reduced pressure at 500 °C according to literature procedures with purity checked by FTIR.[43] KH in mineral oil (30%) was purchased from Sigma Aldrich and thoroughly rinsed with hexane before use.

Y(SiMe^{t}Bu$_2$)$_3$Cl(μ-Na(THF)$_3$)(THF), 5.1. In a 20 mL scintillation vial, a colorless slurry of YCl_3 (0.052g, 0.246 mmol) in ca. 7 ml of THF for five minutes before being placed in a freezer for 1 h, alongside a separate scintillation vial containing a yellow solution of NaSiMe^{t}Bu$_2$ in ca. 7 mL THF, to cool to −35 °C. Once chilled, the solution containing NaSiMe^{t}Bu$_2$ was added portionwise to the vial containing the YCl_3 slurry and the reaction was stirred for 3 h, forming a yellow slurry. This was then centrifuged and a yellow supernatant was decanted away from yellow solids. Solvent was removed under reduced pressure, resulting in the formation of small yellow crystals of **5.1** (0.071g, 0.126 mmol, 30% yield). ^{1}H NMR (500 MHz, C_6D_6) δ 3.64 (16H, m, OC*H*$_2$CH$_2$), 1.40 (16H, m, OCH$_2$C*H*$_2$), 0.99 (54H, s, Si(C[C*H*$_3$]$_3$)$_2$CH$_3$) , 0.00 (9H, s, Si(C[CH$_3$]$_3$)$_2$C*H*$_3$). IR (cm^{-1}) : 2935m, 2919m, 2873m, 2832s, 2754w, 2722w, 2689w, 2657w, 2641w, 2574w, 2560w, 2428w, 2394w, 2374w, 2357w, 2321w, 1461m, 1413m, 1377m, 1352m, 1293m, 1248w, 1228w, 1201w, 1044w, 1006m, 927w, 888w, 872w, 806s, 780m, 753m, 675w.

CRYSTALLOGRAPHIC INFORMATION

Y(SiMe^{t}Bu$_2$)$_3$Cl(μ-Na(THF)$_3$)(THF), 5.1. A yellow crystal of approximate dimensions 0.091 x 0.100 x 0.410 mm was mounted in a cryoloop and transferred to a Bruker X8 Prospector diffractometer system. The APEX3[44] program package was used to determine the unit-cell parameters and for data collection (10 sec/frame scan time). The raw frame data was processed using SAINT[45] and SADABS[46] to yield the reflection data file. Subsequent calculations were carried out using the SHELXTL[47] program package. The diffraction symmetry was 2/*m* and the systematic absences were consistent with the monoclinic space group $P2_1/c$ that was later determined to be correct. The structure was solved by direct methods and refined on F^2 by full-

matrix least-squares techniques. The analytical scattering factors[48] for neutral atoms were used throughout the analysis. Hydrogen atoms were included using a riding model. Disordered atoms were included using multiple components, partial site-occupancy-factors, and displacement (SIMU, ISOR, DFIX,) constraints. Least-squares analysis yielded wR2 = 0.2132 and Goof = 1.086 for 848 variables refined against 9836 data (0.83 Å), R1 = 0.0736 for those 7293 data with I > 2.0σ(I).

Table 5.1 Crystal data and structure refinement for $Y(SiMe^tBu_2)_3Cl(\mu\text{-}Na(THF)_3)(THF)$, 5.1.	
Identification code	kgb10 (Kito Gilbert-Bass)
Empirical formula	$C_{43}H_{95}ClNaO_4Si_3Y$
Formula weight	907.80
Temperature/K	92.85
Crystal system	monoclinic
Space group	$P2_1/c$
a/Å	15.4697(16)
b/Å	21.243(2)
c/Å	16.1934(18)
α/°	90
β/°	92.471(6)
γ/°	90
Volume/Å^3	5316.7(10)
Z	4

ρ_{calc}g/cm^3	1.134
μ/mm^{-1}	2.989
F(000)	1976.0
Crystal size/mm^3	0.41 × 0.1 × 0.091
Radiation	CuKα (λ = 1.54178)
2Θ range for data collection/°	5.718 to 138.082
Index ranges	-18 ≤ h ≤ 18, -25 ≤ k ≤ 25, -19 ≤ l ≤ 19
Reflections collected	143195
Independent reflections	9836 [R_{int} = 0.1513, R_{sigma} = 0.0611]
Data/restraints/parameters	9836/776/848
Goodness-of-fit on F^2	1.088
Final R indexes [I>=2σ (I)]	R_1 = 0.0736, wR_2 = 0.1943
Final R indexes [all data]	R_1 = 0.0941, wR_2 = 0.2135
Largest diff. peak/hole / e Å^{-3}	0.86/-1.38

NaSiMe^{t}Bu$_2$. A yellow crystal of approximate dimensions 1.375 × 0.588 × 0.486 mm was mounted in a cryoloop and transferred to a Bruker SMART APEX II diffractometer system. The APEX2[49] program package was used to determine the unit-cell parameters and for data collection (15 sec/frame scan time). The raw frame data was processed using SAINT[50] and SADABS[46] to yield the reflection data file. Subsequent calculations were carried out using the SHELXTL[47] program package. The diffraction symmetry was 2/*m* and the systematic absences were consistent with the monoclinic space group $P2_1/c$ that was later determined to be correct.

The structure was solved by direct methods and refined on F^2 by full-matrix least-squares techniques. The analytical scattering factors[48] for neutral atoms were used throughout the analysis. Hydrogen atoms were included using a riding model. Disordered atoms were included using multiple components, partial site-occupancy-factors. There were four high residuals present in the final difference-Fourier map. It was not possible to determine the nature of the residuals although it was probable that these were lone pairs on the Si atoms, due to their position and proximity to those atoms (ca. 1.3 Å) and occupancy of 0.33 of one carbon atom each (ca. 2 electrons). Least-squares analysis yielded wR2 = 0.1180 and Goof = 1.032 for 455 variables refined against 13844 data (0.73 Å), R1 = 0.0916 for those 10160 data with $I > 2.0\sigma(I)$. Note: When the four high residuals were modeled as carbon atoms at 1/3 occupancy, least-squares analysis yielded wR2 = 0.1153 and Goof = 1.021 for 495 variables refined against 13844 data (0.73 Å), R1 = 0.0437 for those 10160 data with $I > 2.0\sigma(I)$.

Definitions:

$wR2 = [\Sigma[w(F_o^2-F_c^2)^2] / \Sigma[w(F_o^2)^2]]^{1/2}$

$R1 = \Sigma||F_o|-|F_c|| / \Sigma|F_o|$

$Goof = S = [\Sigma[w(F_o^2-F_c^2)^2] / (n-p)]^{1/2}$ where n is the number of reflections and p is the total number of parameters refined.

The thermal ellipsoid plot is shown at the 50% probability level.

Table 5.2 Crystal data and structure refinement for $NaSiMe^tBu_2$.	
Identification code	kgb41
Empirical formula	$C_{36}H_{84}Na_4Si_4$

Formula weight	721.35
Temperature/K	133.15
Crystal system	monoclinic
Space group	$P2_1/c$
a/Å	18.6359(17)
b/Å	13.1988(12)
c/Å	20.3222(19)
α/°	90
β/°	108.361(2)
γ/°	90
Volume/Å^3	4744.2(8)
Z	4
ρ_{calc}g/cm^3	1.010
μ/mm^{-1}	0.183
F(000)	1600.0
Crystal size/mm^3	1.375 × 0.588 × 0.486
Radiation	MoKα (λ = 0.71073)
2Θ range for data collection/°	2.302 to 61.14
Index ranges	$-26 \leq h \leq 26$, $-18 \leq k \leq 16$, $-28 \leq l \leq 29$
Reflections collected	60168
Independent reflections	13844 [R_{int} = 0.0473, R_{sigma} = 0.0412]

Data/restraints/parameters	13844/0/455
Goodness-of-fit on F^2	1.032
Final R indexes [I>=2σ (I)]	R_1 = 0.0916, wR_2 = 0.2627
Final R indexes [all data]	R_1 = 0.1180, wR_2 = 0.2913
Largest diff. peak/hole / e $Å^{-3}$	5.12/-0.45

REFERENCES

(1) Arnold, P. L.; Cloke, G. N.; Nixon, J. F. The First Stable Scandocene: Synthesis and Characterisation Ofbis(h-2,4,5-Tri-Tert-Butyl-1,3-Diphosphacyclopentadienyl)Scandium(II). *Chemical Communications* **1998**, No. 7, 797–798.

(2) Du, J.; Cobb, P. J.; Ding, J.; Mills, D. P.; Liddle, S. T. F-Element Heavy Pnictogen Chemistry. *Chemical Science*. Royal Society of Chemistry December 4, 2023, pp 13–45.

(3) Baldwin, J.; Brookfield, A.; Whitehead, G. F. S.; Natrajan, L. S.; McInnes, E. J. L.; Oakley, M. S.; Mills, D. P. Synthesis and Characterization of Solvated Lanthanide(II) Bis(Triisopropylsilyl)Phosphide Complexes. *Inorganic Chemistry* **2024**, *63* (43), 20295–20306.

(4) Pearson, R. G. Hard and Soft Acids and Bases. *Journal of the American Chemical Society* **1963**, *85* (22), 3533–3539.

(5) Shannon, R. D. Revised Effective Ionic Radii and Systematic Studies of Interatomic Distances in Halides and Chalcogenides. *Acta Cryst* **1976**, *32*, 751.

(6) Kückmann, T. I. Silyl Chalcogenolates: Synthesis, Reactivity and Transition Metal Complexes, Johann Wolfgang Goethe-Universität, 2006.

(7) Igonin, V. A.; Ovchinnikov, Y. E.; Dement'ev, V. V; Shklover, V. E.; Timofeeva, T. V; Fnuue, T. M.; Struchkov, Y. T. Crystal Structures of Cycloheteropentasilanes $(\eta^5\text{-Cp})_2\text{Ti}(\text{SiPh}_2)_5$ and $\text{O}(\text{SiPh}_2)_5$. *Journal of Organometallic Chemisrry* **1989**, *371*, 187–196.

(8) Parkanyi, L.; Pannell, K. H.; Hernandez, C. Organometalloidal Derivatives of the Transition Metals IX * SYNTHESIS AND THE CRYSTAL STRUCTURE OF $(\eta^5\text{-C}_5\text{H}_5)_2\text{Fe(CO)}_2\text{SiMe}_2\text{-SiPh}_3$. *Journal of Organometallic Chemistry* **1983**, *252*, 127–132.

(9) Réant, B. L. L.; Berryman, V. E. J.; Basford, A. R.; Nodaraki, L. E.; Wooles, A. J.; Tuna, F.; Kaltsoyannis, N.; Mills, D. P.; Liddle, S. T. ^{29}Si NMR Spectroscopy as a Probe of S- And f-Block Metal(II)-Silanide Bond Covalency. *Journal of the American Chemical Society* **2021**, *143* (26), 9813–9824.

(10) Schuhknecht, D.; Truong, K. N.; Spaniol, T. P.; Maron, L.; Okuda, J. Molecular Hydrides of Divalent Ytterbium Supported by a Macrocyclic Ligand: Synthesis, Structure and Olefin Hydrofunctionalization Catalysis. *Chemical Communications* **2018**, *54* (80), 11280–11283.

(11) Bochkarev, L. N.; Makarov, V. M.; Hrzhanovskaya, Y. N.; Zakharov, L. N.; Fukin, G. K.; Yanovsky, A. I.; Struchkov, Y. T. Synthesis and Structure of Organosilicon and Organogermanium Complexes of Ytterbium $(\text{Ph}_3\text{E})_2\text{Yb(THF)}_4$ with YbSi and YbGe Bonds. *Journal of Organometallic Chemistry* **1994**, *467* (2).

(12) Zitz, R.; Hlina, J.; Gatterer, K.; Marschner, C.; Szilvási, T.; Baumgartner, J. Neutral "Cp-Free" Silyl-Lanthanide(II) Complexes: Synthesis, Structure, and Bonding Analysis. *Inorganic Chemistry* **2015**, *54* (14), 7065–7072.

(13) Zitz, R.; Hlina, J.; Aghazadeh Meshgi, M.; Krenn, H.; Marschner, C.; Szilvási, T.; Baumgartner, J. Using Functionalized Silyl Ligands To Suppress Solvent Coordination to Silyl Lanthanide(II) Complexes. *Inorganic Chemistry* **2017**, *56* (9), 5328–5341.

(14) Corradi, M. M.; Frankland, A. D.; Hitchcock, P. B.; Lappert, M. F.; Lawless, G. A. Synthesis, Structure and Reactivity of [Yb(η-C_5Me_5){$Si(SiMe_3)_3$}$(THF)_2$]. *Chem. Commun.* **1996**, No. 20, 2323–2324.

(15) Niemeyer, M. Reactions of Hypersilyl Potassium with Rare-Earth Metal Bis(Trimethylsilylamides): Addition versus Peripheral Deprotonation. *Inorganic Chemistry* **2006**, *45* (22), 9085–9095.

(16) Lampland, N. L.; Pindwal, A.; Yan, K.; Ellern, A.; Sadow, A. D. Rare Earth and Main Group Metal Poly(Hydrosilyl) Compounds. *Organometallics* **2017**, *36* (23), 4546–4557.

(17) Zitz, R.; Arp, H.; Hlina, J.; Walewska, M.; Marschner, C.; Szilvási, T.; Blom, B.; Baumgartner, J. Open-Shell Lanthanide(II+) or -(III+) Complexes Bearing -Silyl and Silylene Ligands: Synthesis, Structure, and Bonding Analysis. *Inorganic Chemistry* **2015**, *54* (7), 3306–3315.

(18) Meshgi, M. A.; Zitz, R.; Walewska, M.; Baumgartner, J.; Marschner, C. Tuning the Si-N Interaction in Metalated Oligosilanylsilatranes. *Organometallics* **2017**, *36* (7), 1365–1371.

(19) Xu, C.; Ye, Z.; Xiang, L.; Yang, S.; Peng, Q.; Leng, X.; Chen, Y. Insertion of Metal-Substituted Silylene into Naphthalene's Aromatic Ring and Subsequent Rearrangement for Silaspiro-Benzocycloheptenyl and Cyclobutenosilaindan Derivatives. *Angewandte Chemie - International Edition* **2021**, *60* (6), 3189–3195.

(20) Chen, Y.; Song, H.; Cui, C. Dehydrosilylation of ArNHSiH3 with Ytterbium(II) Amide: Formation of a Dimeric Ytterbium(II) Silanimine Complex. *Angewandte Chemie - International Edition* **2010**, *49* (47), 8958–8961.

(21) Evans, W. J.; Perotti, J. M.; Ziller, J. W.; Moser, D. F.; West, R. Evaluation of a Silylene Divalent Lanthanide Interaction in the Metallocene Complex $(C^5Me^5)^2Sm[SiN^tBuCHCHN^tBu]$. *Organometallics* **2003**, *22* (5), 1160–1163.

(22) Woen, D. H.; Huh, D. N.; Ziller, J. W.; Evans, W. J. Reactivity of Ln(II) Complexes Supported by $(C_5H_4Me)^{1-}$ Ligands with THF and $PhSiH_3$: Isolation of Ring-Opened, Bridging Alkoxyalkyl, Hydride, and Silyl Products. *Organometallics* **2018**, *37* (18), 3055–3063.

(23) Hitchcock, P. B.; Lappert, M. F.; Maron, L.; Protchenko, A. V. Lanthanum Does Form Stable Molecular Compounds in the +2 Oxidation State. *Angewandte Chemie International Edition* **2008**, *47* (8), 1488–1491.

(24) Fieser, M. E.; Macdonald, M. R.; Krull, B. T.; Bates, J. E.; Ziller, J. W.; Furche, F.; Evans, W. J. Structural, Spectroscopic, and Theoretical Comparison of Traditional vs Recently Discovered Ln^{2+} Ions in the $[K(2.2.2\text{-Cryptand})][(C_5H_4SiMe_3)_3Ln]$ Complexes: The Variable Nature of Dy^{2+} and Nd^{2+}. *Journal of the American Chemical Society* **2015**, *137* (1), 369–382.

(25) Sekiguchi, A.; Fukawa, T.; Nakamoto, M.; Lee, V. Y.; Ichinohe, M. Isolable Silyl and Germyl Radicals Lacking Conjugation with π-Bonds: Synthesis, Characterization, and Reactivity. *Journal of the American Chemical Society* **2002**, *124* (33), 9865–9869.

(26) Nakamoto, M.; Yamasaki, T.; Sekiguchi, A. Stable Mononuclear Radical Anions of Heavier Group 13 Elements: $[(^tBu_2MeSi)3E^{\bullet-}][K^+(2.2.2\text{-Cryptand})]$ (E = Al, Ga). *Journal of the American Chemical Society* **2005**, *127* (19), 6954–6955.

(27) Lickiss, P. D.; Smith, C. M. Silicon Derivatives of the Metals of Groups 1 and 2. *Coordination Chemistry Reviews* **1995**, *145*, 75–124.

(28) Addison, A. W.; Nageswara Rao, T.; Reedijk, J.; van Rijn, J.; Verschoor, G. C. Synthesis, Structure, and Spectroscopic Properties of Copper(II) Compounds Containing Nitrogen-Sulphur Donor Ligands ; the Crystal and Molecular Structure of Aqua[l,7-Bis(N-Methylbenzimidazol-2'-Yl)-2,6-Dithiaheptane]Copper(II) Perchlorate. *Journal of the Chemical Society, Dalton Transactions* **1984**, No. 7, 1349–1356.

(29) Sgro, M. J.; Piers, W. E. Synthesis, Characterization and Reactivity of Yttrium and Gadolinium Silyl Complexes. *Inorganica Chimica Acta* **2014**, *422*, 243–250.

(30) Sun, X.; Simler, T.; Kraetschmer, F.; Roesky, P. W. Thermally Stable Rare-Earth Metal Complexes Supported by Chelating Silylene Ligands. *Organometallics* **2021**, *40* (13), 2100–2107.

(31) Pöcheim, A.; Marschner, C.; Baumgartner, J. Rare-Earth-Silyl Ate-Complexes Opening a Door to Selective Manipulations. *Inorganic Chemistry* **2021**, *60* (11), 8218–8226.

(32) Guzei, I. A.; Wendt, M. An Improved Method for the Computation of Ligand Steric Effects Based on Solid Angles. *Dalton Transactions* **2006**, No. 33, 3991–3999.

(33) Fulmer, G. R.; Miller, A. J. M.; Sherden, N. H.; Gottlieb, H. E.; Nudelman, A.; Stoltz, B. M.; Bercaw, J. E.; Goldberg, K. I. NMR Chemical Shifts of Trace Impurities: Common Laboratory Solvents, Organics, and Gases in Deuterated Solvents Relevant to the Organometallic Chemist. *Organometallics* **2010**, *29* (9), 2176–2179.

(34) Anderson-Sanchez, L. M.; Ziller, J. W.; Evans, W. J. Synthesis of *Bis*-(2,6-Diadamantyl Aryloxide) Ln(II) Complexes of Samarium, Europium, and Ytterbium and Their Ln(III) Precursors. *Inorganic Chemistry* **2024**, *63* (45), 21416–21422.

(35) Anderson-Sanchez, L. M.; Yu, J. M.; Ziller, J. W.; Furche, F.; Evans, W. J. Room-Temperature Stable Ln(II) Complexes Supported by 2,6-Diadamantyl Aryloxide Ligands. *Inorganic Chemistry* **2023**, *62* (2), 706–714.

(36) Queen, J. D.; Anderson-Sanchez, L. M.; Stennett, C. R.; Rajabi, A.; Ziller, J. W.; Furche, F.; Evans, W. J. Synthesis of Crystallographically Characterizable Bis(Cyclopentadienyl) Sc(II) Complexes: $(C_5H_2TBu_3)_2Sc$ and $\{[C_5H_3(SiMe_3)_2]_2ScI\}^{1-}$. *Journal of the American Chemical Society* **2024**, *146* (5), 3279–3292.

(37) Queen, J. D.; Rajabi, A.; Ziller, J. W.; Furche, F.; Evans, W. J. Redox Studies of the Scandium Metallocene $(C_5H_2TBu_3)_2Sc^{II}$ Lead to a Terminal Side-On $(N{=}N)^{2-}$ Complex: $[(C_5H_2TBu_3)_2Sc^{II}I(H_2\text{-}H_2)]$-. *Journal of the American Chemical Society* **2025**.

(38) Moehring, S. A.; Miehlich, M.; Hoerger, C. J.; Meyer, K.; Ziller, J. W.; Evans, W. J. A Room-Temperature Stable Y(II) Aryloxide: Using Steric Saturation to Kinetically Stabilize Y(II) Complexes. *Inorganic Chemistry* **2020**, *59* (5), 3207–3214.

(39) Rees, W. S. Jr.; Just, O.; Schumann, H.; Weimann, R. Angew Chem Int Ed Engl - March 1 1996 - Rees - Structural Characterization of a Tris-Agostic Lanthanoid H Si. *Angewandte Chemie* **1996**, *35* (4), 419–422.

(40) Eppinger, J.; Spiegler, M.; Hieringer, W.; Herrmann, W. A.; Anwander, R. C2-Symmetric Ansa-Lanthanidocene Complexes. Synthesis via Silylamine Elimination and β-SiH Agostic Rigidity. *Journal of the American Chemical Society* **2000**, *122* (13), 3080–3096.

(41) Zitz, R.; Hlina, J.; Aghazadeh Meshgi, M.; Krenn, H.; Marschner, C.; Szilvási, T.; Baumgartner, J. Using Functionalized Silyl Ligands To Suppress Solvent Coordination to Silyl Lanthanide(II) Complexes. *Inorganic Chemistry* **2017**, *56* (9), 5328–5341.

(42) Scarel, G.; Wiemer, C.; Fanciulli, M.; Fedushkin, I. L.; Fukin, G. K.; Domrachev, G. A.; Lebedinskii, Y.; Zenkevich, A.; Pavia, G. [(Me3Si)2N]3Lu: Molecular Structure and Use as Lu and Si Source for Atomic Layer Deposition of Lu Silicate Films. *Zeitschrift fur Anorganische und Allgemeine Chemie* **2007**, *633* (11–12), 2097–2103.

(43) Armarego, W. L. F.; Chai, C. L. Lin. *Purification of Laboratory Chemicals*; Elsevier/BH, 2009.

(44) APEX3, Version 2018.1-0. Bruker AXS Inc.: Madison, WI 2018.

(45) SAINT, Version 8.38a. Bruker AXS inc. : Madison, WI 2013.

(46) Sheldrick, G. M. SADABS, Version 2014/5. Bruker AXS, Inc.: Madison, WI 2014.

(47) Sheldrick, G. M. SHELXTL, Version 2014/7. Bruker AXS, Inc.: Madison, WI 2014.

(48) International Tables for Crystallography. *Dordrecht: Kluwer Academic Publishers*. 1992.

(49) APEX2, Version 2014.11-0. Bruker AXS, Inc.: Madison, WI 2014.

(50) SAINT, Version 8.34a. Bruker AXS, Inc.: Madison, WI 2013.

–Chapter 6–

A Tripodal Oxygen Scorpionate Ligand Can Support Ytterbium in the 2+ Oxidation State

INTRODUCTION

The development of divalent lanthanide chemistry has been dominated by the use of X-type anionic ligands in which the negatively charged donor atom is bound directly to the cationic lanthanide in complexes like LnX_2. Although exploration of ligands like cyclopentadienide $(C_5H_5)^{1-}$ $(Cp)^{1-}$ and its derivatives has certainly been effective toward the aim of understanding the behavior of the Ln(II) ions,[1–6] the development of less traditional ligands has been under-explored. Tripodal tris(pyrazolyl)borate ligands, which are abbreviated as $(Tp)^{1-}$ and called scorpionates, are of interest for divalent lanthanide metal stability because, like $(Cp)^{1-}$, they offer three electron pairs with only a 1– charge.[7,8] The tris(pyrazolyl)borate ligand binds to the central metal through the nitrogen atoms of the three pyrazolyl moieties anchored by a negatively-charged boron atom, Figure 6.1. These L_2X-type ligands are also very modular and can be modified to sterically manipulate the ligand sphere.[9–11] Scorpionate ligands have coordinated various Ln(III) ions[12–14] and some traditional $4f^{n+1}$ Ln(II) ions (Ln = Sm, Eu, Tm, Yb).[12,15–19] However, a non-traditional $4f^n5d^1$ Ln(II) scorpionate complex has not yet been obtained.

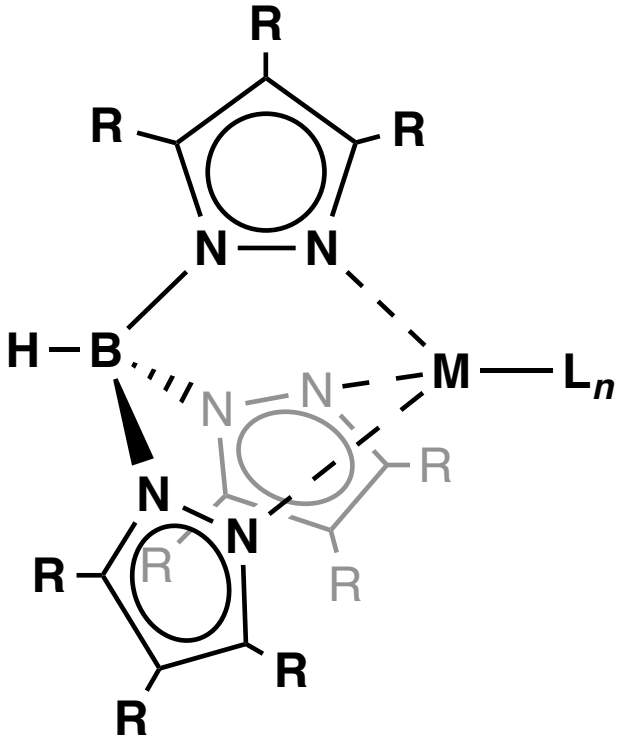

Figure 6.1. A general scaffold of the binding mode of the tris(pyrazolyl)borate ligand bound to some metal (M) with supporting anionic or neutral ligands (L_n) and customizable substituents (R).

The $(Tp)^{1-}$ have provided stability to Ln(III) ions in many solvents including water.[20–23] They have been used for single molecule magnet design[12] and they have been used with transition metals for a variety of special applications including anticancer, antibiotic and other medical uses.[24] A relatively new class of sterically demanding scorpionate ligand has been developed by the Parkin group invovling the tris(2-oxo-1-tert-butylimidazolyl)hydroborato $(TpO^{tBu})^{1-}$ and tris(2-oxo-methylbenzimidazolyl)hydroborato $(TpO^{MeBenz})^{1-}$ ligands, Figure 6.2.[9,11]

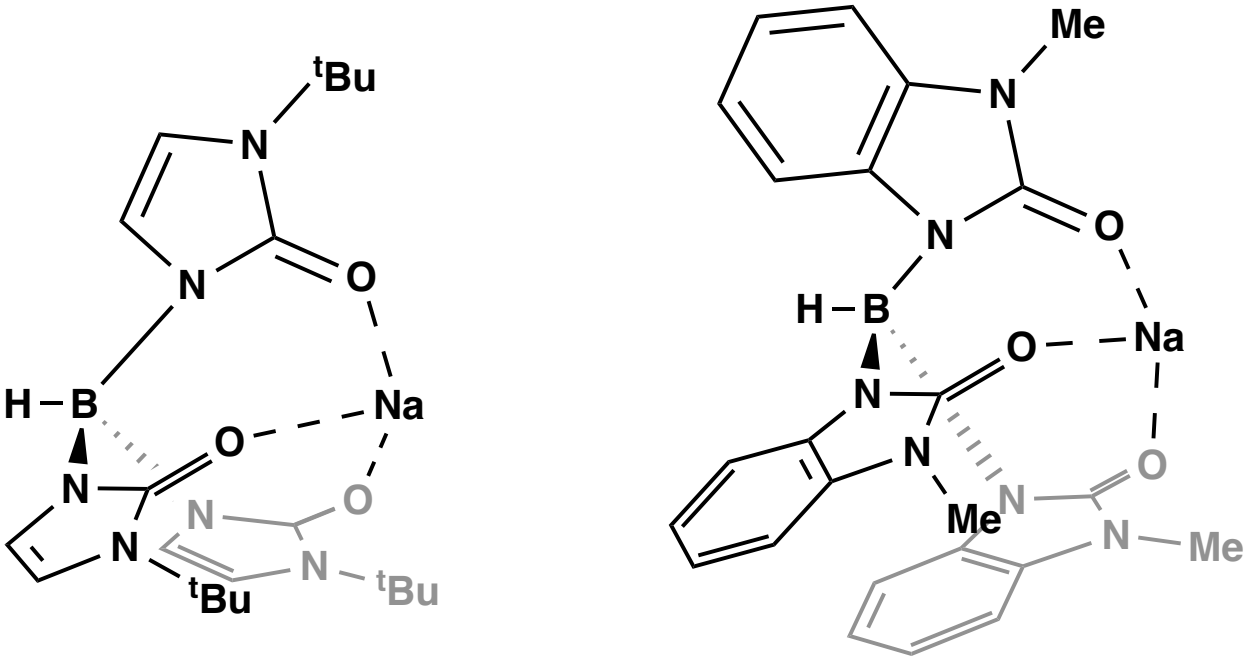

Figure 6.2. Sodium salts of the tris(2-oxo-1-tert-butylimidazolyl)hydroborato $(TpO^{tBu})^{1-}$ (left) and tris(2-oxo-methylbenzimidazolyl)hydroborato $(TpO^{MeBenz})^{1-}$ (right) ligands developed by Parkin.[9,11]

These new ligands bind through three neutral oxygen atoms on carbonyl groups and have coordinated to Na, Fe, Co, Zn, Zr, Re, and Tl[9,11] to make mononuclear complexes. However, there were no crystal structures in the Cambridge Crystal Data Centre (CCDC) with a $(TpO^{R})^{1-}$ (R = *t*Bu, MeBenz) bound to a lanthanide most likely due to the harsh conditions of the ligand's synthesis. Given that steric saturation around the metal center has shown to support non-traditional Ln(II) species effectively,[1,25–27] this study aimed to explore the $(TpO^{tBu})^{1-}$ ligand with the lanthanide metals. The compatibility of these ligands with a Ln(II) ion is demonstrated by the synthesis of the complex $Yb^{II}(TpO^{tBu})_2$ described in this Chapter.

RESULTS

The NaTpO^{tBu} reagent was prepared according to literature procedures with slight modification from a three-step synthesis, beginning with the aminolysis reaction via Hoffman rearrangement of 2,2-dimethoxyethanamine and *tert*-butylisocyanide to afford N-tert-butyl-N'-(2,2-dimethoxyethyl)urea in 99% yield, Scheme 6.1, step (a).[28]

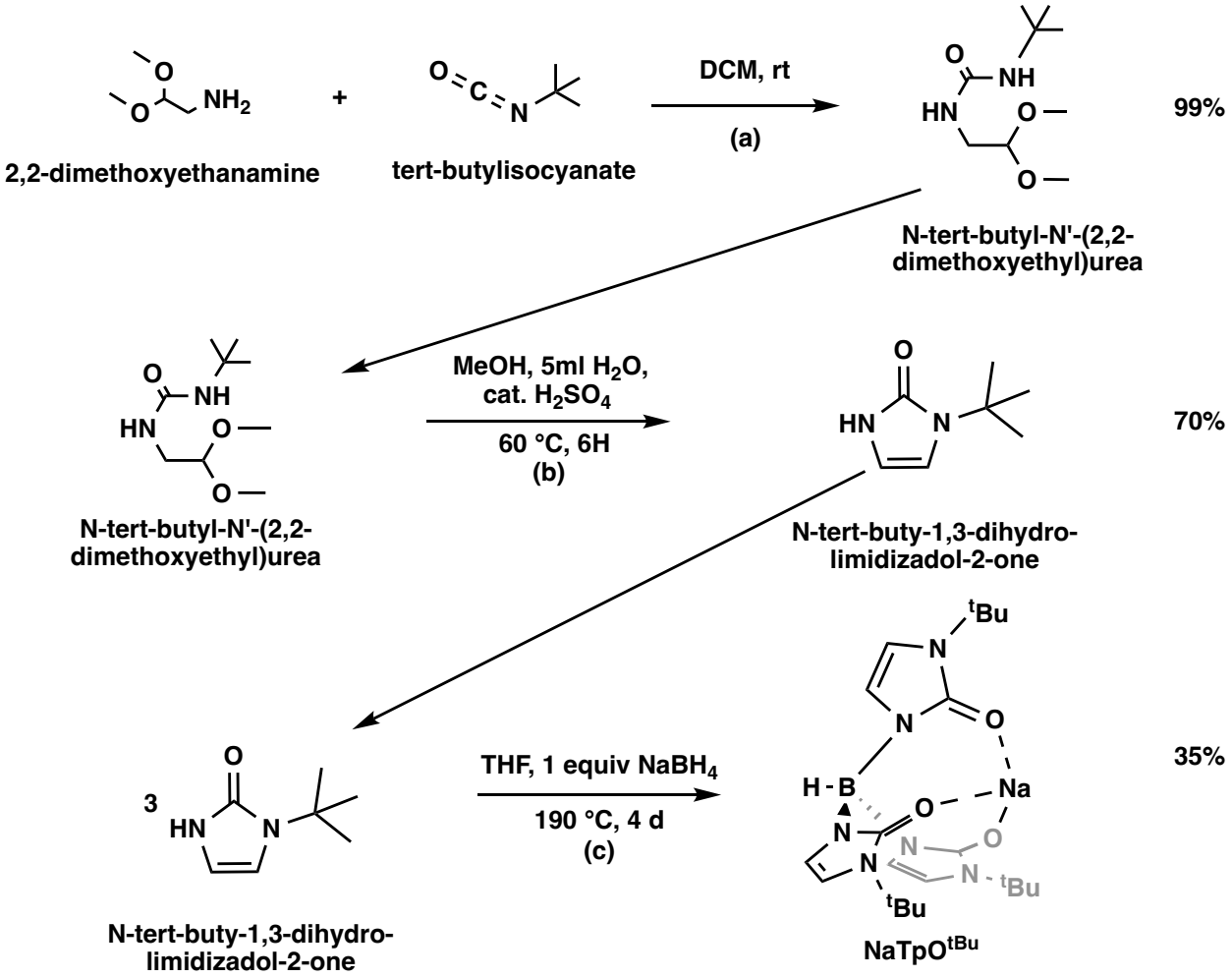

Scheme 6.1. The three-step synthesis of NaTpO^{tBu}. Steps (a), (b), and (c) are described below. Percent yields are given in after each step.

Heating of the resulting urea compound in the presence of H_2SO_4 in MeOH for 6 h caused the undocumented formation of a pink solution.[9,28] When quenched with 1.1 equiv of $NaHCO_3$ and extracted into (and recrystallized from) benzene, this afforded the compound N-*tert*-buty-1,3-dihydro-limidizadol-2-one in 70% yield, Scheme 6.1, step (b). Finally, treatment of

three equiv N-*tert*-buty-1,3-dihydro-limidizadol-2-on with one equiv of $NaBH_4$ in a high-pressure reaction flask in minimal THF (ca. 5 mL) for four days at 190 °C instead of the suggested nine days resulted in the formation of $NaTpO^{tBu}$ in 35% yield compared to the 7% yield reported, Scheme 6.1, step (c). It should be noted that H_2 gas generated from reaction (c) can reduce the C=C bond in N-*tert*-buty-1,3-dihydro-limidizadol-2-one to form N-*tert*-butylimidazolidin-2-one.[9]

A colorless solution of two equiv of $NaTpO^{tBu}$ in ca. 10 mL toluene was treated with one equiv of bright yellow $YbI_2(THF)_4$ and stirred at 60 °C for 72 h and formed a dark orange mixture. After filtration of colorless solids, solvent was removed under reduced pressure. Crystallization in minimal THF (ca. 1 mL) layered beneath hexane (ca. 1 mL) and placed in the glovebox freezer at −35 °C for 18 h led to yellow crystals of $Yb^{II}(TpO^{tBu})_2$, **6.1**, in 84% yield, eq 6.1, Figure 6.3.

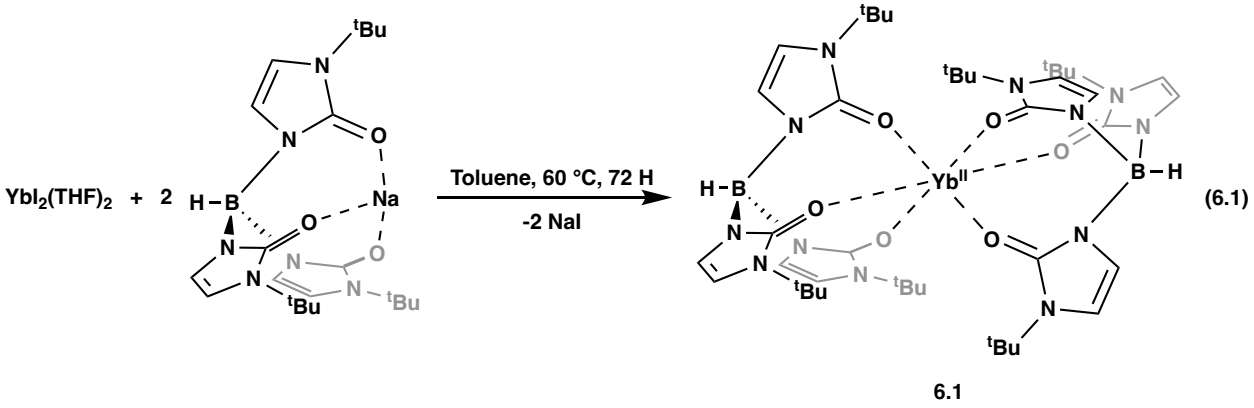

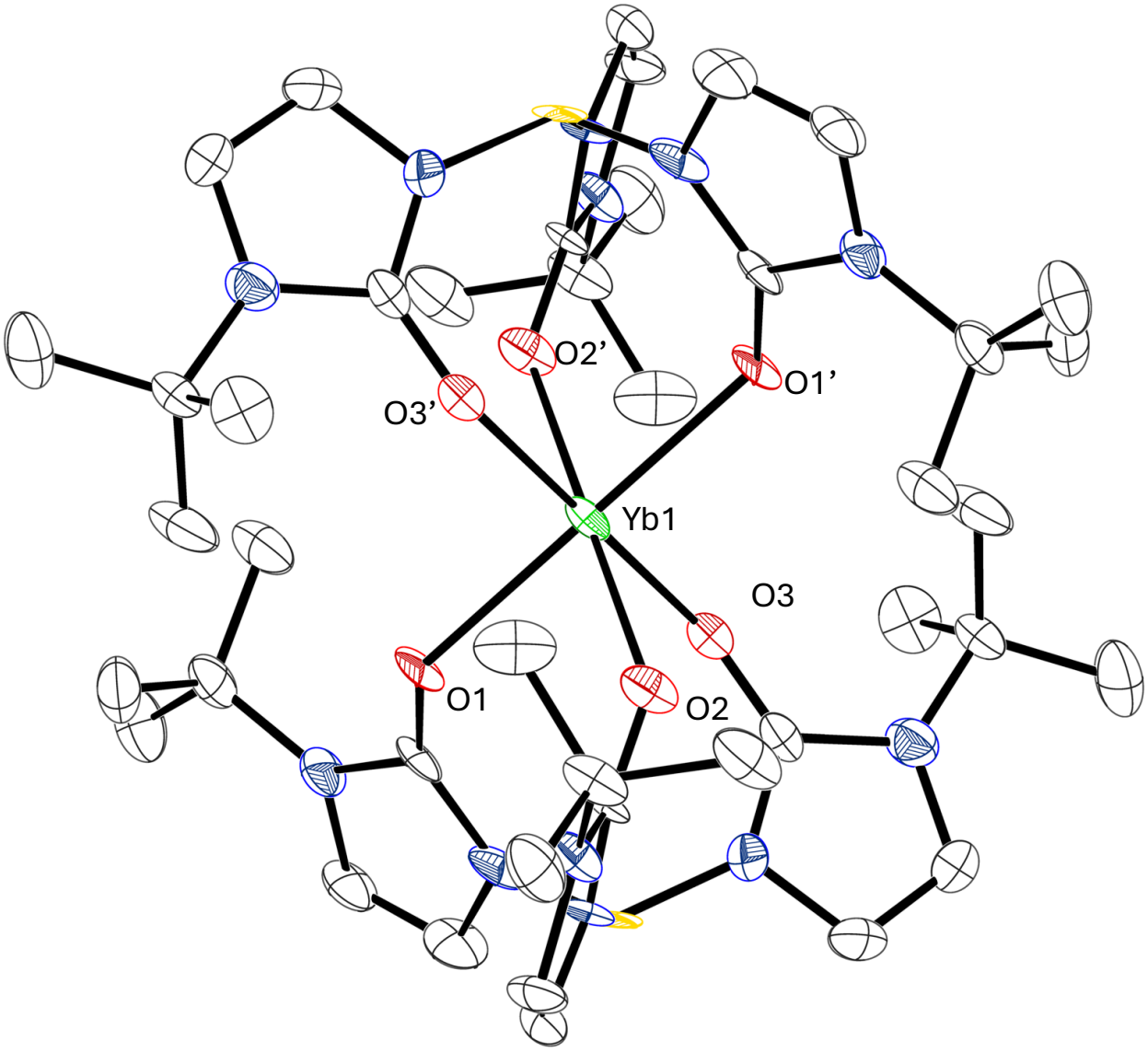

Figure 6.3. Graphical representation of Yb(TpO^{tBu})$_2$, **6.1**, with thermal ellipsoids drawn at the 50% probability level. Hydrogen atoms are not shown for clarity.

Complex **6.1** crystallizes in the P-1 space group with no solvent present in the lattice. The central metal, Yb1 is located on an inversion axis so that one of the ligands is symmetry-generated. Both (TpO^{tBu})$^{1-}$ligands bind through the three oxygen atoms to the Yb(II) center in a distorted octahedral geometry which allows the *t*Bu groups to stagger, providing a Guzei *G*

parameter, which assesses the steric saturation of the metal center as a percentage, 87%[29] (equivalent to a cone angle of 165° for each ligand), Figure 6.4.

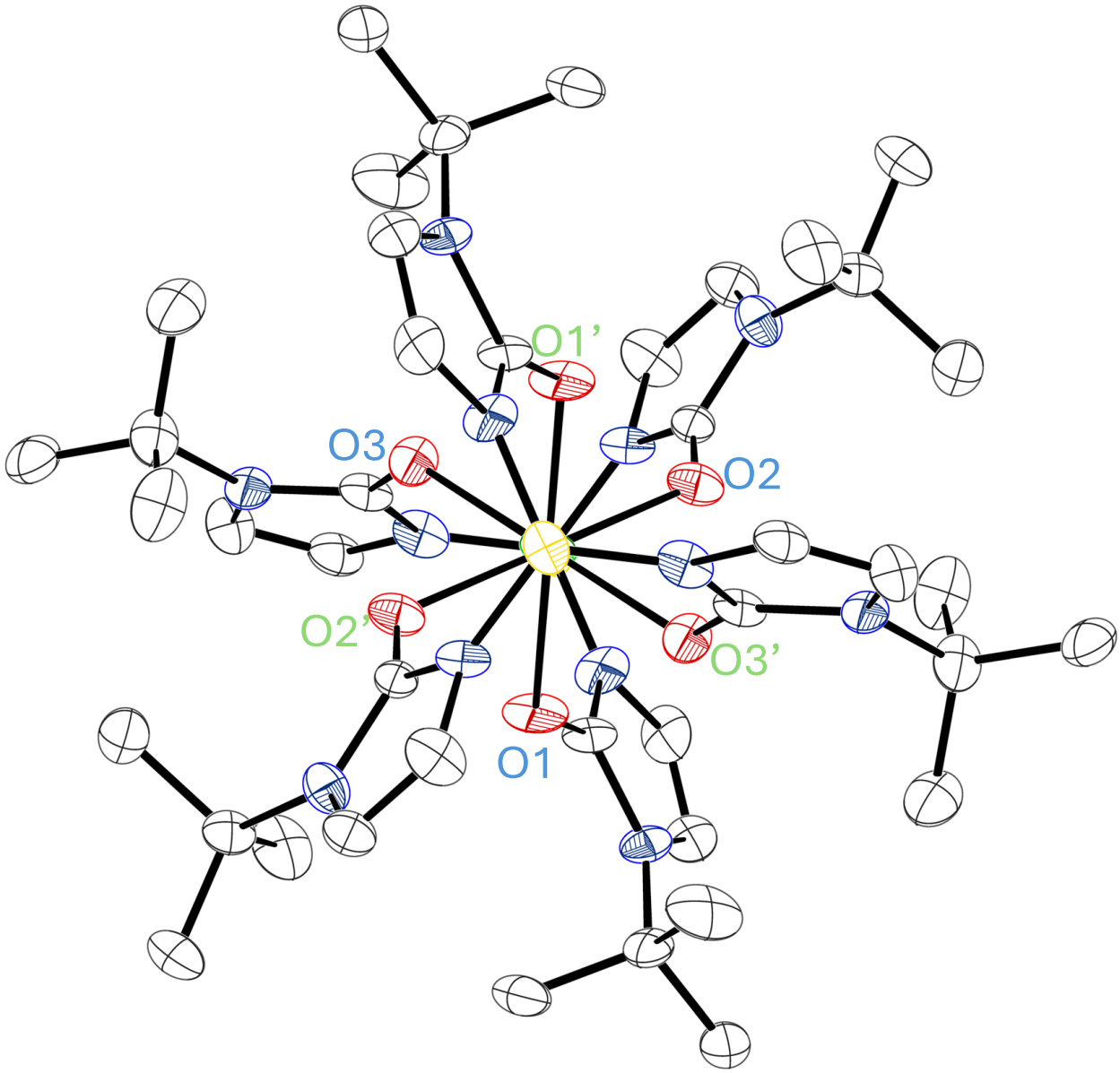

Figure 6.4. Graphical representation of Yb(TpO^{tBu})$_2$, **6.1**, shown down the B–Yb–B axis to illustrate staggering ligand formation with thermal ellipsoids drawn at the 50% probability level. Hydrogen atoms are not shown for clarity.

Each of the 2-oxo-1-*tert*-butylimidazolyl moieties is canted slightly in the same direction, most likely to afford more room for the tert-butyl substituents present. It should be noted here that although the data show 100% completeness on this structure, due to an interference with the beam stop, all data are correct except those for the Yb(II) atom, which shows as 50% occupancy. However, the Yb–O bond lengths of 2.338(7), 2.342(6) and 2.353(6) Å are typical of those distances found in other Yb^{II} complexes with six neutral oxygen ligands bound, Table 6.1. The O-Yb-O angles for oxygen atoms on the same ligand are similar to one another at 85.2(2), 83.3(2) and 83.3(2)°.

Table 6.1: Selected bond lengths (Å) and angles [°]of 6.1-Yb and other complexes with six Yb-O bonds

$Yb^{II}(TpO^{tBu})_2$, **6.1**		$Yb^{II}Ph_3BSi(SiMe_2OMe)_3$-$\kappa_3]_2$[16]		$[Yb^{II}(THF)_6]$ $[BPh_4]_2$[30]	
Yb1-O1	2.338(7)	Yb1–O1	2.4174(1)	Yb1–O1	2.388(4)
Yb1-O2	2.342(6)	Yb1–O2	2.4263(1)	Yb1–O2	2.392(4)
Yb1-O3	2.353(6)	Yb1–O3	2.4465(1)	Yb1–O3	2.350(4)
Avg. Yb-O	2.34	Avg. Yb-O	2.43	Avg. Yb-O	2.37
O1-Yb1-O2	85.2(2)	O1-Yb1-O2	89.27(5)	O1-Yb1-O2	88.14(15)
O1-Yb1-O3	83.3(2)	O1-Yb1-O3	86.69(4)	O1-Yb1-O3	88.13(15)
O2-Yb1-O3	83.3(2)	O2-Yb1-O3	88.82(5)	O2-Yb1-O3	89.50(16)
O1-Yb1-O2'	94.8(2)	O1-Yb1-O2'	90.73(5)	O1-Yb1-O2'	91.86(15)
O1-Yb1-O3'	96.7(2)	O1-Yb1-O3'	93.31(4)	O1-Yb1-O3'	91.87(15)
O2-Yb1-O3'	96.7(2)	O2-Yb1-O3'	91.18(5)	O2-Yb1-O3'	90.50(16)
O1-Yb1-O1'	180	O1-Yb1-O1'	180	O1-Yb1-O1'	180.0(3)

Avg. O-Yb-O (w/o 180° angle)	90	Avg. O-Yb-O (w/o 180° angle)	90	Avg. O-Yb-O (w/o 180° angle)	90

As Yb(II) contains a closed shell $4f^{14}$ electron configuration, ^{1}H NMR spectroscopy is easily determined. The ^{1}H NMR of **6.1** shows three main resonances at δ 6.53, 6.02 and 1.39 ppm, Figure 6.5.

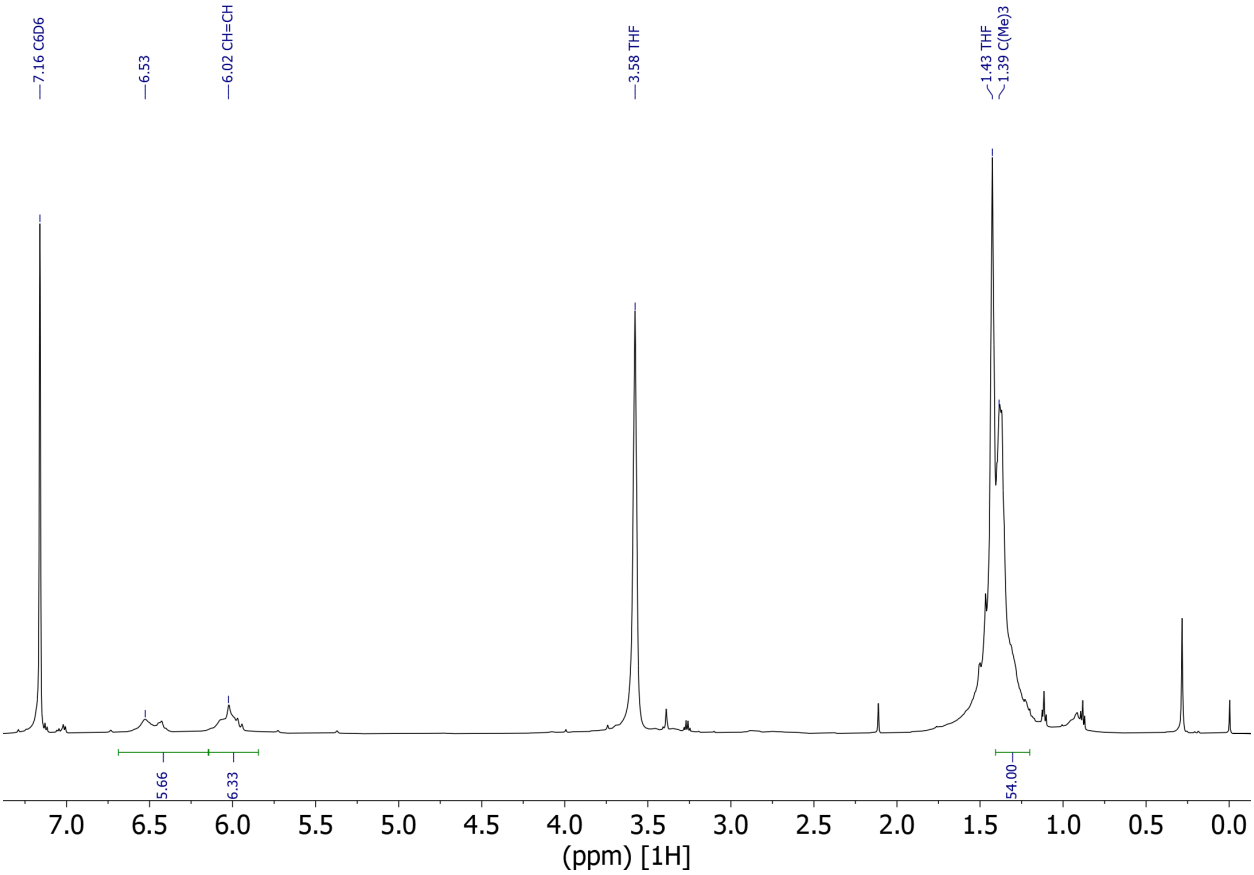

Figure 6.5. ^{1}H NMR (500 MHz, 298K) spectrum of **6.1** in deuterated benzene (residual proton peak marked at δ = 7.16 and TMS internal standard at 0.00 ppm). Note**:** Residual resonances for THF marked at δ = 3.58 and 1.43 and for silicone grease impurity at 0.29 ppm.

The absence of surplus peaks suggests that the $(TpO^{tBu})^{1-}$ligand is bound tightly to the Yb(II) ion and the O atoms are not labile. Though these values are similar to those found in the

Na(TpO^{tBu}) precursor at δ = 6.56, 6.08 and 1.38 ppm, this is not surprising, as both metals are diamagnetic.

DISCUSSION

As shown by the synthesis and structure of Yb(TpO^{tBu})$_2$, **6.1**, the TpO^{tBu} ligand can form lanthanide divalent complexes.[1,27] The Guzei *G* value of 87% for **6.1** is in the range of some of the most stable divalent rare-earth complexes to date, namely $Sc^{II}(C_5H_2{}^tBu_3\text{-}1,3,4\text{-})_2$ at 87%,[31,32] and $Ln^{II}(OAr^*)_2(THF)_2$ (Ar* = $C_6H_2Ad_2$-2,6-^{t}Bu-4; Ad = 1-adamantyl) (Ln = Sm, Yb),[25] $Ln^{II}(OAr^*)_2$ (Sm = Eu)[25] and $[Ln^{II}(OAr^*)_3]^-$ (Ln = La, Ce, Nd, Gd, Dy, Y, Yb and Lu) at 85-92%.[26,33] Since this high steric shielding of the metal center, has been shown to increase the longevity of complexes of the Ln 2+ oxidation state,[1,27] this ligand may be useful for other lanthanides.

CONCLUSION

The tripodal tris(2-oxo-1-tert-butylimidazolyl)hydroborato (TpO^{tBu}) oxygen donor ligand has been shown here to form a crystallographically characterizable complex with an Ln(II) ion, specifically Yb. With a high degree of steric crowding around the metal center, it is conceivable that this ligand could serve to stabilize a non-traditional $4f^n5d^1$ metal center under similar conditions.

EXPERIMENTAL DETAILS

All manipulations and syntheses described below were conducted with the rigorous exclusion of air and water using standard Schlenk line and glovebox techniques under an argon or dinitrogen atmosphere. Solvents were sparged with UHP argon and dried by passage through columns containing Q-5 and molecular sieves prior to use. Deuterated NMR solvents were dried

over NaK alloy, degassed by three freeze-pump-thaw cycles, and vacuum transferred before use. ^{1}H NMR spectra were recorded on a Bruker CRYO600 MHz. spectrometers at 298 K and referenced internally to residual protio-solvent resonances. $YbI_2(THF)_4$[34] and $NaTpO^{tBu}$ (TpO^{tBu} = tris(2-oxo-1-tert-butylimidazolyl)hydroborato)[9] starting materials were synthesized via literature procedures with minimal adjustments.

$Yb^{II}(TpO^{tBu})_2$, 6.1. A 20 mL scintillation vial was charged with a colorless solution of two equiv of $NaTpO^{tBu}$ (0.058 g, 0.129 mmol) in ca. 10 mL of toluene. This was treated with one equiv of bright yellow powdered $YbI_2(THF)_4$ (0.048g, 0.067 mmol) and stirred at 60 °C for 72 h. The solution turned to a dark orange mixture. The mixture was centrifuged and the orange supernatant was decanted away from a colorless pellet. The solvent was removed from the supernatant under reduced pressure and treated with ca. 1 mL of THF to form an orange solution. Ca. 1 mL of hexane was layered on top of this, yellow solids immediately formed at the solvent front. This was placed in the glovebox freezer at −35 °C for 18 h to yield yellow crystals of $Yb^{II}(TpO^{tBu})_2$, **6.1** (0.056g, 0.054 mmol, 84% yield). ^{1}H NMR (600 MHz, C_6D_6) δ 6.56 (6 H, d, HC=C*H*), 6.08 (6 H, d, *H*C=CH), 1.38 (54 H, s, C(CH_3)).

REFERENCES

(1) Evans, W. J. Tutorial on the Role of Cyclopentadienyl Ligands in the Discovery of Molecular Complexes of the Rare-Earth and Actinide Metals in New Oxidation States. *Organometallics* **2016**, *35* (18), 3088–3100.

(2) Windorff, C. J.; Dumas, M. T.; Ziller, J. W.; Gaunt, A. J.; Kozimor, S. A.; Evans, W. J. Small-Scale Metal-Based Syntheses of Lanthanide Iodide, Amide, and Cyclopentadienyl Complexes as Analogues for Transuranic Reactions. *Inorg Chem* **2017**, *56* (19), 11981–11989.

(3) Evans, W. J.; Davis, B. L. Chemistry of Tris(Pentamethylcyclopentadienyl) f-Element Complexes, $(C_5Me_5)_3M$. *Chem Rev* **2002**, *102* (6), 2119–2136.

(4) Huh, D. N.; Ziller, J. W.; Evans, W. J. Isolation of Reactive Ln(II) Complexes with C5H4Me Ligands (CpMe) Using Inverse Sandwich Countercations: Synthesis and Structure of [(18-Crown-6)K(μ-CpMe)K(18-Crown-6)][$CpMe_3$L(II)] (Ln = Tb, Ho). *Dalton Transactions* **2018**, *47* (48), 17285–17290.

(5) Cassani, M. C.; Duncalf, D. J.; Lappert, M. F. The First Example of a Crystalline Subvalent Organolanthanum Complex: [K([18]Crown-6)- $(\eta_2\text{-}C_6H_6)_2$][$(LaCp^{tt}_2)_2(\mu\text{-}\eta_6\text{:}\eta_6\text{-}C_6H_6)$] · $2C_6H_6$ (Cp^{tt} =η_5-$C_5H_3Bu^t_2$-1,3). *J Am Chem Soc* **1998**, *120* (49), 12958–12959.

(6) Hitchcock, P. B.; Lappert, M. F.; Maron, L.; Protchenko, A. V. Lanthanum Does Form Stable Molecular Compounds in the +2 Oxidation State. *Angewandte Chemie International Edition* **2008**, *47* (8), 1488–1491.

(7) Santini, C.; Marinelli, M.; Pellei, M. Boron-Centered Scorpionate-Type NHC-Based Ligands and Their Metal Complexes. *Eur J Inorg Chem* **2016**, *2016* (15–16), 2312–2331.

(8) Wang, G. C.; So, Y. M.; Wong, K. L.; Au-Yeung, K. C.; Sung, H. H. Y.; Williams, I. D.; Leung, W. H. Synthesis, Structure, and Reactivity of a Tetranuclear Cerium(IV) Oxo Cluster Supported by the Kläui Tripodal Ligand $[Co(\eta^5\text{-}C_5H_5)\{P(O)(OEt)_2\}_3]^-$. *Chemistry - A European Journal* **2015**, *21* (45), 16126–16135.

(9) Al-Harbi, A.; Sattler, W.; Sattler, A.; Parkin, G. Synthesis and Structural Characterization of Tris(2-Oxo-1-Tert-Butylimidazolyl) and Tris(2-Oxo-1-Methylbenzimidazolyl)Hydroborato Complexes: A New Class of Tripodal Oxygen Donor Ligand. *Chemical Communications* **2011**, *47* (11), 3123–3125.

(10) Tricoire, M.; Hsueh, F. C.; Keener, M.; Rajeshkumar, T.; Scopelliti, R.; Zivkovic, I.; Maron, L.; Mazzanti, M. Siloxide Tripodal Ligands as a Scaffold for Stabilizing Lanthanides in the +4 Oxidation State. *Chem Sci* **2024**, *15* (18), 6874–6883.

(11) Al-Harbi, A.; Kriegel, B.; Gulati, S.; Hammond, M. J.; Parkin, G. Bis- and Tris(2-Oxobenzimidazolyl)Hydroborato Complexes of Sodium and Thallium: New Classes of Bidentate and Tridentate Oxygen Donor Ligands. *Inorg Chem* **2017**, *56* (24), 15271–15284.

(12) Vostrikova, K. E. The Tripodal Ligand's 4f Complexes: Use in Molecular Magnetism. *Inorganics (Basel)* **2023**, *11* (7), 307.

(13) Rieser, T. E.; Schädle, D.; Maichle-Mössmer, C.; Anwander, R. Terminal Dysprosium and Holmium Organoimides. *Chem Sci* **2024**, *15* (10), 3562–3570.

(14) Matveeva, A. G.; Kudryavtsev, I. Y.; Pasechnik, M. P.; Vologzhanina, A. V.; Baulina, T. V.; Vavina, A. V.; Sukat, G. Y.; Matveev, S. V.; Godovikov, I. A.; Turanov, A. N.; Karandashev, V. K.; Brel, V. K. Coordination and Extraction of Lanthanides(III) with Tripodal Ligands on the Triphenylphosphine Oxide Platform: Effect of Uncoordinating Substituents. *Polyhedron* **2018**, *142*, 71–82.

(15) Momin, A.; Carter, L.; Yang, Y.; McDonald, R.; Essafi, S.; Nief, F.; Del Rosal, I.; Sella, A.; Maron, L.; Takats, J. To Bend or Not to Bend: Experimental and Computational Studies of Structural Preference in $Ln(Tp^{i}Pr_2)_2$ (Ln = Sm, Tm). *Inorg Chem* **2014**, *53* (22), 12066–12075.

(16) Thalangamaarachchige, V. D.; Unruh, D. K.; Cordes, D. B.; Krempner, C. Synthesis, Structure, and Reactivity of Zwitterionic Divalent Rare-Earth Metal Silanides. *Inorg Chem* **2015**, *54* (9), 4189–4191.

(17) Andrez, J.; Bozoklu, G.; Nocton, G.; Pécaut, J.; Scopelliti, R.; Dubois, L.; Mazzanti, M. Lanthanide(II) Complexes Supported by N,O-Donor Tripodal Ligands: Synthesis, Structure, and

Ligand-Dependent Redox Behavior. *Chemistry - A European Journal* **2015**, *21* (43), 15188–15200.

(18) Reichart, F.; Kischel, M.; Zeckert, K. Lanthanide(II) Complexes of a Dual Functional Tris(2-Pyridyl)Stannate Derivative. *Chemistry - A European Journal* **2009**, *15* (39), 10018–10020.

(19) Morissette, M.; Haufe, S.; McDonald, R.; Ferrence, G. M.; Takats, J. Steric Saturation of the Ytterbium Coordination Environment: (Tp^{t}Bu, Me)Yb(OMes), a Four Coordinate, Monomeric, Base-Free Divalent Lanthanide Complex, Its Solvation with Tetrahydrofuran, and Comparison to the β-Diketonate Complex, (TptBu, Me)Yb(Dpm). *Polyhedron* **2004**, *23* (2–3), 263–271.

(20) Mikhalyova, E. A.; Yakovenko, A. V.; Zeller, M.; Gavrilenko, K. S.; Kiskin, M. A.; Smola, S. S.; Dotsenko, V. P.; Eremenko, I. L.; Addison, A. W.; Pavlishchuk, V. V. Crystal Structures and Intense Luminescence of Tris(3-(2′-Pyridyl)-Pyrazolyl)Borate Tb^{3+} and Eu^{3+} Complexes with Carboxylate Co-Ligands. *Dalton Transactions* **2017**, *46* (11), 3457–3469.

(21) Amoroso, A. J.; Thompson, A. M. C.; Jeffery, J. C.; Jones, P. L.; Mccleverty, J. A.; Ward, M. D. Synthesis of the New Tripodal Ligand Tris-[3-(2'-Pyridyl)Pyrazol-1-Yl]Hydroborate, and the Crystal Structure of Its Europium(III) Complex. *Journal of the Chemical Society, Communications* **1994**, 2751–2752.

(22) Rheingold, A. L.; Incarvito, C. D.; Trofimenko, S. Hydrotris[3-(Carboxypyrrolidido)Pyrazol-1-yl]Borate, the First Proven N_3)(O_3-Hexadentate Homoscorpionate Ligand. *Journal of the Chemical Society, Dalton Transactions* **2000**, No. 8, 1233–1234.

(23) Sun, C.-D.; Wong, W. T. Heteroleptic Polypyrazolylborate Complexes of the Lanthanides: Syntheses and Molecular Structures of [Nd{$HB(Pz)_3$}$_2$Cl(H_2O)] ($HB(Pz)_3$ = Hydrotris (Pyrazol-1-Yl)Borate) and [Nd{$HB(Pz^*)_3$}LCl_2] (HB (Pz^*)$_3$ = Hydrotris (3,5-Dimethylpyrazol-1-Yl) Borate; L = 4,4'-Di-Tert-Butyl-2,2'-Bipyridine). *Inorganica Chim Acta* **1997**, *255*, 355–360.

(24) Muñoz-Molina, J. M.; Belderrain, T. R.; Pérez, P. J. Trispyrazolylborate Coinage Metals Complexes: Structural Features and Catalytic Transformations. *Coord Chem Rev* **2019**, *390*, 171–189.

(25) Anderson-Sanchez, L. M.; Ziller, J. W.; Evans, W. J. Synthesis of *Bis*-(2,6-Diadamantyl Aryloxide) Ln(II) Complexes of Samarium, Europium, and Ytterbium and Their Ln(III) Precursors. *Inorg Chem* **2024**, *63* (45), 21416–21422.

(26) Anderson-Sanchez, L. M.; Yu, J. M.; Ziller, J. W.; Furche, F.; Evans, W. J. Room-Temperature Stable Ln(II) Complexes Supported by 2,6-Diadamantyl Aryloxide Ligands. *Inorg Chem* **2023**, *62* (2), 706–714.

(27) Macdonald, M. R.; Bates, J. E.; Ziller, J. W.; Furche, F.; Evans, W. J. Completing the Series of +2 Ions for the Lanthanide Elements: Synthesis of Molecular Complexes of Pr^{2+}, Gd^{2+}, Tb^{2+}, and Lu^{2+}. *J Am Chem Soc* **2013**, *135* (26), 9857–9868.

(28) Quast, H.; Nahr, U. Photochemische Stickstoff-Eliminierung Aus 1-(1-Alkenyl)-4-tert-butyl-1,4-dihydro-5H-tetrazol-5-onen. Konkurrenz Zwischen Methanol-Addition Und Cyclisierung Einer Dipolaren Zwischenstufe. *Chem Ber* **1984**, *117* (8), 2761–2778.

(29) Guzei, I. A.; Wendt, M. An Improved Method for the Computation of Ligand Steric Effects Based on Solid Angles. *Dalton Transactions* **2006**, No. 33, 3991–3999.

(30) Evans, W. J.; Johnston, M. A.; Greci, M. A.; Gummersheimer, T. S.; Ziller, J. W. Divalent Lanthanide Complexes Free of Coordinating Anions: Facile Synthesis of Fully Solvated Dicationic $[LnL_x]_2^-$ Compounds. *Polyhedron* **2003**, *3*, 119–126.

(31) Queen, J. D.; Rajabi, A.; Ziller, J. W.; Furche, F.; Evans, W. J. Redox Studies of the Scandium Metallocene $(C_5H_2TBu_3)_2Sc^{II}$ Lead to a Terminal Side-On $(N{=}N)^{2-}$ Complex: $[(C_5H_2TBu_3)_2Sc^{II}I(H_2\text{-}H_2)]$-. *J Am Chem Soc* **2025**.

(32) Queen, J. D.; Anderson-Sanchez, L. M.; Stennett, C. R.; Rajabi, A.; Ziller, J. W.; Furche, F.; Evans, W. J. Synthesis of Crystallographically Characterizable Bis(Cyclopentadienyl) Sc(II) Complexes: $(C_5H_2TBu_3)_2Sc$ and $\{[C_5H_3(SiMe_3)_2]_2ScI\}^{1-}$. *J Am Chem Soc* **2024**, *146* (5), 3279–3292.

(33) Moehring, S. A.; Miehlich, M.; Hoerger, C. J.; Meyer, K.; Ziller, J. W.; Evans, W. J. A Room-Temperature Stable Y(II) Aryloxide: Using Steric Saturation to Kinetically Stabilize Y(II) Complexes. *Inorg Chem* **2020**, *59* (5), 3207–3214.

(34) Girard, P.; Namy, J. L.; Kagan, H. B. Divalent Lanthanide Derivatives in Organic Synthesis: Mild Preparation of SmI_2 and YbI_2 and Their Use as Reducing or Coupling Agents. *J Am Chem Soc* **1980**, *102* (8), 2693–2698.

–Appendix A–

Synthesis of $Bi(OBMes_2)_3$

INTRODUCTION

As discussed in Chapters 3 and 4, the di(mesityl)boroxide $(OBMes)^{1-}$ ligand has been explored with many transition metals and group 1 and 2 metals,[1,2] group 1 and 2 metals[3,4] and some f-block elements,[5–7] In Chapters 3 and 4, specifically, it was coordinated to the lanthanide metals in the attempt to reduce them to the Ln(II) oxidation state, or oxidize them to the Ln(IV) oxidation state. However, of the main group metals, only the crystal structures of di(aryl)boroxides bound to Al,[8–10] Ga,[11] and Pb[12] have been reported. The chemistry of the heavy main group metal, bismuth, has seen promising advancements in redox and catalytic reactions,[13–19] but its compatibility with the di(mesityl)boroxide ligand has yet examined. Reported here is the synthesis and characterization of the homoleptic, monometallic complex $Bi(OBMes_2)_3$.

RESULTS AND DISCUSSION

A colorless slurry of $Bi(OBMes)_2$ in THF was treated with three equiv of a clear, colorless solution of $KOBMes_2$ in THF. This was allowed to stir for 18 h, resulting in a colorless mixture, eq A.1. Subsequent workup in hexane and hot toluene resulted in the formation of large, colorless, hexagonal and triangular crystals of $Bi(OBMes_2)_3$, **A.1** upon removal of solvent under reduced pressure, Figure A.1.

$$BiCl_3 + 3\ KOBMes_2 \xrightarrow[-3\ KCl]{THF,\ rt,\ 18\ h} \textbf{A.1} \qquad \text{(A.1)}$$

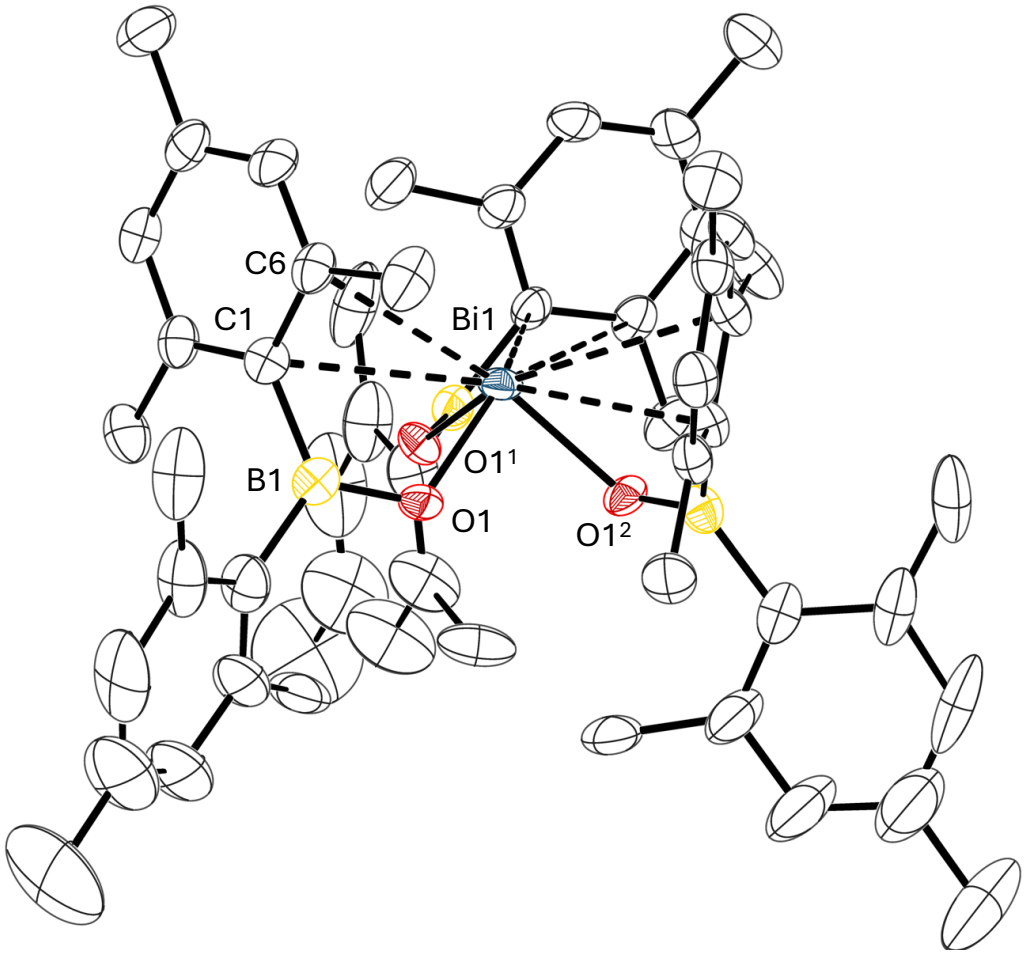

Figure A.1. Graphical representation of $Bi(OBMes_2)_3$, **A.1**, with thermal ellipsoids drawn at the 50% probability level. Hydrogen atoms and one disordered toluene molecule are not shown for clarity.

Complex **A.1** crystallizes in the *R*3 space group with one disordered THF molecule in the crystal lattice and the Bi1 atom located on an inversion plane. The Bi–O bond length of 2.102(5) is ca. 0.1-0.05 Å longer than other monomolecular Bi(III) tris(alkoxide) and tris(siloxide) compounds, table **A.1**.[20–24] This could be due to the weaker electron donation of the boroxide ligand to the Bi(III) metal center.[2,4,25]

Table A.1. Selected Average Bond Distances (Å) and angles [°] of Complex **A.1** and Similar Complexes in Literature

Compound	Bi–O avg (Å)	O–Bi–O avg [°]	Bi–O–R avg [°]

$Bi(OBMes_2)_3$, **A.1**	2.102(5)	89.3(2)	119.6(5)
$Bi(OCPh_3)_3$[20]	2.076(3)	86.5(9)	124.2(2)
$Bi(OC^iPr_3)_3$[21]	2.054(2)	92.4(6)	132.5(1)
$Bi(OC^tBu_3)_3$[21]	2.059(1)	89.6(1)	120.6(5)
$Bi(OSi^iPr_3)_3$[22]	2.012(2)	93.0(8)	154.1(1)
$Bi(OSiMe_2{}^tBu)_3$[24]	2.055(2)	92.5(7)	142.2(3)
$Bi(OSiPh_2{}^tBu)_3$[23]	2.033(5)	96.7(2)	142.4(1)
Average	2.055(5)	89.9(1)	139.1(6)

The near 90° O–Bi–O angle in **A.1** of 89.3(2)° is typical of complexes of this class of compound, Table A.1. It is likely due Bi–O bonding of the 6p orbitals on Bi combined with the presence of an unhybridized and nonbonding 6s orbital, an effect of orbital "dehybridization" that occurs in the heavier p-block elements.[20,26] The Bi–O–R (R = ipso atom) angle of 119.6(5)° is the widest of the monometallic Bi tris(alkoxide) and tris(aryloxide) compounds with crystallographic data available for comparison in the Cambridge Crystal Data Centre (CCDC). This said, the wide Bi–O–R angle range of ca. 36.9° is further evidence that typical binding angles of this type vary widely. In complex **A.1**, the Bi–O–B angle is determined by the large mesityl substituents bound to the boron atom. This is shown by the orientation of these substituents in parallel to one another and canted at a Bi1–O1–B1–C1 torsion angle of 165.2(4)° to accommodate for the steric bulk of the mesityl groups, ultimately resulting a complex with C_{3V} symmetry.

On each di(mesityl)boroxide ligand, one mesityl group is oriented away from the boron and the other is oriented toward it. A similar orientation of aryl rings is found in the compound closest in morphology to **A.1**, $Bi(OCPh_3)_3$,[20] synthesized by Hana et. al. The close proximity of these aryl substituents to the Bi(III) core and the absence of dimerization of these complexes is explained by short Bi–C_{ipso} interactions in a range of 3.052 to 3.179 Å, which are shorter than the

Bi–C_{aryl} 4.0 Å Van der Waals radius (the smallest distance between two atoms that are not bound together).[20,27] Although Bi–arene interactions are rather rare,[20,23,28,29] the shortest metal-carbon Bi1–C1 and Bi1–C6 distances of 3.171(8) and 3.340(8) respectively in complex **A.1** are also below the 4.0Å threshold, and are likely participating in metal-arene interactions as well.

CONCLUSION

Described here is the facile synthesis of $Bi(OBMes_2)_3$, **A.1**. **A.1** is a rare example of a monomeric Bi(III) which shows probable Bi–C_{arene} interactions, as the distances of these rings fall below the 4.0 Å threshold of Van der Waals radii.[26,27] This suggests that the steric bulk of these ligands may help to maintain the monomeric nature of the complex in the solid state.[20]

EXPERIMENTAL DETAILS

All manipulations and syntheses described below were conducted with the rigorous exclusion of air and water using standard Schlenk line and glovebox techniques under an argon or dinitrogen atmosphere. Solvents were sparged with UHP argon and dried by passage through columns containing Q-5 and molecular sieves prior to use. Deuterated NMR solvents were dried over NaK alloy, degassed by three freeze-pump-thaw cycles, and vacuum transferred before use. ^{1}H, NMR spectra were recorded on Bruker an AVANCE600 MHz spectrometers at 298 K unless otherwise stated and referenced internally to residual protio-solvent resonances. ^{11}B NMR are not reported, as the resonances of the ^{11}B nuclei in the lanthanide complexes could not be differentiated from ligand resonances. $KOB(C_6H_2Me_3\text{-}2,4,6)_2$ ($KOBMes_2$) was synthesized in accordance with the process described in chapter 3. $[CsOBMes_2]_5(THF)_4$ was synthesized by treatment of $HOBMes_2$ with one equiv Cs metal in THF, followed by washing with hexane. $HOBMes_2$ was purchased from The Synnovator or synthesized via literature preparations.[4] KH in mineral oil (30%) was purchased from Sigma Aldrich and thoroughly rinsed with hexane before use. Cs was

purchased from Sigma Aldrich and used without further purification. $BiCl_3$ was purchased from Fischer Scientific and used without purification.

$Bi(OBMes_2)_3$, A.1. To a colorless slurry of $BiCl_3$ (0.174 g, 0.552 mmol) in ca. 30 mL THF, three equiv $KOBMes_2$ (0.495 g, 1.63 mmol) was added and stirred for 18 h. Solvent was removed under reduced pressure and ca. 60 mL of hexane was added to the resulting colorless solids. This was heated to near boiling while stirring and created a hazy colorless slurry. The slurry was centrifuged and the clear, colorless supernatant was decanted. The solvent of the supernatant was removed under reduced pressure and treated with ca. 10 mL toluene, precipitating a white powder. This colorless mixture was centrifuged once more and the colorless supernatant was decanted away from the white powder. Upon removing solvent under reduced pressure, colorless triangular prismatic crystals of $Bi(OBMes_2)_3$ formed (0.256g, 0.255 mmol, 47% yield). ^{1}H NMR (600 MHz, C_6D_6) δ 6.68 (12 H, s, Ar-*H*), 2.30 (36 H, s, o-*Me*), 2.12 (18 H, s, p-*Me*).

CRYSTALLOGRAPHIC INFORMATION

X-ray Data Collection, Structure Solution and Refinement for $Bi(OBMes_2)_3$•(THF), **A.1**.

A colorless crystal of approximate dimensions 0.144 x 0.299 x 0.325 mm was mounted in a cryoloop and transferred to a Bruker SMART APEX II diffractometer system. The APEX2[30] program package was used to determine the unit-cell parameters and for data collection (60 sec/frame scan time). The raw frame data was processed using SAINT[31] and SADABS[32] to yield the reflection data file. Subsequent calculations were carried out using the SHELXTL[33] program

package. The systematic absences were consistent with the hexagonal space groups *R*3 and $R\bar{3}$. The noncentrosymmetric space group *R*3 was assigned and later determined to be correct.

The structure was solved by direct methods and refined on F^2 by full-matrix least-squares techniques. The analytical scattering factors[34] for neutral atoms were used throughout the analysis. Hydrogen atoms were included using a riding model. The molecule was located on a three-fold rotation axis.

Least-squares analysis yielded wR2 = 0.0708 and Goof = 1.102 for 191 variables refined against 5153 data (0.72 Å), R1 = 0.0311 for those 5128 data with $I > 2.0\sigma(I)$. The structure was refined as a two-component inversion twin (BASF = 0.086(11).

There were high residuals present in the final difference-Fourier map consistent with a disordered tetrahydrofuran solvent. Refinement of the solvent was unsatisfactory. The SQUEEZE[35] routine in the PLATON[35] program package was used to account for the electrons in the solvent accessible voids.

Table A.2 Crystal data and structure refinement for kgb70.	
Identification code	kgb70
Empirical formula	$C_{58}H_{74}B_3O_4Bi$
Formula weight	1076.58
Temperature/K	93(2)

Crystal system	trigonal
Space group	R3
a/Å	11.833(2)
b/Å	11.833(2)
c/Å	34.075(10)
α/°	90
β/°	90
γ/°	120
Volume/Å^3	4132(2)
Z	3
ρ_{calc}g/cm^3	1.298
μ/mm^{-1}	3.243
F(000)	1656.0
Crystal size/mm^3	0.325 × 0.299 × 0.144
Radiation	MoKα (λ = 0.71073)
2Θ range for data collection/°	3.586 to 59.37
Index ranges	-16 ≤ h ≤ 16, -16 ≤ k ≤ 16, -47 ≤ l ≤ 47
Reflections collected	28123
Independent reflections	5153 [R_{int} = 0.0482, R_{sigma} = 0.0386]
Data/restraints/parameters	5153/1/191
Goodness-of-fit on F^2	1.102

Final R indexes [I>=2σ (I)]	R_1 = 0.0311, wR_2 = 0.0705
Final R indexes [all data]	R_1 = 0.0316, wR_2 = 0.0708
Largest diff. peak/hole / e Å^{-3}	1.42/-1.55
Flack parameter	0.086(11)

(1) Weese, K. J.; Bartlett, R. A.; Murray, B. D.; Olmstead, M. M.; Power, P. R. Synthesis and Spectroscopic and Structural Characterization of Derivatives of the Quasi-Alkoxide Ligand $[OBMes_2]^-$ (Mes = 2,4,6-$Me_3C_6H_2$). *Inorganic Chemistry* **1987**, *26* (15), 2409–2413.

(2) Cole, S. C.; Coles, M. P.; Hitchcock, P. B. Boroxide Complexes of the Group 4 Metals: A "Noninnocent" Ligand in Olefin Polymerization. *Ogranometallics* **2005**, *24* (13), 3279–3289.

(3) Cole, S. C.; Coles, M. P.; Hitchcock, P. B. Sodium Boroxide Containing an Unusual Na_4O_4 Ladder Core. *Inorganic Chemistry Communications* **2010**, *13* (10), 1163–1165.

(4) Le Coz, E.; Hammoud, J.; Roisnel, T.; Cordier, M.; Dorcet, V.; Kahlal, S.; Carpentier, J. F.; Saillard, J. Y.; Sarazin, Y. Bonding in Barium Boryloxides, Siloxides, Phenoxides and Silazides: A Comparison with the Lighter Alkaline Earths. *Chemistry - A European Journal* **2021**, *27* (46), 11966–11982.

(5) Arnold, P. L.; Puig-Urrea, L.; Wells, J. A. L.; Yuan, D.; Cruickshank, F. L.; Young, R. D. Applications of Boroxide Ligands in Supporting Small Molecule Activation by U(III) and U(IV) Complexes. *Dalton Transactions* **2019**, *48* (15), 4894–4905.

(6) Yan, H.; Wu, B.; Zhao, X. K.; Yu, C.; Wei, J.; Hu, H. S.; Zhang, W. X.; Xi, Z. Rare-Earth Metal Boroxide with Formal Triple Metal–Oxygen Orbital Interaction: Synthesis from

B(C₆F_5)$_3$·H₂O and Radical-Anion Ligated Rare-Earth Metal Amides. *CCS Chemistry* **2021**, *3* (11), 2772–2781.

(7) Arnold, P. L.; Halliday, C. J. V.; Puig-Urrea, L.; Nichol, G. S. Instantaneous and Phosphine-Catalyzed Arene Binding and Reduction by U(III) Complexes. *Inorganic Chemistry* **2021**, *60* (6), 4162–4170.

(8) Anulewicz-Ostrowska, R.; Luliński, S.; Serwatowski, J.; Suwińska, K. Diverse Reactivity of Dialkylaluminum Dimesitylboryloxides [(μ-Mes_2BO)AlR_2]$_2$. Synthetic and Structural Study. *Inorganic Chemistry* **2000**, *39* (25), 5763–5767.

(9) Gibson, V. C.; Mastroianni, S.; White, A. J. P.; Williams, D. J. Formation and Unexpected Catalytic Reactivity of Organoaluminum Boryloxides. *Inorganic Chemistry* **2001**, *40* (5), 826–827.

(10) Kurumada, S.; Yamashita, M. A Tetraorganyl-Alumaborane with An Al-B σ-Bond and Two Adjacent Lewis-Acidic Centers. *Journal of the American Chemical Society* **2022**, *144* (10), 4327–4332.

(11) Zheng, X.; Heilmann, A.; McManus, C.; Aldridge, S. A Xanthene-Based Mono-Anionic PON Ligand: Exploiting a Bulky, Electronically Unsymmetrical Donor in Main Group Chemistry. *Chemistry - A European Journal* **2021**, *27* (9), 3159–3165.

(12) Someşan, A. A.; Roisnel, T.; Dorcet, V.; Silvestru, C.; Sarazin, Y. Aminofluoroalkoxide Amido and Boryloxo Lead(II) Complexes. *Dalton Transactions* **2019**, *48* (27), 9944–9948.

(13) Planas, O.; Peciukenas, V.; Cornella, J. Bismuth-Catalyzed Oxidative Coupling of Arylboronic Acids with Triflate and Nonaflate Salts. *Journal of the American Chemical Society* **2020**, *142* (26), 11382–11387.

(14) Brym, M.; Jones, C.; Junk, P. C. Rare Examples of Mononuclear, Homoleptic Antimony(III) and Bismuth(III) Aryloxides. *Main Group Chemistry* **2006**, *5* (1), 13–19.

(15) Silvestru, C.; Breunig, H. J.; Althaus, H. Structural Chemistry of Bismuth Compounds. I. Organobismuth Derivatives. *Chemical Reviews* **1999**, *99* (11), 3277–3327.

(16) Hejda, M.; Jirásko, R.; Růžička, A.; Jambor, R.; Dostál, L. Probing the Limits of Oxidative Addition of C(Sp3)-X Bonds toward Selected N,C,N-Chelated Bismuth(I) Compounds. *Organometallics* **2020**, *39* (23), 4320–4328.

(17) Moon, H. W.; Cornella, J. Bismuth Redox Catalysis: An Emerging Main-Group Platform for Organic Synthesis. *ACS Catalysis*. American Chemical Society January 21, 2022, pp 1382–1393.

(18) Pang, Y.; Leutzsch, M.; Nöthling, N.; Cornella, J. Catalytic Activation of N2O at a Low-Valent Bismuth Redox Platform. *Journal of the American Chemical Society* **2020**, *142* (46), 19473–19479.

(19) Greenacre, V. K.; Levason, W.; Reid, G. Developments in the Chemistry of Stibine and Bismuthine Complexes. *Coordination Chemistry Reviews*. Elsevier B.V. April 1, 2021.

(20) Hanna, T. A.; Keitany, G.; Ibarra, C.; Sommer, R. D.; Rheingold, A. L. Synthesis and Crystal Structure of a Three-Coordinate Bismuth Alkoxide with Bismuth-β-Phenyl Secondary Interactions, $Bi(OCPh_3)3$. *Polyhedron* **2001**, *20*, 2451–2455.

(21) Hatanpää, T.; Vehkamäki, M.; Ritala, M.; Leskelä, M. Study of Bismuth Alkoxides as Possible Precursors for ALD. *Dalton Transactions* **2010**, *39* (13), 3219.

(22) Paalasmaa, S.; Mansfeld, D.; Schürmann, M.; Mehring, M. Synthesis and Characterization of Three Homoleptic Bismuth Silanolates: $[Bi(OSiR_3)_3]$ (R = Me, Et,*i*Pr). *Zeitschrift für anorganische und allgemeine Chemie* **2005**, *631* (12), 2433–2438.

(23) Mansfeld, D.; Mehring, M.; Schürmann, M. [Bi(OSi*t*BuPh$_2$)$_3$]: A Metal Silanolate with a Weak Bismuth - π Arene Interaction. *Zeitschrift für anorganische und allgemeine Chemie* **2004**, *630* (12), 1795–1797.

(24) Mansfeld, D.; Mehring, M.; Schürmann, M. From a Monomeric Bismuth Silanolate to a Molecular Bismuth Oxo Cluster: [Bi$_{22}$O$_{26}$ (OSiMe$_2$*t*Bu)$_{14}$]. *Angewandte Chemie International Edition* **2005**, *44* (2), 245–249.

(25) Coles, M. P. Metal Compounds of Boron-Substituted Alkoxide ('Boroxide') Ligands. *Coordination Chemistry Reviews* **2016**, *323*, 52–59.

(26) Pyykko, P.; Desclaux, J. P. Relativity and the Periodic System of Elements. *Accounts of Chemical Research* **1979**, *12* (8), 276–281.

(27) Mantina, M.; Chamberlin, A. C.; Valero, R.; Cramer, C. J.; Truhlar, D. G. Consistent van Der Waals Radii for the Whole Main Group. *The Journal of Physical Chemistry A* **2009**, *113* (19), 5806–5812.

(28) Evans, W. J.; Hain, J. H.; Ziller, J. W. Synthesis and First X-Ray Crystal Structure of a Bi(OR)$_3$ Complex: Tris(2,6-Dimethylphenoxo)Bismuth. *Journal of the Chemical Society, Chemical Communications* **1989**, No. 21, 1628.

(29) Massiani, M.-C.; Papiernik, R.; Hubert-Pfalzgraf, L. G.; Daran, J.-C. Molecular Precursors of Bismuth Oxides; β-Diketonates and Alkoxides. Molecular Structure of [Bi$_2$(μ^2,η^1-OC$_2$H$_4$OMe)$_4$ (η^1-OC$_2$H$_4$OMe)$_2$], And Of Bi(OSiPh$_3$)(THF)$_3$. *Polyhedron* **1991**, *10* (4/5), 437–445.

(30) APEX2, Version 2014.11-0. Bruker AXS, Inc.: Madison, WI 2014.

(31) SAINT, Version 8.34a. Bruker AXS, Inc.: Madison, WI 2013.

(32) Sheldrick, G. M. SADABS, Version 2014/5. Bruker AXS, Inc.: Madison, WI 2014.

(33) Sheldrick, G. M. SHELXTL, Version 2014/7. Bruker AXS, Inc.: Madison, WI 2014.

(34) International Tables for Crystallography. *Dordrecht: Kluwer Academic Publishers*. 1992.

(35) Spek, A. L. PLATON SQUEEZE: A Tool for the Calculation of the Disordered Solvent Contribution to the Calculated Structure Factors. *Acta Crystallographica* **2015**, *C71*, 9–19.

–Appendix B–

Some Heteroleptic Terphenlythiolate Lanthanide (III) Complexes.

INTRODUCTION

As discussed in Chapter 2, the coordination chemistry of yttrium and f-block elements using the hexaisopropylterphenyl ligands $(EAr^{iPr6})^{1-}$ (E = anionic donor atom; $Ar^{iPr6} = C_6H_3$-2,6-$(C_6H_2$-2,4,6-$^iPr)_2$) has recently expanded [1–3] from it earlier development by Power and Niemeyer.[4–11] This big, bulky ligand is an excellent scaffold for the reduction and analysis of non-traditional $4f^{n+1}$ Ln(II) ions as it offers excellent steric crowding around the metal center, and forms easily-crystallizable complexes. In Chapter 2, the $Ln^{III}(SAr^{iPr6})_2I$ (Ln = La, Nd) precursors were synthesized for reduction to the Ln(II) oxidation state and concurrent elimination of KI. However, during optimization of the synthetic techniques of the hexaisopropylterphenylthiolate complexes $Ln^{III}(SAr^{iPr6})_2I$ as precursor for $Ln^{II}(SAr^{iPr6})$ molecules,[1] various methods of salt metathesis and protonolysis syntheses were employed, eventually contributing to the necessity of donor-free LnI_3 reactants.[12] In non-optimal conditions, the use of two equiv of ligand resulted in the formation of a product with only one ligand bound to the Ln(III) metal center. For example, salt metathesis of $YI_3(THF)_{3.5}$ and two equiv $KSAr^{iPr6}$ led to the isolation of $Y(SAr^{iPr6})I_2(THF)_2$. Furthermore, when $Sm(NPh_2)_2I(THF)_2$ was synthesized for protonolysis with $HSAr^{iPr6}$, this instead led to the isolation of $Sm(SAr^{iPr6})(NPh_2)I(THF)$. To synthesize the $Ln^{III}(SAr^{iPr6})_2I$ (Ln = La, Nd),[1] the first method employed was salt metathesis via treatment of $LnI_3(THF)_{3.5}$. In the literature, analogous reactions with the thiolate and other terphenyl potassium salts with metal halide salts have shown to afford

the compounds $M^{III}(EAr^{iPr6})_2X$ and $Sm^{II}(SAr^{iPr6})_2$ with $UI_3(THF)_4$,[3] SmI_2,[6] and $LnCl_3$ (Ln = Y,[2] Pr,[8] Eu[8]), Scheme B.1.

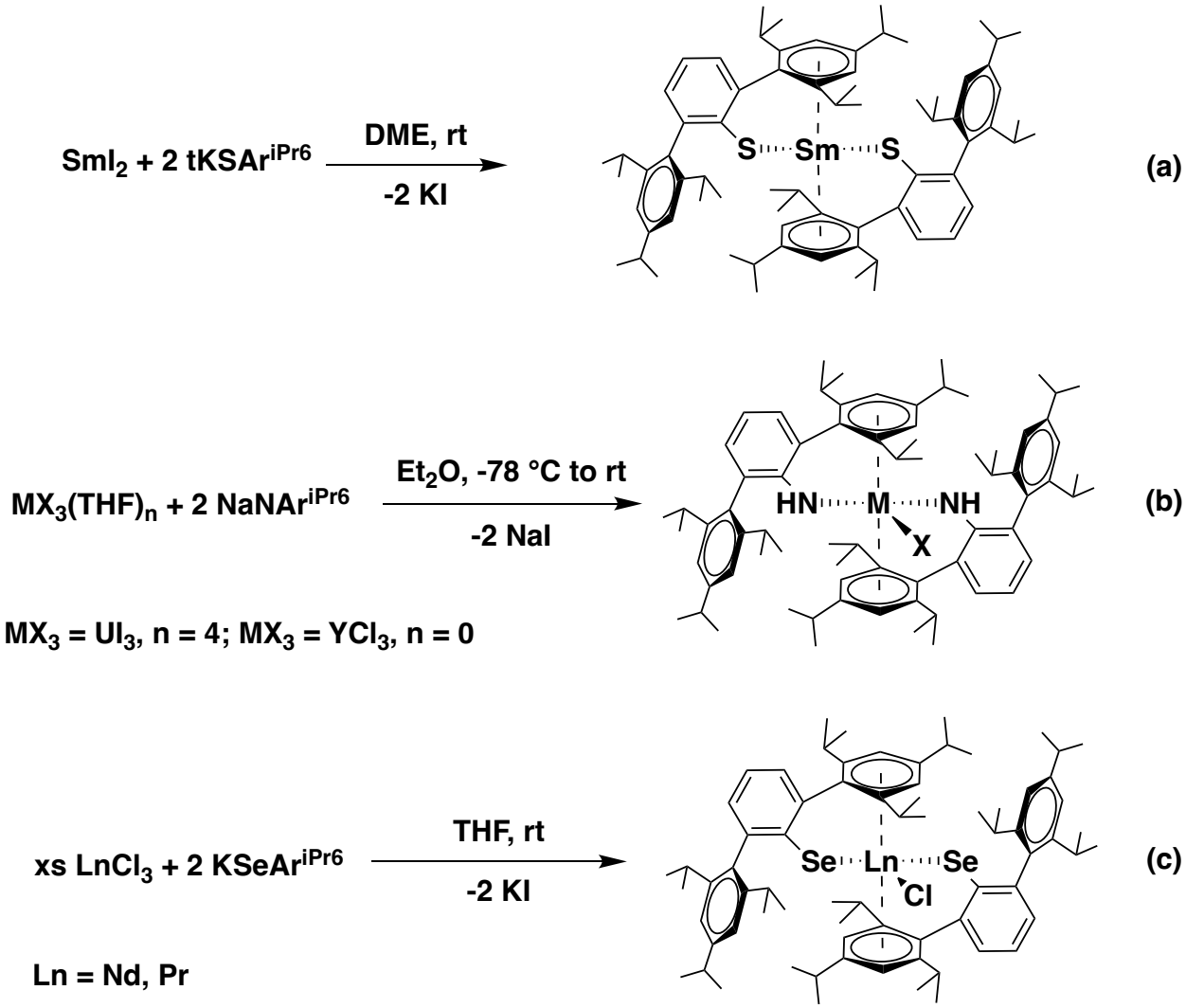

Scheme B.1. Salt metathesis reactions of crystallographically characterized compounds $Sm^{II}(SAr^{iPr6})_2$[6] (a), $M^{III}(NHAr^{iPr6})_2X$[2,3] (b), and $Ln^{III}(SeAr^{iPr6})_2Cl$.[8] (c)

RESULTS AND DISCUSSION

Synthesis of $Y(SAr^{iPr6})I_2(THF)_3$, B.1. To form a $Y^{III}(SAr^{iPr6})_2I$ precursor for reduction to $Y^{II}(SAr^{iPr6})_2$, a yellow slurry of $YI_3(THF)_{3.5}$ was treated with a colorless solution of 1.8 equiv of $KSAr^{iPr6}$ in THF. No immediate change was seen of the yellow slurry, but after stirring for 48 h,

the slurry seemed more pale yellow than before. The mixture was centrifuged and the yellow supernatant was decanted away from the colorless pellet. Solvent was removed under reduced pressure, and the resulting yellow residue was treated with ca. 1 mL toluene and placed in the freezer at −35 °C to afford small block crystals of $Y(SAr^{iPr6})I_2(THF)_3$, complex **B.1** in 31% yield, eq B.1, Figure B.1.

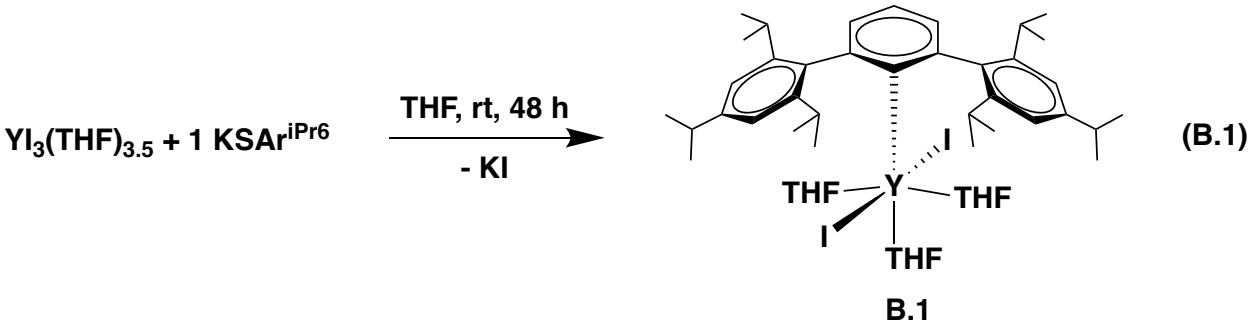

(B.1)

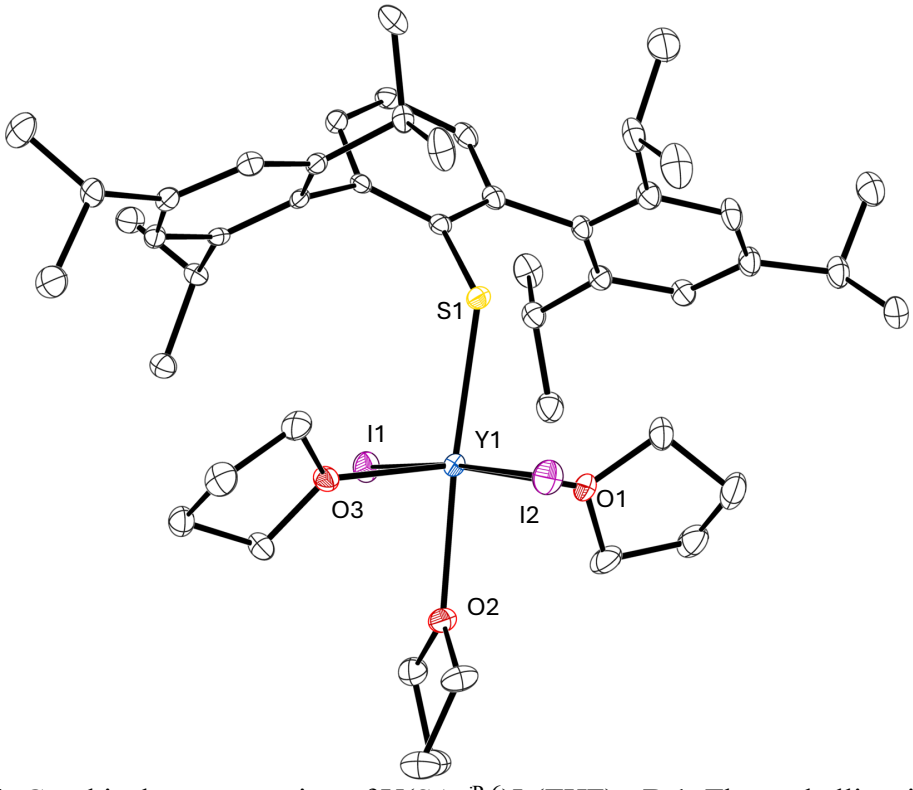

Figure B.1. Graphical representation of $Y(SAr^{iPr6})I_2(THF)_3$, **B.1.** Thermal ellipsoids are drawn at the 50% probability level and hydrogen atoms are not shown for clarity.

Complex **B.1** crystallizes in the orthorhombic space group $P2_12_12_1$ with no solvent molecules present in the lattice. In the molecular structure of **B.1,** a total of three THF molecules, two I^{1-} anions and a $(SAr^{iPr6})^{1-}$ ligand bound to the central Y(III) atom in a distorted octahedral geometry. The THF atoms are organized in a *mer* orientation at adjacent O–Y–O angles of 84.42(7) and 81.78(7)°. The O1–Y1-O3 angle is 164.80(7), which is likely less than 180° due to the bulkiness of the $(SAr^{iPr6})^{1-}$ ligand. This is also reflected in the I–Y–I angle of 175.744(1) The Y–O distances of 2.2943(2), 2.3063(2), and 2.4193(2) and the Y–I distances of 2.9469(4) and 3.0100(4) are typical of Y-O_{THF} and Y-I distances of other complexes that have three THF molecules and two I^{1-} ions bound. [13–17] It is notable that, likely due to the saturation of the coordination sphere of the metal, the arene ring of the terphenylthiolate ligand is not coordinated to the metal, such as it is in most other lanthanide terphenyl complexes. However, this monodenticity of the $(SAr^{iPr6})^{1-}$ is also seen in the other complexes $Yb^{II}(SAr^{iPr6})_2(THF)_4$[4] and $Yb^{II}(SAr^{iPr6})_2(DME)_2$[4], which all also exhibit steric crowding by neutral ligands at the metal center. Interestingly, **B.1** is isomporphous to the analogous ytterbium molecule $Yb^{III}(SAr^{iPr6})I_2(THF)_3$.[4] The compound $Yb^{III}(SAr^{iPr6})I_2(THF)_3$.however, was synthesized via oxidation of the protonolysis product $Yb^{II}(SAr^{iPr6})_2(THF)_4$ with elemental I_2. Regardless, the metrical parameters are very similar, including the Ln–S–C_{aryl} angle of 124.85(9) for **B.1** and 125.1(3) for $Yb^{III}(SAr^{iPr6})I_2(THF)_3$, Table **B.1**.

Table B.1. Select bond distances Å and angles [°]for B.1 and $Yb^{III}(SAr^{iPr6})I_2(THF)_3$			
B.1		$Yb^{III}(SAr^{iPr6})I_2(THF)_3$	
Y1-I1	2.9469(4)	Yb1-I1	2.9100(9)
Y1-I2	3.0100(4)	Yb1-I2	2.9840(1)

Y1-S1	2.6191(7)	Yb1-S1	2.581(2)
Y1-O1	2.2943(2)	Yb1-O1	2.390(6)
Y1-O2	2.4193(2)	Yb1-O2	2.270(6)
Y1-O3	2.3063(2)	Yb1-O3	2.275(6)
I1-Y1-I2	175.744(1)	I1-Yb-I2	176.74(3)
S1-Y1-I1	97.435(2)	S1-Yb-I1	96.81(6)
S1-Y1-I2	86.819(2)	S2-Yb-I2	86.45(6)
O1-Y1-I1	93.19(5)	O1-Yb-I1	86.75(2)
O1-Y1-I2	86.46(5)	O1-Yb-I2	89.99(2)
O1-Y1-S1	92.67(5)	O1-Yb-S	175.86(2)
O1-Y1-O2	84.42(7)	O2-Yb-I1	93.64(2)
O1-Y1-O3	164.80(7)	O2-Yb-I2	86.19(2)
O2-Y1-I1	85.73(5)	O2-Yb-S1	93.74(2)
O2-Y1-I2	90.01(5)	O2-Yb-O2	83.9(2)
O2-Y1-S1	175.83(5)	O2-Yb-O3	164.5(2)
O3-Y1-I1	92.11(5)	O3-Yb-I1	91.90(2)
O3-Y1-I2	87.21(5)	O3-Yb-I2	87.46(2)
O3-Y1-S1	100.76(5)	O3-Yb-S1	99.98(2)
O3-Y1-O2	81.78(7)	O3-Yb-O2	81.9(2)
C1-S1-Y1	124.85(9)	C1-S-Yb1	125.1(3)

Synthesis of $Sm(NPh_2)_2I(THF)$, B.2. Two of the previously synthesized Ln(II) terphenyl complexes in the literature were formed from protonolysis reactions of the lanthanide amides,

$Yb[NR_2]$ and $Sm[NR_2]_2(THF)_2$ (R = $SiMe_3$) to make $Yb^{II}(SAr^{iPr6})_2$ and $Sm^{II}(OAr^{iPr6})_2$ respectively. However, as the Ln(II) metals with electron configuration $4f^n5d^1$ (Ln = La, Ce, Nd, Gd, Tb, Dy, Ho, Er, Lu) amide complexes have only been found to be available as $[M(chelate)][Ln(NR_2)_3]$ (M = K, Rb; chelate = 2.2.2 cryptand, 18-c-6) and are rather thermally unstable,[18,19] these starting materials were not pursued. Alternatively, the protonolysis of previously-synthesized heteroleptic lanthanide amide complexes, $[Ln(NR_2)_2X(THF)]_2$ (X = Cl, I),[20–25] could lead to the formation of the $Ln(SAr^{iPr6})_2I$ precursors that could then be reduced to form the desired $Ln^{II}(SAr^{iPr6})_2$ complexes.[21–24] However their syntheses tended to lead to ligand redistribution to form $Ln(NR_2)_3$ compounds, and thus, a different amide ligand explored.

One such amide was $(NPh_2)^{1-}$. Previously the $(NPh_2)^{1-}$ has been used to bind to the lanthanides to make a wide variety of homo- and heteroleptic species,[26–43] however, a mononuclear $M(NPh_2)_2X$ (M = any metal, X = any halogen) complex has not been recorded in the CCDC. Reported here, is the synthesis of $Sm(NPh_2)I(THF)$, complex **B.2**.

The precursor of complex **B.2**, $KNPh_2(THF)_{1.5}$ was synthesized via treatment of crystalline, colorless $HNPh_2$ with one equiv KH in a 2:5 Et_2O to THF mixture, followed by vigorous bubbling of H_2, eq B.2. Workup in hexane afforded the brown powder, $KNPh_2(THF)_{1.5}$, verified by ^1H NMR in 85% yield, figure **B.2**, eq, B.2**.**

$$KH + HNPh_2 \xrightarrow[-\ H_2]{Et_2O,\ THF} KNPh_2(THF)_{1.5} \quad \textbf{(B.2)}$$

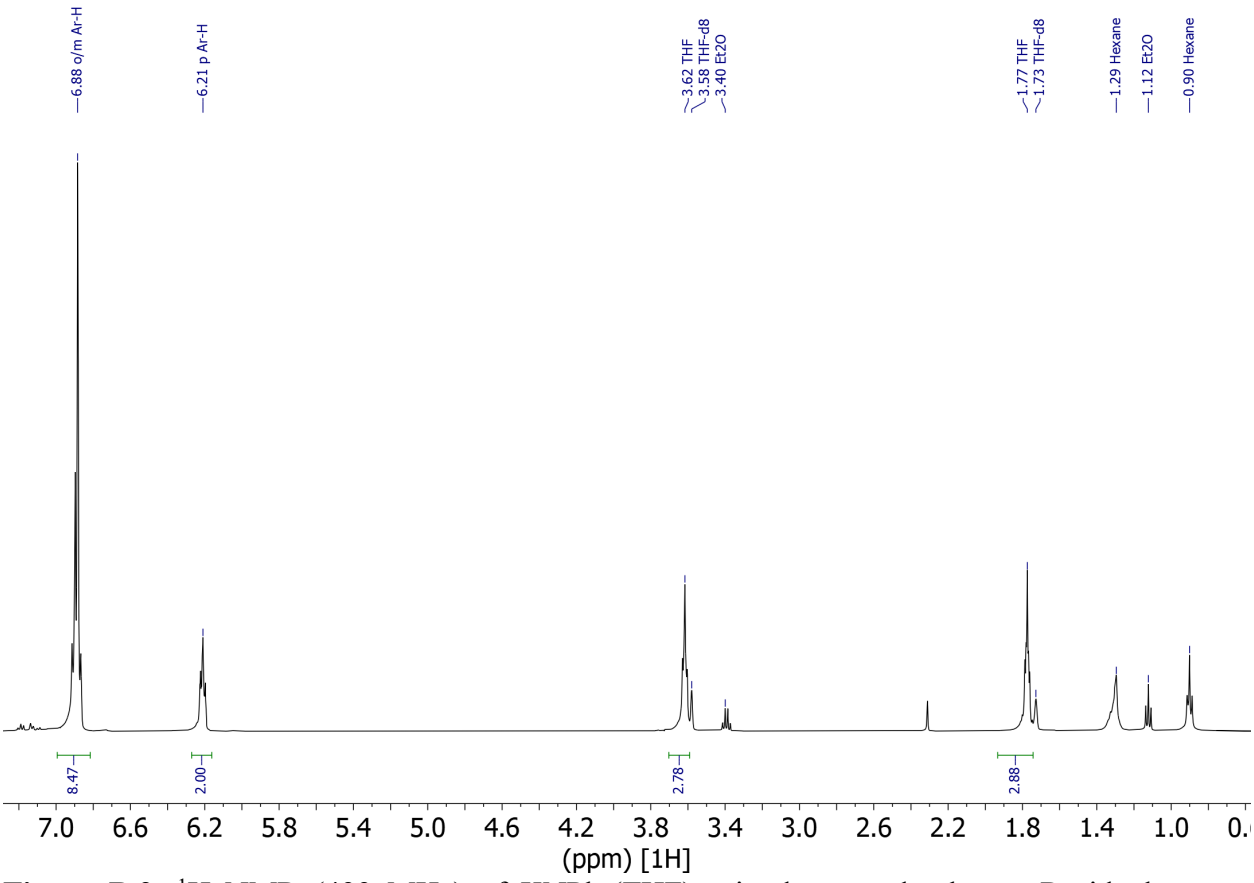

Figure B.2. ^{1}H NMR (499 MHz) of $KNPh_2(THF)_{1.5}$ in deuterated toluene. Residual proton resonances are marked at δ 3.58 and 1.75 ppm. Note: Resonances of Et_2O, toluene and hexane impurities are noted on the spectrum.

With $KNPh_2(THF)_{1.5}$ in hand the application to the lanthanide metals could be explored. To see if a lanthanide bis(amide)iodide could be formed with $(NPh_2)^{1-}$, a light yellow slurry of $SmI_3(THF)_{3.5}$ in THF was treated with $KNPh_2(THF)_{1.5}$, immediately forming an intense red color, eq B.3. After stirring for 1 h, the colorless solids were filtered away from the red supernatant, and the resulting vibrant red solution was reduced in volume under low pressure, followed by cooling to −35 °C in the freezer. This afforded a crop of large, red crystals of $Sm(NPh_2)_2I(THF)_2$, complex **B.2** in 42% yield, Figure **B.3**, eq B.3.

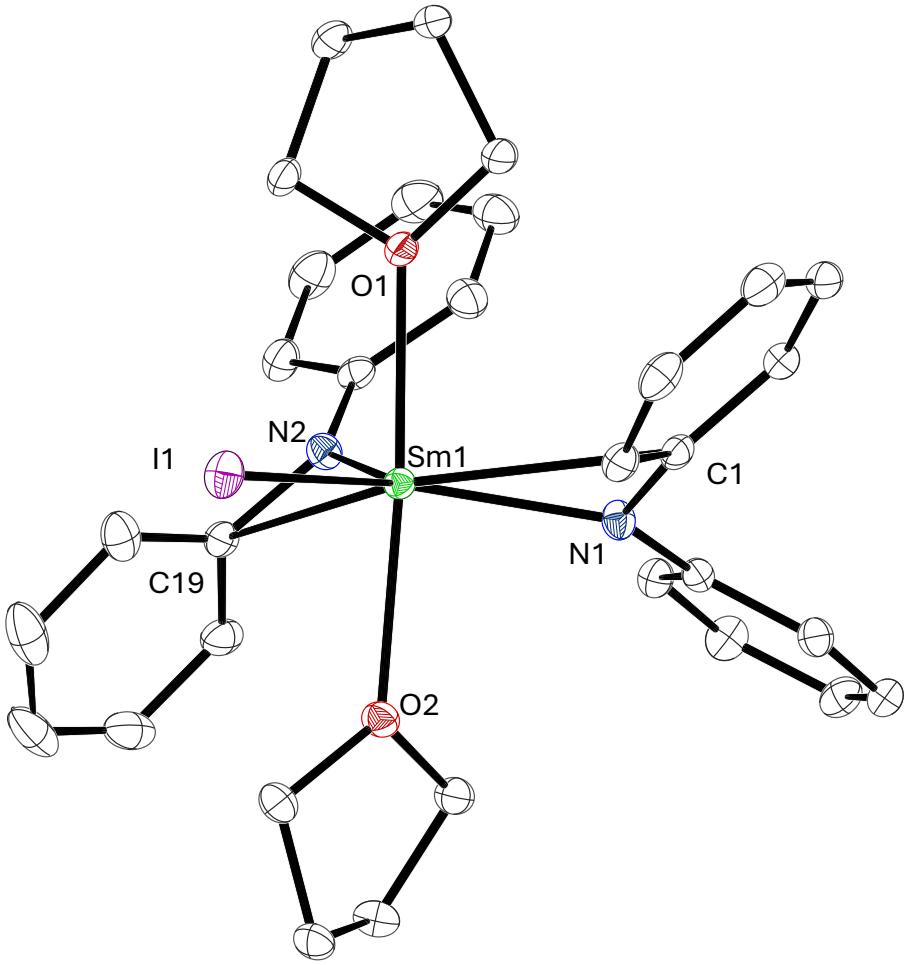

Figure B.3. Graphical representation of $Sm(NPh_2)_2I(THF)_2$, **B.2.** Thermal ellipsoids are drawn at the 50% probability level and hydrogen atoms are not shown for clarity.

$$SmI_3(THF)_{3.5} + KNPh_2(THF)_{1.5} \xrightarrow[-2\ KI]{THF,\ rt,\ 1\ h} \underset{\textbf{B.2}}{\overset{THF}{\underset{I}{Ph_2N,,,,\ Sm\ NPh_2}}\ \overset{}{THF}} \qquad \textbf{(B.3)}$$

Complex **B.2** crystallizes in the triclinic *P*-1 space group in a distorted trigonal bipyramidal geometry with a τ_5 geometry index of 0.70 (where 0 = square planar and 1 = trigonal bipyramidal).[44] The axial THF ligands are located at an O–Sm–O angle of 173.63(4)°, the equatorial N–Sm–N angle is 104.39(5)° and the N–Sm–I angles are 124.19(3)° and 131.42(3)°.

The Sm–I bond length of 3.07000(2) Å is shorter than that of the two known monomolecular complexes in which a Sm(III) atom bonds to two negatively charged nitrogen atoms, two THF molecules and one iodide ion, namely Sm(1,1′-fc(NSiMe$_2$^{t}Bu)$_2$)I(THF)$_2$ (Fc = ferrocene) (3.0763(5) Å)[45] and Sm(NR$_2$)$_2$I(THF)$_2$ (3.1011(2)),[46] but the Sm–N distances of **B.2** are longer 2.2911(1) and 2.2846(1) are longer than those of Sm(1,1′-fc(NSiMe$_2$^{t}Bu)$_2$)I(THF)$_2$, Table B2.

Table B.2. Selected Bond Lengths (Å) and angles [°] of complexes similar to B.2

B.2		Sm(1,1′-fc(NSiMe$_2$^{t}Bu)$_2$)I(THF)$_2$		Sm(NR$_2$)$_2$I(THF)$_2$	
Sm1-I1	3.07000(17)	Sm1-I1	3.0763(5)	Sm1-I1	3.10107(16)
Sm1-O1	2.3957(11)	Sm1-O1	2.460(3)	Sm1-O1	2.4213(13)
Sm1-O2	2.4190(12)	Sm1-O2	2.430(2)	Sm1-O2	2.4299(13)
Sm1-N1	2.2911(14)	Sm1-N1	2.263(3)	Sm1-N1	2.3099(15)
Sm1-N2	2.2846(14)	Sm1-N2	2.263(3)	Sm1-N2	2.2853(15)
O1-Sm1-I1	86.48(3)	O1-Sm1-I1	84.90(7)	O1-Sm1-I1	86.19(3)
O1-Sm1-O2	173.63(4)	O1-Sm1-O2	166.00(9)	O1-Sm1-O2	162.68(5)
O2-Sm1-I1	87.18(3)	O2-Sm1-O1	166.00(9)	O2-Sm1-I1	84.12(3)
N1-Sm1-I1	131.42(3)	N1-Sm1-I1	114.21(7)	N2-Sm1-I1	102.15(4)
N1-Sm1-O1	99.24(4)	N1-Sm1-O1	92.34(10)	N2-Sm1-O1	98.62(5)
N1-Sm1-O2	85.46(5)	N1-Sm1-O2	93.88(9)	N2-Sm1-O2	97.44(5)
N2-Sm1-I1	124.19(3)	N2-Sm1-I1	114.16(7)	N2-Sm1-N1	124.16(5)
N2-Sm1-O1	84.22(4)	N2-Sm1-O1	90.89(11)	N1-Sm1-I1	133.63(4)
N2-Sm1-O2	98.85(4)	N2-Sm1-O2	94.31(10)	N1-Sm1-O1	84.99(5)
N2-Sm1-N1	104.39(5)	N2-Sm1-N1	131.62(10)	N1-Sm1-O2	91.36(5)

The extension of this Sm–N bond length may be due to the rather close Sm1–C1 and Sm1–C19 proximities of distances 2.9423(16) and 2.9671(16) respectively. These interactions are evidenced by the unusual Sm1–N1–C1 angle of 102.97(10)° and Sm1–N2–C19 angle of 104.05(10)°, which are smaller than the expected 120°.

Synthesis of $Sm(NPh_2)(SAr^{iPr6})_2I(THF)$, B.3. Treatment of a dark red solution of **B.2** with two equiv $HSAr^{iPr6}$ in THF for 18h resulted in a deep red solution, eq B.4. Workup in hexane followed by crystallization at −35 °C led to small, red crystals of $Sm(NPh_2)(SAr^{iPr6})_2I(THF)$, complex **B.3**, Figure B.4.

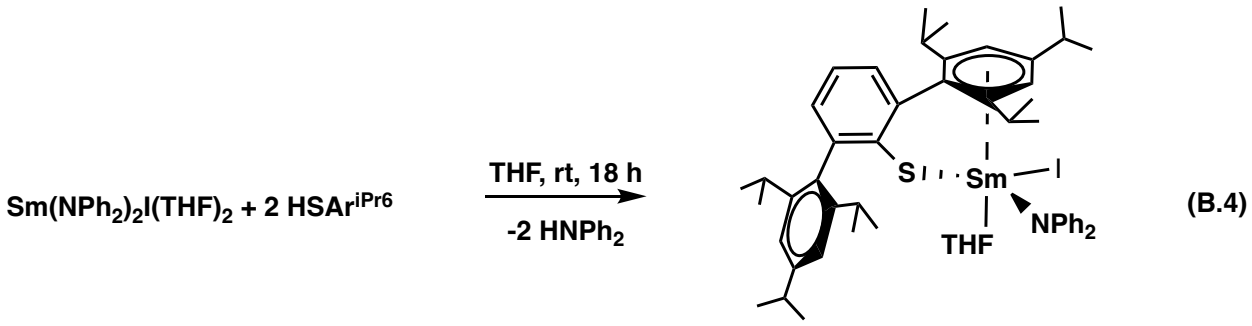

B.3

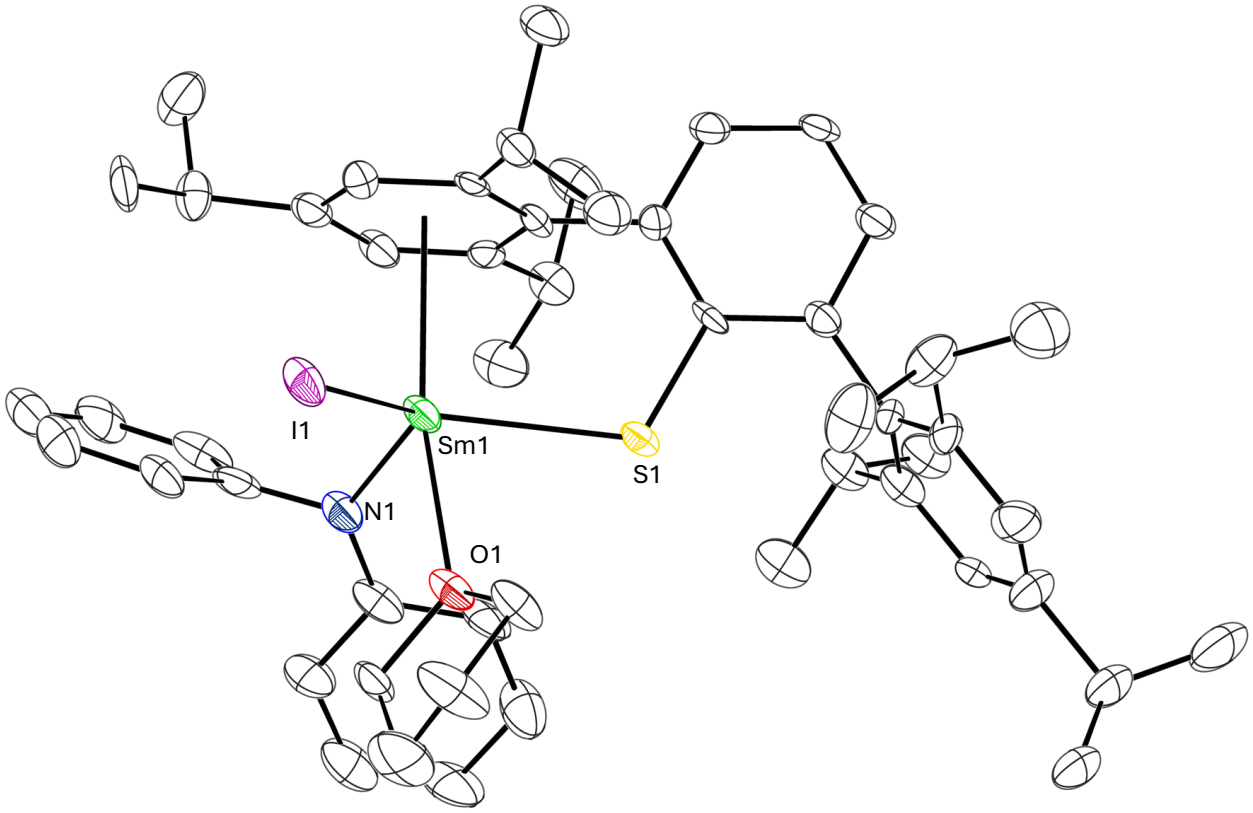

Figure B.4. Graphical representation of $Sm(NPh_2)(SAr^{iPr6})I(THF)$, **B.3.** Thermal ellipsoids are drawn at the 50% probability level and hydrogen atoms are not shown for clarity.

Complex **B.3** crystallizes in the triclinic *P*-1 space group. It contains one THF ligand, one iodide ligand and one $(SAr^{iPr6})^{1-}$ ligand bound to the central Sm(III) metal. It is also bound η^6 to one flanking aryl ring of the terphenyl ligand in a way that is typical of terphenyl coordination complexes.[1–5,7–11,47–50] The S-Sm-I, S-Sm-N and I-Sm-N angles of 120.10(4)°, 111.08(1)°, and 118.85(12)°, respectively, suggest a near-trigonal plane, similar to the S–Ln–S and S–Ln–I angles of $Ln(SAr^{iPr6})_2I$ (Ln = La, Nd) (See Chapter 2, Table 2.1). Similarly, the Sm–C_{arene} average distance of 2.969(5) Å is similar to the reported distances of 2.618 in other Sm(III) arene bonds.[51–53]

CONCLUSION

By exploring alternative syntheses to form the precursor for reduction, $Ln(SAr^{iPr6})_2I$, three new Ln(III) complexes have been crystallographically characterized. $Y(SAr^{iPr6})I_2(THF)_3$, a

compound analogous to the previously reported Yb(SAr^{iPr6})$I_2(THF)_3$,[4] **B.1** was synthesized via salt metathesis with $YI_3(THF)_{3.5}$ and $KSAr^{iPr6}$. Additionally, on the path to find alternatives to protonolysis reactions with $HSAr^{iPr6}$, the complex $Sm(NPh_2)_2I(THF)_2$, **B.2** was crystallographically characterized, showing an opportunity for silicon-free protonolysis reactions with the lanthanides. **B.2** was then treated with $HSAr^{iPr6}$ to form the complex $Sm(NPh_2)(SAr^{iPr6})I(THF)$, **B.3**, a heteroleptic Sm(III) complex that coordinates η^6 to the Sm center, highlighting the variability of binding modes that the $(SAr^{iPr6})^{1-}$ ligand can undergo.

EXPERIMENTAL DETAILS

General Considerations. All manipulations were performed by using modified Schlenk techniques or in a Vacuum/Atmospheres glovebox under argon. Solvents were degassed by sparging with dry argon before drying and collection using an S2 Grubbs-type[54] solvent purification system (JC Meyer). All physical measurements were recorded under strictly anaerobic and anhydrous conditions. Infrared spectra were recorded on compressed solid samples using an Agilent Cary 630 ATR/FTIR instrument. NMR spectra were recorded using a Bruker AVANCE 600 MHz spectrometer or a Bruker AVANCE 500 MHz spectrometer at 298 K unless otherwise stated and referenced to residual solvent signals $SmI_3(THF)_{3.5}$ and $YI_3(THF)_{3.5}$ were prepared from samarium or yttrium metal and iodine as previously described.[15] $HNPh_2$ was purchased from Sigma Aldrich and used without purification. $KSAr^{iPr6}$ was prepared by the reaction of $HSAr^{iPr6}$ with potassium metal in toluene as previously described.[7]

Synthesis of $KNPh_2(THF)_{1.5}$. A grey slurry of KH (0.224 g, 5.58 mmol) in a solution of 2 mL Et_2O and 8 mL THF was treated portionwise with light brown $HNPh_2$ (1.032g, 6.10 mmol),

immediately resulting in vigorous bubbling. The mixture was stirred for 30 min until it had turned orange and the bubbling had ceased. Solvent was removed under reduced pressure to yield orange solids of $KNPh_2(THF)_{1.5}$ (1.49 g, 4.75 mmol, 85% yield). ^{1}H NMR (499 MHz, THF) δ 6.88 (m, 8H, *o/m*-Ar-*H*), 6.21 (t, 2H, *p*-Ar-*H*), 3.62 (s, 3 H, OC*H*$_2$CH$_2$), 3.40, 1.77, 1.73 (s, 3 H, OCH$_2$C*H*$_2$), 1.29, 1.12, 0.90.

Sm(NPh$_2$)$_2$I(THF)$_2$, B.2. A yellow slurry of $SmI_3(THF)_{3.5}$ (0.508 g, 0.778 mmol) in ca. 10 mL THF was treated with powdered orange $KNPh_2(THF)_{1.5}$ (0.265 g, 0.844 mmol), immediately turning the mixture bright red. The reaction was stirred for 30 min and then stirring was turned off to allow the white powdered solids to settle to the bottom. The dark red supernatant was decanted away from the white powdered solids and filtered through a PTFE syringe filter to remove particulate solids. The solution was concentrated by solvent removal under reduced pressure to ca. 1 mL, then placed in a freezer at −35 °C for 18 h, resulting in large, bright red crystals of $Sm(NPh_2)_2I(THF)_2$, **B.2** (0.249 g, 0.329 mmol, 42% yield). ^{1}H NMR ^{1}H NMR (600 MHz, C_6D_6) δ 7.02(m, 8 H, *m*-Ar-*H*), 6.73 (m, 4 H, *p*-Ar-*H*), 6.63 (m, 8 H, *o*-Ar-*H*), 3.91(s, 8 H, OC*H*$_2$CH$_2$), 1.03 (s, 8 H, OCH$_2$C*H*$_2$).

Sm(NPh$_2$)(SAr$^{i\text{Pr}6}$)I(THF), B.3. A deep red solution of complex **B.2** (0.107 g, xx mmol) in ca. 10 mL THF was treated with white, powdered HSAr$^{i\text{Pr}6}$ (0.135g, xx mmol) and stirred for 18 h with no immediate change observed. Solvent was removed under reduced pressure to leave a purple-red residue. This residue was treated with ca. 20 mL hexane resulting in a dark purple precipitate. The mixture was then centrifuged and the deep red supernatant was decanted away from the dark purple pellet. The pellet was then dissolved in ca. 2 mL THF, filtered with a filter pipette and cooled to −35 °C to yield purple crystals of Sm(NPh$_2$)(SAr$^{i\text{Pr}6}$)I(THF), **B.3** in very low yield. The yield was too low to accurately characterize besides crystallographically.

CRYSTALLOGRAPHIC INFORMATION

X-ray Data Collection, Structure Solution and Refinement for $Y(SAr^{iPr6})I_2(THF)_3$, **B.1**.

A light brown crystal of approximate dimensions 0.304 x 0.322 x 0.354 mm was mounted on a glass fiber and transferred to a Bruker SMART APEX II diffractometer system. The APEX2[55] program package was used to determine the unit-cell parameters and for data collection (60 sec/frame scan time). The raw frame data was processed using SAINT[56] and SADABS[57] to yield the reflection data file. Subsequent calculations were carried out using the SHELXTL[58] program package. The diffraction symmetry was *mmm* and the systematic absences were consistent with the orthorhombic space group $P2_12_12_1$ that was later determined to be correct.

The structure was solved by direct methods and refined on F^2 by full-matrix least-squares techniques. The analytical scattering factors[59] for neutral atoms were used throughout the analysis. Hydrogen atoms were included using a riding model. The data were refined as an inversion twin with BASF = [-0.023(4)].

Least squares analysis yielded wR2 = 0.0508 and Goof = 0.999 for 15207 variables refined against 509 data (0.70 Å), R1 = 0.0234 for those 13608 data with $I > 2.0\sigma(I)$. The absolute structure was assigned by refinement of the Flack parameter.[60]

Table B.3 Crystal data and structure refinement for kgb43_k.	
Identification code	kgb43_k

Empirical formula	$C_{48}H_{73}I_2O_3SY$
Formula weight	1072.83
Temperature/K	93.15
Crystal system	orthorhombic
Space group	$P2_12_12_1$
a/Å	13.5168(10)
b/Å	15.8380(12)
c/Å	23.3796(18)
α/°	90
β/°	90
γ/°	90
Volume/Å^3	5005.1(7)
Z	4
ρ_{calc}g/cm^3	1.424
μ/mm^{-1}	2.476
F(000)	2184.0
Crystal size/mm^3	0.354 × 0.312 × 0.307
Radiation	MoKα (λ = 0.71073)
2Θ range for data collection/°	3.962 to 61.088
Index ranges	$-19 \leq h \leq 19$, $-22 \leq k \leq 22$, $-32 \leq l \leq 33$
Reflections collected	72943

Independent reflections	15207 [R_{int} = 0.0301, R_{sigma} = 0.0463]
Data/restraints/parameters	15207/0/509
Goodness-of-fit on F^2	0.999
Final R indexes [I>=2σ (I)]	R_1 = 0.0234, wR_2 = 0.0496
Final R indexes [all data]	R_1 = 0.0296, wR_2 = 0.0508
Largest diff. peak/hole / e $Å^{-3}$	1.28/-0.36
Flack parameter	-0.023(4)

X-ray Data Collection, Structure Solution and Refinement for $Sm(NPh_2)_2I(THF)_2$, **B.2**.

A red crystal of approximate dimensions 0.190 x 0.219 x 0.336 mm was mounted in a cryoloop and transferred to a Bruker SMART APEX II diffractometer system. The APEX2[55] program package was used to determine the unit-cell parameters and for data collection (30 sec/frame scan time). The raw frame data was processed using SAINT[56] and SADABS[57] to yield the reflection data file. Subsequent calculations were carried out using the SHELXTL[58] program package. There were no systematic absences nor any diffraction symmetry other than the Friedel condition. The centrosymmetric triclinic space group $P\bar{1}$ was assigned and later determined to be correct.

The structure was solved by direct methods and refined on F^2 by full-matrix least-squares techniques. The analytical scattering factors[59] for neutral atoms were used throughout the analysis. Hydrogen atoms were included using a riding model.

Least-squares analysis yielded wR2 = 0.0394 and Goof = 1.114 for 343 variables refined against 8957 data (0.73 Å), R1 = 0.0171 for those 8356 data with I > 2.0σ(I).

Table B.4 Crystal data and structure refinement for kgb42_k.	
Identification code	kgb42_k
Empirical formula	$C_{32}H_{36}N_2O_2ISm$
Formula weight	757.88
Temperature/K	93.15
Crystal system	triclinic
Space group	P-1
a/Å	9.8902(5)
b/Å	10.3258(5)
c/Å	15.5537(8)
α/°	107.4380(10)
β/°	98.4810(10)
γ/°	93.8810(10)
Volume/Å^3	1488.26(13)
Z	2
ρ_{calc}g/cm^3	1.691
μ/mm^{-1}	3.040
F(000)	746.0
Crystal size/mm^3	0.339 × 0.217 × 0.189

Radiation	MoKα (λ = 0.71073)
2Θ range for data collection/°	4.194 to 61.024
Index ranges	$-14 \leq h \leq 13$, $-14 \leq k \leq 14$, $-22 \leq l \leq 22$
Reflections collected	35492
Independent reflections	8957 [R_{int} = 0.0194, R_{sigma} = 0.0179]
Data/restraints/parameters	8957/0/343
Goodness-of-fit on F^2	1.113
Final R indexes [I>=2σ (I)]	R_1 = 0.0171, wR_2 = 0.0386
Final R indexes [all data]	R_1 = 0.0196, wR_2 = 0.0394
Largest diff. peak/hole / e $Å^{-3}$	0.63/-0.54

X-ray Data Collection, Structure Solution and Refinement for Sm(SAr$^{i\text{Pr}6}$)(NPh_2)I(THF), **B.3**.

A red crystal of approximate dimensions 0.078 x 0.113 x 0.141 mm was mounted in a cryoloop / on a glass fiber and transferred to a Bruker SMART APEX II diffractometer system. The APEX2[55] program package was used to determine the unit-cell parameters and for data collection (90 sec/frame scan time). The raw frame data was processed using SAINT[56] and SADABS[57] to yield the reflection data file. Subsequent calculations were carried out using the SHELXTL[58] program package. There were no systematic absences nor any diffraction symmetry other than the Friedel condition. The centrosymmetric triclinic space group $P\bar{1}$ was assigned and later determined to be correct.

The structure was solved by direct methods and refined on F^2 by full-matrix least-squares techniques. The analytical scattering factors[59] for neutral atoms were used throughout the analysis. Hydrogen atoms were included using a riding model.

Least-squares analysis yielded wR2 = 0.1647 and Goof = 0.931 for 556 variables refined against 18293 data (0.71 Å), R1 = 0.0627 for those 9192 data with $I > 2.0\sigma(I)$.

There were several high residuals present in the final difference-Fourier map. It was not possible to determine the nature of the residuals although it was probable that three hexane solvent molecules were present. The SQUEEZE[61] routine in the PLATON[61] program package was used to account for the electrons in the solvent accessible voids.

Table B.5 Crystal data and structure refinement for kgb44.	
Identification code	kgb44
Empirical formula	$C_{70}H_{108}INOSSm$
Formula weight	1288.88
Temperature/K	93.15
Crystal system	triclinic
Space group	P-1
a/Å	11.5627(15)
b/Å	14.590(2)
c/Å	19.374(3)

α/°	84.890(2)
β/°	75.895(2)
γ/°	72.267(2)
Volume/Å^3	3019.0(7)
Z	2
ρ_{calc}g/cm^3	1.418
μ/mm^{-1}	1.563
F(000)	1348.0
Crystal size/mm^3	0.152 × 0.111 × 0.09
Radiation	MoKα (λ = 0.71073)
2Θ range for data collection/°	4.336 to 61.15
Index ranges	-16 ≤ h ≤ 16, -20 ≤ k ≤ 20, -27 ≤ l ≤ 27
Reflections collected	61965
Independent reflections	18293 [R_{int} = 0.1322, R_{sigma} = 0.1724]
Data/restraints/parameters	18293/84/556
Goodness-of-fit on F^2	0.931
Final R indexes [I>=2σ (I)]	R_1 = 0.0627, wR_2 = 0.1380
Final R indexes [all data]	R_1 = 0.1448, wR_2 = 0.1647
Largest diff. peak/hole / e Å^{-3}	1.73/-1.65

REFERENCES

(1) Gilbert-Bass, K.; Stennett, C. R.; Grotjahn, R.; Ziller, J. W.; Furche, F.; Evans, W. J. Exploring Sulfur Donor Atom Coordination Chemistry with La(II), Nd(II), and Tm(II) Using a Terphenylthiolate Ligand. *Chemical Communications* **2024**, *60* (34), 4601–4604.

(2) Jena, R.; Benner, F.; Delano, F.; Holmes, D.; Mccracken, J.; Demir, S.; Odom, A. L. A Rare Isocyanide Derived from an Unprecedented Neutral Yttrium(II) Bis(Amide) Complex. *Chemical Science* **2023**, *14*, 4257–4264.

(3) Billow, B. S.; Livesay, B. N.; Mokhtarzadeh, C. C.; McCracken, J.; Shores, M. P.; Boncella, J. M.; Odom, A. L. Synthesis and Characterization of a Neutral U(II) Arene Sandwich Complex. *Journal of the American Chemical Society* **2018**, *140* (50), 17369–17373.

(4) Niemeyer, M. σ-Donor versus η^6-π-Arene Interactions in Monomeric Europium(II) and Ytterbium(II) Thiolates - An Experimental and Computational Study. *European Journal of Inorganic Chemistry* **2001**, No. 8, 1969–1981.

(5) Niemeyer, M. A Sterically Crowded Ytterbium(II) Thiolate: Trans-Bis(2,4,6,2'',4'',6''-Hexaisopropyl-1,1':3',1''-Terphenyl-2'-Thiolato-S)Tetrakis(Tetrahydrofuran-O)Ytterbium(II). *Acta Crystallographica Section E Structure Reports Online* **2001**, *57* (9), m396–m398.

(6) Cofone, A.; Niemeyer, M. A Monomeric, Base-Free Samarium(II) Thiophenolate with a π-Encapsulated Rare-Earth Metal. In *Zeitschrift fur Anorganische und Allgemeine Chemie*; 2006; Vol. 632, pp 1930–1932.

(7) Niemeyer, M.; Power, P. P. Donor-Free Alkali Metal Thiolates: Synthesis and Structure of Dimeric, Trimeric, AndTetrameric Complexes with Sterically Encumbered Terphenyl Substituents. *Inorganic Chemistry* **1996**, *13*, 7264–7272.

(8) Hauber, S. O.; Niemeyer, M. π-Bonding Encapsulation in Aryl-Substituted Lanthanide Selenolates: Monomeric Compounds with Apparent Low-Coordinate Metal Atoms. *Chemical Communications* **2007**, No. 3, 275–277.

(9) Power, P. P.; Niemeyer, M. Donor-Free Alkali Metal Thiolates: Synthesis and Structure of Dimeric, Trimeric, and Tetrameric Complexes with Sterically Encumbered Terphenyl Substituents. *Inorganic Chemistry* **1996**, *35* (25), 7264–7272.

(10) Angelkort, J.; Van Smaalen, S.; Hauber, S. O.; Niemeyer, M. Phase Transition and Crystal Structure of the Monomeric Europium(II) Thiolate $Eu(SC_{36}H_{49})_2$. *Zeitschrift fur Anorganische und Allgemeine Chemie* **2007**, *633* (7), 1031–1035.

(11) Niemeyer, M.; Power, P. P. Synthesis and Characterization of Some Group 1 and 2 Metal Derivatives of the Crowding Terphenyl Thiolate and Selenolate Ligands-EC_6H_3-2,6-$Trip_2$ (E = S or Se; Trip = 2,4,6-*i*-$Pr_3C_6H_2$-). *Inorganica Chimica Acta* **1997**, *263* (1–2), 201–207.

(12) Stennett, C. R.; Luevano, M. R.; Queen, J. D.; Nguyen, J. Q.; Moore, W. N. G.; Evans, W. J. Large- and Small-Scale Syntheses of Donor-Free Rare-Earth Triiodides from the Metals and Ammonium Iodide. *Inorganic Chemistry* **2024**, *63* (36), 16855–16860.

(13) Sgro, M. J.; Piers, W. E. Synthesis, Characterization and Reactivity of Yttrium and Gadolinium Silyl Complexes. *Inorganica Chimica Acta* **2014**, *422*, 243–250.

(14) Liddle, S. T.; Arnold, P. L. Synthesis and Characterisation of Yttrium Complexes Supported by the β-Diketiminate Ligand {$ArNC(CH_3)CHC(CH_3)NAr$} - (Ar = 2,6-$Pri_2C_6H_3$). *Dalton Transactions* **2007**, No. 30, 3305–3313.

(15) Izod, K.; Liddle, S. T.; Clegg, W. A Convenient Route to Lanthanide Triiodide THF Solvates. Crystal Structures of $LnI_3(THF)_4$ [Ln = Pr] and $LnI_3(THF)_{3.5}$ [Ln = Nd, Gd, Y]. *Inorganic Chemistry* **2004**, *43* (1), 214–218.

(16) Cornish, A. D.; Mills, D. P.; Lewis, W.; Blake, A. J.; Liddle, S. T. Reactions of Alkali Metal and Yttrium Alkyls with a Sterically Demanding Bis(Aryloxysilyl)Methane: Formation of Aryloxide Complexes by Si-O Bond Cleavage. *Comptes Rendus Chimie* **2010**, *13* (6–7), 593–602.

(17) Goodwin, C. A. P.; Reta, D.; Ortu, F.; Liu, J.; Chilton, N. F.; Mills, D. P. Terbocenium: Completing a Heavy Lanthanide Metallocenium Cation Family with an Alternative Anion Abstraction Strategy. *Chemical Communications* **2018**, *54* (66), 9182–9185.

(18) Ryan, A. J.; Ziller, J. W.; Evans, W. J. The Importance of the Counter-Cation in Reductive Rare-Earth Metal Chemistry: 18-Crown-6 Instead of 2,2,2-Cryptand Allows Isolation of $[Y^{(II)}(NR_2)_3]^{1-}$ and Ynediolate and Enediolate Complexes from CO Reactions. *Chemical Science* **2020**, *11* (7), 2006–2014.

(19) Ryan, A. J.; Darago, L. E.; Balasubramani, S. G.; Chen, G. P.; Ziller, J. W.; Furche, F.; Long, J. R.; Evans, W. J. Synthesis, Structure, and Magnetism of Tris(Amide) $[Ln\{N(SiMe_3)_2\}_3]^{1-}$ Complexes of the Non-Traditional +2 Lanthanide Ions. *Chemistry - A European Journal* **2018**, *24* (30), 7702–7709.

(20) Collin, J.; Giuseppone, N.; Jaber, N.; Domingos, A.; Maria, L.; Santos, I. *Iodo Bis Bistrimethylsilylamido Lanthanides*; 2001; Vol. 628. www.elsevier.nl/locate/jorganchem.

(21) Berg, D. J.; Gendron, R. A. L. Synthesis, Solid State Structure, and Solution Behaviour of the Lighter Lanthanide Bis(Trimethylsilyl)Amido Chlorides, $[Ln\{N(SiMe_3)_2\}_2(THF)(\mu\text{-}Cl)]_2$(Ln = Ce, Nd). **2000**.

(22) Zhou, F.; Zhang, S.; Zhao, Y.; Li, C. Z.; Cheng, X.; Zheng, L.; Zhang, Y.; Li, Y. Dinuclear Dysprosium and Ytterbium Complexes Incorporating N,NBis(Pyrrolylαmethyl)-N-Methylamine Ligand: Syntheses and Structures. *Zeitschrift fur Anorganische und Allgemeine Chemie* **2009**, *635* (15), 2636–2641.

(23) Hitchcock, P. B.; Hulkes, A. G.; Lappert, M. F. Oxidation in Nonclassical Organolanthanide Chemistry: Synthesis, Characterization, and X-Ray Crystal Structures of Cerium(III) and -(IV) Amides. *Inorganic Chemistry* **2004**, *43* (3), 1031–1038.

(24) Hemmer, E.; Cavelius, C.; Huch, V.; Mathur, S. Templating Influence of Molecular Precursors on $Pr(OH)_3$ Nanostructures. *Inorganic Chemistry* **2015**, *54* (13), 6267–6280.

(25) Bradley, D. C.; Ghotra, J. S.; Hart, F. A. Low Co-Ordination Numbers in Lanthanide and Actinide Compounds. Part 1. The Preparation and Characterization of Tris{bis(Trimethylsilyl)-Amido}lanthanides. *Journal of the Chemical Society, Dalton Transactions* **1973**, 1021–1023.

(26) Coles, M. P.; Hitchcock, P. B.; Khvostov, A. V.; Lappert, M. F.; Li, Z.; Protchenko, A. V. Crystalline Amidocerium(IV) Oxides and a Side-on Bridging Dioxygen Complex. *Dalton Transactions* **2010**, *39* (29), 6780.

(27) Minhas, R. K.; Ma, Y.; Song, J.-I.; Gambarotta, S. Synthesis, Reactivity, and Stability of Di-and Trivalent Samarium Amides. *Inorganic Chemistry* **1996**, *35*, 1866–1873.

(28) Guan, J.; Jin, S.; Lin, Y.; Shan, Q. Syntheses of Methylcyclopentadlenyl Derivatives of Lanthanides (Ln = La-Nd) and Crystal Structures of $[(THF)_2Li(u\text{-}CI)_2]_2[MeCpNd(THF)]$ and $[Li(DME)_3][MeCpLa(NPh_2)_3]$. *Organometallics* **1992**, *11*, 2483–2487.

(29) Karl, M.; Dashti-Mommertz, A.; Neumüller, B.; Dehnicke, K. $[(THF)_2Na(Ph_2N)_2Sm\{N(SiMe_3)_2\}_2]$, Ein Amido-Komplex Des Samariums Mit Sandwichartig Koordiniertem Natriumion. *Zeitschrift fur Anorganische und Allgemeine Chemie* **1998**, *624* (3), 355–356.

(30) Gamer, M. T.; Roesky, P. W. Lanthanide - Potassium Wheels. *Inorganic Chemistry* **2005**, *44* (17), 5963–5965.

(31) Xu, X.; Yao, Y.; Zhang, Y.; Shen, Q. Synthesis, Reactivity, and Structural Characterization of Sodium and Ytterbium Complexes Containing New Imidazolidine-Bridged Bis(Phenolato) Ligands. *Inorganic Chemistry* **2007**, *46* (9), 3743–3751.

(32) Karl, M.; Harms, K.; Dehnicke, K. Synthese Und Kristallstrukturen Der Natrium-Amido-Metallate $[(THF)_2Na(Ph_2N)_2Ln\{N(SiMe_3)_2\}_2]$ Mit Ln = Gd Und Yb. *Zeitschrift für anorganische und allgemeine Chemie* **1999**, *625* (11), 1774–1776.

(33) Wang, Y.; Shen, Q.; Xue, F.; Yu, K. Novel Anionic Lanthanocene Amide Complexes: Syntheses and X-Ray Crystal Structures of $[Na(THF)2(\mu\text{-}\eta_5\text{:}\eta_5\text{-}MeC_5H_4)_2Ln(NPh_2)_2]_n$ (Ln = Sm, Er). *Organometallics* **2000**, *19* (3), 357–360.

(34) Yu, K. X.; Ding, Y. S.; Han, T.; Leng, J. D.; Zheng, Y. Z. Magnetic Relaxations in Four-Coordinate Dy(III) Complexes: Effects of Anionic Surroundings and Short Dy-O Bonds. *Inorganic Chemistry Frontiers* **2016**, *3* (8), 1028–1034.

(35) Wong, W.-K.; Zhang, L.; Xue, F.; Mak, T. C. W. *Effects of Metal-Size and Auxiliary Ligand on the Alkylation of Lanthanide-Halide with Li[(CH2)(CH2)PPh2]. X-Ray Crystal Structures of [Me2PPh2] [Sm(h5-C5H4Bu)3Cl] and [Li(C4H8O) 4] [Er(NPh2)4]*; 2013; Vol. 16.

(36) Weiss, C. J.; Marks, T. J. Organo-f-Element Catalysts for Efficient and Highly Selective Hydroalkoxylation and Hydrothiolation. *Dalton Transactions* **2010**, *39* (29), 6576–6588.

(37) Mao, L.; Shen, Q. I.; Jin, S. SYNTHESIS AND CRYSTAL STRUCTURE OF $[Li(THF)_4][(TBuCp)Yb(NPh_2)_3]$. *Polyhedron* **1994**, *13* (6), 102–1025.

(38) Guan, J.; Shen, Q.; Jin, S.; Lin, Y. *Synthesis And Crystal Structure Of Bis(Cyclopentadienyl)Amido Complex Of Neodymium, [Li(DME)3] [(η5-C5H5)2Nd(Nph2)2]*; 1994; Vol. 13.

(39) Hitchcock, P. B.; Khvostov, A. V; Lappert, M. F.; Protchenko, A. V. *Ytterbium(II) Amides and Crown Ethers: Addition versus Amide Substitution*; 2002; Vol. 647. www.elsevier.com/locate/jorganchem.

(40) Wang, W.-K.; Zhang, L.; Xueb, F.; Makb, T. C. W. Synthesis and X-Ray Crystal Structure of[$Li(C_4H_8O)_4$] [$Yb(NPh_2)_4$]. **1997**, *16* (2), 345–347.

(41) Xue, M.; Yao, Y.; Shen, Q.; Zhang, Y. The Salt-Free Diamido Complexes of Lanthanide Supported by β-Diketiminate: Synthesis, Characterization, and Their Catalytic Activity for the Polymerization of Acrylonitrile and ε-Caprolactone. *Journal of Organometallic Chemistry* **2005**, *690* (21–22), 4685–4691.

(42) Synthese Und Röntgenstrukturanalyse von [$Li(THF)_4$] [$(C_5H_5)_2Lu(NPh_2)_2$].

(43) Palumbo, C. T.; Kotyk, C. M.; Ziller, J. W.; Evans, W. J. Synthesis and Crystallographic Characterization of Diphenylamide Rare-Earth Metal Complexes $Ln(NPh_2)_3(THF)_2$ and [$(Ph_2N)_2Ln(\mu\text{-}NPh_2)]_2$. *Acta Crystallographica Section E Crystallographic Communications* **2020**, *76* (9), 1447–1453.

(44) Yang, L.; Powell, D. R.; Houser, R. P. Structural Variation in Copper(i) Complexes with Pyridylmethylamide Ligands: Structural Analysis with a New Four-Coordinate Geometry Index, T4. *Journal of the Chemical Society. Dalton Transactions* **2007**, No. 9, 955–964.

(45) Huang, W.; Brosmer, J. L.; Diaconescu, P. L. In Situ Synthesis of Lanthanide Complexes Supported by a Ferrocene Diamide Ligand: Extension to Redox-Active Lanthanide Ions. *New Journal of Chemistry* **2015**, *39* (10), 7696–7702.

(46) Bienfait, A. M.; Wolf, B. M.; Törnroos, K. W.; Anwander, R. Trivalent Rare-Earth-Metal Bis(Trimethylsilyl)Amide Halide Complexes by Targeted Oxidations. *Inorganic Chemistry* **2018**, *57* (9), 5204–5212.

(47) Barnett, B. R.; Mokhtarzadeh, C. C.; Figueroa, J. S.; Lummis, P.; Wang, S.; Queen, J. D.; Gavenonis, J.; Schüwer, N.; Tilley, T. D.; Boynton, J. N.; Power, P. P. Terphenyl Ligands and Complexes; 2018; pp 85–122.

(48) Ni, C.; Rekken, B.; Fettinger, J. C.; Long, G. J.; Power, P. P. Two-Coordinate, Homoleptic Manganese(II) Primary Terphenyl Amido Complexes: The Effects of Secondary Coordination on Geometry and Lewis Base Complexation. *Dalton Transactions* **2009**, No. 39, 8349–8355.

(49) Schiemenz, B.; Power, P. P. Synthesis of Sterically Encumbered Terphenyls and Characterization of Their Metal Derivatives $Et_2OLiC_6H_3$-$_{2,6}$-$Trip_2$ and $Me_2SCuC_6H_3$-2,6-$Trip_2$ (Trip = 2,4,6-i-$Pr_3C_6H_2^-$). *Organometallics* **1996**, *15*, 958–964.

(50) Pratt, J.; Bryan, A. M.; Faust, M.; Boynton, J. N.; Vasko, P.; Rekken, B. D.; Mansikkamäki, A.; Fettinger, J. C.; Tuononen, H. M.; Power, P. P. Effects of Remote Ligand Substituents on the Structures, Spectroscopic, and Magnetic Properties of Two-Coordinate Transition-Metal Thiolate Complexes. *Inorganic Chemistry* **2018**, *57* (11), 6491–6502.

(51) Fan, B.; Shen, Q.; Lii, Y. Synthesis and Molecular Structure of H6-Xylenesamariumtris(Aluminum Tetrachlorides). *Journal of Organometallic Chemistry* **1989**, *376*, 61–66.

(52) Cotton, F. A.; Schwotzer, W. $Sm(H6\text{-}C_6Me_6)(H2\text{-}AlCl_4)_3$: The First Structure of a Rare Earth Complex with a Neutral π-Ligand. *Journal of the American Chemical Society* **1986**, *108*, 4657–4658.

(53) Hossain, M. E.; Guo, Z.; Wang, J.; Deacon, G. B.; Junk, P. C.; Diether, D.; Anwander, R. H6-Arene(Halogenidoaluminato)Lanthanoid(III) Complexes: Synthesis, Characterization and Catalytic Activity for Isoprene Polymerization. *European Journal of Inorganic Chemistry* **2022**, *2022* (7).

(54) Pangborn, A. B.; Giardello, M. A.; Grubbs, R. H.; Rosen, R. K.; Timmers, F. J. Safe and Convenient Procedure for Solvent Purification. *Organometallics* **1996**, *15* (5), 1518–1520.

(55) APEX2, Version 2014.11-0. Bruker AXS, Inc.: Madison, WI 2014.

(56) SAINT, Version 8.34a. Bruker AXS, Inc.: Madison, WI 2013.

(57) Sheldrick, G. M. SADABS, Version 2014/5. Bruker AXS, Inc.: Madison, WI 2014.

(58) Sheldrick, G. M. SHELXTL, Version 2014/7. Bruker AXS, Inc.: Madison, WI 2014.

(59) International Tables for Crystallography. *Dordrecht: Kluwer Academic Publishers*. 1992.

(60) Parsons, S.; Flack, H. D.; Wagner, T. Use of Intensity Quotients and Differences in Absolute Structure Refinement. *Acta Crystallographica* **2013**, *B69*, 249–259.

(61) Spek, A. L. PLATON SQUEEZE: A Tool for the Calculation of the Disordered Solvent Contribution to the Calculated Structure Factors. *Acta Crystallographica* **2015**, *C71*, 9–19.

If you made it this far, you're a real one. Thanks for reading.

-Kito